Tailoring Applications-Relevant Properties in Poly(Vinylidene Fluoride)-based Homo-, Co- and Ter-Polymers through Modification of Their Three-Phase Structure

Thulasinath Raman Venkatesan

Faculty of Science
Institute of Physics and Astronomy
University of Potsdam

Faculty of Science
Department of Physics and Astronomy
KU Leuven

Dissertation in partial fulfillment of the requirements for the joint degree of
Doctor of Natural Sciences (Dr. rer. nat.) & Doctor of Science (Ph. D.): Physics
January 2022

Supervisor (University of Potsdam): Prof. Dr. Reimund Gerhard
Supervisor (KU Leuven): Prof. Dr. Michael Wübbenhorst

Published online on the
Publication Server of the University of Potsdam:
https://doi.org/10.25932/publishup-54966
https://nbn-resolving.org/urn:nbn:de:kobv:517-opus4-549667

Reviewers:

1st Reviewer: Prof. Dr. Reimund Gerhard
Institute of Physics and Astronomy, University of Potsdam

2nd Reviewer: Prof. Dr. Michael Wübbenhorst
Department of Physics and Astronomy, KU Leuven

3rd Reviewer: Prof. Dr. Yuri Feldman
Department of Applied Physics, The Hebrew University of Jerusalem

---

Thesis Committee/ Joint Examination Committee:

Prof. Dr. Reimund Gerhard
Institute of Physics and Astronomy, University of Potsdam

Prof. Dr. Michael Wübbenhorst
Department of Physics and Astronomy, KU Leuven

Prof. Dr. Pavlik Lettinga
Department of Physics and Astronomy, KU Leuven

Prof. Dr. Andreas Taubert
Institute of Chemistry, University of Potsdam

Prof. Dr. Yuri Feldman
Department of Applied Physics, The Hebrew University of Jerusalem

Prof. Dr. Valeri Afanasiev
Department of Physics and Astronomy, KU Leuven

Prof. Dr. Dieter Neher
Institute of Physics and Astronomy, University of Potsdam

Prof. Dr. Ruth Cardinaels
Department of Physics and Astronomy, KU Leuven

"கற்றது கைமண் அளவு, கல்லாதது உலகளவு"

- ஔவையார், பெண் புலவர் (~12ஆம் நூற்றாண்டு)

"What one knows is just a handful of sand, while the unknown is as big as Earth"

- Avvaiyar, Tamil poetess (circa 12th century)

என்னை ஈன்ற தாய்க்கும் தந்தைக்கும் அர்ப்பணிப்பு

To my beloved mother and father
for their endless love and support

Declaration

I, Thulasinath Raman Venkatesan, formally submit my thesis titled, **'Tailoring Applications-Relevant Properties in Poly(Vinylidene Fluoride)-based Homo-, Co- and Ter-Polymers through Modification of Their Three-Phase Structure'** in partial fulfillment of the requirements set forth by the regulations for awarding the title '***doctor rerum naturalium***' **(Dr. rer. nat.)** in the Faculty of Science at the University of Potsdam and for awarding the title **'Doctor of Science (Ph.D.): Physics'** in Arenberg Doctoral School at KU Leuven, within the framework of a Convention de Cotutelle de thése/Joint Doctorate.

I declare that the content presented in this thesis has not been submitted as an exercise for a degree to any other university.

I hereby confirm that the work described herein is based on the research I have performed in the University of Potsdam and KU Leuven without contributions from any sources other than those cited in the text, the references, and the acknowledgements. This applies explicitly to all graphics, drawings, and images included in the thesis.

Thulasinath Raman Venkatesan

Summary

Poly(vinylidene fluoride) (PVDF)-based homo-, co- and ter-polymers are well-known for their ferroelectric and relaxor-ferroelectric properties. Their semi-crystalline morphology consists of crystalline and amorphous phases, plus interface regions in between, and governs the relevant electro-active properties. In this work, the influence of chemical, thermal and mechanical treatments on the structure and morphology of PVDF-based polymers and on the related ferroelectric/relaxor-ferroelectric properties is investigated.

Polymer films were prepared in different ways and subjected to various treatments such as annealing, quenching and stretching. The resulting changes in the transitions and relaxations of the polymer samples were studied by means of dielectric, thermal, mechanical and optical techniques. In the Introductory chapter, a brief history of electro-active materials along with a basic description of ferroelectric and relaxor-ferroelectric materials is provided. The motivation for the work, and the various experimental and characterization methods that have been used are described in Chapters 2 and 3, respectively. The different PVDF-based polymers employed for the experiments and the various sample preparation techniques utilized are mentioned in Chapter 4.

While Chapter 5 summarizes the important properties and characteristics of ferroelectric and relaxor-ferroelectric materials, the relaxations and transitions that can be observed in these materials are included in Chapter 6. Both chapters 5 and 6 list and discuss the key features of PVDF-based polymers that are subsequently studied in more details in futher chapters. In particular, the origin(s) behind the mysterious mid-temperature transition (T_{mid}) that is observed in all PVDF-based polymers is assessed in Chapter 7. A new hypothesis is proposed to describe the T_{mid} transition as a result of multiple processes taking place within the temperature range of the transition. Chapter 8 explains in detail how the contributions of the individual processes to the observed overall T_{mid} transition depend on the chemical structure of the monomer units, and the processing conditions which also affect the melting transition.

In order to prepare high-quality films under laboratory conditions, PVDF-based polymers were subjected to rapid quenching in liquid nitrogen from their melt or annealed state, the

results of which are discussed in Chapter 9. Quenching results in a decrease of the overall crystallinity and in smaller crystallites. On samples quenched after annealing, notable differences in the fractions of the different crystalline phases have been observed when compared to samples that had been slowly cooled.

Poly(vinylidene fluoride-tetrafluoroethylene) (P(VDF-TFE)) films were stretched at different temperatures and their effect on the crystalline phases and dielectric properties is analyzed in Chapter 10. The results show that stretching of P(VDF-TFE) films causes an increase in the fraction of the ferroelectric β phase with simultaneous increments in the melting point (T_m) and the crystallinity (χ_c) of the copolymer. While an increase in the stretching temperature does not have a profound effect on the amount of the ferroelectric phase, its stability appears to improve - as seen in the reduction of the Full Width at Half Maximum (FWHM) of the WAXD peaks in both parallel and perpendicular directions to the molecular chain axis. This observation is also supported by the reduction of dissipation losses that is observed with an increase in stretching temperature. In addition, the impact of stretching temperature on the mid-temperature transition is observed in DSC heating curves from the change in the shape of the transition from that of an endothermic peak at low temperatures of stretching to a relaxation step at higher stretching temperatures.

Chapter 11 demonstrates the use of non-linear dielectric spectroscopy (NLDS) as an effective tool to study relaxation processes and phase transitions in a poly(vinylidene fluoride-trifluoroethylene-chlorofluoroethylene) (P(VDF-TrFE- CFE)) relaxor-ferroelectric (R-F) terpolymer. Measurements of the non-linear dielectric permittivity ε_2' reveal peaks at 30 and 80 °C that cannot be identified in conventional dielectric spectroscopy. By combining the results from NLDS experiments with those from other techniques such as Thermally-Stimulated-Depolarization Currents (TSDCs) and dielectric-hysteresis studies, it is possible to explain the processes behind the additional peaks. The former peak is associated with T_{mid} and may help to understand the non-zero ε_2' values that are found for the paraelectric terpolymer phase. The latter peak can also be observed during cooling of P(VDF-TrFE) copolymer samples at 100 °C and is due to conduction processes and space-charge polarization as a result of the accumulation of real charges at the electrode-sample interface.

Effects of thermal processing on micro- and nano-structural features and thus on relaxor-ferroelectric properties of a P(VDF-TrFE-CFE) terpolymer were investigated by means of dielectric experiments and are discussed in Chapter 12. The results are correlated with those obtained from thermal and optical methods. Annealing lowers the Curie-transition temperature of the terpolymer as a consequence of its smaller ferroelectric-phase fraction,

which by default exists even in terpolymers with relatively high CFE content. Changes in the transition temperatures are in turn related to the behavior of the hysteresis curves observed on differently heat-treated samples. Upon heating, the hysteresis curves evolve from those known for a ferroelectric to those of a typical relaxor-ferroelectric material. Comparing dielectric-hysteresis loops obtained at various temperatures, we find that annealed terpolymer films show higher electric-displacement values and lower coercive fields than the non-annealed samples - irrespective of the measurement temperature - and also exhibit ideal relaxor-ferroelectric behavior at ambient temperatures, which makes them excellent candidates for related applications at or near room temperature. However, non-annealed films – by virtue of their higher ferroelectric activity – show a larger and more stable remanent polarization at room temperature, while annealed samples need to be poled below $0\,^{\circ}\mathrm{C}$ to exhibit a well-defined polarization.

Overall, by modifying the three phases in PVDF-based polymers, it has been demonstrated how the preparation steps and processing conditions can be tailored to achieve the desired properties that are optimal for specific applications.

Kurzfassung

Homo-, Ko- und Terpolymere auf der Basis von Poly(vinylidenfluorid) (PVDF) sind für ihre ferroelektrischen und relaxor-ferroelektrischen Eigenschaften bekannt. Die teilkristalline Morphologie dieser Fluorpolymere, bestehend aus kristallinen und amorphen sowie den dazwischen liegenden Grenzflächen, bestimmt die relevanten elektroaktiven Eigenschaften. In dieser Arbeit wird der Einfluss chemischer, thermischer und mechanischer Behandlungen auf die Struktur und Morphologie von Polymeren der PVDF-Familie untersucht, die wiederum direkt mit den ferroelektrischen/relaxor-ferroelektrischen Eigenschaften zusammenhängen. Daher wurden Polymerfilme mit verschiedenen Methoden hergestellt und vielfältigen Prozessschritten wie z.B. Tempern, Abschrecken und Recken unterzogen. Die sich daraus ergebenden Veränderungen bei Phasenübergängen und Relaxationen in den Proben wurden mit dielektrischen, thermischen, mechanischen und optischen Verfahren untersucht. Insbesondere wurden die Ursachen für den mysteriösen Übergang bei mittleren Temperaturen (T_{mid}) untersucht, der an allen PVDF-basierten Polymeren beobachtet werden kann.

Es wurde eine neue Hypothese aufgestellt, die den T_{mid}-Übergang als Ergebnis mehrerer Prozesse beschreibt, die innerhalb eines Temperaturbereichs mehr oder weniger gleichzeitig ablaufen. Der Beitrag dieser einzelnen Übergänge zum Gesamtübergang hängt sowohl von der chemischen Struktur der Monomereinheiten als auch von den Verarbeitungsbedingungen ab. Die verschiedenen Verarbeitungsbedingungen wirken sich auch auf den Schmelzübergang der Polymere aus. Der Prozess des Abschreckens führt zu einer Abnahme der Gesamtkristallinität mit einer geringeren Kristallitgröße. Bei Proben, die nach dem Tempern abgeschreckt wurden, werden im Vergleich zu Proben, die langsam aus dem getemperten Zustand abgekühlt wurden, bemerkenswerte Unterschiede im Anteil der verschiedenen kristallinen Phasen festgestellt. Das Recken von Poly(vinylidenfluorid-tetrafluorethylen) (P(VDF-TFE))-Filmen führt zu einem Anstieg des Anteils der ferroelektrischen β-Phase bei gleichzeitiger Erhöhung von Schmelzpunkt (T_{m}) und Kristallinität (χ_{c}) des Kopolymers. Während eine Erhöhung der Strecktemperatur keinen tiefgreifenden Einfluss auf die Menge der ferroelektrischen Phase hat, scheint sich die Stabilität der ferroelektrischen Phase zu verbessern.

Messungen der nichtlinearen dielektrischen Dielektrizitätskonstante ε_2' zeigen in einem relaxor-ferroelektrischen (R-F) Terpolymer aus Poly(vinyliden-fluorid-trifluorethylen-chlorfluorethylen) (P(VDF-TrFE- CFE)) Maxima bei 30 und 80 °C, die in der herkömmlichen dielektrischen Spektroskopie nicht identifiziert werden können. Das erste Maximum hängt mit T_{mid} zusammen und kann dabei helfen, die von Null verschiedenen ε_2'-Werte zu verstehen, die an der paraelektrischen Phase des Terpolymers beobachtet werden. Das zweite Maximum kann auch während des Abkühlens von P(VDF-TrFE)-Kopolymerproben bei 100 °C beobachtet werden und ist auf elektrische Leitungsprozesse und Raumladungspolarisationen infolge der Ansammlung von realen Ladungen an den Grenzflächen der Elektroden zum Polymermaterial zurückzuführen.

Das Tempern verringert die Curie-Übergangstemperatur des Terpolymers als Folge der Verringerung des ferroelektrischen Phasenanteils, der standardmäßig sogar in Terpolymeren mit relativ hohem CFE-Gehalt vorhanden ist. Die Änderungen der Übergangstemperaturen stehen wiederum im Zusammenhang mit dem Verhalten der Hysteresekurven bei unterschiedlich wärmebehandelten Proben. Während der Erwärmung kommt es zu einer deutlichen Veränderung der Hysteresekurven von einem typisch ferroelektrischen Verhalten hin zu relaxor-ferroelektrischem Verhalten. Vergleicht man die bei verschiedenen Temperaturen beobachteten dielektrischen Hystereseschleifen, so stellt man fest, dass getemperte Terpolymerfilme - unabhängig von der Messtemperatur - höhere dielektrische Verschiebungen und niedrigere Koerzitivfelder aufweisen als nicht getemperte Proben und dass sie auch bei Raumtemperatur ein ideales relaxor-ferroelektrisches Verhalten zeigen, was sie zu ausgezeichneten Kandidaten für Anwendungen in der Nähe der Raumtemperatur macht. Allerdings zeigen nicht getemperte Filme aufgrund ihrer höheren Ferroelektrizität einen höheren und stabilen Wert der remanenten Polarisation bei Raumtemperatur, während getemperte Proben unter 0 °C gepolt werden müssen, um eine eindeutige Polarisation aufzuweisen. Insgesamt konnte gezeigt werden, dass durch die Modifizierung der drei Phasen in PVDF-basierten Polymeren die Präparationsschritte und Verarbeitungsbedingungen so angepasst werden können, dass die gewünschten Eigenschaften für bestimmte Anwendungen optimal sind.

Samenvatting

Poly(vinylideenfluoride) (PVDF)-gebaseerde homo-, co- en ter-polymeren staan bekend om hun ferro-elektrische en relaxor-ferro-elektrische eigenschappen. Hun semi-kristallijne morfologie bestaat uit kristallijne en amorfe fasen met daartussen interfaceregio's, en bepaalt de relevante elektro-actieve eigenschappen. In dit werk wordt de invloed onderzocht van chemische, thermische en mechanische behandeling op de structuur van op PVDF gebaseerde polymeren en op de daarmee samenhangende ferro-elektrische/relaxor-ferro-elektrische eigenschappen. Polymeerfilms werden op verschillende manieren bereid en onderworpen aan verschillende behandelingen zoals warmte behandelen, afschrikken en uitrekken. De resulterende veranderingen in de overgangen en relaxaties van de polymeersamples werden bestudeerd met behulp van diëlektrische, thermische, mechanische en optische technieken. In het bijzonder werd nagegaan wat de oorsprong(en) is (zijn) van de mysterieuze overgang in het middentemperatuur gebied (T_{mid}) die in alle op PVDF gebaseerde polymeren wordt waargenomen.

Een nieuwe hypothese wordt voorgesteld om de T_{mid} te beschrijven als een resultaat van meerdere processen die plaatsvinden binnen het temperatuur bereik van de overgang. De bijdrage van de afzonderlijke processen tot de waargenomen totale overgang hangt af van zowel de chemische structuur van de monomeereenheden als de verwerkingsomstandigheden die ook de smeltovergang beïnvloeden. Quenchen resulteert in een afname van de totale kristalliniteit en kleinere kristallieten. Bij samples die na annealing zijn afgekoeld, zijn opmerkelijke verschillen in de fracties van verschillende kristallijne fasen waargenomen in vergelijking met stalen die langzaam waren afgekoeld. Uitrekken van poly(vinylideen-fluoride-tetrafluorethyleen) (P(VDF-TFE)) films veroorzaakt een toename in de fractie van de ferro-elektrische β-fase met gelijktijdige toenames in het smeltpunt (T_{m}) en de kristalliniteit (χ_{c}) van het copolymeer. Terwijl een verhoging van de uitrektemperatuur geen diepgaand effect heeft op de hoeveelheid van de ferro-elektrische fase, lijkt de stabiliteit ervan te verbeteren.

Metingen van de niet-lineaire diëlektrische permittiviteit ε_2' een poly(vinylideenfluoride-trifluorethyleen-chloorfluorethyleen) (P(VDF-TrFE- CFE)) relaxor-ferro-elektrisch (R-F) terpolymeer leiden tot pieken bij 30 en 80 °C die niet kunnen worden geïdentificeerd via con-

ventionele diëlektrische spectroscopie. De eerste piek is geassocieerd met T_{mid} en kan helpen om de niet-nul ε_2' waarden die worden gevonden voor de para-elektrische terpolymeer fase te begrijpen. De laatste piek kan ook worden waargenomen tijdens afkoeling van P(VDF-TrFE) copolymeer samples bij 100 °C en is te wijten aan geleidingsprocessen en ruimtelading polarisatie als gevolg van de accumulatie van reële ladingen op het grensvlak tussen elektrode en polymeer.

Annealing verlaagt de Curietemperatuur van het terpolymeer als gevolg van de kleinere ferro-elektrische fractie, die algemeen aanwezig is, zelfs in terpolymeren met een relatief hoog CFE-gehalte. Veranderingen in de overgangstemperaturen zijn op hun beurt gerelateerd aan het gedrag van de hysteresiscurven die zijn waargenomen bij verschillend warmtebehandelde stalen. Bij opwarming evolueren de hysteresiscurven van typisch ferro-elektrisch naar de karakteristieke vorm voor relaxor-ferroelektrica. Bij vergelijking van de diëlektrische-hysterese krommen verkregen bij verschillende temperaturen, vinden we dat warmtebehandelde terpolymeer films hogere elektrische verplaatsingswaarden en lagere coërcitiefvelden vertonen dan de niet- warmtebehandelde samples - ongeacht de meettemperatuur - en ook ideaal relaxor-ferro-elektrisch gedrag vertonen bij omgevingstemperaturen, waardoor ze uitstekende kandidaten zijn voor gerelateerde toepassingen bij of nabij kamertemperatuur. Niet- warmtebehandelde films vertonen echter - op grond van hun hogere ferro-elektrische activiteit - een hogere en stabiele remanente polarisatie bij kamertemperatuur, terwijl warmtebehandelde samples onder 0 °C moeten worden gepoold om een goed gedefinieerde polarisatie te vertonen. Door de drie fasen in op PVDF gebaseerde polymeren op een gecontroleerde manier te wijzigen, is in het algemeen aangetoond hoe de preparatiestappen en verwerkingsomstandigheden kunnen worden aangepast om de gewenste eigenschappen te verkrijgen met oog voor specifieke toepassingen.

Glossary

$\alpha_{\mathbf{a}}$	relaxation in amorphous phase and glass-transition
$\alpha_{\mathbf{c}}$	relaxation in crystalline phase
$\chi_{\mathbf{c}}$	crystallinity
ΔH	enthalpy of fusion
μ	dipole moment
ω	applied stress
τ	relaxation time, characteristic time constant for the electric dipoles to reach the new equilibrium state under an alternating electric field
θ	diffraction angle
ε'	real part of dielectric permittivity
ε''	imaginary (loss) part of dielectric and permittivity
$L_{\mathbf{c}}$	coherence length of crystals
T_{C}	Curie-transition temperature
$T_{\mathbf{c}}$	crystallization temperature
$T_{\mathbf{g}}$	glass-transition temperature
$T_{\mathbf{g}}(U)$	upper glass-transition temperature
$T_{\mathbf{mid}}$	mid-temperature transition
$T_{\mathbf{m}}$	melting temperature
$T_{\mathbf{s}}$	stretching temperature

d	inter-planer distance/lattice constant
a-c	amorphous-crystalline
a.u.	arbitary units
ATR	Attenuated Total Reflection, a mode of Fourier transform-infrared spectroscopy where the incident infrared beam is attenuated after incident with the sample through total reflection inside a crystal of high refractive index.
CHN	CycloHexaNone, solvent
condis	conformational disorder
D	dielectric displacement
d	piezoelectric strain coefficient
DC	Direct Current
DHL	Double Hysteresis Loop
DMA	Dynamic Mechanical Analysis, a thermomechanical technique used to measure the viscoelastic response of a material by subjecting the material to an oscillating force
DMF	DiMethylFormamide, solvent
DRS	Dielectric Relaxation Spectroscopy, a spectroscopic technique used for the electric characterization of dielectric and semi-conducting materials based on the interaction of an external electric field with the dipole moment of the sample
DSC	Differential Scanning Calorimetry, a thermodynamic technique used to study the physical properties of a polymer by measuring the difference in heat flow of a sample and reference.
E	applied electric field
e.g.	abbreviated form of the Latin term *exempli gratia*, meaning 'for example'
etc.	abbreviated form of the Latin term *et cetera*, meaning 'and so on'
F-P	Ferroelectric-to-Paraelectric transition, the phenomenon in which ferroelectric materials when heated above a particular temperature (Curie temperature), lose their spontaneous polarization and are converted to a non-polar paraelectric phase

FTIR Fourier-Transform InfraRed spectroscopy, a technique used to identify a sample material from the characteristic vibrations of its chemical bonds in the infrared region of the spectrum.

FWHM Full Width at Half Maximum

HEEIP High-Energy Electron-Irradiated Poly(vinylidene fluoride-trifluoroethylene) copolymer

i.e. abbrevated form of the Latin term *id est*, meaning 'that is'

mDSC modulated Differential Scanning Calorimetry, an extension of standard differential scanning calorimetry where a sinusoidal temperature oscillation is overlaid on the conventional linear heating ramp

MWI Maxwell-Wagner Interface polarization

NLDS Non-Linear Dielectric Spectroscopy, a spectroscopic technique used to measure the non-linear permittivities ε_2^* and ε_3^*

P polarization

p pyroelectric coefficient

P(VDF-HFP) Poly(VinyliDene Fluoride-HexaFluoroPropylene), a copolymer of vinylidene fluoride with hexafluoropropylene showing high electrostrictive response

P(VDF-TFE) Poly(VinyliDene Fluoride-TetraFluoroEthylene), a copolymer of vinylidene fluoride with tetrafluoroethylene showing similar ferroelectric properties as Poly(vinylidene fluoride-trifluoroethylene)

P(VDF-TrFE) Poly(VinyliDene Fluoride-TriFluoroEthylene), a copolymer of vinylidene fluoride with trifluoroethylene showing a broad electrical hysteresis with a clear ferroelectric-paraelectric transition

P(VDF-TrFE-CFE) Poly(VinyliDene Fluoride-TriFluoroEthylene-ChloroFluoroEthylene), a terpolymer of vinylidene with trifluoroethylene and chlorofluoroethylene showing relaxor-ferroelectric characteristics

P(VDF-TrFE-CTFE) Poly(VinyliDene Fluoride-TriFluoroEthylene-ChloroTriFluoroEthylene), a terpolymer of vinylidene with trifluoroethylene and chlorotrifluoroethylene showing relaxor-ferroelectric characteristics

PLM Polarized Light Microscope, a microscopy method used for observing the crystalline structure in polymers

PTFE Poly(TetraFluoroEthylene), a fluorinated polymer used in filters.

PVDF Poly(VinyliDene Fluoride), a semi-crystalline polymer containing C-F dipoles with a dipole moment of 2.3 D, showing a glass-transition temperature of around $-40\,^{\circ}$C and melting point around $177\,^{\circ}$C

RT Room Temperature

SAXD Small Angle X-ray Diffraction, X-ray diffraction measurement covering a narrow range of Braggs angle 2θ from about few seconds of arc to a few degrees

SHL Single Hysteresis Loop

T temperature

tan δ dielectric dissipation factor (DRS)/ mechanical loss factor (DMA)

WAXD Wide-Angle X-ray Diffraction, X-ray diffraction measurement covering a broad range of Braggs angle 2θ from about 2 to 60°

XRD X-Ray Diffraction, an analytical technique in which the diffraction of X-rays on to a crystalline sample are used to identify and study the phase structures in the sample.

Contents

1

Introduction

1.1 Electro-active Materials

Electric charges have aroused the curiosity of mankind for several thousands of years. The ancient Egyptians, Greeks and Romans were already familiar with electric fishes that delivered shock [1, 2]. The first scientific description about attraction and repulsion between certain electrically charged objects was probably given by Thales of Miletus, a Greek merchant and philosopher, already more than 2500 years ago [3]. He identified *amber* as one such material. The word *electron* (*electrum* in Latin) refers to amber in Greek and the term *electric* was used by William Gilbert (1544-1603) [4] to describe materials like amber, sulphur and glass that can attract objects. These materials are now known as *electrets*. The term 'electret' was coined by Oliver Heaviside in 1885 [5]. By definition, electret is a piece of dielectric material that possesses a quasi-permanent polarization [5] or electric charge [6]. The electric charges can be 'real' charges on the surface or bulk of the electret and/or arise as a result of electric dipoles in the material.

Some of these naturally charged materials release charges when heated or cooled down producing a voltage. This property is referred to as *pyroelectricity* (*pyr* meaning 'fire' in Greek). The phenomenon has been observed already more than 2400 years ago and is mentioned in the work of the Greek philosopher Theophrastus, who had attributed mythical origin for the source of these pyroelectric crystals (most probably in tourmaline) [7]. After two millennia, another property known as piezoelectricity was discovered in Rochelle, tourmaline, quartz and other crystals by Pierre and Jacques Curie during the year 1880 [8]. The term *piezo* originates from the Greek word *piezo* meaning 'to press'. Hence, piezoelectricity refers to the process of producing charges by subjecting the material to a mechanical stress. Further, ferroelectricity was identified in Rochelle salts about a century ago by Valasek [9]. Subsequently, further research led to the discovery of these interesting properties in several inorganic, mono- and poly-crystalline materials.

Out of the 32 classes into which all the crystalline materials fall, 21 are non-centrosymmetric (not having a center of symmetry). Except for the cubic class '432', the remaining 20 classes exhibit piezoelectricity. Within these 20 classes, 10 possess a unique polar axis (direction in which the dipoles point) and thus exhibit pyroelectricity. If the polarity can be reversed by the application of an electric field, then the material is also *ferroelectric* ('ferro' derived from the Latin word *ferrum* meaning iron). As shown in Figure 1.1, pyroelectricity is a sub property of piezoelectric materials and ferroelectricity is again a sub property of pyroelectric materials. This means, all ferroelectric materials are pyro- and piezo-electric, but piezoelectricity does not always encompass true pyroelectricity and pyroelectricity does not necessarily lead to ferroelectricity. For example, Poly(vinylidene fluoride) is a ferro-, pyro- and piezo-electric material, while quartz is piezoelectric, but not ferroelectric.

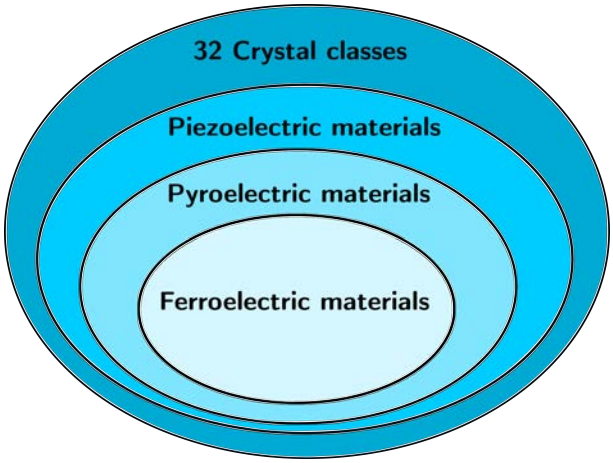

Figure 1.1: Overview of different crystalline electro-active materials.

The afore-mentioned properties in crystalline materials can be primarily explained due to the structure and anisotropy of these crystals [1]. Polymers in general are less anisotropic than crystals and do not possess a perfect crystal lattice. However, they mostly have a non-centrosymmetric crystalline structure (semi-crystalline polymers), and the necessary anisotropy and symmetry breaking required for piezoelectricity can be achieved by means of suitable preparation and processing conditions (e.g. stretching, poling or foaming with charging). Seminal research on piezoelectricity in natural and synthetic polymers was carried out by Fukada, by Kawai and by others in the second half of the 20th century [10, 11]. The electro-activity of these materials arises from the molecular dipoles present in the chemical structure of the monomer. Later in the 1990s, phenomenologically, piezoelectric properties were also identified in non-polar polymers with electrically charged internal cavities. These bipolar electrets are referred to as *ferroelectrets* or *piezoelectrets* [1].

Apart from the above mentioned electrets, there are other types of electro-active materials as shown in Figure 1.2. This includes space-charge electrets with real charges on the surface and in the bulk of

polymers such as polypropylene, poly(tetrafluoroethylene), and electro-electrets consisting of dielectric elastomers. In the latter, opposite charges on the compliant electrodes in contact with the dielectric elastomer act as a macroscopic dipole, bringing about changes in the mechanical properties of the material when subjected to an external electric field. In addition, composite materials can be prepared by loading polar fillers in a dielectric material resulting in piezo- and pyro-electric composites. The electro-active and electromechanical properties of these materials can be exploited in myriad applications as sensors, actuators and transducers [12]. These properties can be described semi-quantitatively using a 'charge-spring' model consisting of charges connected to springs between two electrodes [13]. Different spring constants and charge layers are used to describe the electrical and mechanical inhomogeneities of the particular material under consideration.

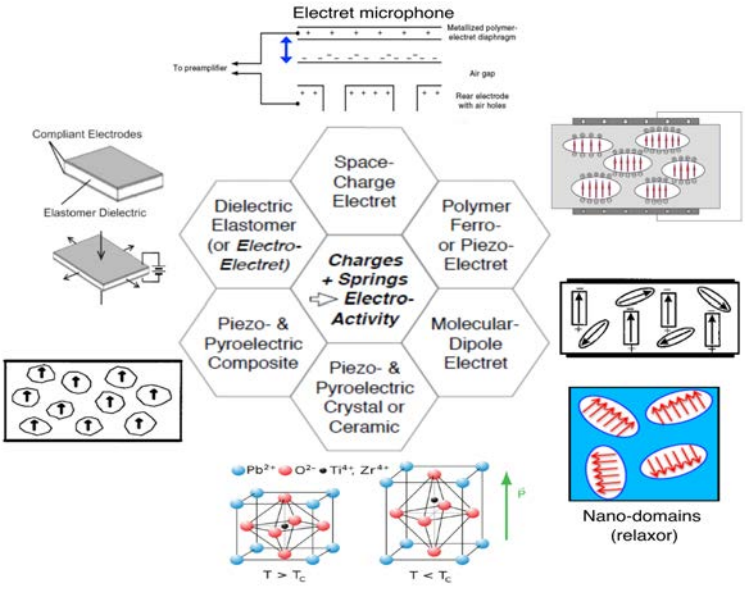

Figure 1.2: Six different types of electro-active materials along with their characteristic features. Adapted from the work of Gerhard [1] and various literature mentioned therein.

1.2 Ferroelectric and Relaxor-Ferroelectric Materials

Ferroelectric materials are the class of materials which show analogous behaviour to ferromagnetic materials even though they do not possess any iron atoms. These materials are characterized by the exhibition of a spontaneous electric polarization (P_s) that is reversible upon the application of an external electric field and also show hysteresis behavior, *i.e.*, the polarization depends not only on the applied electric field but also its history, similar to ferromagnetic materials which show a spontaneous magnetization and hysteresis behavior. Additionally, these materials when heated above a particular temperature called the

Curie Temperature (T_C), lose their spontaneous polarization and are converted to a non-polar paraelectric phase. This transition is called ferroelectric to paraelectric (F-P) or Curie transition. Above T_C, the dielectric permittivity (ε) of these materials follows a Curie-Weiss law (Equation 1.1). Similar to ferromagnetic domains, there exist different regions of the crystal which are polarized in different directions with a P_s, each volume of uniform polarization referred to as a ferroelectric domain.

$$\frac{\varepsilon}{\varepsilon_0} = \frac{C}{T - T_0}, \tag{1.1}$$

where ε_0 is vacuum permittivity or permittivity of free space, equal to 8.85×10^{-12} Fm^{-1}, C is material specific Curie constant, and T_0 is the Curie-Weiss temperature ; $T_0 < T_C$ in the case of a first order phase transition, $T_0 = T_C$ in the case of a second order phase transition.

Up to date, more than 1000 materials have been found to be ferroelectric in nature consisting mostly of inorganic single crystals or ceramic materials such as Barium Titanate, Potassium-Sodium Tartrate-Tetrahydrate (Rochelle Salt), etc. When Kawai first reported piezoelectricity in poly(vinylidene fluoride) (PVDF) [11] in 1969, it aroused much curiosity among the material-science community. Since then extensive research has been carried out to identify newer ferroelectric material systems based on polymers because of their pronounced ferroelectric properties and related electromechanical response, in particular, their marked ferroelectric-hysteresis as well as their piezo- and pyro-electric activity. This has led to the discovery of copolymers, polyureas, polyamides and ferroelectric liquid-crystalline polymers. In addition, relaxor-ferroelectric behavior has been identified in irradiated P(VDF-TrFE) copolymers and in PVDF-based terpolymers, a phenomenon that had been observed previously only on inorganic ceramics such as lead magnesium niobate (PMN) and lead lanthanum zirconate titanate (PLZT) [14].

A large number of fundamental and application-oriented studies have been dedicated to the detailed investigation of structure-property relationships and underlying molecular mechanisms behind the useful properties of the PVDF family of fluoropolymers [15, 16, 17, 18, 19, 20, 21, 22, 23, 24]. Further, these polymers have been employed in sensor and actuator applications, as piezoelectric sensors, motion detectors, ultrasound detectors, micro-actuators, and organic electronics (OFETs) [12, 22, 25, 26, 27, 28]. As in inorganic ferroelectrics and relaxor-ferroelectrics, the electroactivity of these polymers is a property of the polar crystalline phase, but the structure and the elastic properties of the amorphous phase embedding the polar crystallites strongly determine the macroscopic behavior. There exist several polar and non-polar crystalline phases depending on processing conditions and pre-history of the film. Moreover, intermediate phases between amorphous and crystalline phases must be considered in order to explain the mechanical and related electro-active properties of these materials. Overall, these polymers compared to conventional ferroelectric/relaxor-ferroelectric crystals and ceramics offer multiple advantages such as

light weight, low density, high flexibility and softness, suitability for large-area thin film applications, and small acoustic impedance that quite well matches that of air and fluids.

1.3 Poly(vinylidene fluoride) (PVDF)[1]

PVDF is the most commonly used ferroelectric polymer. It is semicrystalline in nature with a repeating unit of $(CH_2 - CF_2)$. PVDF can be prepared by free radical polymerization of gaseous 1,1-difluoroethylene. It can be easily crystallized as it does not have any problems associated with tacticity of the asymmetric carbon atom, and the small fluorine atoms easily enter into crystallographic lattices. The crystalline fraction is generally limited to $50-60\%$ due to the presence of configurational defects such as head to head $(CF_2 - CF_2)$ and tail to tail $(CH_2 - CH_2)$. The presence of a high difference in electronegativity between the carbon and fluorine atom in the C-F bond produces a large net dipole moment (μ) of 6.4×10^{-30} Cm or 1.92 D (traditional unit of μ – Debye D = 3.34×10^{-30} Cm) in VDF monomers [25]. Overall, the monomer has a μ of 2.3 D, paving the way for the large ferro-, pyro- and piezo-electric responses in suitably prepared VDF-based polymers [29].

PVDF-based co- and ter-polymers can crystallize into at least five different phases that are commonly referred to as α (form II), β (form I), γ (form III), δ (form IIp or IV), and ϵ (form V) phases [15, 29, 30]. The molecular chains in the five crystalline forms assume three different conformations: All-*trans*, TG^+TG^-, and $T_3G^+T_3G^-$ (Figure 1). *T (trans)* and $G^{\pm}$ (*gauche*$^{\pm}$) refer to the torsional bond arrangements in the molecule with substituents at angles 180° and $\pm 60^\circ$ to each other respectively. The dipole moments in both TG^+TG^- and $T_3G^+T_3G^-$ chain conformations are inclined with respect to the chain axis. The net dipole moment in the direction normal and parallel to the chain axis are 1.2 D and 1 D, respectively. When cooled from the melt, PVDF chains mostly adopt the TG^+TG^- conformation and crystallize into the α phase, which is the thermodynamically preferred phase. In α crystals, the dipole moments of neighboring chains point in opposite directions and thus cancel each other – resulting in a macroscopically non-polar phase.

Poling of α crystals at strong electric fields can orient the neighboring dipole moments parallel to each other leading to the formation of the polar δ phase [31]. On the other hand, stretching of the α phase to high ratios results in the alignment of all fluorine atoms at the same side of the backbone with a zig-zag all-*trans* chain conformation, resulting in β crystals. Here, all the C-F dipoles in PVDF are perpendicular to the chain axis and as a result, exhibits the highest dipole moment of all PVDF phases (2.1 D) [29]. Hence, in order to prepare PVDF with the best possible ferroelectric characteristics, it is necessary to achieve a high fraction of the crystalline β phase.

[1] Parts of this section are adapted from T. Raman Venkatesan *et al.*, "Structure-Property Relationships in Three-Phase Relaxor-Ferroelectric Terpolymers", *Ferroelectrics*, 586(1), 60-81, 2022 [24].

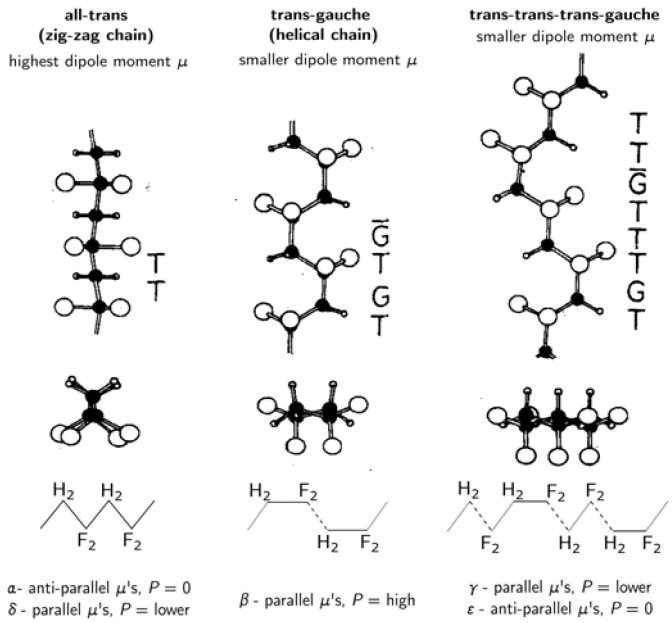

Figure 1.3: Schematic overview of the various conformations found in the different crystalline phases of VDF-based polymers with a brief description of their typical characteristics. Adapted from the work of Tashiro *et al.* [32]

Poling at very high electric fields also results in the β phase. High-temperature annealing of the α phase can convert the polymer chains into the $T_3G^+T_3G^-$ conformation, which is either polar with parallel dipole moments of all macromolecular chains in a crystal (γ phase) or non-polar with anti-parallel dipole moments of neighboring chains (ϵ phase) [30]. However, only a minor fraction of ϵ PVDF crystals is usually generated, as the γ phase is thermodynamically favoured over the ϵ phase. A schematic overview of the three conformations present in the five crystalline phases of PVDF-based polymers is shown in Figure 1.3. The five crystalline phases (Form I to V) can be inter-converted by thermal, mechanical and electrical means as depicted in Figure 1.4. This is facilitated by the small difference in the potential energies of the different conformations. In addition, the solvent used to prepare the polymer films also influences the final crystalline phase as depicted in the figure.

1.4 PVDF Derived Polymers

It has been shown before that ferroelectric polymers show enhanced electromechanical properties near the F-P transition region [33]. Therefore, by reducing the F-P transition temperature, the applicability of these materials for electromechanical sensors and actuators under ambient conditions can be improved. However, in β PVDF the dipolar forces in the ferroelectric phase are sufficiently strong that the polymer melts before undergoing F-P transition. By introducing molecular defects in PVDF, one can alter the physical properties of the polymer, making it more useful for practical applications. This can

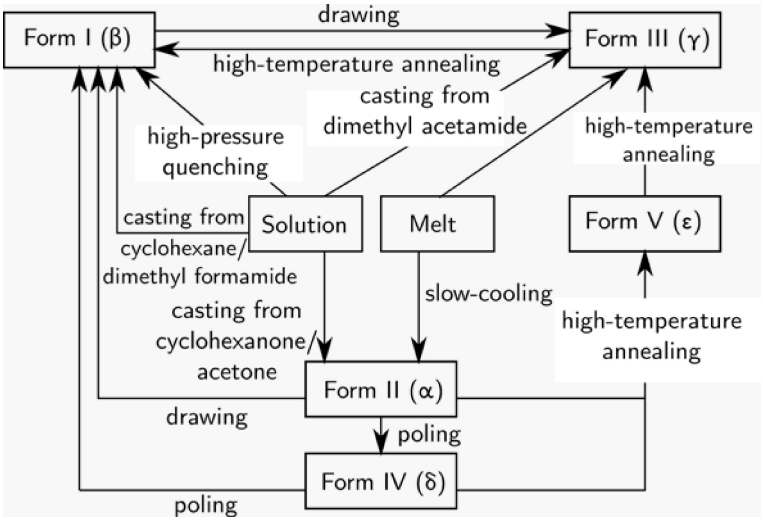

Figure 1.4: Interconvertion between different crystalline phases in PVDF using thermal, mechanical and electrical energy (adapted from the work of Tashiro *et al.* [32]).

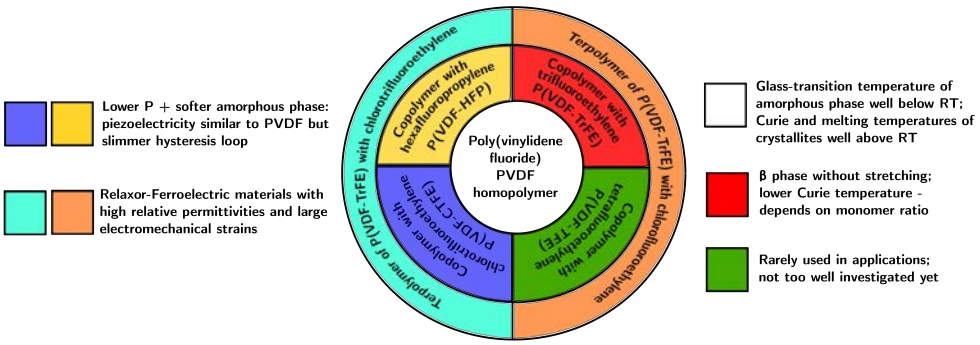

Figure 1.5: Schematic overview of the different PVDF-based polymers with a brief description of their typical characteristics.

be done by polymerizing VDF along with a comonomer. In the past, various comonomers such as trifluoroethylene (TrFE), tetrafluoroethylene (TFE), chlorotrifluoroethylene (CTFE), hexafluoropropylene (HFP), *etc*. have been polymerized with VDF. The comonomers have different effects on the relevant properties of the copolymers – as briefly summarized in Figure 1.5. The most important VDF-based copolymers are the random copolymers of VDF with TrFE (P(VDF-TrFE)), TFE (P(VDF-TFE)), and HFP (P(VDF-HFP)).

1.4.1 P(VDF-TrFE) Copolymer

Although studies with P(VDF-TrFE) were done even before piezoelectricity in PVDF was reported [34], it was only around 1979, its ferroelectric behavior was started to be studied [35]. TrFE is a bulky comonomer when compared with VDF (Figure 1.6). This along with the steric and electronic repulsion of -CFH in

TrFE with -CF_2 in VDF, increases the interchain distance compared with the homopolymer and subsequently weakens the interchain interaction. This in turn decreases the F-P transition compared to β PVDF. As the concentration of TrFE is increased, the stability of the ferroelectric β phase is reduced with respect to the paraelectric phase and hence the T_C is increased. The T_C in P(VDF-TrFE) varies from 60-135 °C according to the TrFE content [36]. As a result, by varying TrFE concentration, the properties of the copolymer can be tailored. For example, the T_C of the copolymer is reduced below its melting point T_m when the molar concentration of TrFE is in the range 50-80 % VDF [37]. In addition, introduction of TrFE restrains the formation of *gauche* bonds and as a result stabilizes the β phase. This is explained in terms of the size of the fluorine atom in TrFE, which is slightly bigger than the hydrogen atom, causing more steric hindrance than VDF, forcing it to take an all-*trans* conformation [23]. Therefore, the stretching process required for the PVDF homopolymer can be eliminated with P(VDF-TrFE).

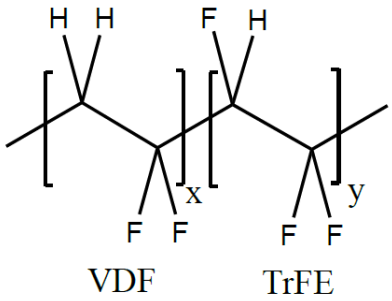

Figure 1.6: Chemical structure of P(VDF-TrFE) copolymer.

Poling P(VDF-TrFE) offers many advantages such as high piezoelectric response, high electromechanical coupling factor, *etc.*, which has led to a broad range of applications such as transducers and sensors. However, compared to traditional ferroelectric materials, TrFE copolymer shows very low strain level (~ 0.1 % strain) and low sensitivity to external stimulus. The response can be improved by operating near the unstable F-P transition range where the transition from ferroelectric phase to paraelectric phase is accompanied by a large strain. This is due to the change in conformation from all-*trans* to TG^+TG^- state. But, this F-P transition occurs over a narrow range at higher temperature and involves a large hysteresis. This limits its enhanced response to be used practically.

1.4.2 P(VDF-TFE) Copolymer

Poly(vinylidenefluoride-tetrafluoroethylene) (P(VDF-TFE)) is a random copolymer of vinylidenefluoride (VDF) with tetrafluoroethylene (TFE). Its chemical structure shown in Figure 1.7 resembles that of the PVDF homopolymer, but with a certain number of -CH_2 groups in VDF having been replaced by -CF_2 groups. Hence, the P(VDF-TFE) copolymer might be regarded as a variant of the PVDF homopolymer with a higher percentage of head-to-head (H-H) ($CF_2 - CF_2$) defects. However, its ferro-,

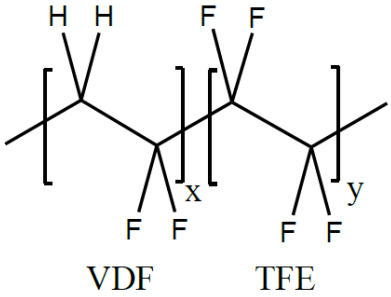

Figure 1.7: Chemical structure of P(VDF-TFE) copolymer.

pyro- and piezo-electric properties are quite similar to those of the often used copolymer of VDF with trifluoroethylene (P(VDF-TrFE)) [15, 16]. In addition to being employed in various electro-active devices such as transducers, pressure sensors, infrared detectors, memories, etc. [28], copolymers of VDF with TFE are mainly used as protective surface coatings due to their excellent chemical and weather resistance [38, 39]. More recently, TFE-based terpolymer elastomers with the third co-monomer propylene (P), *i.e.* P(VDF-TFE-P), have been developed for applications as electrode binders and separators in lithium-ion batteries [39, 40].

1.4.3 P(VDF-HFP) Copolymer

In HFP, all the hydrogen atoms in propylene are replaced by fluorine atoms (Figure 1.8). As a result, when HFP is copolymerised with VDF, it can be described as certain number of -CH_2 units in PVDF being replaced by -$CF(CF_2)$ units. P(VDF-HFP) was developed in the 1960s as an easily soluble, lower-melting copolymer of PVDF for applications such as chemically resistive films and coatings [41]. It was only in the 2000s they attracted interest from the ferroelectric community because of their high electrostrictive strain response [42, 43]. This is attributed to the bulky -CF_3 groups in HFP which in turn causes less favourable thermodynamical conditions for crystallization. This results in P(VDF-HFP) exhibiting lower elastic modulus and thus higher piezoelectric and strain response with external electric field. Previously, a high elecrostrictive strain response of over 4 % was reported on a melt-quenched non-stretched P(VDF-HFP) film containing 5 % HFP [42].

A diffuse F-P transition in the temperature range of 50-70 °C has been reported in P(VDF-HFP) 93/7 and 86/14 mol % copolymers before [44]. Uniaxial stretching renders the polymer structure more polar by inducing the β phase in PVDF, thus significantly increasing the modulus at ambient temperature for possible electromechanical applications. At the same time, this does not immobilize most parts contributing to polarization structurally which results in their low thermal stability [45].

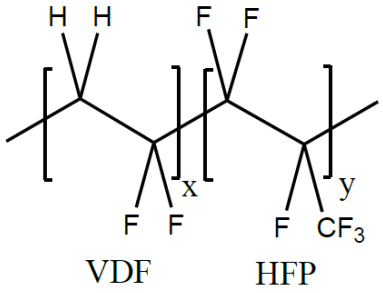

Figure 1.8: Chemical structure of P(VDF-HFP) copolymer.

1.4.4 Irradiated P(VDF-TrFE) Copolymer

Ferroelectric materials show hysteresis behavior due to the existence of an energy barrier when switching from one phase to another or from one polarization direction to the other. By reducing this energy barrier, the electrostrictive strain response of these materials can be enhanced, thus improving their applicability in electromechanical sensors and actuators.

In 1985, Odajima *et al.* first showed that by irradiating P(VDF-TrFE) copolymer it is possible to reduce its F-P transition temperature [46] and in 1998, Zhang *et al.* demonstrated that these high-energy electron-irradiated P(VDF-TrFE) (referred as HEEIP) show exceptionally high electrostrictive response ($\sim 4\%$), which is related to typical relaxor-ferroelectric behavior as previously found in some inorganic ceramics such as lead magnesium niobate (PMN) and lead lanthanum zirconate titanate (PLZT) [14]. This behavior was proposed to be caused by irradiation-induced defects in the material. High-energy irradiation breaks the long-range polar order in the ferroelectric phase into nanodomains, thus reducing the dipole interaction and stabilizing the non-polar paraelectric phase at room temperature. It was concluded that the F-P transition is reduced to room temperature or even eliminated. Consequently, at room temperature, in the presence of an external field it is possible to induce a reversible change between the polar and non-polar phases with only little hysteresis.

1.4.5 PVDF Terpolymers[1]

In 2002, Chung and Petchsuk demonstrated that it is also possible to chemically modify the P(VDF-TrFE) copolymer so that it exhibits R-F properties [47]. To this end, a third bulky chlorine-containing monomer was added to the P(VDF-TrFE) copolymer, which reduces the interaction between the dipolar regions and leads to the formation of nano-domains – similar to the effect of irradiation [47, 48]. However, the chemical route eliminates undesirable side effects of irradiation such as cross-linking, chain

[1]Parts of this section are adapted from T. Raman Venkatesan *et al.*, "Structure-Property Relationships in Three-Phase Relaxor-Ferroelectric Terpolymers", *Ferroelectrics*, 586(1), 60-81, 2022 [24].

scission and formation of free radicals. In the past, chlorine-contaning termonomers such as chlorofluoroethylene (CFE), chlorodifluoroethylene (CDFE), chlorotrifluoroethylene (CTFE), and trifluoropropene (TFP) have been used [25]. When compared to their ferroelectric counterparts, R-F terpolymers show a slimmer hysteresis loop, a lower coercive field (E_c) and a higher saturation polarization (P_s), which leads to higher energy dissipation and lower switching voltages that may be advantageous for applications. Furthermore, the chemically modified R-F polymers show high permittivities at RT, since their Curie-transition temperatures lie within the ambient temperature range [49]. Similar to the synthesis of PVDF and its copolymers, free-radical polymerization of the monomers via bulk, suspension, solution, and emulsion methods have been used to also synthesize the terpolymers [47, 48, 50].

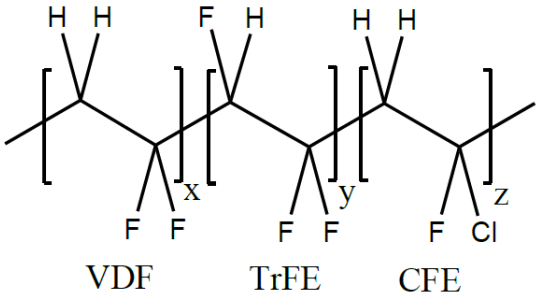

Figure 1.9: Chemical structure of P(VDF-TrFE-CFE) terpolymer.

The type of termonomer and also its relative content have an effect on the R-F properties of the resulting terpolymer. Out of all the termonomers used with P(VDF-TrFE), CFE leads to the highest electrostrictive strain of the terpolymer [51]. In addition, a lower CFE fraction is needed to convert the P(VDF-TrFE) copolymer into an R-F polymer. While only about 4 mol % of CFE is needed for achieving R-F behavior, 10 mol % is required in the case of CTFE [51]. This is probably a result of the larger size and the lower dipole moment of CTFE molecules (0.64 D) than CFE (1.8 D), which stabilizes the all-*trans* conformation to a larger extent than CFE. Consequently, a 62/38/4 mol % P(VDF-TrFE-CFE) terpolymer (Figure 1.9) shows a higher elastic modulus resulting in a higher elastic-energy density and a higher electromechanical coupling factor when compared to a 65/35/10 mol % P(VDF-TrFE-CTFE) terpolymer.

Klein *et al.* [52] varied the CFE content in the terpolymer between 0 and 9 mol % and studied its influence on the relaxor-ferroelectric and the electromechanical properties. The crystallinity of the sample decreases with increasing CFE content, and this in turn affects the electrostrictive strain response of the material. Increasing the CFE content to more than 9 mol % reduces crystallinity and Young's modulus drastically. On the other hand, decreasing the CFE fraction below ~8 mol % results in a terpolymer with a significant amount of ferroelectric regions [53]. The Curie transition of the material is also affected by the CFE content. In a previous study, it has been shown that a higher CFE content results in a lower

Curie temperature T_C. This is expected because a higher overall CFE fraction will result in a higher CFE content in the crystalline phase, further reducing the interaction between P(VDF-TrFE) segments and ultimately lowering the F-P transition temperature [49, 54].

Polymer	S_m [%]	Y [Gpa]	Energy density [J/cm^3]	k_{33}
Piezo P(VDF-TrFE) (65/35 mol %)	0.2	3.3	0.0066	0.27
HEEIP	-5.0	0.4	0.50	0.30
P(VDF-TrFE-CTFE) (58.5/31.5/10 mol %)	-4.0	0.4	0.32	0.28
P(VDF-TrFE-CFE) (59.5/36.5/4 mol %)	-4.5	1.1	1.10	0.55

Table 1.1: Comparison of the electromechanical properties of P(VDF-TrFE) and modified P(VDF-TrFE) polymers. Y is Young's modulus, S_m is the maximum strain and k_{33} is electromechanical coupling factor [51].

In the optimal case when the CFE molar content in the terpolymer is about 8.5 mol %, the material is completely relaxor-ferroelectric in nature and also shows the highest strain with little hysteresis [52]. Addition of CTFE, however, does not affect the crystallinity of the sample much, and the result is similar to that of cross-linking in irradiated P(VDF-TrFE) copolymers where the CTFE units serve as defects that limit the extent of crystallization and result in thinner crystalline lamellae [55, 56]. In comparison with CFE, a higher mol % of CTFE is required to achieve comparable electromechanical properties in the terpolymer [51]. Table 1.1 lists the electromechanical properties of both P(VDF-TrFE) and modified P(VDF-TrFE) copolymers. From the table, we can observe that the terpolymer with a relatively low fraction of CFE shows higher strain than the terpolymer with a higher fraction of CTFE.

2

Motivation

As mentioned in the Introduction (Section 1.2), the semi-crystalline nature of PVDF-based homo-, co- and ter-polymers presents itself with at least three different phases that influence its mechanical and related electro-active properties. This includes the ordered crystalline phase, disordered amorphous phase and the interphase between these two phases. The preparation and processing conditions affect all these phases and determine the macroscopic behavior. This is relevant from an application point of view as it serves as a tool to control the ferroelectric/relaxor-ferroelectric properties of PVDF-based polymers.

Though it has been about 50 years since the discovery of piezoelectricity in PVDF [11], the underlying mechanisms responsible for the electro-active properties are still not completely understood and continue to arouse the curiosity of researchers. At the same time, active research is being performed to develop new materials, to improve the existing properties and to propose novel applications of this interesting class of polymers. A detailed structure-property study will help us to have a better understanding of the fundamental ferroelectric/relaxor-ferroelectric mechanisms and to tailor the end properties according to the required application. With this aim and motivation, this study was dedicated towards modifying the structure (three electro-active phases) of different PVDF-based polymers by using chemical, thermal and mechanical treatments and studying their impact on the dielectric and morphological properties. Particular attention was dedicated towards finding the origin(s) of the mid-temperature transition observed in all PVDF-based polymers, which has remained elusive until now.

3

Experimental and Characterization Methods

3.1 Infrared Spectroscopy

3.1.1 Introduction

InfraRed (IR) spectroscopy is one of the first logical steps in identifying organic compounds and especially polymers. It is a powerful tool used for identifying the types of chemical bonds in organic and inorganic molecules by producing an infrared spectrum that is like a molecular 'fingerprint' of the material. The resulting spectral scan (absorbance or transmittance) is usually specific to a general class of material. It can be utilized to identify the components of an unknown mixture by comparing spectral scans of known materials. It can be applied to the analysis of solids, liquids and gases.

3.1.2 Working Principle

Molecular bonds vibrate at different frequencies depending on the elements and the type of bonds, *i.e.*, for any given bond there are several specific frequencies at which it can vibrate. According to quantum mechanics, these frequencies correspond to the ground state and several excited states. One way to increase the frequency of molecular vibration is to excite the bond by allowing it to absorb light energy. IR radiations ranging from 4000 to 400 cm^{-1} cause bending and stretching of organic bonds, giving rise to close packed absorption bands known as IR absorption spectrum [57].

3.1.3 Fourier Transform InfraRed (FTIR) Spectrometer

FTIR spectrometer is the commonly used form of IR spectroscopy. A FTIR spectrometer generally consists of an IR source, an interferometer and a detector. The interferometer used in most FTIR spectrometers are based on the two-beam interferometer originally designed by Michelson. A simplified schematic diagram of the FTIR setup is shown in Figure 3.1. Infrared energy is emitted from a glowing black body

source. The interferometer consists of a moving mirror, a fixed mirror and a beam splitter. Radiation from the infrared source is collimated by a mirror and the resultant beam is divided at the beam splitter; half the beam passes to a fixed mirror, and half is reflected to the moving mirror. After reflection, the two beams recombine at the beam splitter and for any particular wavelength, constructively or destructively interfere. A part of this interfered beam is transmitted to the sample. The sample transmits or reflects this beam which is then read by the detector [58].

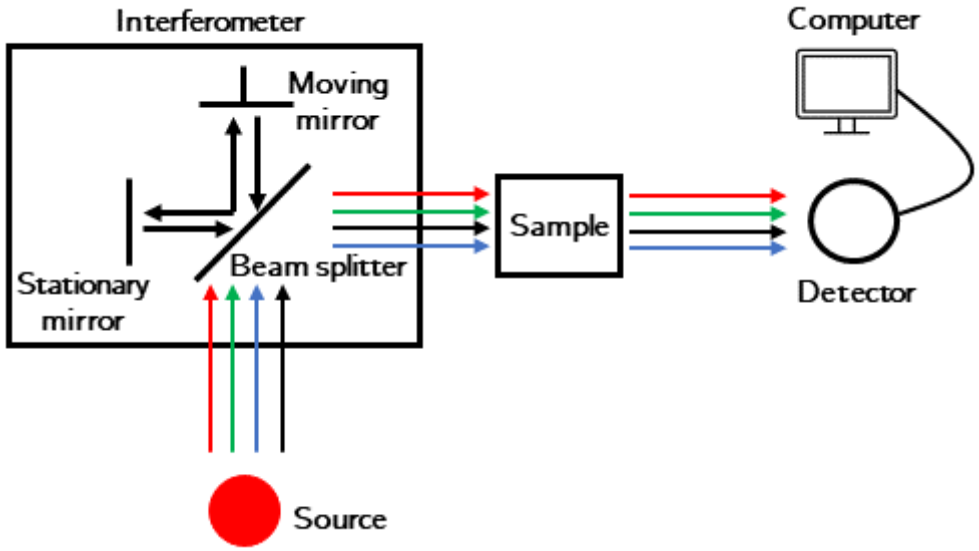

Figure 3.1: Schematic diagram of a typical FTIR setup. Redrawn from [59].

The detector receives information about each single wavelength in the measured IR range. In order to convert it to a single continuous spectrum, a Fourier transformation is performed on the interferogram by the software. A background measurement without the sample is measured and the ratio of the sample beam to the background single beam gives the transmittance of the sample. The negative $\log_{10}$ of the transmittance gives the absorbance of the spectrum.

FTIR spectroscopy is mostly used for qualitative and quantitative estimation of functional groups, degree and kinetics of polymerization, type of microstructure of different polymers, identification of tacticity, among other uses. It has also been widely used these days to detect the various crystalline phases in polymer because of its high sensitivity.

3.1.4 Attenuated Total Reflection (ATR) mode FTIR

FTIR spectroscopy has been increasingly performed in ATR mode as it offers the possibility to measure a sample directly in its solid, liquid form without any complex sample preparation. In ATR mode, the sample is placed on top of a transparent crystal with a high refractive index. The IR beam is transmitted into

the crystal at a typical angle of 45 ° relative to the surface of the crystal and is totally internally reflected at the crystal-sample interface rather than the boundary of the crystal as shown in Figure 3.2. Due to the wave property of the IR beam, instead of being reflected on the boundary of the crystal, it is reflected on the virtual layer of the sample as it has a lower refractive index than the crystal (inset in Figure 3.2). This layer is about 0.5-3 µm from the crystal and the fraction of wave which enters the sample is referred to as the evanescent wave. The evanescent wave is attenuated at the regions where the sample absorbs the energy and the remaining wave after several internal reflections exits the ATR crystal and reaches the detector [60].

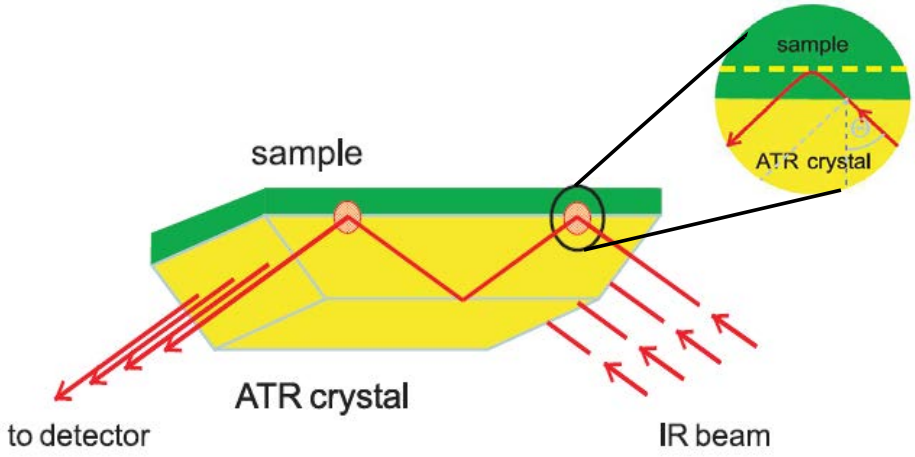

Figure 3.2: Principle of ATR. Adapted from [60].

3.1.5 Measurement

In this current work, a Bruker Alpha-P® FTIR spectrometer operated in ATR mode at room temperature was used to study qualitatively and quantitatively the crystalline phases present in the sample polymer films. Prior to the measurement, a blank background measurement was made without the sample. A small portion of the sample film was then placed on top of the crystal and a uniform static pressure was applied on it, before the measurement was carried out.

3.2 X-Ray Diffraction (XRD)

3.2.1 Introduction

The study of arrangement of polymer molecules into crystalline regions forms the basic objective of using X-ray diffraction with polymers. The subject is based on the system of ideal crystals and the physical aspect of X-rays, and the way they interact with matter to the nature of crystallization of a polymer and polymer morphology. It is primarily used to determine the degree of crystallinity in polymers. Apart

from that, it can be also used to identify polymers, calculate the lamellar thickness of the crystalline phase. Depending on the angular regions of diffracted rays, XRD can be categorized into two: Wide Angle X-Ray Diffraction (WAXD) covers a broad range of Bragg's angle 2θ from 2° up to 60° and is the commonly used type. Small Angle X-ray Diffraction (SAXD) experiments are carried out from a few seconds of arc up to a few degrees. SAXD is particularly used to analyze information from nano size polymer crystallites as their scattering is intense at smaller angles.

3.2.2 Working Principle

A crystalline solid material consists of regularly spaced atoms (electrons), which could be described by a set of imaginary planes. The distance between these planes is called the d-spacing. When the wavelength of the incoming X-rays is comparable to the d-spacing in the crystalline planes, they constructively interfere. This results in the diffraction of the X-rays as shown in Figure 3.3. This can be described by Bragg's law which forms the basis of XRD measurements (Equation 3.1).

$$n\lambda = 2d\sin\theta, \tag{3.1}$$

where n is the order of refraction, λ is the wavelength of X-ray, d is the distance between crystalline planes, and θ is half of the scattering angle measured from the incident beam.

The diffraction pattern depends upon the internal structure, phase composition, texture of the sample. Every crystalline solid has a unique pattern of d-spacing which is a 'finger print' of that solid. As a result, solids with the same chemical composition, but different phases can be identified by their XRD pattern [57].

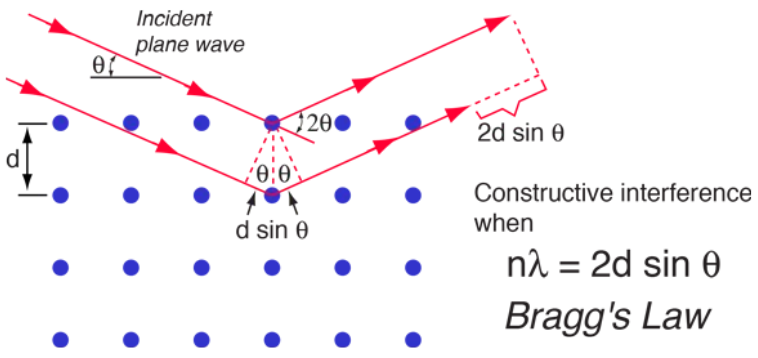

Figure 3.3: Working principle of XRD using Bragg's law [61].

3.2.3 Experimental Setup

A typical X-ray setup is composed of three major components: the X-ray source (X-ray tube, rotating anode, synchrotron radiation), the monochromator (monocrystal, curved mirrors, monochromator) and the detector (scintillator, CCD camera, curved detector, image plate) as depicted in Figure 3.4. X-rays are generated by the impact of fast moving electrons on a metal target in vacuum tubes. Copper target producing an X-ray of wavelength 1.54 Å in conjunction with nickel filter to eliminate β-radiation is ideal for polymer diffraction work. The generated X-rays are directed towards the sample which lies in the center of a goniometer circle, rotating with an angular velocity of 2ω. Simultaneously, the detector rotates also at a velocity of 2ω which makes it possible to measure the sample at various angles. The diffracted rays are recorded either photographically or by X-ray sensitive contours in conjunction with a computer. In the latter case, the recorded intensity is plotted as a function of 2θ.

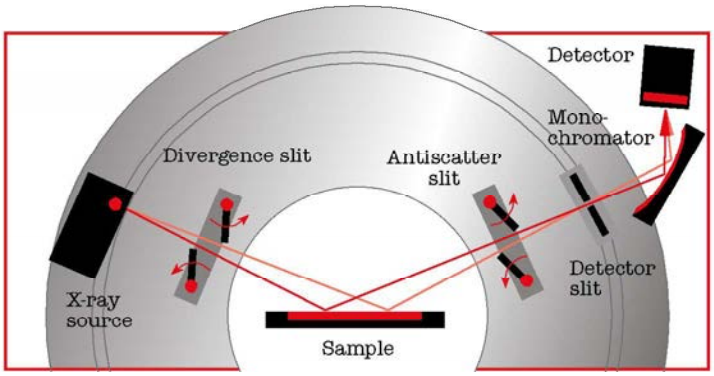

Figure 3.4: Simplified schematic diagram of a typical XRD setup in reflection mode [62].

In principle, there are two modes in which the XRD can be done. The first is the reflection mode where the incident X-ray is spread all over the sample surface with various incident angles in the vicinity of θ. Defocusing effect is observed in reflection mode as the diffracted beam at lower 2θ angle is narrower than that at higher 2θ (Figure 3.4). The second is the transmission mode in which the incident beam is perpendicular to the sample surface as displayed in Figure 3.5. No defocusing effect is observed in the case of transmission mode [62].

3.2.4 Measurement

In this work, Wide angle X-ray diffraction (WAXD) measurements on a PANalytical Empyrean® powder X-ray diffractometer were performed at room temperature in transmission mode operating at 40 kV and

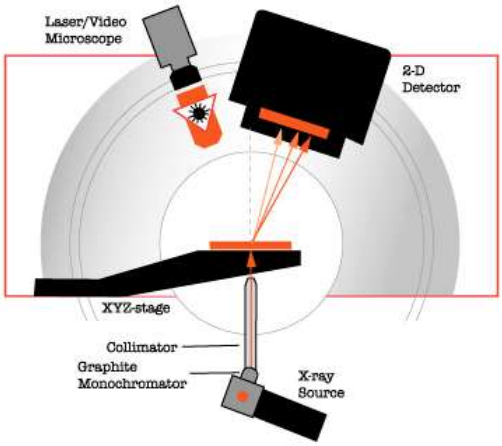

Figure 3.5: Simplified schematic diagram of a typical XRD setup in transmission mode [62].

40 mA. The instrument was configured with a focusing X-ray mirror for Copper radiation (λ= 1.5419 Å) and a PIXcel$^{1D®}$ detector. θ-θ scans were run during 72 minutes over a 2θ range of 2-70 $^\circ$ with a step size of 0.0131 $^\circ$ and a sample rotation time of 1 s. The free-standing polymer films were placed between two polyimide films (Kapton®).

3.3 Differential Scanning Calorimetry (DSC)

3.3.1 Introduction

Differential Scanning Calorimetry (DSC) is a thermo-analytical technique which can be used to characterize the physical properties of a polymer by measuring the amount of heat required to increase the temperature of a sample and a reference as a function of temperature. Typical applications of this technique include determination of melting, crystallization temperatures, and the corresponding changes associated with enthalpy and entropy. It can be also used to measure the glass-transition temperature, curing and phase transitions which show either changes in heat capacity or latent heat. Commonly, there exist two variants of DSC. The first is the 'Heat flux DSC', where the sample and the reference are heated by the same heat source. The temperature difference ΔT between them is measured and is converted to a power difference ΔP ($\Delta P = \Delta Q/\mathrm{d}t$). In the second type called as the 'Power compensated DSC', the sample and reference are heated separately by different heat sources. The temperature difference between them is maintained closely to zero and the difference in power ΔP required to maintain both the sample and reference at the same temperature is measured. Both the Heat flux DSC and Power compensated DSC give similar thermograms.

3.3.2 Modulated DSC

Modulated DSC (mDSC) is an extension of the standard DSC in which a sinusoidal temperature oscillation is overlaid on the conventional linear temperature heating ramp as shown in Figure 3.6. In this case, the actual heating rate depends on the underlying overall heating rate, amplitude and frequency of modulation. The temperature modulation makes it possible to separate complex transitions as a result of which mDSC has a higher resolution than standard DSC.

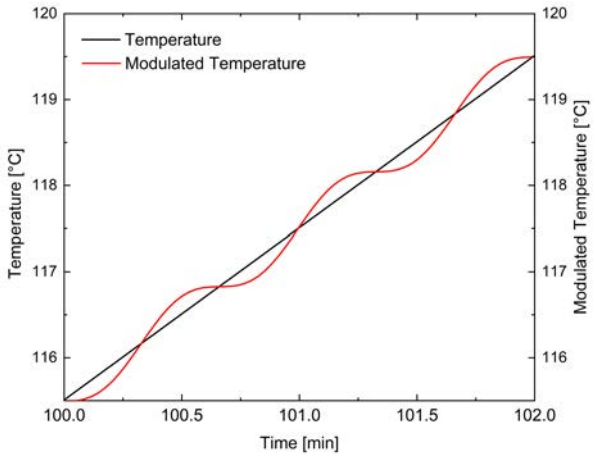

Figure 3.6: Temporal plot of the linear and modulated heating rates used in a typical mDSC measurement.

3.3.3 Measurement Principle

The heat flow measured in DSC has the following contributions:

$$\frac{\mathrm{d}q}{\mathrm{d}t} = C_\mathrm{p}\frac{\mathrm{d}T}{\mathrm{d}t} + f(t,T), \tag{3.2}$$

where $\mathrm{d}q/\mathrm{d}t$ is the heat flow, C_p is the sample heat capacity, $\mathrm{d}T/\mathrm{d}t$ is the heating rate and f(t,T) is a function of time and temperature. The C_p depending on the heating rate represents the reversible contribution to heat flow and is influenced by the thermodynamical changes occurring in the sample. The other component which is a function of time and temperature is referred to as non-reversible heat flow and does not depend on the modulated heating rate.

In conventional DSC, only the total heat flow is measured and it is not possible to separate the individual contributions. Using mDSC, it is possible to deconvolute the measured signal into reversible and non-reversible contributions to the total heat flow. Discrete Fourier Transform (DFT) of the measured signal is performed to separate the signal into the average or total heat flow and amplitude. This is done by the mDSC software, which continuously measures the amplitudes of the sample temperature and raw

heat flow signals by comparing the data to a reference sine wave of the same frequency. From these amplitudes the heat capacity of the sample is calculated using the following relation:

$$C_{\mathrm{p}} = K_{C_p} \times \frac{q_{\mathrm{amp}}}{T_{\mathrm{amp}}} \times \frac{Period}{2\pi}, \tag{3.3}$$

where K_{C_p} is the heat capacity calibration constant, q_{amp} is the heat flow amplitude, T_{amp} is the temperature amplitude and Period is the modulation time period. The calculated C_{p} is then multiplied by the negative of the average heating rate to obtain the reversible heat flow contribution. Multiplying by the negative of the average heating rate results in the inversion of the heat flow signal so that the endothermic processes result in valleys and exothermic processes result in peaks. Finally, the non-reversible heat flow is calculated by subtracting the reversible heat flow from the total heat flow [63].

3.3.4 Thermal Transitions in Polymers

A semi-crystalline polymer during heating can undergo the following transitions as seen in Figure 3.7:

1. **Glass-transition temperature:** The temperature below which the polymer is hard and brittle, and above which it is soft and flexible is known as the glass-transition temperature (T_{g}). It is a second-order transition meaning that the transition involves a change in heat capacity but does not involve a latent heat. It occurs over a temperature range and it is determined by the mid-point of the inclined region in the graph where the heat capacity steadily increases.

2. **Melting and Crystallization temperature:** Above T_{g}, the polymer chains start to absorb more energy and start to move more freely. As the temperature increases, slowly the ordered arrangement in the polymer is lost and the polymer starts to melt. It is an endothermic process and the temperature remains constant despite constant heating. This is due to the excess heat added to the chains during the melting process and this heat is the latent heat of melting. The temperature at which this occurs is known as the melting temperature T_{m}.

   During cooling of the polymer from the melt condition, at a certain temperature range they begin to arrange again into ordered chains. This process is known as crystallization and the temperature at which this occurs is known as the crystallization temperature (T_{c}). This process observed during cooling corresponds to the melting transition seen in the heating step. It is an exothermic reaction and occurs only in semi-crystalline polymers which have a certain degree of crystallinity. Unlike T_{g}, the crystallization transition undergoes a change in heat capacity and also gives latent heat. Hence, it is a first-order transition.

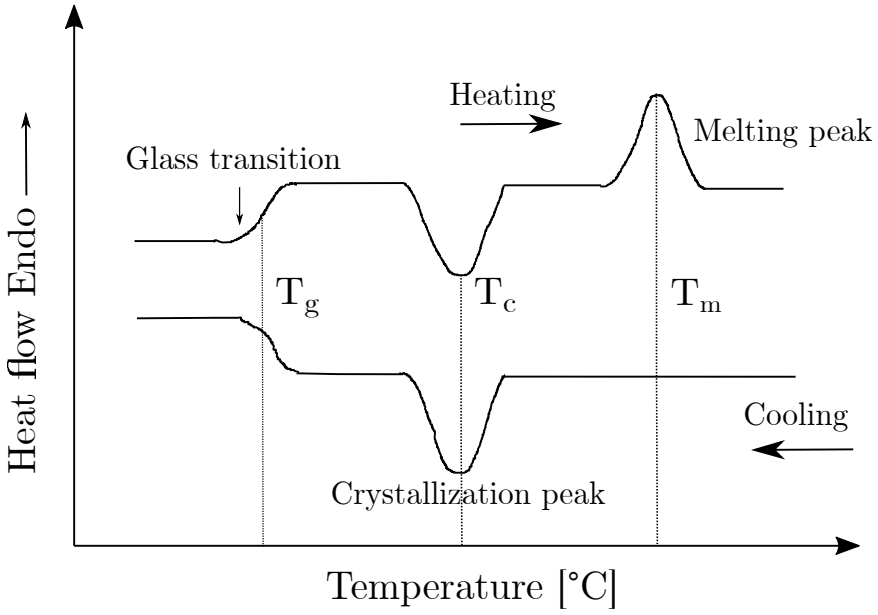

Figure 3.7: A typical DSC plot of a semi-crystalline polymer.

3.3.5 Comparison between DSC and mDSC

Both conventional DSC and mDSC could be used to identify various transitions, latent heats of phase transitions as well as heat capacity of the sample being measured. However, conventional DSC suffers from certain limitations. Since DSC measures only the sum of all thermal events that occur at a certain temperature, it is difficult to separate and analyze complex transitions. For example, enthalpic relaxation – an endothermic process – normally occurs with the glass transition and its magnitude depends on the thermal history of the sample. In certain cases, it can cause the glass transition to resemble a melting peak instead of a step in the measured heat flow of DSC. Similarly, the process of melting and crystallization can both occur simultaneously in some polymers. This would make it impossible to determine the crystallinity of the sample using conventional DSC. However, as in mDSC the reversible and non-reversible heat flow are separated, the complex transitions can be individually identified. Thermal processes such as the enthalpy relaxation associated with T_g and secondary crystallization can be clearly observed in the non-reversible heat flow contribution [64, 65].

Another constraint with conventional DSC is its ability to detect weak transitions. This depends both on the short-term noise (seconds) in the heat flow signal and long term (minutes) variation of the shape of the baseline. While the short-term noise can be removed by signal averaging, the long-term noises are difficult to be eliminated as they depend on a number of factors such as the changes occurring in the properties of the different materials used in the construction of the measurement cell and properties of the purge gas with temperature. mDSC avoids this problem as a result of using the ratio of two signals

(Equation 3.3) instead of relying on the absolute heat flow signal measured.

In order to have a better resolution (ability to distinguish multiple transitions occurring in the same temperature range), smaller samples and higher heating rates are required. However, this reduces the strength of the measured signal in DSC, thereby reducing the sensitivity of the measurements. mDSC has an upper hand because of the two different heating rates used. While the resolution of the measurement can be improved by decreasing the average heating rate, the sensitivity can be increased by using a higher instantaneous heating rate (modulated heating rate). Hence, mDSC offers additional advantages when compared to conventional DSC measurements.

3.3.6 Experimental Setup

The Heat flux DSC equipment consists of a heating chamber with two pans, one which consists of the polymer sample and the other, the reference pan as depicted in Figure 3.8. Both pans are heated to the same temperature and the difference in heat supplied is measured using a computer connected to the DSC equipment. The computer is also used to specify the heating rate and other parameters during the experiment. The measurement chamber is closed and purged with nitrogen gas to maintain inert atmosphere. The plot of the difference in heat flow versus temperature is plotted directly on the computer.

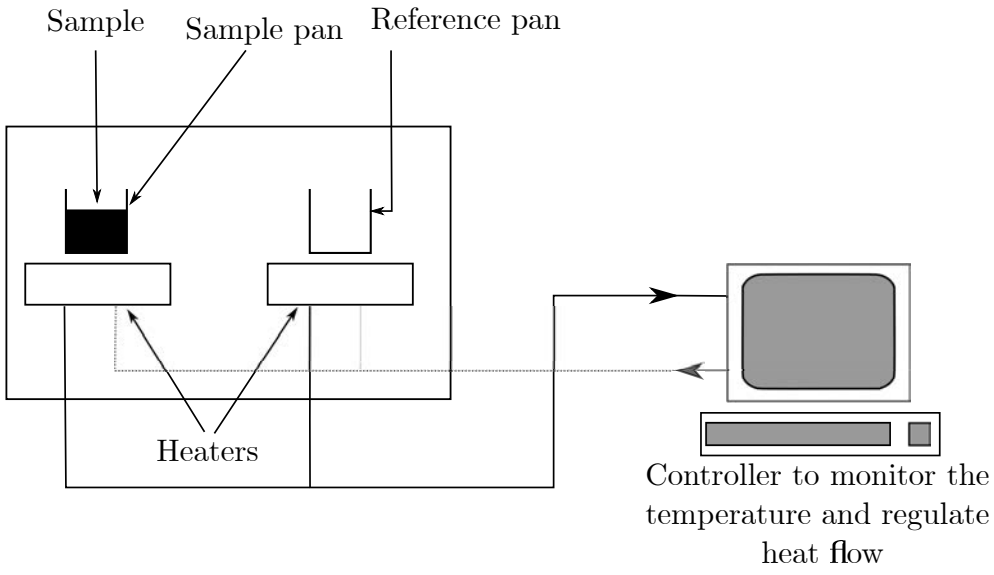

Figure 3.8: Simple sketch of a Heat flux DSC setup.

3.3.7 Measurement

The DSC measurements were performed using a Netzsch DSC 214 Polyma® calorimeter. Approximately, 1-5 mg of the sample was placed inside the aluminum sample pan and it was heated and cooled at

a fixed heating rate, usually at 10 K/min. Modulated DSC measurements were performed using a Q2000 DSC® from TA Instruments (U.K.) using 3-4 mg of sample. A linear heating rate of 2.5 K/min with a modulation amplitude of ±0.21 K for every 40 s was used. Proteus® 7.0 and Universal analysis software 5.5 were used to analyze the DSC and mDSC curves, respectively.

3.4 Dielectric Relaxation Spectroscopy (DRS)

3.4.1 Introduction

Dielectric spectroscopy (DRS) is an important tool to investigate the electric characteristics of dielectric (non-conducting) and semi-conducting materials with respect to their chemical structure. Polymer materials which are dielectric or semi-conducting in nature are ideal candidates to be inspected by DRS technique.

3.4.2 Basic Concepts of Dielectric Relaxation

An ideal dielectric material has zero DC conductivity and when an external field is applied to it, both the positive and negative charged particles of an atom are displaced (positive particles are pushed in the direction of the field and negative charges move in the opposite direction) from their equilibrium positions. This produces an electric dipole in the material and this process is referred to as polarization.

The polarization vector ($\vec{P}$) is defined as the dipole moment ($\vec{\mu}$) per unit volume (unit C/m^2):

$$\vec{P} = \frac{\mathrm{d}\vec{\mu}}{\mathrm{d}V}, \tag{3.4}$$

$\vec{\mu}$ (unit C.m) is defined as

$$\vec{\mu} = \sum_{i=1}^{N} q_{\mathrm{i}}\vec{r_{\mathrm{i}}}, \tag{3.5}$$

where q_i is the charge and $\vec{r_i}$ is the coordinate of the charge, and N is the total number of charges. The induced dipole moments create an internal field, which lowers the applied external field. The resulting mean internal field $\vec{E}$ is called the macroscopic electric field.

At small electric fields the polarization is directly proportional to $\vec{E}$:

$$\vec{P} = \varepsilon_0 \chi \vec{E}. \tag{3.6}$$

where ε_0 is the permittivity of free space (8.854×10^{-12} Fm^{-1}) and χ is the electric susceptibiliy of the material which explains how easily the material can be polarized. The polarization saturates at high electric fields.

There are various types of polarization which includes electronic polarization (displacement of positive and negative charges in an atom), atomic polarization (displacement of positive and negative

ions), orientational polarization (orientation of permanent dipoles in the material in the direction of applied electric field) and space-charge polarization (displacement of real charges inside the dielectric sample, sometimes referred to as ionic polarization). The space-charges can be present at an interface leading to interfacial polarization [66].

In an alternating electric field, the movement of the charged masses are governed by two physical mechanisms; resonance and relaxation. Figure 3.9 displays the frequency response of the various dielectric polarization processes that take place in a dielectric material under an alternating field. Displacement polarizations (electric and atomic polarizations) resonate with resonant frequencies of 10^{15} to 10^{14} Hz for the electronic and of 10^{13} to 10^{12} Hz for the atomic polarization. Hence, electronic polarization is the fastest process and occurs in the optical frequency region and governs the absorption of material in the UV-visible range. On the other hand, atomic polarization is comparatively a slower process and governs the vibration of atomic bonds in the infrared region. However, orientational polarization is a non-resonant process. This leads to a retarded response of the dipoles when an electric field is applied. This process is referred to as *dielectric relaxation*. The characteristic time constant of such a relaxation process required to attain the new equilibrium after changing the exciting field is called the *relaxation time* (τ). As this is closely related to the viscosity of the material, it is strongly dependent on temperature. In polymers, depending on the temperature, the relaxation times can be from few seconds to several hours [67].

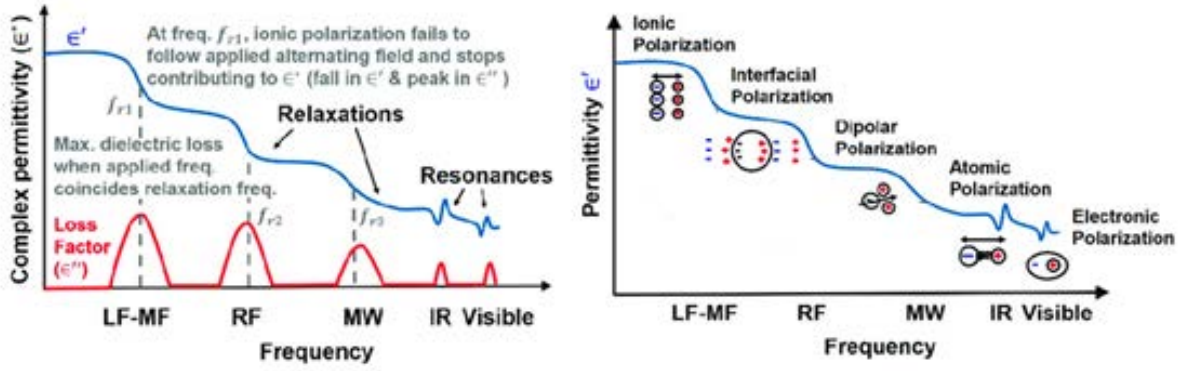

Figure 3.9: Frequency response of the various dielectric polarization mechanisms under an alternating field. Reprinted from the work of Mehrotra *et al.* [68] under Open Access Creative Commons Attribution 4.0.

3.4.2.1 Linear Response Theory for Dielectric Relaxation

The dielectric relaxation theory for small electric fields is a special case of linear response theory [69, 70]. By this approach the time dependent response *y(t)* of a system following a disturbance *x(t)* can be described using a linear equation. In dielectrics, the disturbance is the time dependent external electric field $x(t) = \vec{E}(t)$ applied to the system and the response is the polarization $y(t) = \vec{P}(t)$.

The applied electric field $E(t)$ results in the re-orientation of permanent dipole moments in the dielectric material along the direction of the field. This causes changes in the molecular orientation and leads to the generation of a macroscopic polarization inside the material, given by:

$$\vec{P}(t) = \vec{P_\infty} + \vec{P_{\text{or}}}, \tag{3.7}$$

P_∞ and P_{or} refers to the contribution from displacement polarization and orientational polarization, respectively. Since the orientational polarization is influenced by the thermal fluctuations, its corresponding dipole moment μ is expressed as a time averaged value. Hence,

$$\vec{P}(t) = \vec{P_\infty} + \frac{1}{V}\Sigma\vec{\mu_{\text{i}}} = \vec{P_\infty} + \frac{N}{V}\langle\vec{\mu}\rangle. \tag{3.8}$$

where N/V is the number of dipoles per unit volume. Due to the process of polarization, image charges Q are induced on the metal electrodes in addition to the displacement charges which are present in vacuum. The total charge per unit area deposited on the electrodes is called the electric displacement $\vec{D}$ and using macroscopic Maxwell approach, which describes the interaction of matter with electromagnetic fields, it can be expressed by:

$$\vec{D} = \varepsilon_0\vec{E}(t) + \vec{P}(t). \tag{3.9}$$

$\vec{D}$ can be also expressed as a function of $\vec{E}$ (for small electric fields) using the complex time-dependent permittivity $\varepsilon^*(t)$ of the material by:

$$\vec{D} = \varepsilon_0\varepsilon^*(t)\vec{E}(t). \tag{3.10}$$

Combining Equations 3.9 and 3.10 we have,

$$\vec{P}(t) = \varepsilon_0(\varepsilon^*(t) - 1)\vec{E}(t) = \varepsilon_0\chi(t)\vec{E}(t). \tag{3.11}$$

Thus for small electric fields, the polarization is directly proportional to $\vec{E}(t)$. The polarization saturates at high electric fields. Using linear response theory [69, 70, 71] the polarization can be expressed as:

$$\vec{P}(t) = \vec{P_\infty} + \varepsilon_0\int_{-\infty}^{t}\varepsilon(t-t')\frac{\mathrm{d}\vec{E}(t')}{\mathrm{d}(t')}\,\mathrm{d}t'. \tag{3.12}$$

The above Equation 3.12 is based on linearity, according to which the response of the system to two disturbances is the sum of two single reactions and causality, and assumes that only disturbances in the past contribute to the response of time (t). In this case, $\varepsilon(t)$ can be measured directly as the time-dependent response caused by a step-like change of external electric field, *i.e.*,

$$\frac{\mathrm{d}(\vec{E}(t))}{\mathrm{d}t} = \vec{E_0}\,\delta(t);\ \varepsilon(t) = \frac{\vec{P}(t) - \vec{P}_\infty}{\vec{E_0}\varepsilon_0}. \tag{3.13}$$

In the case a stationary periodic disturbance $\vec{E}(t,\omega) = \vec{E_0}\,exp(-i\omega t)$ is applied to the system with angular frequency $\omega = 2\pi\upsilon$, Equation 3.12 is transformed to

$$\vec{P}(t,\omega) = \varepsilon_0(\varepsilon^*(\omega) - 1)\,\vec{E}(t,\omega) \text{ with } \varepsilon^*(\omega) = \varepsilon'(\omega) - i\varepsilon''(\omega), \tag{3.14}$$

where $\varepsilon'(\omega)$ is proportional to the amount of reversible energy stored per period (commonly referred to as dielectric permittivity) and $\varepsilon''(\omega)$ is proportional to the amount of energy dissipated as heat per period (commonly referred to as dielectric loss). $\varepsilon^*(\omega)$ is related to the time-dependent dielectric function $\varepsilon(t)$ by

$$\varepsilon^*(\omega) = \varepsilon_\infty - \int_0^\infty \frac{\mathrm{d}(\varepsilon(t))}{\mathrm{d}t} \exp(-i\omega t)\,\mathrm{d}t. \tag{3.15}$$

Equation 3.15 is a one-sided Fourier or full imaginary Laplace transformation [71]. Therefore, $\varepsilon^*(\omega)$ can be transformed to both the time dependent dielectric function $\varepsilon(t)$ and the dielectric relaxation time distribution $\mathrm{L}(\tau)$. This infers that both the real and imaginary contributions to $\varepsilon^*(\omega)$ are related according to Kramers-Kronig [69, 70, 71]. Hence, by analyzing one contribution the other can determined;

$$\varepsilon'(\omega) = \varepsilon_\infty + 2/\pi \int_0^\infty \varepsilon''(\omega)\left(\frac{\omega}{\omega^2 - \omega_0^2}\right)\mathrm{d}\omega, \tag{3.16}$$

$$\varepsilon''(\omega) = \frac{\sigma}{\varepsilon_0\omega_0} + 2/\pi \int_0^\infty \varepsilon'(\omega)\left(\frac{\omega_0}{\omega^2 - \omega_0^2}\right)\mathrm{d}\omega. \tag{3.17}$$

σ is the electrical conductivity and the term $\sigma/\varepsilon_0\omega_0$ describes the possible contribution from ionic conductivity.

3.4.3 Analyzing Dielectric Relaxation Spectra

In order to characterize and analyze the various dielectric relaxations in materials, different features and parameters such as the shape of the loss peak, frequency at maximum loss and dielectric strength are used. The dielectric strength is expressed as $\Delta\varepsilon = \varepsilon_s - \varepsilon_\infty$, where ε_s and ε_∞ refer to the static (low frequency limit), and infinite (unrelaxed) permittivity (high frequency limit), respectively. From the above, the relaxation time (τ) and its distribution for the individual processes can be estimated. Different model functions have been proposed to analyze the dielectric relaxation spectra and calculate the characteristic relaxation parameters. They can be divided into Debye and non-Debye relaxation models.

3.4.3.1 Debye Relaxation

The Debye model is the most simplified model used to analyze a dielectric spectrum [72]. It assumes that the dipoles in the system undergo a single relaxation process and decays according to an exponential distribution function. By neglecting the effects of inertia and the interaction of neighbouring molecules, the time dependence of the polarization after a step in the applied field is assumed to be described by the following first order differential equation [70, 71, 72]:

$$\frac{dP(t)}{dt} = -\frac{1}{\tau}P(t). \tag{3.18}$$

By solving Equation 3.18, we obtain

$$P(t) = P(0)\exp\left(\frac{-t}{\tau}\right), \tag{3.19}$$

which leads to an exponential decay for the correlation function $\phi(\tau)$:

$$\phi(\tau) = \varepsilon(t) = \exp\left(-\frac{t}{\tau}\right). \tag{3.20}$$

On further derivation using the fluctuation-dissipation theorem [70], the following complex dielectric function $\varepsilon^*(\omega)$ can be obtained:

$$\varepsilon^*(\omega) = \left(\varepsilon_\infty + \frac{\Delta\varepsilon}{1+i\omega\tau}\right). \tag{3.21}$$

The real and imaginary parts of ε can be expressed individually using Debye functions by Equations 3.22 and 3.23, respectively.

$$\varepsilon^{'}(\omega) = \varepsilon_\infty + \left(\frac{\Delta\varepsilon}{1+\omega^2\tau^2}\right), \tag{3.22}$$

$$\varepsilon^{''}(\omega) = \omega\tau\frac{\Delta\varepsilon}{1+\omega^2\tau^2}. \tag{3.23}$$

Another useful quantity is the loss or dissipation factor $\tan\delta$ given by:

$$\tan\delta = \frac{\varepsilon''}{\varepsilon'}. \tag{3.24}$$

3.4.3.2 Non-Debye Relaxation

Equation 3.23 predicts a symmetrical loss peak with a half width spanning 1.14 decades. However, in polymers the dielectric loss peaks are asymmetric with a high frequency tail and their half width is much broader than predicted by the Debye function. This is described as non-Debye relaxation behavior. Modified Debye functions have been developed to describe the non-ideal behavior such as the Cole-Cole function (Equation 3.25) which describes the broadening of the loss peak:

$$\varepsilon^*_{CC}(\omega) = \varepsilon_\infty + \frac{\Delta\varepsilon}{1+(i\omega\tau_{CC})^\beta}, \tag{3.25}$$

where $0 < \beta \leq 1$. The asymmetric broadening can be described using the Fuoss-Kirkwood or the Cole-Davidson function as mentioned in Equation 3.26:

$$\varepsilon^*_{CD}(\omega) = \varepsilon_\infty + \frac{\Delta\varepsilon}{(1+i\omega\tau_{CD})^\gamma}, \tag{3.26}$$

where $0 < \gamma \leq 1$. The real and imaginary parts of complex dielectric permittivity determined from Equations 3.21, 3.25 and 3.26 are plotted in Figure 3.10 [73].

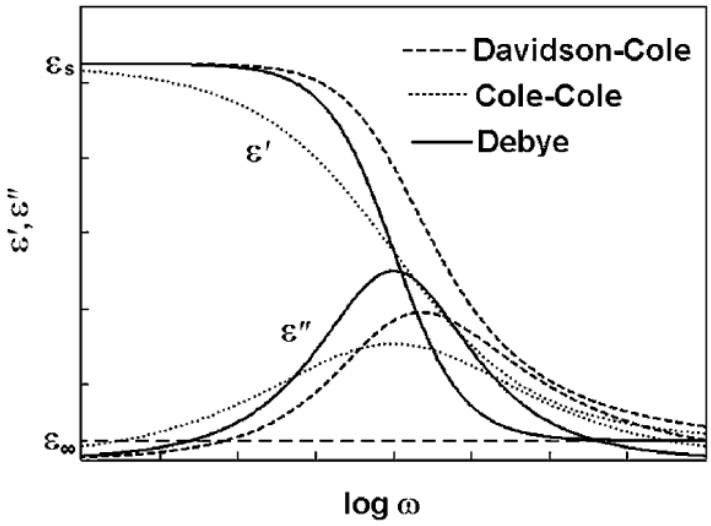

Figure 3.10: Real and imaginary parts of ε for Debye, Cole-Cole and Cole-Davidson relaxation models *vs.* logarithmic frequency. Reprinted from the work of Lukichev [73] with permission from © 2014 Elsevier.

By combining both the Cole-Cole and Cole-Davidson plot, a more general function was introduced by Havriliak and Negami (HN-function), which is described in Equation 3.27.

$$\varepsilon^*_{HN}(\omega) = \varepsilon_\infty + \frac{\Delta\varepsilon}{(1+(i\omega\tau_{CD})^\beta)^\gamma}. \tag{3.27}$$

The dielectric strength $\Delta\varepsilon$, relaxation time τ, and the shape parameters β and γ give a complete description about the dielectric relaxation processes. By performing a least square fit of the dielectric data with the HN-function one can obtain all these parameters [70].

3.4.3.3 Derivative Techniques

While analyzing the dielectric loss $\varepsilon''(\omega)$ spectra, frequently problems arise with ohmic conduction, especially above the glass-transition temperature. One approach to remove the conduction component $\varepsilon''_{\text{cond}} = \sigma/(\varepsilon_0\omega_0)$ (frequency independent) is using Equation 3.17 and transforming the permittivity ε' into an imaginary part $\varepsilon''_{\text{KK}}$ that is only based on relaxation phenomena [74]. In this case, the term $\varepsilon''_{\text{KK}}$ would lack contribution from Ohmic conduction. This can be achieved using numerical techniques described in [75, 76, 77]. Alternatively, the logarithmic derivative $\varepsilon''_{\text{der}}$ defined in Equation 3.28 can also be used [77, 78, 79, 80].

$$\varepsilon''_{\text{der}} = -\frac{\pi}{2}\frac{\partial\,\varepsilon'(\omega)}{\partial \ln\omega}\,. \tag{3.28}$$

The above equation holds for broad peaks such as those for α transition or secondary relaxations [79]. For Debye relaxations the derivative results in sharper peaks than the measured loss:

$$\frac{\partial\,\varepsilon'(\omega)}{\partial \ln\omega} = -\frac{\varepsilon''^{2}}{\varepsilon''_{\text{max}}}\,. \tag{3.29}$$

In other words, by using $\varepsilon''_{\text{der}}$ the Ohmic conduction is suppressed and the resolution of neighbouring sharp peaks is significantly improved.

A second derivative method is used to determine the temperature coefficient of permittivity α_ε given by [74, 80, 81]:

$$\frac{1}{\varepsilon'}\frac{\partial\,\varepsilon^{'}(T)}{\partial\,T} = \frac{\partial\, ln\,\varepsilon'(T)}{\partial\,T} = \alpha_\varepsilon\,. \tag{3.30}$$

By calculating the derivative $\partial\,\varepsilon^{'}(T)/\partial\,T$, loss peaks from mechanisms with a high activation energy is enhanced with respect to those with a lower activation energy. The implication is that peaks arising from relaxations of the main chain are intensified comparing to the side chain relaxations [79]. In addition, dynamic glass-transition temperature manifests as a local maximum in the $\partial\,\varepsilon^{'}(T)/\partial\,T$ *vs.* T plot, indicating the temperature at which the material deviates from time-temperature superposition (Williams-Landel-Ferry behavior). First-order transitions such as melting and crystallization processes exhibiting frequency-independent behavior also gives rise to peak maximum. However, they are not observed in $\varepsilon''_{\text{der}}$ *vs.* T plot [80, 81]. Hence, derivative analysis is very helpful to identify and distinguish the various relaxations and phase transitions occurring in polymers.

3.4.4 Dielectric Relaxation in Polymers

Dielectric spectroscopy is used to study the dipolar, structural transitions and charge-carrier relaxations in polymers. It measures the permittivity as a function of frequency or/and temperature. Polymers typically characterized by the presence of various dipolar entities in different environments lead to a broad distribution of their relaxation times. This gives rise to corresponding loss peaks extending to several frequency decades.

At low frequencies in isothermal conditions or at higher temperatures with constant frequency conditions, α relaxation occurs. As it has the highest strength, it is also referred to as the primary relaxation. This relaxation is usually associated with glass transition, due to the onset of segmental motions in the amorphous regions of the polymer. The loss peak has an asymmetrical shape and its temperature dependence obeys the Vogel-Fulcher-Tammann (VFT) law:

$$\tau(T) = \tau_0 \exp\left(\frac{T_\mathrm{a}}{T - T_\mathrm{V}}\right), \tag{3.31}$$

where τ_0 is the relaxation rate in the high temperature limit, T_a is the activation temperature, and T_V is the Vogel temperature, also referred as ideal glass-transition temperature. T_V is found approximately about 40 K below the dynamic glass-transition temperature [70]. The VFT behavior and the assymetrical loss peak are typical features of a co-operative process. Dynamic glass-transition temperature is defined as the temperature at which the relaxation time reaches 100 s [82]. The β relaxation occurs at higher frequencies or at lower temperatures compared to α relaxation, involving local intra-molecular movements such as rotation of side groups and other such motions. This is usually followed by the γ relaxation, which involves the motion of even smaller molecular units. These are referred as secondary relaxations. Molecular impurities if present in the polymer, give rise to a δ relaxation. All these loss peaks are symmetric in the frequency domain and follows an Arrhenius-type temperature dependence:

$$\tau(T) = \tau_0 \exp\left(\frac{E_\mathrm{a}}{\mathrm{k_B} T}\right), \tag{3.32}$$

where E_a is the activation energy, $\mathrm{k_B}$ is the Boltzmann's constant. These are typical behaviors of a non-cooperative process. Apart from this, in semi-crystalline polymers additional relaxations can originate from partial mobilization of polymer chains in amorphous regions embedded within crystalline regions and from secondary ordering/reordering crystallization processes (referred as α_c relaxation).

3.4.5 Experimental Setup

A schematic of the experimental setup is shown in Figure 3.11. The sample is mounted onto a sample holder which is directly connected to the input terminals of the impedance analyzer. The sample holder is

then placed inside a temperature controlled chamber (cryosat) which belongs to the QUATRO® cryosystem. The sample is heated or cooled inside the cryosat using dry nitrogen gas. Both the controller of the impedance analyzer and the cryosystem are connected to a computer.

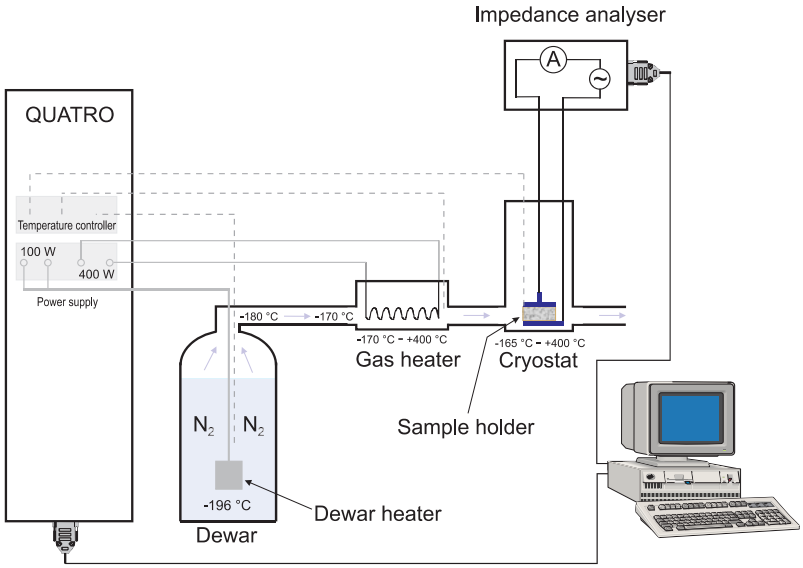

Figure 3.11: Experimental setup used for DRS measurement [67].

A simplified sketch of the measuring circuit is shown in Figure 3.12. A potential V_1 is supplied by the voltage generator at the high end terminal of the sample. The zero-voltage detector detects a potential at the low terminal and in turn changes the magnitude and phase of the output potential V_2 of the variable amplitude-phase generator until the current I_2 (generated through the range-resistor) balances the sample current I_1, and the voltage detected by the detector becomes zero. Under this condition we have:

$$I_1 = -I_2, \tag{3.33}$$

$$I_1 = \frac{V_1}{Z}; I_2 = \frac{V_2}{R}, \tag{3.34}$$

where Z is the impedance of the sample and R is the resistance of the range-resistor. From Equations 3.33 and 3.34, we get:

$$Z = -\frac{V_1}{V_2}R. \tag{3.35}$$

This balancing operation is automatically performed over the full frequency range. As the impedance of the sample is directly measured by the impedance analyzer, dielectric spectroscopy is also known as

impedance spectroscopy. Using the impedance, we can determine the capacitance and the permittivity of the sample using the following equation:

$$\frac{1}{Z_(\omega)} = i\omega C(\omega), \tag{3.36}$$

where ω is the angular frequency.

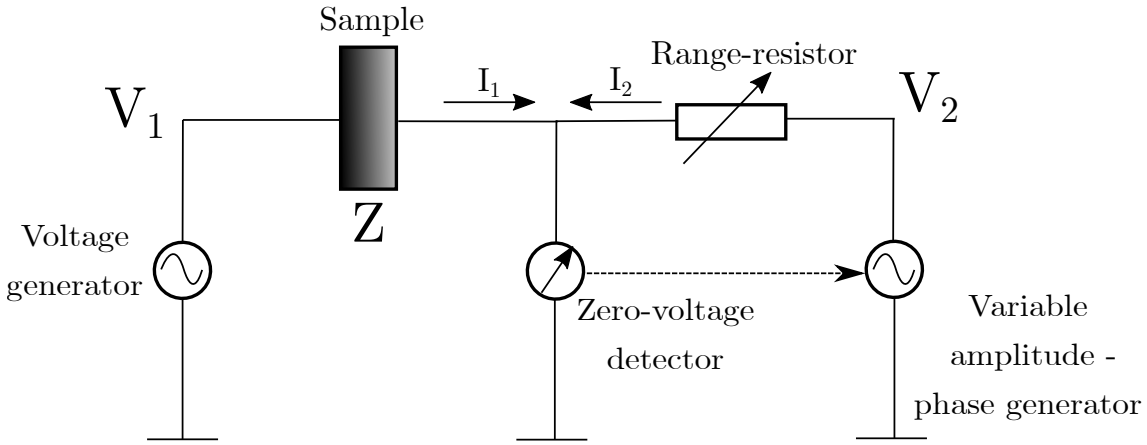

Figure 3.12: Simplified measuring circuit used in DRS measurement.

3.4.6 Measurement

The DRS measurements were carried out under dry nitrogen atmosphere by use of the Novocontrol Quatro® cryosystem together with the Novocontrol Alpha dielectric analyzer®. Free-standing films metalized on both sides with aluminum electrodes were used for the measurements.

3.4.7 Dielectric Non-linearity[1]

Landau theory provides a phenomenological description of ferroelectric materials [84], according to which the ferroelectric contribution to free energy (F) can be expressed in terms of even powers of the dielectric displacement (D) for electric field $E = 0$ as follows [85]:

$$F = F_0 + \frac{1}{2}\alpha D^2 + \frac{1}{4}\gamma D^4 + \frac{1}{6}\delta D^6, \tag{3.37}$$

where α, γ and δ are known as Landau parameters. The Landau parameters depend in general on temperature T. In simple cases, the ferroelectric transitions can be described by the Devonshire theory

[1]This section is adapted from T. Raman Venkatesan *et al.*, "Non-Linear Dielectric Spectroscopy for Detecting and Evaluating Structure-Property Relations in a P(VDF-TrFE-CFE) Relaxor-Ferroelectric Terpolymer", *Appl. Phys. A*, 127: 756 (10 pages), 2021. [83]

in which α is assumed to be proportional to temperature $\alpha = \beta(T - T_0)$, while β, γ and δ are constant. With an electric field applied the free energy becomes [86]

$$F = F_0 + \frac{1}{2}\alpha D^2 + \frac{1}{4}\gamma D^4 + \frac{1}{6}\delta D^6 - ED. \tag{3.38}$$

As the Landau parameters depend on temperature, the free energy is a function of both D and temperature (T). The electric field (E) as a function of D is then obtained from the partial derivative of F with respect to D:

$$E = \frac{\partial F(D,T)}{\partial D} = \alpha D + \gamma D^3 + \delta D^5. \tag{3.39}$$

D can be expressed by a power series representation of the electric displacement in terms of E with $D = P_s$ (spontaneous polarization) at $E = 0$;

$$D = P_s + \varepsilon_0\varepsilon_1 E + \varepsilon_0\varepsilon_2 E^2 + \varepsilon_0\varepsilon_3 E^3 + ... \tag{3.40}$$

Thus the odd- and even-order permittivities, and in particular ε_1, ε_2 and ε_3, can be calculated from the coefficients of the series expansion of D as a function of E in Equation 3.40 [87]. As seen in the equation, ε_2 and ε_3 describe non-linear contributions of the electric field to the displacement. They are referred to as first- and second-order non-linear permittivities.

In the paraelectric phase, the spontaneous polarization disappears (P_s = 0), and the nonlinear permittivities ε_1, ε_2 and ε_3 may be calculated from the Landau parameters [85] as follows:

$$\varepsilon_0\varepsilon_1 = 1/\alpha, \;\; \varepsilon_0\varepsilon_2 = 0, \;\; \text{and} \;\; \varepsilon_0\varepsilon_3 = -\gamma/\alpha^4. \tag{3.41}$$

3.4.7.1 Order of Phase Transition

As explained in Section 1.2, ferroelectric and relaxor-ferroelectric materials undergo a transition from the polar ferroelectric state to a non-polar paraelectric state above a characteristic transition temperature (T_C) [22, 88] where the phase transition can be of first or second order [22, 84].

The signs of the Landau parameters in the paraelectric phase can be used to determine the type of phase transition in ferroelectric and relaxor-ferroelectric materials [89, 90]. While the sign of β and δ always remains positive, γ is positive in the case of a second-order transition and negative if the transition is of first order. Thus it is possible to infer the order of the phase change also from the sign of ε_3 [85, 89]. For a second-order transition, the sign of ε_3 changes from positive to negative at T_C, and for a first-order transition, the sign remains unchanged, *i.e.*, the same below and above T_C. On the other hand, the sign of ε_2 is always opposite to that of P_r below T_C, and at $T = T_C$, the value disappears for both the second- and the first-order transitions.

3.4.7.2 Remanent Polarization

When the material is in its ferroelectric state, ε_2 depends on the P_s and the remanent polarization (P_r) [89, 91] according to

$$\varepsilon_0\varepsilon_2 = -P_r(\varepsilon_0\varepsilon_1)^3\,(3\gamma + 10\delta P_s^2). \tag{3.42}$$

Due to the temperature dependence of $1/\varepsilon_1$, we have $10\delta P_s^2 \ll 3\gamma$. In this case, the ratio $\varepsilon_2/\varepsilon_1^3$ is approximately proportional to P_r [85] according to

$$\varepsilon_0\varepsilon_2/3(\varepsilon_0\varepsilon_1)^3 \approx -P_r\gamma. \tag{3.43}$$

Hence, by measuring non-linear dielectric permittivities, we can estimate the remanent polarization without subjecting the sample to very high electric fields.

3.4.7.3 Non-Linear Dielectric Relaxation Spectroscopy (NLDS) Measurement

Figure 3.13 displays the schematic of a measurement setup used to measure the non-linear permittivities using a lock-in amplifier. A sinusoidal electric field with an amplitude $E_\sim$ = 5 V/µm below the coercive field (E_c) was applied at a frequency f_0 of 1 kHz to the capacitor-film sample from a lock-in amplifier (type SR830). The current response from the sample was recorded over a reference resistor connected in series with the sample. A Fourier transform of the current density ($j(t)$) was performed to obtain the spectral components:

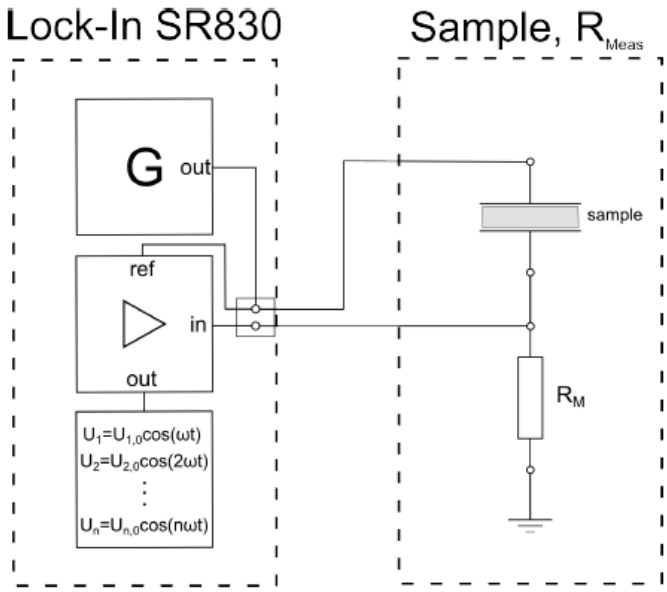

Figure 3.13: Experimental setup for NLDS measurement using a lock-in amplifier. Reprinted from [92].

$$j(t) = \frac{\mathrm{d}D(t)}{\mathrm{d}t} = \sum_{i=0}^{\infty} (j_{\mathrm{i}}' \cos i\omega_0 t + j_{\mathrm{i}}'' \sin i\omega_0 t). \tag{3.44}$$

The linear and non-linear permittivities ε_{n} were then calculated from a sum of the Fourier coefficients j_{i}'' [87]. If the excitation amplitude is chosen sufficiently small for the coefficients j_{n}'' to decrease strongly with increasing order n, the ε_{n} values can be calculated according to the approximate equation [93]:

$$\varepsilon_0 \varepsilon_{\mathrm{n}} \approx \frac{-1}{\omega_0} \times \frac{2^{\mathrm{n}-1}}{n E_{\sim}^{\mathrm{n}}} \times j_{\mathrm{n}}''. \tag{3.45}$$

The permittivities ε_{n} defined in Equations 3.40 and 3.45 refer to the real parts $\varepsilon_{\mathrm{n}}'$ of the respective complex non-linear permittivities. Their imaginary parts $\varepsilon_{\mathrm{n}}''$ can be calculated by replacing the non-vanishing component j_{n}'' with j_{n}' in Equation 3.45.

Spin-coated polymer samples with aluminum electrodes evaporated on the top and bottom side of the films were used for the NLDS measurements. Ice or liquid nitrogen was used as the cooling medium, while the sample was heated using an oil-filled heater.

3.5 Thermally Stimulated Depolarization Currents (TSDCs)

3.5.1 Introduction

As the spontaneous discharge of electret materials takes several years in ambient temperature conditions, Frei and Groetzinger [94, 95] proposed a thermal stimulation of the decay, in order to accelerate the mobility of the frozen-in dipoles which can help to study the decay in short periods of time. The technique consisted of slowly heating the electret between two electrodes, connected to an ammeter which measures this discharge current from the electret. This method was further improved by Turnhoult where he employed linear heating of the material [96]. Today, TSDC measurement technique has become a commonly used technique to investigate the various molecular motions and charge carrier relaxations in dielectric materials. It can also be used to quantitatively measure impurity concentrations, characterize the state of polymers and its local environments, study chemical effects such as degradation, curing and other such phenomena in polymer materials. It complements the frequency and time domain measurements from dielectric spectroscopy.

3.5.2 Working Principle and Experimental Setup

The experimental setup of a short-circuit TSDC measurement instrument is shown in Figure 3.14. A typical experimental scheme during the TSDC measurement is shown in Figure 3.15. At first, the dielectric sample (placed in a parallel plate capacitor configuration) is heated to an elevated temperature above the glass-transition temperature and near the melting temperature of the sample in order to remove any

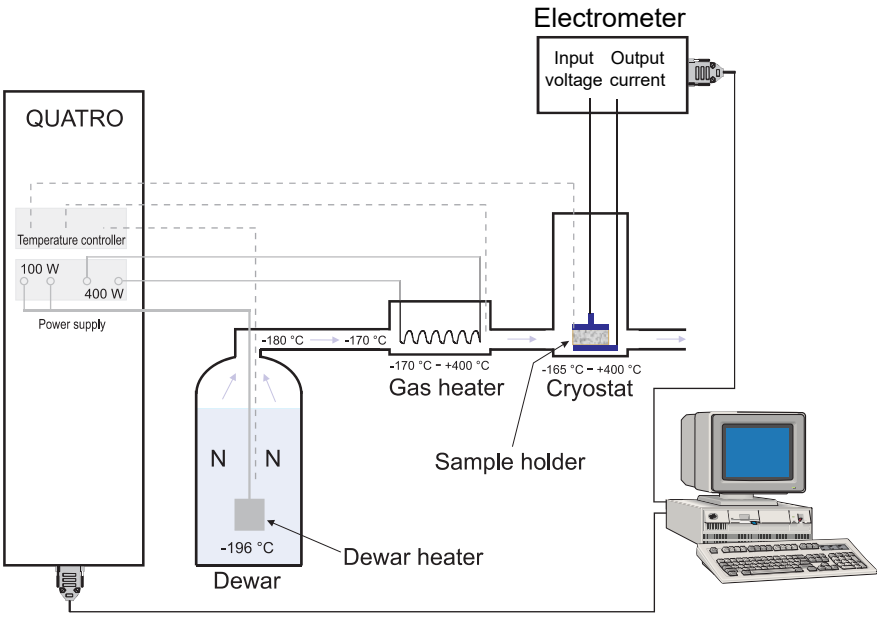

Figure 3.14: Experimental setup for TSDC measurement (adapted from [67]).

previous polarization in the sample. Then the sample is cooled down to the poling temperature T_p (at which the dipoles and free charges are mobile). At a time t_0, an electric field E_p is applied to pole the sample. After poling the sample for a period t_p, the sample temperature is reduced to a temperature T_f below the T_g of the sample to freeze all the dipoles inside, while the poling field is still applied. The field is finally removed after a period of time t_f. The sample is now electrically polarized and this polarization will persist for a very long time. The polarization inside the sample will induce in the adjacent electrode charges of equal magnitude and opposite polarity called *image charges*. These electrodes are then short circuited to an electrometer, which can measure currents with high sensitivity. The TSDC of the sample is finally measured by heating the sample with a linear heating rate.

As the temperature of the sample rises, the polarization induced in the sample begins to decay, and whenever a temperature range at which the decay rate matches the time scale of the experiment is encountered, some of the image charges are released from the electrodes, which constitute the depolarization current. The depolarization current as a function of temperature is plotted in a typical TSDC thermogram. As this is an electrical technique, even subtle effects can be detected, and also as the test frequencies used are very low, TSDC is a highly sensitive technique with high resolution. It is similar to the results obtained from DRS measurements operated at a very low frequency, typically in the range of 10^{-3} to 10^{-4} Hz [97].

Similar to DRS measurements, various molecular motions can be identified from TSDC measurements. Secondary relaxations which occur due to partial mobility of polymer chain segments such as rotation of single chemical group or side groups can be identified. In the TSDC thermogram, these relax-

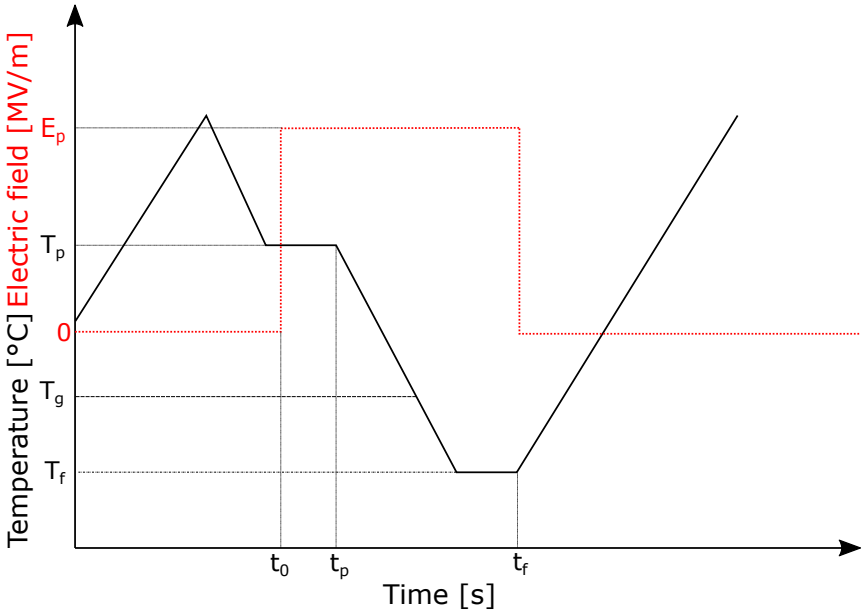

Figure 3.15: Experimental scheme for TSDC measurement.

ations occur at lower temperatures. At higher temperatures, when whole segments of polymer backbone can move (tens of repeat unit) such as during glass transition, α relaxation occurs, which is observed in the form of a peak similar to α peak from DRS measurements.

The persistent polarization in the dielectric is considered to arise from various contributions. They are primarily divided into contributions from hetero- and homo-charges. Heterocharges can be visualized as charges which arise as a result of imposing electric field on the sample (due to polarization of dipolar units). They have charges which are opposite in polarity than the image charges induced in the adjacent electrodes. The second contribution comes from homocharges from charged species displaced from their centroid points. They can arise from charges injected by the electrodes into the materials or from the charged species already present in the sample (impurities). They carry the same sign as the charges in their adjacent electrodes. The redistribution of these homocharges takes places at temperatures about 20-40 °C above T_g [98]. The discharge current peak in the TSDC thermogram corresponding to this redistribution of charges depends on the conductivity of the dielectric material, and so can be considered as a measure of the bulk distribution due to the transport of charged species themselves. In other words, it is an indication of the amount of space-charge polarization in the material. These discharge peaks are referred to as ρ peaks or space-charge peaks.

3.5.3 Measurement

TSDC measurements were carried out under dry nitrogen atmosphere by use of the Novocontrol Quatro cryosystem® together with the Keithley 6578 electrometer®. The TSDC thermograms of the samples

as a function of temperature were obtained at different fields. Similar to samples used for DRS, the free-standing or spin-coated films were metalized on both sides with aluminum electrodes.

3.6 Electrical Hysteresis

3.6.1 Introduction

The dipoles in ferroelectric and relaxor-ferroelectric polymers contain randomly oriented dipoles with a spontaneous polarization. In the absence of an electric field, they cancel each other and hence have a zero net polarization. By subjecting them to an external electric field it is possible to orient these dipoles in the direction of electric field, thus inducing a macroscopic polarization (P_s) in the sample. On removal of the field, a certain amount of dipoles retain their polarization leading to the observation of a remanent polarizarion (P_r) in ferroelectric polymers. When the field is reversed the dipoles switch in the opposite direction and at a certain electric field termed as the coercive field (E_c), the polarization becomes zero. This indicates the minimum electric field needed to orient the dipoles. The process of poling in one direction followed by field reversal results in the observation of a hysteresis loop in ferroelectric polymers such as that depicted in Figure 3.16. The samples can be poled by a corona discharge [31, 99] or by direct contact poling of the samples *via* metallic electrodes [29, 100, 101] using a varying electric field (sinusoidal, triangular, etc.). During poling, in addition to orientation of dipoles and domains, injection and trapping of charges can occur. These lead to ageing effect in the materials.

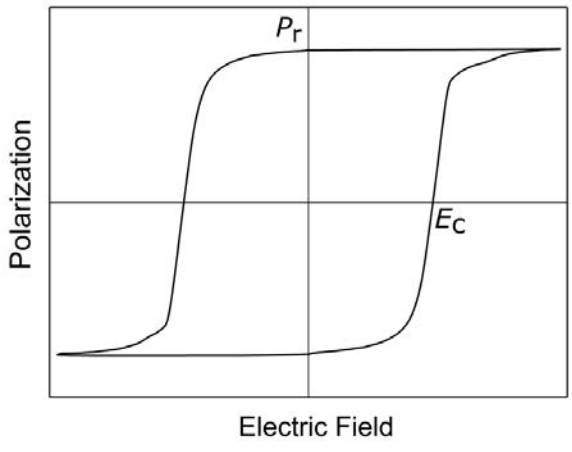

Figure 3.16: Typical dielectric hysteresis curve observed in a ferroelectric polymer.

3.6.2 Experimental Setup

For the measurement of dielectric hysteresis, a method demonstrated by Sawyer-Tower already in 1930 was used [102]. The setup consists of a Sawyer-Tower circuit such as that schematically shown in

Figure 3.17. A high-voltage supply controlled by an arbitrary-waveform generator (together indicated as signal generator) applies the necessary voltage to the sample. Bipolar triangular signals were used to minimize fatigue behavior as suggested by Zhu *et al.* [103]. The sample which has a capacitance C_s is connected in series with a reference capacitor. The capacitance C_{ref} of the reference capacitor is very large compared to that of the sample, for example $C_s/C_r < 0.01$. As a result, when a poling voltage is applied, the maximum voltage drop occurs across the sample capacitor, i.e, V_{ref} (voltage across reference capacitor) $<<$ V_s (voltage across sample). V_s on sample capacitor is almost equal to the poling voltage (V_p). V_{ref} is proportional to the dielectric displacement (D) and polarization of the sample, and is applied to the vertical plates of the oscilloscope. On the other hand, the sample bias V_p is proportional to the electric field, and after attenuation is applied to the horizontal plates of the oscilloscope. The hysteresis loop is displayed directly on the oscilloscope as a plot of dielectric displacement *vs.* electric field.

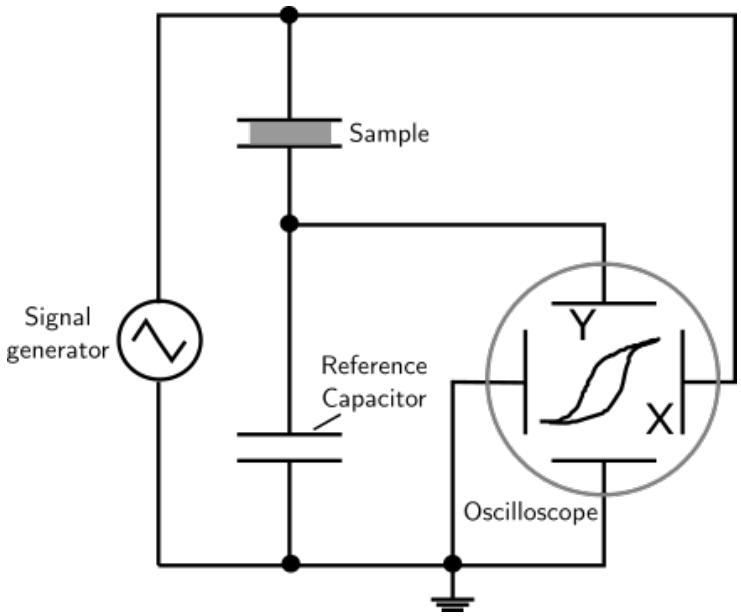

Figure 3.17: Sketch of a Sawyer-Tower circuit used for the measurement of dielectric hysteresis.

The current in the circuit consists of contributions from polarization ($I_p(t)$), capacitance ($I_c(t)$) and conductivity ($I_{cond}(t)$) of the sample as mentioned in Equation 3.46 [100]. Since bipolar loops are used during the measurement, the individual contributions are not separated and hence the measured current is proportional to the electric displacement D and is given by Equation 3.47 [104].

$$I(t) = I_p(t) + I_c(t) + I_{cond}(t) = A\frac{dP}{dt} + C\frac{dV_p}{dt} + \frac{V_p}{R} \tag{3.46}$$

$$I(t) = A\frac{dD}{dt}, \tag{3.47}$$

A is the electrode area of the sample. The charges Q collected in the reference capacitor is given by:

$$Q = \int_0^t I \, \mathrm{d}t = A \int_0^t \frac{\mathrm{d}D}{\mathrm{d}t} = A \int_0^D \mathrm{d}D, \tag{3.48}$$

and V_{ref} is related to the polarization by:

$$V_{\mathrm{ref}} = \frac{Q}{C_{\mathrm{ref}}} = \frac{A}{C_{\mathrm{ref}}} \int_0^D \mathrm{d}D. \tag{3.49}$$

Therefore, the displacement D can be calculated from A, C_{ref} and the measured V_{ref} from Equation 3.50.

$$D = \int_0^D \mathrm{d}D = \frac{C_{\mathrm{ref}} \times V_{\mathrm{ref}}}{A} \tag{3.50}$$

The electric field E applied to the sample with thickness d is determined by:

$$E = \frac{V_{\mathrm{p}}}{d}. \tag{3.51}$$

3.7 Polarized Light Microscopy

3.7.1 Introduction

A polarized light microscope (PLM) helps to view samples under a polarized light. They are suitable for studying the morphology of optically anisotropic materials such as semi-crystalline polymers. They act as beam splitters and divide the light rays into two parts. This phenomenon is exploited in polarized microscopy where the interference of the split beams after they are re-united along the same optical path is used to obtain information about the structure of semi-crystalline polymers.

3.7.2 Measurement Principle

When linearly polarized light is incident on a birefringent (anisotropic) sample with a vibration direction parallel to the optical axis, the illumination vibrations will coincide with the principal axis of the sample and hence the sample will appear dark. In the case, the polarized light hits the sample at 45°, it splits into two polarized waves of equal amplitude, parallel to the directions of the major refractive indices of the sample. These two waves then transverse the sample with different velocities and upon emerging, combine to form an elliptically polarized light wave that passes through an analyzer to yield interference patterns. Since the analyzer is placed at 90° with respect to the polarizer (cross-polars), only the portion polarized parallel to the analyzer is transmitted resulting in bright areas, while other areas appear dark [57, 105, 106]. This contrast helps to view the different spherullitic structures in polymers. In addition, the destructive interference of white light in the analyzer vibration plane often produces a spectrum of colour that can be used to obtain information about path differences and sample thickness if the refractive indices of the sample are known [106].

3.7.3 Experimental Setup

A simple schematic of a PLM is displayed in Figure 3.18. It consists of a polarizer positioned at right angles to an analyzer. The unpolarized light from the light source such as a Xenon lamp is linearly polarized by the polarizer and then projected on to the sample. After interacting with the sample, the light is elliptically polarized and is magnified by the objective lens. The light finally passes through the analyzer and can be viewed under an eyepiece or recorded with a CCD camera. In this work a Zeiss Axio ImagerA1m PLM was used to image the spherullites of free-standing PVDF films.

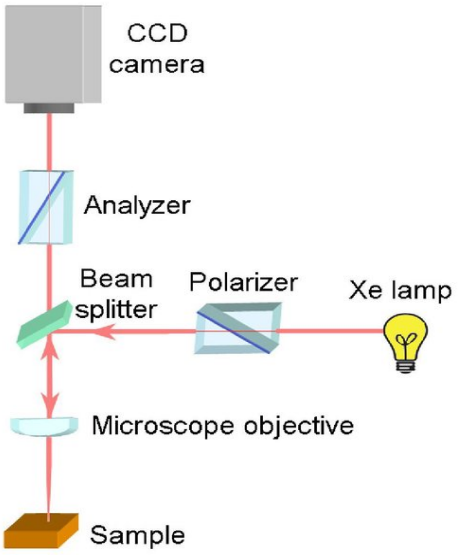

Figure 3.18: Schematic representation of a typical polarized light microscope [107].

3.8 Dynamic Mechanical Analysis

Dynamic mechanical analysis (DMA) is a thermomechanical technique used to measure the viscoelastic response of a material by subjecting the material to an oscillating force. The technique is similar to DRS where a periodic external field is applied to the sample, the difference being here in DMA, a mechanical force is applied instead of an electrical field. DMA can be used in conjunction with DRS for identifying glass transition and other relaxational processes in polymers. In addition to it, it can be also used to determine the degree of phase separation in multicomponent systems, effect of adding fillers in composites, influence of processing conditions, *etc*. [57, 70].

3.8.1 Measurement Principle

Consider a sinusoidal strain being applied to a test sample and measuring the corresponding stress developed in the material. The phase shift angle δ between the applied strain and the measured stress can be in between 0 and 90°. For a perfectly elastic material a δ of 0° and for a perfectly viscous fluid a δ 90° is observed. In the case of a polymer, due to the viscoelastic nature of the material, an angle between these two values can be observed.

In a viscoelastical material, for a sinusoidal applied strain, the resulting stress will be also sinusoidal and is described by Equation 3.52.

$$\sigma(t) = \sigma_0 sin(\omega t + \delta), \tag{3.52}$$

where σ_0 is the stress amplitude. The ratio between the dynamic stress and dynamic strain is given by the complex modulus (E^*) and can resolved into two components; the energy stored in the system due to elastic deformation, referred to as the storage modulus (E') and the energy dissipated as heat owing to viscous motions, denoted by loss modulus (E''). Mathemacially,

$$E^* = E' + \mathrm{i}E''. \tag{3.53}$$

The ratio of the loss and storage modulus is the mechanical dissipation factor ($\tan\delta$), which is independent of the shape and dimensions of the sample. When a polymer material undergoes a thermodynamical process such as a glass transition or a structural relaxation, a corresponding change in its viscoelastic response is observed. These changes can be observed in the complex modulus E^* of the sample either as a function of temperature, time or deforming frequency.

3.8.2 Experimental Setup

The sample is mounted in the setup in a number of ways depending on the characteristics and type of sample and accordingly subjected to different forces. The most commonly used configurations are tensile mode, compression mode, shear loading, single cantilever, dual cantilever and three-point bending. In this work, a Netzsch DMA 242C setup operated in tensile mode at a frequency of 5 Hz was used. The sample temperature was controlled using dry nitrogen.

4

Materials and Sample Preparation Techniques

4.1 Materials

In this work, PVDF homopolymer, P(VDF-TFE), P(VDF-TrFE) copolymers and P(VDF-TrFE-CFE) terpolymer were used. PVDF Solef^{TM} 1008 powder was purchased from Solvay S.A. (Belgium). Apart from it commercial extruded PVDF films which were uniaxially or biaxially stretched were utilized (Piezotech S.A., France). Extruded P(VDF-TFE) films with a VDF/TFE ratio of 70/30 mol %, respectively, and thickness of 100-200 μm were provided by F2ME, Russia, and P(VDF-TFE) 80/20 mol % powder under the trade name Kynar^{TM} 7201 was obtained from Atofina (currently Arkema-Piezotech S.A., France). P(VDF-TrFE) with a comonomer composition of 75/25 mol % was procured in powder form from Piezotech S.A. P(VDF-TrFE-CFE) terpolymer with a VDF/TrFE/CFE ratio of 62.2/29.4/8.4 mol%, respectively, was provided by Arkema-Piezotech.

4.2 Sample Preparation

4.2.1 Drop-Casting

For the drop-casting or solvent-casting technique, the polymer is dissolved in a suitable solvent and the solvent is then allowed to evaporate after casting it onto a substrate. The different solvents, the concentration of polymer solutions used during drop-casting for various polymers are listed in Table 4.1.

The procedure started with dissolving the weighed quantity of polymer in its appropriate solvent. The solution is then filtered through a poly(tetrafluoroethylene) (PTFE) syringe filter with a pore size of 0.2 μm. The filtered solution was drop cast onto a 80×80 mm glass plate. The glass plates were cleaned thoroughly prior to drop-casting with first laboratory soap solution, then ultrapure water, acetone and again finally with ultrapure water. After drop casting, the solvent was allowed to be evaporated at room

Table 4.1: Table of different polymers and solvents used for drop-casting and spin-coating films.

Sample	Composition [mol %]	Method	Concentration	Solvent
PVDF	homopolymer	drop-casting	10 wt %	Dimethylformamide/ Cyclohexanone
P(VDF-TFE)	80/20	drop-casting	10 wt %	Acetone/ Acetonitrile
P(VDF-TrFE)	75/25	drop-casting spin-coating	10 wt % 20 wt %	Acetonitrile Acetonitrile
P(VDF-TrFE-CFE)	62.2/29.4/8.4	drop-casting spin-coating	10 wt %	Acetone

temperature overnight. Finally, the film was peeled off from the substrate. The thickness of the free-standing films was between 20 and 40 µm. The films were then subjected to an annealing procedure unless otherwise specified. The samples were annealed at a particular pre-set temperature in vacuum for about 12 h and then slowly cooled to room temperature (RT). The non-annealed films were also dried in a vacuum oven at RT to remove traces of solvent.

4.2.2 Spin-coating

Spin-coating allows to prepare much thinner films than that obtained by drop-casting. Here, the polymer solution is dropped onto a substrate that is held under vacuum on a rotating platform. This is followed by a rotating step where the solution flows across the substrate due to centripetal force. The solvent and excess solution is then pushed out leaving behind a thin film.

To prepare spin-coated films, the polymer solution was prepared using the same procedure described for drop-casting. To prepare thinner films a lower concentration of the polymer was used as specified in Table 4.1. Two rotating steps were used. In the first step, the substrate was rotated for 30 s at 2500 rpm, followed by a second step with a higher rotating time of 45 s and speed of 3500 rpm.

4.2.3 Melt-pressing

For preparing thicker films, polymer powders were heated to a temperature above its melting point in between two heating plates under pressure. The sample powder was covered on the top and bottom with PTFE films. PTFE films have a very high softening point when compared to PVDF-based polymers and were used to prevent the polymer films from sticking to the heat plates. The samples were held at a temperature at least 20 °C above its melting point for a period of 20 min under a pressure of 100 bar. After this, the heating was switched off and the sample melt was cooled down to RT with the pressure still applied to obtain the melt-pressed films.

4.2.4 Commercial Extruded Films

Commercial films used in this study were prepared by melt-extrusion technique. In this technique polymer in the form of powder or granules are melt inside a heated barrel. The sample is gradually heated to temperatures above its melting point as it travels through rotating screws located inside the barrel. Usually two-screw arrangement is used. The polymer melt is then pushed through a flat metal die to produce thin films, which are immediately quenched in an ice or water bath. The films can also be uniaxially (in the direction of the film) or biaxially oriented as they exit the die.

4.2.5 Evaporation of Metal Electrodes

For dielectric measurements, the films were coated on both sides with aluminium electrodes of 60 nm thickness in Univex 350® vacuum system with the help of INFICON SQC-310® deposition controller. In the case of spin-coated films, the substrate was first deposited with a 10 nm thick chromium layer before evaporating a bottom aluminum layer. This was followed by the spin-coating step and finally a top aluminum electrode was deposited on to the sample film. In order to make electrical contact with the bottom electrode, a portion of the polymer film layer was removed [108].

5

Properties and Characteristics of PVDF-based Ferro- and Relaxor-Ferroelectric Polymers[1]

PVDF and its related co- and ter-polymers that are either ferroelectric or relaxor-ferroelectric in nature exhibit certain properties and characteristics that are unique for these class of materials, which are briefly discussed in this chapter.

5.1 Polarization and Dielectric-Hysteresis Characteristics

As mentioned in the Introduction (Section 1.2), one of the criteria for a material to be ferroelectric or relaxor-ferroelectric is its ability to exhibit a dielectric-hysteresis behavior. It is a measure of the amount of electric energy spent to align the dipoles in the direction of an applied electric field (E). Ferroelectric polymers such as β PVDF and P(VDF-TrFE) have a large number of dipoles. This leads to the observation of a broad hysteresis loop with a high coercive field (E_c) and remanent polarization (P_r)/displacement (D_r) as shown in Figure 5.1 in a P(VDF-TrFE) sample [100, 101, 109, 110, 111]. In the case with relaxor ferroelectric (R-F) terpolymers, they exhibit very high dielectric permittivities and have a lower number of dipoles in comparison to ferroelectric polymers. Hence, the dipoles can rotate easily upon application of an electric field. Consequently, R-F terpolymers exhibit slim hysteresis loops with small values of E_c and D_r as shown in Figure 5.1 for a P(VDF-TrFE-CFE) terpolymer annealed at 60 °C (measured at 25 °C).

R-F terpolymers can also produce double-hysteresis-loop (DHL) behavior where the displacement is reduced to values close to zero on removing the electric fields as depicted in a terpolymer sample

[1]Parts of this chapter are adapted from T. Raman Venkatesan *et al.*, "Structure-Property Relationships in Three-Phase Relaxor-Ferroelectric Terpolymers", *Ferroelectrics*, 586(1), 60-81, 2022 [24] and T. Raman Venkatesan *et al.*, "Tuning the Relaxor-Ferroelectric properties of Poly(vinylidene fluoride-trifluoroethylene-chlorofluoroethylene) Terpolymer by Thermally Induced Micro- and Nanostructures", under review in *Macromolecules*, 2022.

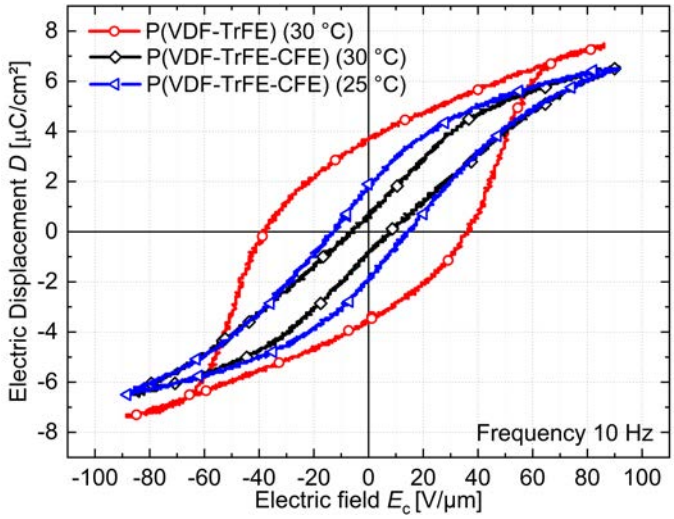

Figure 5.1: Comparison of dielectric-hysteresis loops in a ferroelectric P(VDF-TrFE) (VDF/TrFE 75/25 mol %) copolymer measured at 30 °C and in a relaxor-ferroelectric P(VDF-TrFE-CFE) (VDF/TrFE/CFE 62.2/29.4/8.4 mol %) terpolymer annealed at 60 °C, measured at 25 and 30 °C. Symbols are added to the continuously measured curves in order to facilitate their identification.

annealed at 60 °C and measured at a temperature of 30 °C. DHL behavior has been observed before in anti-ferroelectric ceramics and is usually explained as a reversible antiferroelectric-to-ferroelectric (AFE-to-FE) transition [112, 113]. In the case of ferroelectric/R-F polymers, DHLs have been previously observed in P(VDF-TrFE) copolymers containing higher fractions of TrFE and in terpolymers containing CFE and CTFE as termonomers [114, 115, 116, 117]. This behavior is attributed to the presence of antiferroelectric (AFE)-like regions which can exist in VDF-TrFE molecular chains [114] or as a result of the bulky termonomer acting as physical pinning sites in the terpolymer [115, 117, 118]. DHLs and R-F hysteresis loops are advantageous for energy-storage applications, since the electric-energy density that can be discharged is very high [53, 115].

In the case of P(VDF-TrFE), Takashi *et al.* stated that the non-polar AFE-like regions during field switching/reversal leads to a two-step polarization response. On application of a field in the direction opposite to that prior to the measurement, it was found that first depolarization occurs in the direction of the applied field followed by repolarization [114]. With respect to P(VDF-TrFE-CFE) terpolymers, Yang *et al.* [115, 118] described that at low applied electric fields, the strength of the field is not high enough to rotate the bulky CFE groups and the VDF-TrFE groups next to them to follow the field (materials in its relaxor-ferroelectric state). Hence, only the dipoles of VDF-TrFE groups far away from CFE can respond to the applied field resulting in a ferroelectric-to-ferroelectric (FE $\rightarrow$ FE) transition and observation of a single hysteresis loop (scenario (a) in Figure 5.2). At high fields, these CFE groups and the VDF-TrFE groups in the immediate vicinity can also be rotated, resulting in an increase in the VDF-TrFE interaction

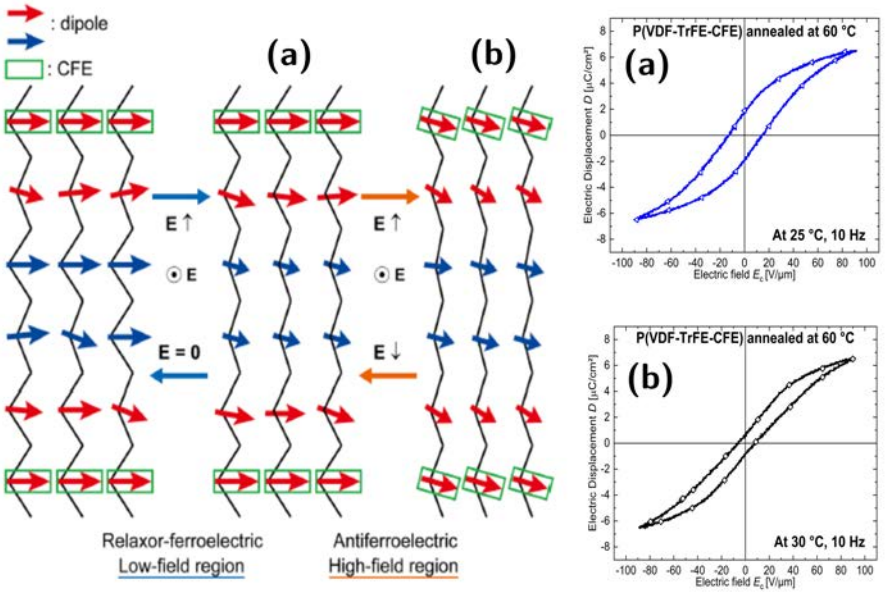

Figure 5.2: Schematic model of dipole switching in a P(VDF-TrFE-CFE) leading to single-hysteresis-loop (SHL) and double-hysteresis-loop (DHL) behavior. Adapted from [117] under Open Access Creative Commons Attribution 4.0.

within the material. This causes an increase in the overall polarization response of the sample thereby leading to a relaxor-ferroelectric-to-ferroelectric (R-F $\rightarrow$ FE) phase transition with DHL behavior (scenario (b) in Figure 5.2). The transition process is reversible, and the terpolymer returns to its R-F state upon removal of the electric field. It has been estimated that just 2 neighboring CFE units can pin about 14 VDF-TrFE groups between them [115, 118].

In terms of the explanation offered by Takashi *et al.* [114], the switching of CFE groups at high fields and the reversal of the bulky termonomers to its prior state on lowering of the field can be considered as the repolarization and depolarization steps, respectively, as shown in Figure 5.3. The threshold voltage at which the field is just high enough to rotate the CFE groups can be determined by taking a derivative of the displacement as a function of time ($\mathrm{d}D/\mathrm{d}t$) and finding the voltage at which the maximum change in D occurs during the increase or decrease of the applied fields [114].

Looking at the shape of the DHL in Figure 5.1, it is similar to the one observed by Tsutsumi *et al.* where the shape of the curve is not symmetrical in the high-field region. The shape of the DHL in terpolymers depends on a number of factors such as the maximum applied field, temperature of the measurement, the fraction of the ferroelectric and relaxor-ferroelectric phases in the respective sample. This can be seen in the difference of the DHLs measured at different temperatures in different processed samples by Yang *et al.* [115] and also in different heat-treated terpolymer samples (Chapter 12). In addition, it should be taken into account that the material undergoes active changes during poling. Previously, it

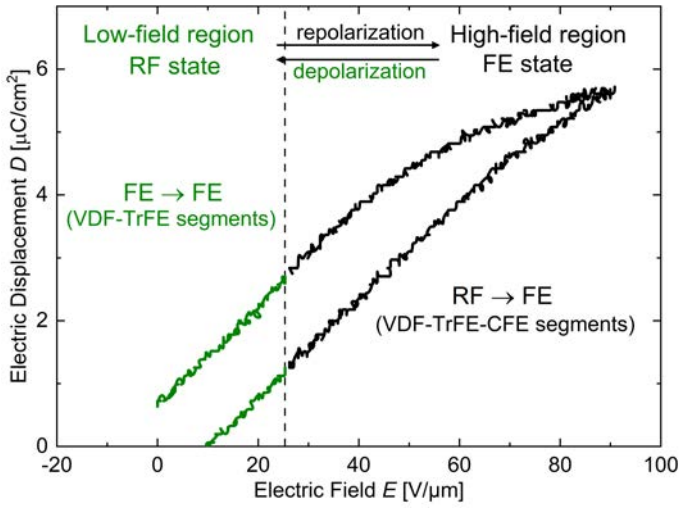

Figure 5.3: D-E double hysteresis loop of a P(VDF-TrFE-CFE) terpolymer film (annealed at 60 °C prior to the measurement) with a VDF/TrFE/CFE ratio of 62.2/29.4/8.4 mol % at 40 °C measured using a frequency of 10 Hz.

has been shown that the poling process can result in the change of crystallinity and the fraction of polar phases in the measured samples [119, 120, 121]. Apart from this, the nature of the termonomer has also been found to influence the type of hysteresis loops observed in the terpolymer [24, 116, 117]. The pinning effect of CFE is weaker when compared to that of CTFE due to its smaller size and higher dipolar moment.

5.2 Piezoelectric and Pyroelectric Coefficients

Ferroelectric polymers show lower piezo- and pyro-electric constants when compared to ferroelectric ceramics such as PZT, primarily due to their high stiffness/low Young's modulus [20, 122]. Typical piezoelectric strain coefficients d_{31} d_{33}, and pyroelectric p_3 coefficient values recorded for PVDF and P(VDF-TrFE) are listed in Table 5.1. In the case of R-F polymers, since they have a very low remanent polarization, they show very low/negligible piezoelectric and pyroelectric constants after poling.

Table 5.1: Typical piezoelectric strain coefficients d_{31}, d_{33}, and pyroelectric coefficient p_3 of PVDF and P(VDF-TrFE) reported in literature.

Ferroelectric polymer	d_{31} **[pC/N]**	d_{33} **[pC/N]**	p_3 **[nC/cm^{2}K^{-1}]**	**References**
Uniaxially stretched PVDF	20	30	3	[20, 123, 124, 125, 126, 127, 128]
Biaxially stretched PVDF	5-20	12	4	
P(VDF-TrFE) (75/25 mol%)	10	20-30	2	[111, 129]

5.3 Electrostrictive Strain

The low Young's modulus of R-F terpolymers results in large electrostrictive strains – higher than those of ceramics – which can be exploited in actuator applications [53]. P(VDF-TrFE-CFE) terpolymers show the highest electrostrictive strain among all R-F polymers known so far [14, 48]: about 7 % in the thickness direction (longitudinal strain, S_3) and 2 % in the transverse direction (S_1), respectively, as shown in Figure 5.4. Additional stretching increases S_1 to $\sim$3 % when an electric field of 150 V/μm is applied [48] (Figure 5.4c). As shown in Figures 5.4a and 5.4c, both S_3 and S_1 show a quadratic dependence of strain at low fields and saturates at high electric fields.

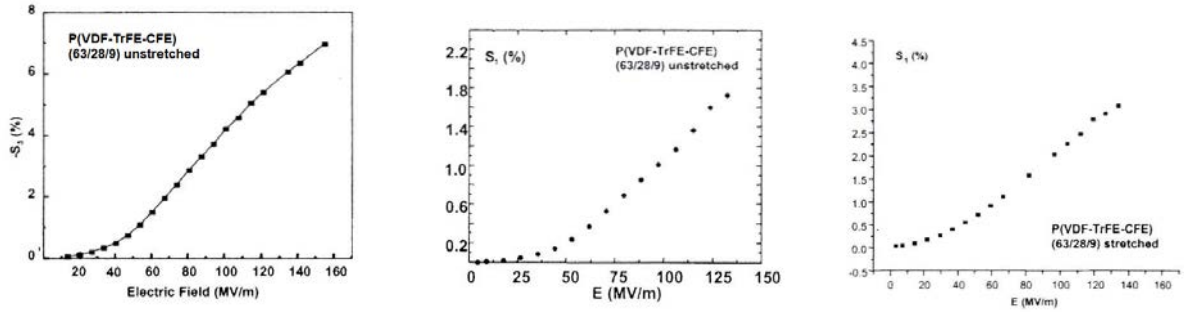

(a) S_3 (unstretched) **(b)** S_1 (unstretched) **(c)** S_1 (stretched)

Figure 5.4: Electrostrictive strain observed in longitudinal (S_3) and transverse (S_1) directions in unstreched and stretched P(VDF-TrFE-CFE) terpolymer films. Reprinted from the work of Bauer *et al.* [48] with permission from © 2004 IEEE.

5.4 Electrocaloric Effect

The process of polarization and relaxation also brings about changes in entropy and temperature of the material when it is exposed to an electric stress, which is known as the electrocaloric effect (ECE) – the reciprocal effect to pyroelectricity. It has been proposed to use this property for solid-state refrigeration in sensors, in microelectronic devices, as well as in small, but highly efficient industrial and domestic cooling appliances [130, 131, 132]. Neese *et al.* reported that a large ECE can be achieved in both ferroelectric and relaxor-ferroelectric polymers operated near their respective F-P transition temperatures [133]. As shown in Figure 5.5a, at 80 °C, with an applied electric field of $\approx$ 209 MV/m, an isothermal entropy change ΔS = 55 J/KgK and an adiabatic temperature change ΔT = 12 °C was obtained with a P(VDF-TrFE) (55/45 mol%) copolymer. Similar levels of ΔS and ΔT were also measured in a P(VDF-TrFE-CFE) (59.2/33.6/7.2 mol%) terpolymer at 55 °C, with an applied electric field of $\approx$ 307 MV/m (Figure 5.5b [133]).

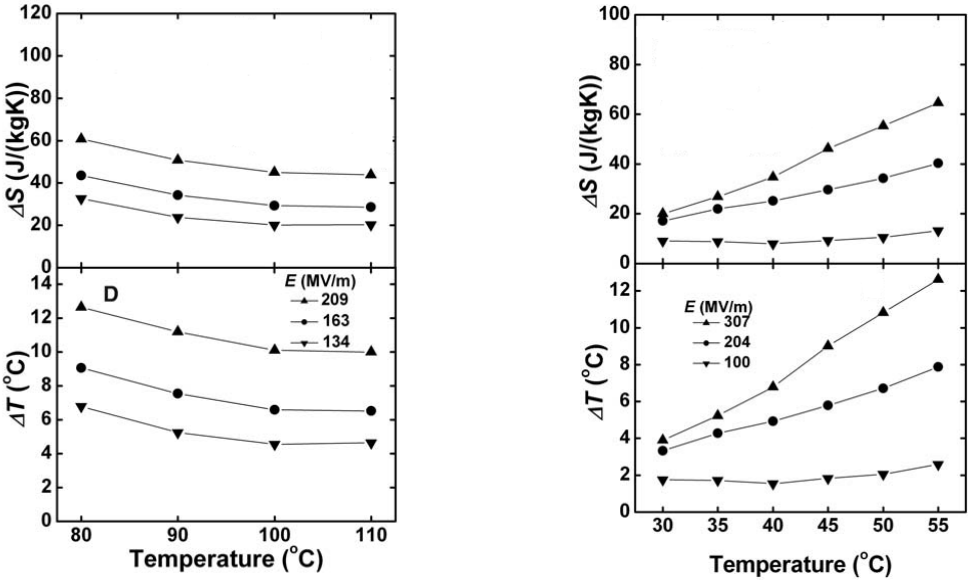

(a) P(VDF-TrFE) copolymer

(b) P(VDF-TrFE-CFE) terpolymer

Figure 5.5: Isothermal entropy change ΔS and adiabatic temperature change ΔT observed in a P(VDF-TrFE) (55/45 mol%) copolymer and a P(VDF-TrFE-CFE) (59.2/33.6/7.2 mol%) terpolymer. Reprinted from the work of Neese *et al.* [133] with permission from © 2008 AAAS.

The ECE of R-F terpolymers is very attractive for real-world applications, since they have a very low T_C. Subsequently, the temperature dependence of the ECE in P(VDF-TrFE-CFE) terpolymers has been investigated [134]. It was shown that the change of the isothermal entropy ΔS is directly proportional to the square of the electric displacement D ($\Delta S = -\beta \Delta D^2/2$) and that the coefficient β increases with temperature. The results indicate that the polarization response from the nanopolar regions in the terpolymer does not generate much change in ΔS and that the major contribution comes from the changes accompanying the ferroelectric-to-paraelectric transition in the crystalline regions.

5.5 Crystalline Phases Present in Ferroelectric and Relaxor-Ferroelectric Polymers

The various crystalline phases present in PVDF-based homo-, co- and ter-polymers can be identified using techniques such as WAXD and FTIR spectroscopy.

5.5.1 Wide-Angle X-ray Diffraction (WAXD)

Figure 5.6 displays a room temperature (RT) WAXD scan of a melt-pressed α PVDF film. The indexing of the lattice planes and assignment of the crystalline peaks to their respective crystalline phases are based on the previous work of Kochervinskii *et al.* [21, 44, 135]. As a result of peak fitting, the composite scan

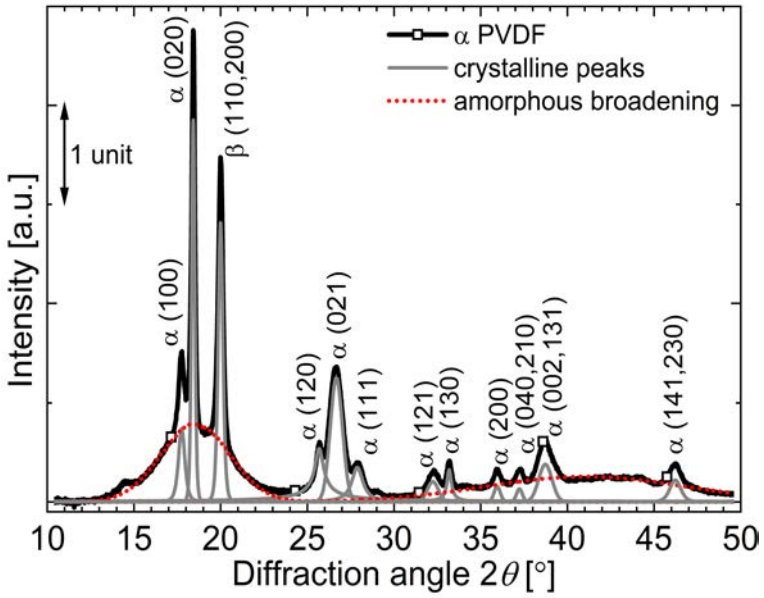

Figure 5.6: RT WAXD scan of a melt-pressed PVDF homopolymer film.

is decomposed into crystalline peaks and amorphous halo as shown in the figure. The melt-pressed film shows majorly α crystalline peaks as expected. However, the diffraction at $2\theta = 20.0^\circ$ near the (110,200) family of planes shows the presence of β phase crystals in the sample.

The RT WAXD scans of other PVDF-based co- and ter-polymers are compared with that of α PVDF in Figure 5.7. The peak position, lattice constant d and the corresponding full width at half maximum (FWHM) of the crystalline peaks associated with the various crystalline phases estimated for the different polymers are listed in Table 5.2. WAXD scans between diffraction angles $2\theta = 15$ and 25° are typically used for the characterization of α and β phase crystals present in the perpendicular direction to the chain axis in PVDF-based polymers [136, 137, 138, 139]. From the figure, we can observe that a 70/30 mol% P(VDF-TFE) sample shows mainly α crystalline peaks with a minor fraction of β phase crystalline peaks similar to α PVDF. The similarity in the crystalline composition of the P(VDF-TFE) copolymer can be explained by the molar ratio of TFE, and its chemical structure, which is similar to that of a VDF homopolymer with higher percentage of H-H defects [140].

By making use of the Scherrer equation (Equation 5.1) [141, 142], the coherence length L_c or crystallite size perpendicular to the lattice plane can be calculated:

$$L_c = \frac{0.9 \times \lambda}{B \times \cos\theta}, \tag{5.1}$$

where λ is the wavelength of X-ray used (1.5419 Å), B is the full width at half maximum (FWHM) in 2θ. However, if the diffraction peak is the juxtaposition of two Bragg peaks which correspond to two

different families of crystallographic planes, L_c cannot be calculated using the Scherrer equation [138]. In this case, it is reasonable to use the FWHM values of the peaks for qualitatively comparing the size of crystalline domains.

Although PVDF homopolymer and a P(VDF-TFE) polymer have a similar chemical structure, still the TFE units modify the size of the paraelectric crystals found near the (100) plane, as evident by the decrease in the coherence length L_c of the crystals in this plane (Table 5.2). The L_c is reduced to about 3.3 nm in the P(VDF-TFE) copolymer from 19.5 nm in a α PVDF. Simultaneously, a decrease in lattice constant d is observed after the addition of TFE units into the crystalline structure. On the other hand, adding 25 mol% of TrFE comonomer into the homopolymer chain forces the VDF units to form β ferroelectric crystals (Figure 5.7). The strongest peak is seen around the (110,200) reflexes, whose d value is similar to that observed in both PVDF and P(VDF-TFE) copolymer (Table 5.2). Yet again, adding a CFE termonomer causes a change in the crystalline phases in the terpolymer. The peak observed near the (100,200) group of planes shifts to a lower 2θ angle of 18.16° corresponding to crystals in the relaxor-ferroelectric phase. The bulky CFE termonomer also expands the spacing between the planes to about 4.89 $\AA$. Though we cannot estimate the size of the crystalline domains in the terpolymer due to the superposition of the (100) and (200) family of planes, yet from the reduction of FWHM of the peak associated with (100,200) planes in the terpolymer on comparison to that in a 70/30 mol % P(VDF-TrFE) copolymer, we can infer that the size of the crystals increase in the terpolymer (Scherrer equation 5.1).

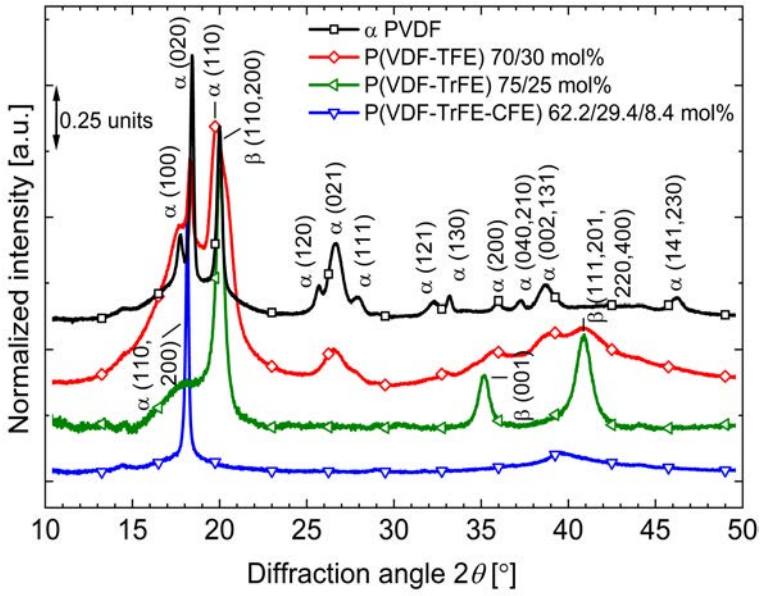

Figure 5.7: RT WAXD scan of various PVDF-based ferroelectric and relaxor-ferroelectric polymers. Symbols are added to the continuously measured spectra in order to facilitate their identification.

Table 5.2: Summary of various crystalline phases along with their designated lattice indices and its corresponding crystalline parameters estimated from the RT WAXD spectra of various PVDF-based polymers between diffraction angles 2θ = 15 and 25°. PE stands for paraelectric phase, FE stands for ferroelectric phase and R-F stands for relaxor-ferroelectric phase.

Sample	Crystalline phase	Lattice indices	Peak position [°]	FWHM [Å]	Lattice constant *d* [Å]
α PVDF	PE	(100)	17.75	0.43	5.00
(melt-pressed)	PE	(020)	18.42	0.22	4.82
	FE	(110,200)	20.00	0.32	4.44
P(VDF-TFE)	PE	(100)	18.04	2.51	4.92
70/30 mol %	PE	(020)	18.31	0.24	4.85
(extruded)	PE	(110)	19.72	0.52	4.5
	FE	(110,200)	20.20	1.10	4.40
P(VDF-TrFE) 75/25 mol % (drop-cast)	FE	(110,200)	20.02	0.60	4.44
P(VDF-TrFE-CFE) 62.2/29.4/8.4 mol % (drop-cast)	R-F	(110,200)	18.16	0.17	4.89

5.5.2 Determining Crystallinity of Semi-Crystalline Polymers

The crystallinity of semi-crystalline polymers χ_c can be estimated from WAXD scans by calculating the area of the amorphous and crystalline peaks using the following equation [143]:

$$\chi_c = \frac{A_c}{A_c + A_a} \times 100, \tag{5.2}$$

where A_c and A_a are the total area of crystalline peaks and amorphous shape, respectively. The fitting of crystalline peaks and amorphous was performed by means of Profex software [144] using a Pearson VII function. A χ_c of 55 % was calculated for a melt-pressed α PVDF film (*cf.* Figure 5.6). The crystallinity can also be calculated from the heat-of-fusion/enthalpy of melting (ΔH_m) values derived from the melting peak in DSC [145] using the below equation [138]:

$$\chi_c = \frac{\Delta H_m}{\Delta H_\infty} \times 100. \tag{5.3}$$

ΔH_∞ is the heat-of-fusion of 100 % crystalline form of the polymer. In case of PVDF, a value of 104.6 J/g is estimated [146]. This yields a χ_c value of 55 % for a melt-pressed α PVDF film with a ΔH_m value of 57.4 J/g, similar to the value determined by WAXD. In the case of a P(VDF-TFE) copolymer, the addition of TFE acts as defects thereby reducing the crystallinity as seen in Table 5.3 (ΔH_∞ value for 100 % PVDF used). For PVDF-based copolymers which show a Curie transition, Teyssédre and Lacabanne [129]

stated that using only the enthalpy of melt will lead to the determination of the crystallinity of the polymer in its paraelectric state which exists prior to its melting. This often leads to difference in the crystallinities observed using WAXD. Hence, they proposed that the enthalpy of the Curie-transition peaks also needs to be considered while determining the crystallinity:

$$\chi_c = \frac{\Delta H_m + \Delta H_{F\text{-}P}}{\Delta H_\infty} \times 100\,. \tag{5.4}$$

By using the above Equation 5.4, a χ_c of 56 % was obtained for a P(VDF-TrFE) copolymer, while using Equation 5.3 yielded a lower value of 27 %. A heat-of-fusion value of 91.45 J/g for 100% crystalline P(VDF-TrFE) was used as calculated by Clements *et al.* [147]. In this work, for calculating χ_c, the method suggested by Teyssédre and Lacabanne [129] was used in the case the polymer exhibited a Curie transition. Inclusion of additional CFE units disrupts the crystalline arrangement further, reducing the total crystallinity to about 20 % in a P(VDF-VDF-CFE) terpolymer (ΔH_∞ for 100 % P(VDF-TrFE) used). Overall, we can observe that the crystallinity decreases from the homopolymer to the terpolymer due to the addition of co- and ter-monomers that act as defects affecting the crystalline arrangement in the polymer.

Table 5.3: Crystallinity of various PVDF-based polymers calculated using different methods along with the enthalpy of melting ΔH_m values from DSC.

Sample	ΔH_m **[J/g]** DSC	X_c **[%]** [a] DSC	X_c **[%]** [b] DSC	X_c **[%]** XRD
α PVDF (melt-pressed)	57.4	55	55	55
P(VDF-TFE) 70/30 mol% (extruded)	30.3	31	31	48
P(VDF-TrFE) 75/25 mol% (drop-cast)	24.6	27	56	40
P(VDF-TrFE-CFE) 62.2/29.4/8.4 mol% (drop-cast)	21.3	20	21	24

[a] ΔH_m; [b] $\Delta H_m + \Delta H_{F\text{-}P}$

5.5.3 Fourier-Transform InfraRed (FTIR) Spectroscopy

Figure 5.8 shows the RT FTIR spectra for various ferroelectric and relaxor-ferroelectric polymers. Using the characteristic peaks present in the PVDF-based polymers it is possible to assign the absorption peaks to the different conformations and in turn to the different crystalline phases present in the sample (Table 5.4). The IR band at 763 cm^{-1} can be assigned to rocking vibrations of CH_2 chains ($r(CH_2)$) in α phase (TG^+TG^- conformation) [26, 148, 149]. Similarly, the IR band at 613 cm^{-1} is assigned to the skeletal bending of the carbon chain ($\delta(CCC)$) coupled with the bending of CF_2 ($\delta(CF_2)$) units of

α phase crystals [136, 150, 151]. From Figure 5.8, we can observe that both PVDF homopolymer and a 70/30 mol % P(VDF-TFE) copolymer show strong absorption at these wavenumbers complementing the observation from their respective WAXD scans. Apart from these characteristic peaks, the peaks at wavenumbers 1212, 977, 855, 795, 532, 485 and 410 cm^{-1} have been also assigned to non-polar para-electric α phase (Table 5.5) [26, 135, 150, 152, 153, 154, 155, 156]. The peak at 1387 cm^{-1} has also been associated with α phase crystals, however this region also overlaps with peaks from the amorphous phase [152].

On the other hand, a 75/25 mol % P(VDF-TrFE) copolymer shows IR peaks at 1285 and 840 cm^{-1}. The band around 1285 cm^{-1} has been assigned to the anti-symmetric stretching of CF_2 ($\upsilon_{as}(CF_2)$), $\upsilon_{as}(CC)$ and $\delta(CCC)$ chains in polar ferroelectric β phase (all-*trans*) [150, 151]. The absorption around 840 cm^{-1} corresponds to symmetric stretching of CF_2 and carbon-carbon backbone chains ($\upsilon_s(CF_2)$ and $\upsilon_s(CC)$, respectively) in β phase [26, 36, 148, 152]. We can confirm that both PVDF and P(VDF-TFE) in addition to the predominant presence of non-polar α crystals also possess β crystalline regions, since PVDF shows a shoulder and P(VDF-TFE) shows peaks at these two wavenumbers – also inferred from the observations of their WAXD scans. The other peaks which are associated with β phase are listed in Table 5.5. The bands at 1075 and 879 cm^{-1} can overlap with amorphous peaks and hence are not usually considered for quantitative analysis [152]. In addition, the *trans* sequences in β phase are difficult to be distinguished from those arising from $T_3G^+T_3G^-$ sequences in γ phase for the peak appearing at 1178 cm^{-1} [155]. Therefore, they are not considered for further analysis.

The band at 506 cm^{-1} corresponds with the bending of CF_2 units (referred as $\delta(CF_2)$) in γ phase ($T_3G^+T_3G^-$ conformation) [150, 151, 157, 158]. Apart from it, the bands at 1243 and 430 cm^{-1} are also assigned to γ crystals [135, 153, 159]. From Figure 5.8, we can see that the terpolymer shows a strong absorption peak and a shoulder at 506 and 1243 cm^{-1}, respectively. In addition, it also shows the presence of α phase band at 613 cm^{-1}. This is consistent with the previous studies showing that P(VDF-TrFE-CFE) terpolymer has predominantly α and γ conformations [51, 150, 151]. However, the presence of a β phase peak is revealed by the peak at 840 cm^{-1}, which is not observed from its corresponding WAXD scan (Figure 5.7).

Table 5.4: Summary of the characteristic IR bands in PVDF-based polymers (υ-stretching, δ-bending, *r*-rocking vibrations in as-asymmetric, and s-symmetric mode).

Wavenumber [cm^{-1}]	Assignment	Conformation	Phase
1283	$\upsilon_{as}(CF_2), \upsilon_{as}(CC), \delta(CCC)$	all-*trans* ($T_{m>3}$)	β
840	$\upsilon_s(CF_2), \upsilon(CC)$	all-*trans* ($T_{m>3}$)	β
763	$r(CH_2)$	TG^+TG^-	α
613	$\delta(CCC), \delta(CF_2)$	TG^+TG^-	α
506	$\delta_s(CF_2)$	$T_3G^+T_3G^-$	γ

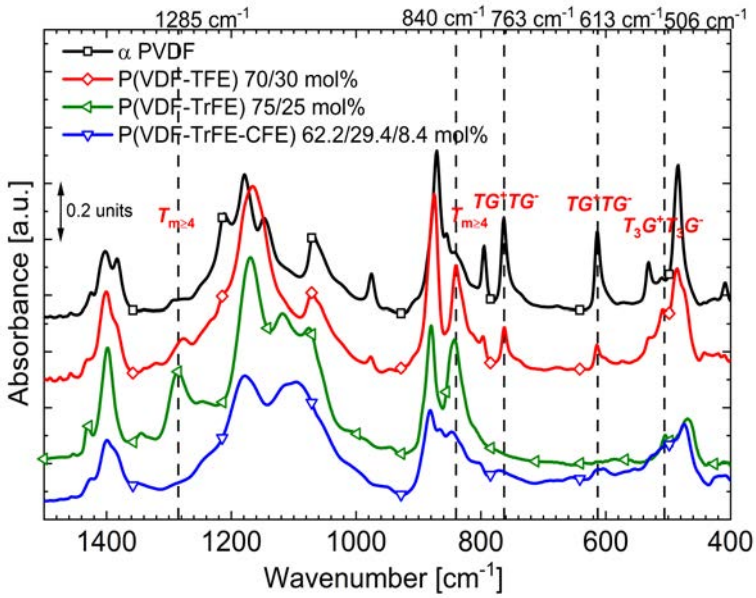

Figure 5.8: RT FTIR spectra of ferroelectric PVDF, P(VDF-TrFE), P(VDF-TFE) and relaxor-ferroelectric P(VDF-TrFE-CFE) polymers. Symbols are added to the continuously measured spectra in order to facilitate their identification.

Table 5.5: Additional IR bands assigned to various crystalline phases in PVDF-based polymers.

Wavenumber [cm^{-1}]	Conformation	Phase	References
1178, 1075, 879 and 468	all-*trans* ($T_{m>3}$)	β	[36, 135, 136, 140, 150, 152, 155]
1212, 977, 855, 795, 532, 485 and 410	TG^+TG^-	α	[26, 135, 150, 152, 153, 154, 155, 156]
1233, 430	$T_3G^+T_3G^-$	γ	[135, 153, 159]

The absorption intensities of the characteristic peaks corresponding to the different crystalline phases can be used to determine the fraction of each phase in the sample. Two different methods are commonly used. In the method proposed by Gregorio and Cestari [148], the wavelengths at 840 and 763 cm^{-1} are considered to be representative of β and α phase, respectively, and the relative fraction of β phase can be determined using the equation:

$$F(\beta) = \frac{A_\beta}{1.3A_\alpha + A_\beta}, \tag{5.5}$$

where A_α and A_β are absorbancies at 763 and 840 cm^{-1}, respectively.

The calculated results are tabulated in Table 5.6. From the table as expected we see that a melt-pressed PVDF homopolymer shows a high fraction of α phase. Interestingly, though a 70/30 P(VDF-

TFE) shows similar characteristics to that of the homopolymer in both WAXD scan and FTIR spectra, it shows a major β phase. 25 mol% of TrFE comonomer results in a copolymer with the highest fraction of all-*trans* β phase (88 %).

Table 5.6: Fraction of different crystalline phases in PVDF-based polymers calculated from characteristic FTIR absorption peaks using the method suggested by Gregorio and Cestari [148].

Polymer	**Preparation technique**	$T_{m>3}$ **[%] 840 cm^{-1}**	TG^+TG^- **[%] 763 cm^{-1}**
PVDF	melt-pressed	34	66
P(VDF-TFE) (70/30 mol %)	extruded	63	37
P(VDF-TrFE) (75/25 mol %)	drop-cast	88	12
P(VDF-TrFE-CFE) (62.2/29.4/8.4 mol %)	drop-cast	63	37

Though this method can be used to determine the fractions of the α and β phases relative to each other in PVDF homo- and co-polymers, it is clearly not suitable for a P(VDF-TrFE-CFE) terpolymer which clearly shows the presence of a γ phase. In fact, we also observe the presence of a certain γ phase in copolymers as well in Figure 5.8. Hence, it is more applicable to use a method which takes into account the presence of γ phase. Previously, a method based on that by Osaki *et al.* [157] has been used to calculate the crystalline fractions in a PVDF-based terpolymer [51, 160] using Equation 5.6.

$$F_i = \frac{A_i}{A_I + A_{II} + A_{III}}, \tag{5.6}$$

where $i = I, II, III$ and A_I, A_{II}, A_{III} are the absorbancies of the chain conformations showing β (all-*trans* $T_{m>3}$ peak at 1283 cm^{-1}), γ (peak at 506 cm^{-1}), and α (peak at 613 cm^{-1}) phase, respectively. These absorption bands were chosen for analysis as they all represent motions associated with CF_2 units up to a reasonable extent [51, 151, 160]. The results of this method are shown in Table 5.7.

Table 5.7: Fraction of different crystalline phases in PVDF-based polymers calculated from characteristic FTIR absorption peaks using the method suggested by Osaki *et al.* [51, 157].

Polymer	**Preparation technique**	$T_{m>3}$ **[%] 1285 cm^{-1}**	TG^+TG^- **[%] 613 cm^{-1}**	$T_3G^+T_3G^-$ **[%] 506 cm^{-1}**
PVDF	melt-pressed	13	59	28
P(VDF-TFE) (70/30 mol %)	extruded	28	24	48
P(VDF-TrFE) (75/25 mol %)	drop-cast	74	3	24
P(VDF-TrFE-CFE) (62.2/29.4/8.4 mol %)	drop-cast	19	30	51

In the case of the terpolymer, we observe that it shows a maximum of γ phase followed by α phase crystals. This is similar to that found in other PVDF-based terpolymers [49, 51] and can be explained by the larger van-der-Waals radius of chlorine (1.8 Å) compared to those of hydrogen and fluorine (1.2 Å, and 1.35 Å, respectively). Considering the steric effects of their intrachain energies, the

larger van-der-Waals radius of chlorine would actually favor the formation of *trans* rather than *gauche* bonds. However, the bulky chlorine atom causes steric congestion in the chain and to relieve it the interchain spacing in the crystalline phase expands, and hence favors the neighboring chains to take up a TG^+TG^- conformation. The delicate balance of these effects leaves room for the inclusion of a certain number of *gauche* bonds in the terpolymer [161]. Thus the terpolymer primarily consists of non-polar and weak polar crystalline phases, which is responsible for its relaxor-ferroelectric behavior.

All the other PVDF-based homo- and co-polymers each show a different behavior. While the P(VDF-TFE) copolymer similar to the terpolymer shows a maximum of γ phase, the P(VDF-TrFE) copolymer shows a predominant β phase crystalline structure. Finally, a PVDF homopolymer similar to the method of Gregorio and Cestari shows high fraction of α phase. Overall, comparing the two different methods for determining the relative fraction of crystalline phases with that of the results from WAXD, it can be stated that the former method by Gregorio *et al.* is more suitable for PVDF-based homo- and co-polymers which show mainly α and β phases, while the method based suggested by Osaki *et al.* is more suitable for PVDF-based terpolymers, which show a strong presence of γ phase crystals.

6

Relaxations and Transitions in PVDF-based Ferroelectric and Relexor-Ferroelectric Polymers

Ferroelectric (FE) and relaxor-ferroelectric (RF) polymers based on PVDF homo-, co-, and ter-polymers show multiple relaxations and transitions, which can be observed using dielectric techniques such as dielectric relaxation spectroscopy (DRS), thermally stimulated depolarization currents (TSDCs) and thermal techniques such as differential scanning calorimetry (DSC).

6.1 Dielectric Techniques

6.1.1 Dielectric Relaxation Spectroscopy (DRS)

Figure 6.1a reveals typical dielectric spectra of a melt-pressed α PVDF film where the real (ε', permittivity) and imaginary parts (ε'', dielectric loss) of complex permittivity are plotted as a function of temperature at different frequencies. From the figure, at least two different processes can be identified, manifesting as steps in permittivity and peaks in dielectric loss. The same dielectric data is plotted as a function of frequencies at selected temperatures in Figure 6.1b. The processes found at low and high temperatures in Figure 6.1a are observed at higher frequencies and lower temperatures, respectively, in Figure 6.1b. Looking at Figure 6.1a, we can notice that as the temperature increases, both the processes show a shift with temperature, *i.e.*, frequency-dependent behavior – characteristic of a relaxation process. The first process present at low temperatures shows the highest loss and can be associated with unfreezing of molecular motions in the amorphous phase of the polymer manifesting as glass transition [162, 163, 164, 165]. This process is commonly referred to as the α_a/β relaxation. On fitting the dielectric loss peaks in Figure 6.1b with the Havriliak Negami (HN)-function and plotting the relaxation times (peak position of loss peaks) in an Arrhenius plot (relaxation time *vs.* inverse temperature) as

Table 6.1: Fit parameters for the α_a and α_c relaxations found in various PVDF-based homo-, co- and ter-polymers.

Sample	Preparation technique	Process	log(τ_0) [s]	E_a [eV]	T_v [K]	T_g [K]
α PVDF	melt-pressed	α_a/T_g	−9.7	0.06	199.7	225.3
		α_c/T_{mid}	−16.4	0.96	[-]	[-]
P(VDF-TFE) 70/30 mol %	extruded	α_a/T_g	−11.5	0.10	181.6	220.5
		α_c/T_{mid}	−17.9	0.97	[-]	[-]
P(VDF-TrFE) 75/25 mol %	drop-cast	α_a/T_g	−11.0	0.10	189.2	227.4
P(VDF-TrFE-CFE) 62.2/29.4/8.4 mol %	drop-cast	α_a/T_g	−13.2	0.17	177.6	234.2

shown in Figure 6.2, we can clearly see that the α_a process shows a non-linear Vogel-Fulcher-Tamman (VFT) behavior with an activation energy E_a of 0.06 eV. The other fit parameters are tabulated in Table 6.1. The obtained values are similar to those calculated previously [166, 167]. The glass-transition temperature T_g can be determined as the temperature at which the VFT curve shows a relaxation time of log τ = 2 s (τ = 100 s) [166, 168]. For α PVDF, a T_g of 225.3 K (−47.9 °C) was obtained by extending the VFT curve to lower temperatures as shown in Figure 6.2, which is the same as that found in literature using DRS [163, 166] and close to the value derived from other methods [129, 167, 169, 170].

On the other hand, the second process occurring at higher temperatures in Figure 6.1a and lower frequencies in Figure 6.1b is commonly referred to as the α_c/α relaxation and usually assigned to motions taking place in the crystalline regions of the polymer [162, 163, 164, 171, 172, 173]. However, as will be explained later in Chapter 7, multiple processes with different origins are proposed to take place in this temperature range referred to as the mid-temperature range transitions. Hence, together this process will be denoted as T_{mid} relaxation. The process obeys Arrhenius' law and yields a linear plot as shown in Figure 6.2. The slope of the curve results in an E_a of 0.96 eV. The fitted parameters (Table 6.1) agree well with those reported in literature [164, 166, 172, 174]. It is to be noted that the notations α_a and α_c refer to the dielectric relaxation processes, while the notation α PVDF is used to denote the crystalline phase of the ferroelectric polymer.

The dielectric spectra of PVDF-based ferroelectric copolymers P(VDF-TFE) and P(VDF-TrFE) are shown in Figures 6.3 and 6.4. Comparing the spectra with that of PVDF (Figure 6.1a), we can observe that similar to PVDF both the copolymers show a glass-transition relaxation at lower temperatures. While the P(VDF-TFE) copolymer clearly shows a T_{mid} process, it is very weak in a P(VDF-TrFE) copolymer, visible only as a shoulder in ε' curve. In addition to it, the TrFE based copolymer shows a new transition around 125 °C whose peak position does not show a shift with temperature, *i.e.*, frequency-independent behavior – characteristic of a structural transition. From literature, this process can be identified with the ferroelectric-to-paraelectric (F-P) transition or Curie transition (T_C) [129, 175]. The corresponding

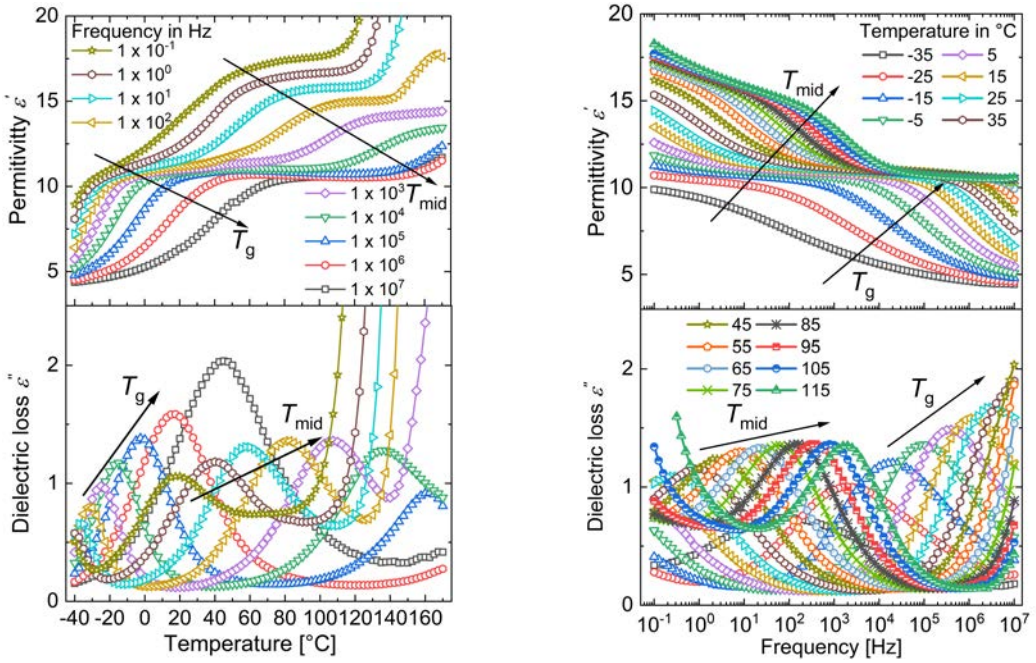

(a) **(b)**

Figure 6.1: Permittivity (ε') and dielectric loss (ε'') of a melt-pressed α PVDF film plotted (a) as a function of temperature at different frequencies and (b) as a function of frequency at different temperatures.

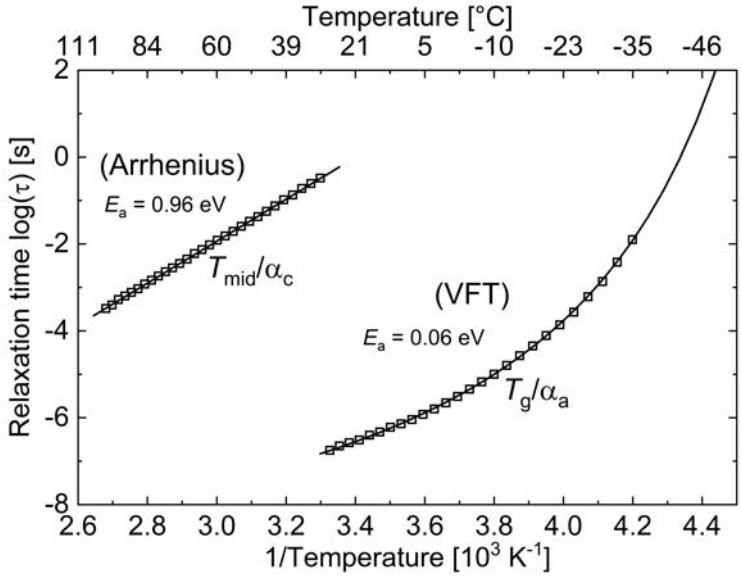

Figure 6.2: Arrhenius plot of a melt-pressed α PVDF film.

peak in ε'' measurement is seen around 122 °C. Adding to it, T_C has also been observed in stretched P(VDF-TFE) copolymer films of similar composition around 110 °C (Section 10.6). Here, in the case of the dielectric spectra of an un-stretched P(VDF-TFE) sample shown in Figure 6.3, the Curie transition is masked by the T_{mid} process which shows a continuous shift with temperature.

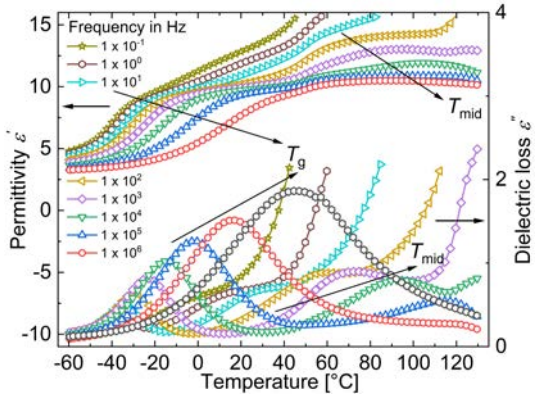

Figure 6.3: Permittivity (ε') and dielectric loss (ε'') of a commercial extruded P(VDF-TFE) 70/30 mol % film plotted as a function of temperature at different frequencies.

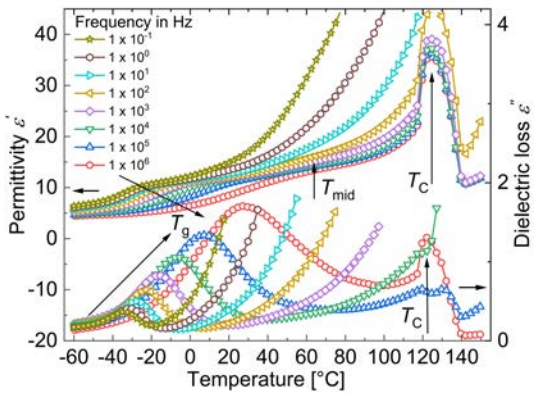

Figure 6.4: Permittivity (ε') and dielectric loss (ε'') of a drop-cast and annealed P(VDF-TrFE) 75/25 mol % film plotted as a function of temperature at different frequencies.

Finally, Figure 6.5 shows the double-log plot of ε' and ε'' recorded on a drop-cast and annealed P(VDF-TrFE-CFE) terpolymer. The permittivity curves show a broad peak around 20 °C, which shifts to higher temperatures with increase in frequency. This broad peak corresponds to the Curie transition, which occurs at a much lower temperature than observed in PVDF-copolymers. These features are characteristic of a typical relaxor-ferroelectric material [48, 136, 176]. Looking at the dielectric loss spectra, as expected, T_g relaxation is observed at lower temperatures similar to ferroelectric polymers. In case of the Curie transition, it is observed around 12 °C at low frequencies (with frequency-independent behavior). As the frequency increases, we can see that both the glass and Curie transitions merge with each other, and at 10 kHz we observe a single peak. Above this frequency, the superimposed peak shows relaxation characteristics [49, 177]. The evolution and subsequent superposition of the two processes can be better visualized on a 3D plot of dielectric loss (ε'') shown in Figure 6.6.

Overall, from the dielectric spectra of PVDF-based FE and R-F polymers, we can see clear differences between them. While an α PVDF homopolymer does not show an observable Curie-transition temperature (T_C), it is masked in the case of an un-stretched 70/30 mol % P(VDF-TFE) copolymer film and seen at a higher temperature in a P(VDF-TrFE) 75/25 mol % copolymer. In the case of an annealed R-F P(VDF-TrFE-CFE) terpolymer (62.2/29.4/8.4 mol %), the addition of the termonomer lowers the T_C below RT ($\approx$12 °C). Looking at the VFT curves in Figure 6.7, clear differences in their T_g are also observed. The calculated T_g values at $\log(\tau) = 2$ s are listed in Table 6.1. The 70/30 mol % P(VDF-TFE)

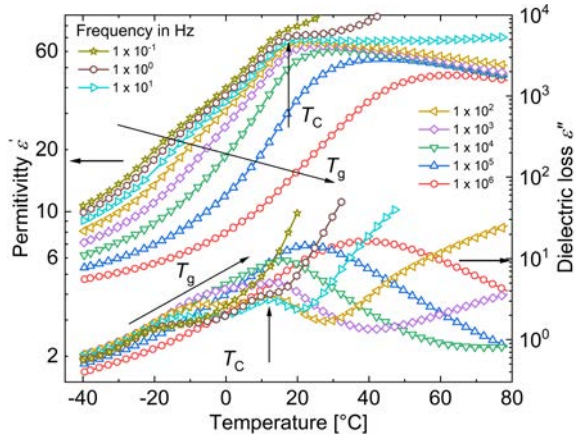

Figure 6.5: Permittivity (ε') and dielectric loss (ε'') (logarithmic scale) of a drop-cast and annealed P(VDF-TrFE-CFE) 62.2/29.4/8.4 mol % terpolymer plotted as a function of temperature at different frequencies.

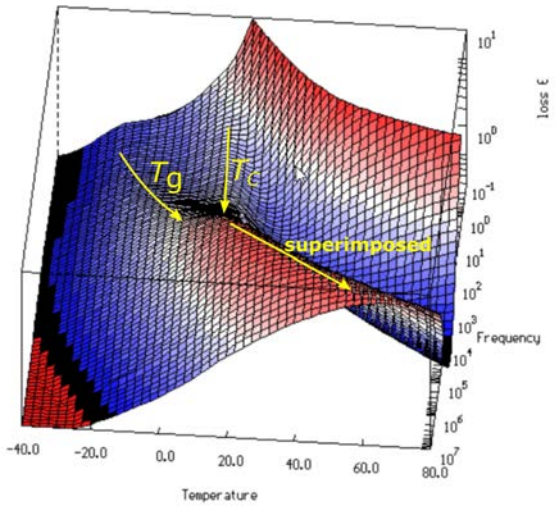

Figure 6.6: 3D dielectric loss (ε'') plot of a drop-cast and annealed P(VDF-TrFE-CFE) 62.2/29.4/8.4 mol % terpolymer as a function of frequency and temperature.

copolymer shows the lowest T_g, followed by an α PVDF and a 75/25 mol % P(VDF-TrFE) copolymer, both of which show very similar values. Finally, a 62.2/29.4/8.4 mol % P(VDF-TrFE-CFE) terpolymer exhibits the highest T_g as expected by the inclusion of the large CFE termonomer. On the other hand, T_{mid} process in both α PVDF and P(VDF-TFE) shows similar activation energies as shown in Figure 6.8 and tabulated in Table 6.1.

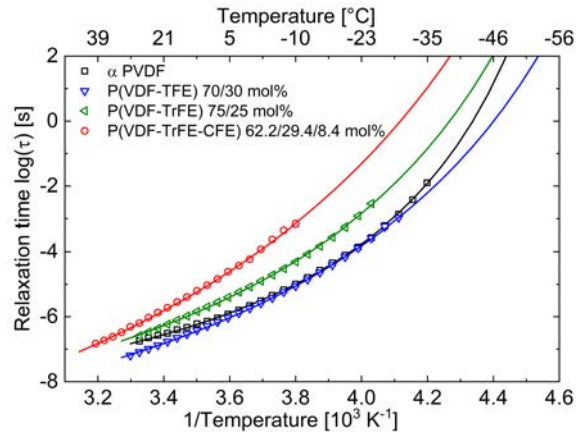

Figure 6.7: Arrhenius plot showing the relaxation times for α_a/T_g relaxation of various PVDF-based homo-, co- and ter-polymers.

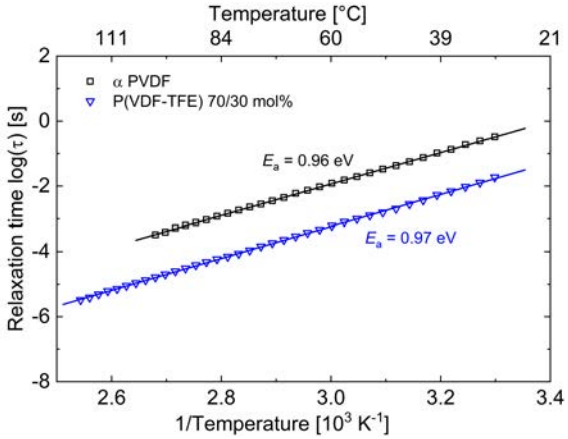

Figure 6.8: Arrhenius plot showing the relaxation times for α_c/T_{mid} relaxation of an α PVDF homopolymer and a P(VDF-TFE) 70/30 mol % copolymer.

Looking at the dielectric properties of the different polymers tabulated in Table 6.2, we can observe that a P(VDF-TrFE-CFE) terpolymer exhibits a very high permittivity near its Curie transition, which

lies near RT, on comparing with PVDF homo- and co-polymers. Big differences are also observed in the permittivities of a 70/30 mol % P(VDF-TFE) and 75/25 mol % P(VDF-TrFE) copolymer. It is to be noted that the dielectric properties of PVDF-based polymers depend on various parameters such as method of preparation, subsequent processing, composition of co- and ter-monomers.

Table 6.2: Important dielectric properties derived from the dielectric spectra of various PVDF-based homo-, co- and ter-polymers.

Sample	**Preparation technique**	ε'_{max} **[-]** 1 **kHz**	T_C [°C] ε' (1 **kHz**)	ε''(1 **kHz**)
α PVDF	melt-pressed	12	[-]	[-]
P(VDF-TFE) 70/30 mol %	extruded	13	[-]	[-]
P(VDF-TrFE) 75/25 mol %	drop-cast	39	125	122
P(VDF-TrFE-CFE) 62.2/29.4/8.4 mol %	drop-cast	73	26	14

6.1.2 Thermally Stimulated Depolarization Currents (TSDCs)

As mentioned in Section 3.5, TSDC serves as a powerful tool to study the relaxations and transitions in polymers. It can be used as a complementary technique to DRS. Figure 6.9 shows the TSDC plot of various PVDF-based polymers. Several peaks can be identified in the depolarization current curve of a melt-pressed α PVDF film. The peak found at the low temperature range at $-46\,^{\circ}$C is identified with the glass-transition process based on the results from DRS and previous measurements on PVDF [169, 174, 178, 179]. The corresponding T_g in the copolymers can be identified in the similar temperature range with P(VDF-TrFE) showing a slightly higher T_g peak than P(VDF-TFE). The peak values are reported in Table 6.3. In the case of an annealed P(VDF-TrFE-CFE) terpolymer, as expected, the glass transition moves to a higher temperature and is observed as a shoulder around $-27\,^{\circ}$C [177, 180, 181].

An additional shoulder is seen around $-50\,^{\circ}$C in the depolarization curve of the terpolymer, suggesting that there might be localized regions in the amorphous phase rich in VDF molecules. As the samples are further heated, a new transition can be identified between -30 and $20\,^{\circ}$C in the form of a peak in the terpolymer and as a shoulder in the PVDF homo- and co-polymers. This has been referred to as an upper glass-transition process, primarily taking place within the tie and cilia molecules in the constrained amorphous phase [129, 174, 177, 180, 182] and can be grouped with the other processes taking place in the mid-temperature region. The presence of this second T_g can be also revealed by peak fitting of dielectric loss data measured using DRS. Figure 6.10 shows the dielectric strength $\Delta\varepsilon$ plotted as a function of temperature which was obtained as a result of fitting loss peaks (fitted using HN function) of a melt-pressed α PVDF film depicted in Figure 6.1b. Two peaks are observed from the figure around 0 and 80 °C. By comparing the first peak around 0 °C with the corresponding TSDC

peak observed around the same temperature in a α PVDF film depicted in Figure 6.9, we can assign it to an upper T_g. The second broad peak centered around 80 °C can be associated with the conformational disorder relaxation process (another mid-temperature transition), as will be shown later using other techniques (Section 7.4). Though this peak can be also used to explain the second depolarization peak of the PVDF sample in Figure 6.9, the depolarization peaks found in the temperature range from 40 to 100 °C in the TSDC plot are due to real charges in the polymer material and hence, do not have origin in distinct dipolar motions [172, 177, 183, 184, 185]. Finally, the peaks around 125 °C in the P(VDF-TrFE) and P(VDF-TrFE-CFE) are as a result of Curie and melting transitions, respectively [177].

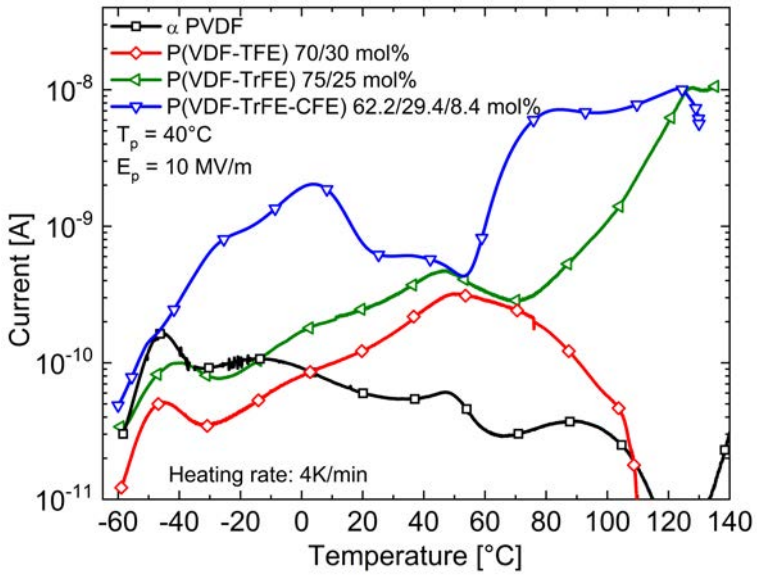

Figure 6.9: TSDC spectra of various PVDF-based homo-, co- and ter-polymers. The samples were poled with electric field E_p = 10 MV/m at a poling temperature T_p = 40 °C. Symbols are added to the continuously measured curves in order to facilitate their identification.

6.2 Thermal Techniques

Differential Scanning Calorimetry (DSC) is yet another useful thermal technique to characterize the various endo- and exo-thermic processes in a polymer material namely glass, melting transition, secondary crystallization, *etc*. The DSC thermogram of various PVDF-based polymers during first heating and cooling is shown in Figure 6.11.

In accordance with DRS and TSDC measurements above, the glass transition occurs as a weak step in the endothermic heating curves between −50 and −30 °C in the homo- and co-polymers, and as a broad step between −30 and 20 °C in the terpolymer. The calculated T_g values are tabulated in Table 6.3. The obtained values are in the similar range of that observed from DRS and TSDC. In the

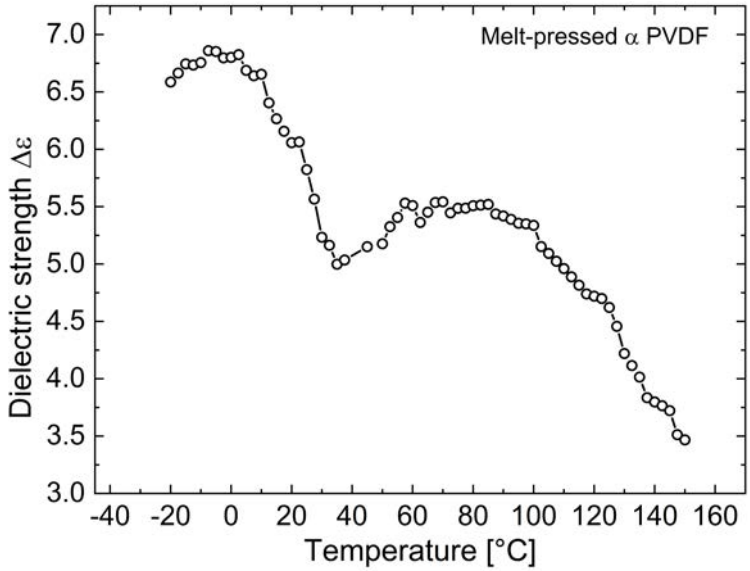

Figure 6.10: Plot of dielectric strength ($\Delta\varepsilon$) *versus* temperature derived from fitting dielectric loss peaks of a melt-pressed α PVDF film shown in Figure 6.1b.

case of a P(VDF-TrFE) copolymer, the step-change is very small. Hence, it is difficult to calculate a reliable value from DSC. The structural transitions in PVDF-based polymers appear as endothermic peaks above the glass-transition temperature range. This includes the Curie transition in the terpolymer around 17 °C and in the case of a P(VDF-TrFE) copolymer around 127 °C. In the temperature range between 30 and 80 °C, an additional peak/step is seen which can be assigned to the T_{mid} temperature transition [81, 119]. This transition appears in all PVDF-based polymers. Finally, at high temperatures, the polymers molecules melt resulting in the melting transition T_{m}. From Figure 6.11 and Table 6.4, we can observe that the homopolymer has the highest melting point, followed by the copolymers. The terpolymer shows the lowest melting point. This denotes that the addition of a second and third monomer to PVDF-homopolymer chains reduces the T_{m} of the resultant polymer.

Table 6.3: Comparison of glass-transition (T_{g}) and Curie-transition (T_{C}) temperatures calculated from various techniques for PVDF-based ferroelectric and relaxor-ferroelectric polymers.

Sample	T_{g} [°C]			T_{C} [°C]		
	DRS (ε'') at log(τ) = 2 s	**TSDC 4 K/min**	**DSC 10 K/min**	**DRS (ε'') 1 kHz**	**TSDC 4 K/min**	**DSC 10 K/min**
α PVDF (melt-pressed)	−47.9	−45.7	−42.7	[-]	[-]	[-]
P(VDF-TFE) 70/30 mol % (extruded)	−52.7	−45.4	−43.0	[-]	[-]	[-]
P(VDF-TrFE) 75/25 mol% (drop-cast)	−45.8	−40.3	[-]	122.0	127.8	127.6
P(VDF-TrFE-CFE) 62.2/29.4/8.4 mol% (drop-cast)	−39.0	−26.0	−17.8	14.0	[-]	17.1

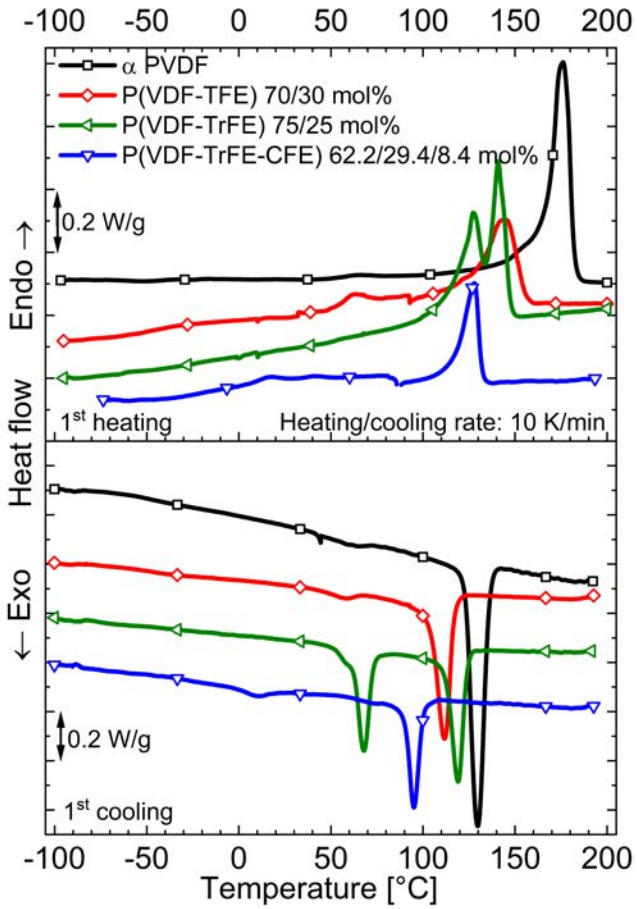

Figure 6.11: DSC thermograms of ferroelectric PVDF-based homo-, co-polymers and relaxor-ferroelectric P(VDF-TrFE-CFE) terpolymer during the first heating and cooling cycle. Symbols are added to the continuously measured thermal scans in order to facilitate their identification.

On cooling the polymer melt, crystallization occurs typically at a lower temperature than the melting point, identified by an exothermic heat peak as seen in Figure 6.11. The PVDF-based polymers follow a similar trend as observed during heating, *i.e.*, the homopolymer crystallizes first, followed by the co- and ter-polymers. The heat-of-fusion/enthalpy of melting (ΔH_m) and enthalpy of crystallization (ΔH_c) values are similar for the respective polymers as observed from Table 6.4. Hence the fraction of primary crystals formed remains the same before and after heating. In case of the Curie transition, during cooling, a shift to a lower temperature is observed for a P(VDF-TrFE) copolymer, *i.e.*, exhibits a thermal hysteresis. On the other hand, a terpolymer shows similar T_C values during heating and cooling. All the PVDF-based ferroelectric and relaxor-ferroelectric polymers show an exothermic peak between 50 and 80 °C corresponding to the T_{mid} transition. In the case of a P(VDF-TrFE) copolymer, though the transition is observed as a relaxation-like step during heating, it is visible as a shoulder in the low-temperature tail of the Curie-transition peak during the cooling cycle. Finally, in the lower temperature end, a glass-

transition step is seen, below which the molecular motions of the polymer chains are restricted.

Table 6.4: Melting point (T_m) and crystallization temperature (T_c) for various PVDF-based polymers along with their enthalpy of melting (ΔH_m) and enthalpy of crystallization values (ΔH_c).

Sample	T_m **[°C]**	ΔH_m **[J/g]**	T_c **[°C]**	ΔH_c **[J/g]**
α PVDF (melt-pressed)	176.2	57.4	129.8	−52.6
P(VDF-TFE) 70/30 mol % (extruded)	145.6	30.3	112.3	−31.7
P(VDF-TrFE) 75/25 mol % (drop-cast)	141.0	24.6	119.1	−24.7
P(VDF-TrFE-CFE) 62.2/29.4/8.4 mol % (drop-cast)	128.0	21.3	95.1	−18.1

7

Origin of Mid-Temperature Range Transitions in PVDF-based Polymers[1]

7.1 Existence of Mid-Temperature Range Transition(s)

Figure 7.1 shows the DSC thermograms of various PVDF-based homo-, co- and ter-polymers subjected to different heat treatments, recorded during the first heating run on film samples. From the figure, on all samples, irrespective of preparation conditions, between 30 and 70 °C either a peak or a step is observed in the heating curve (red box). This transition occurs at an intermediate temperature either between the glass transition (occuring below 0 °C) and the Curie transition (in P(VDF-TrFE) and P(VDF-TFE)), or between the glass and melting transition in PVDF-based homo- and co-polymers (where no clear Curie transition is observed) or between the Curie and melting transitions in a P(VDF-TrFE-CFE) terpolymer, respectively. Hence, it can be referred to as the mid-temperature transition (T_{mid}). This transition has been identified and studied already as early as in the 1960s [163, 165], *i.e.*, even before the discovery of ferroelectricity in PVDF in 1969 [11]. However, in spite of its well-known existence, even five decades later, a complete understanding of this transition was yet to be reached. Multiple explanations – some contradictory to each other – have been proposed to explain the origins of this transition. Some of the different theoretical approaches are listed and briefly reviewed below.

[1]Parts of this chapter are adapted from T. Raman Venkatesan *et al.*, "Origin of the mid-temperature transition in vinylidenefluoride-based ferro-, pyro- and piezoelectric homo-, co- and ter-polymers", *Mater. Res. Express*, 7(6): 065301, 2020 [81] and T. Raman Venkatesan *et al.*, "The Mystery behind the Mid-Temperature Transition(s) in Vinylidenefluoride-based Homo-, Co- and Terpolymers – Has the Puzzle been Solved?", *IEEE Trans. Dielectr. Electr. Insul.*, 27(5), 1446-1464, 2020 [119].

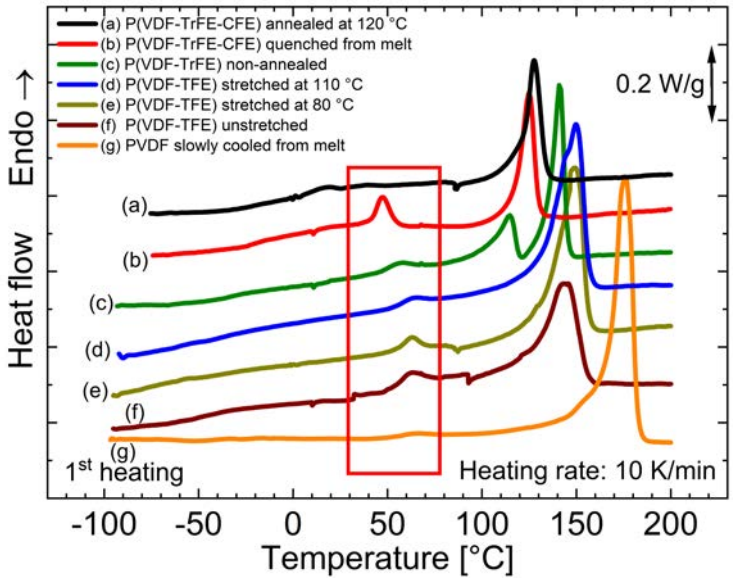

Figure 7.1: DSC thermograms of PVDF, P(VDF-TFE), P(VDF-TrFE) and P(VDF-TrFE-CFE) subjected to different heat treatments, recorded during the first heating run on film samples.

7.2 Proposed Origins of the Mid-Temperature Transition(s) - The Situation

Figure 7.2 shows the permittivity and dielectric-loss spectra of an un-stretched poly(vinylidene fluoride-tetrafluroethylene) (P(VDF-TFE)) film with a VDF/TFE molar ratio of 70/30, respectively, plotted as a function of frequency at selected temperatures. The spectra look similar to that of α PVDF shown in Figure 6.1b, which reveals at least two processes. From Section 6.1, we know that the process at higher frequencies and lower temperatures (below RT) corresponds to the glass-transition (T_g) relaxation – exhibiting VFT behavior. The other process occurring at lower frequencies and at higher temperatures, and exhibiting a frequency-dependent peak shift obeys Arrhenius' law. This latter process commonly referred to as the α_c relaxation can be associated with the T_{mid} transition found in DSC (Figure 7.1). Upon stretching, the T_{mid} process tends to disappear – as shown in Figure 7.3.

The frequency dependence of the T_{mid} transition and the fact that it disappears after stretching can be explained as an upper glass transition ($T_g(U)$) that is associated with the constrained amorphous regions between crystallites. Constrained amorphous phase refers to those amorphous regions which are adjacent or embedded between crystallites [186, 187, 188]. As their movement is restricted between crystalline regions, they do not undergo a conventional glass transition (T_g or $T_g(L)$) at which the chains in continuous amorphous regions gain sufficient energy to move. As stretching leads to the removal of the constrained amorphous regions, it is expected to eliminate the $T_g(U)$ associated with it. This behavior was first shown in the work of Peterlin and Elwell [165] and later in the work of other authors [189,

190, 191]. A little later, Boyer proposed a second glass transition in other semi-crystalline polymers in addition to PVDF [192]. This explanation was later adopted by several other authors (*e.g.* [182, 186, 193, 194]).

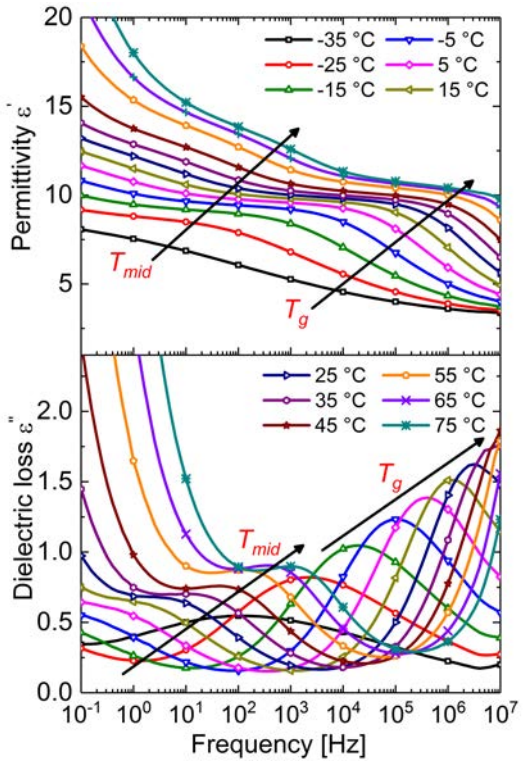

Figure 7.2: The permittivity and dielectric loss of an un-stretched P(VDF-TFE) film as a function of frequency from 10^{-1} to 10^{7} Hz, plotted at selected temperatures. The curves were measured with 10 data points per frequency decade, and a few symbols were added to each curve in order to facilitate identification.

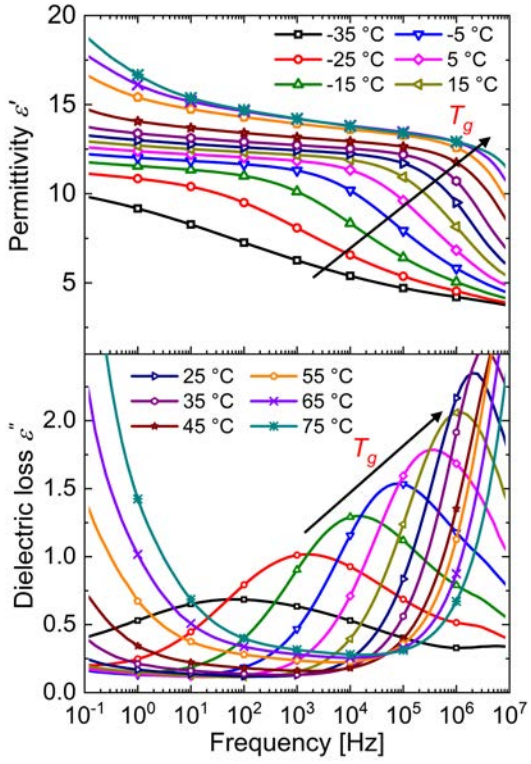

Figure 7.3: The permittivity and dielectric loss of a P(VDF-TFE) film stretched at a temperature of 110 °C, plotted as a function of frequency from 10^{-1} to 10^{7} Hz at selected temperatures. The curves were measured with 10 data points per frequency decade, and a few symbols were added to each curve in order to facilitate identification.

However, when the dielectric spectra of the stretched sample are plotted as a function of temperature at different frequencies as in Figure 7.4, we observe – even after stretching – a small residue of the mid-temperature transition as a shoulder around 60 °C. The transition is more clearly seen in the permittivity spectra on the top of the Figure as a frequency-independent peak – characteristic for a structural transition. From the DSC endotherms shown in Figure 7.1, we notice the T_{mid} transition to be present also in stretched P(VDF-TFE). Additionally, a similar result has also been previously observed by Frübing *et al.* in stretched films of a poly(vinylidenefluoride-hexafluoropropylene) P(VDF-HFP) copolymer film several years ago [45]. Further, it was calculated that the specific heat capacity C_{p} of PVDF already reaches its expected value when PVDF undergoes the conventional glass transition at T_{g}, so it was stated

that there is no possibility for it to increase further at T_{mid} [195]. All the above observations either contradict the hypothesis of an upper glass transition or at least do not provide a complete picture of the mid-temperature transition.

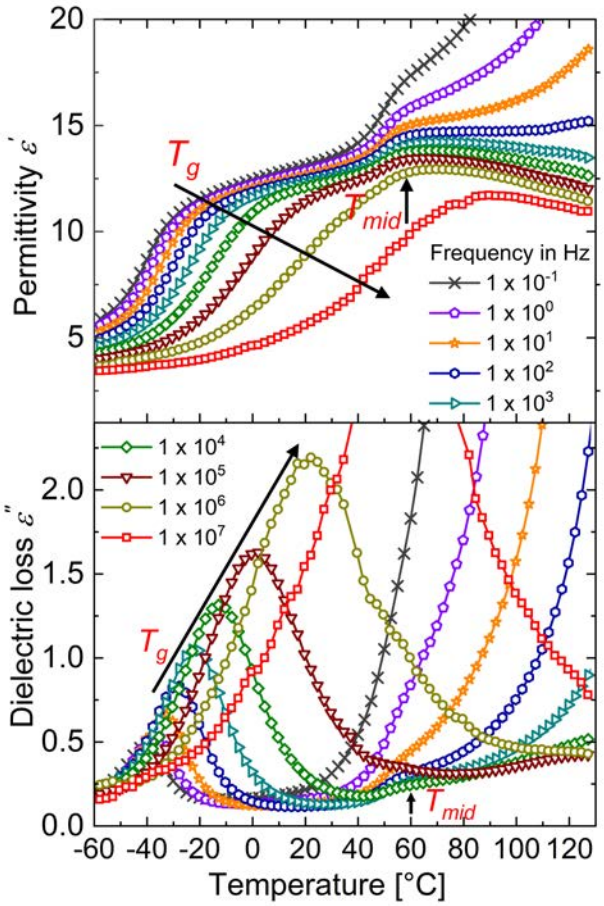

Figure 7.4: The permittivity and dielectric loss of a P(VDF-TFE) film stretched at 110 °C plotted as a function of temperature at fixed frequencies from 10^{-1} to 10^{7} Hz.

The frequency-independence of the transition in Figure 7.4 may also indicate a structural transition associated with the melting of secondary crystals formed during storage of the sample above its conventional T_g. In 1976, Callens *et al.* showed from their static and dynamic mechanical, as well as their TSDC measurements on a α PVDF that the α relaxation shows Arrhenius behavior. They proposed that the α process is due to motions in the crystalline phase [169] and suggested two hypotheses to explain the origins of the process. The first proposal was pre-melting crystalline transitions related to specific molecules present in both amorphous and crystalline regions. This process is observed in more than 50 % of all semi-crystalline polymers [196]. The second hypothesis was the presence of different crystalline fractions. However, when comparing their work with that of Kakutani [171], they had described the latter process as less suitable, since it is observed at high temperatures around 110 °C. Shortly after this, Kepler

and Anderson suggested that secondary crystals that melt at T_{mid} can contribute to the pyroelectricity of PVDF observed at RT [197]. This idea of the melting of secondary crystals at T_{mid} was concluded from several studies on PVDF and other semi-crystalline polymers [45, 65, 162, 198, 199, 200]. Further, the non-reversible heat-flow endothermic peak associated with the T_{mid} transition seen around 60 °C from the modulated DSC (mDSC) thermogram of a stretched P(VDF-TFE) film during first heating shown in Figure 7.5 points towards a structural process such as secondary crystallization [65].

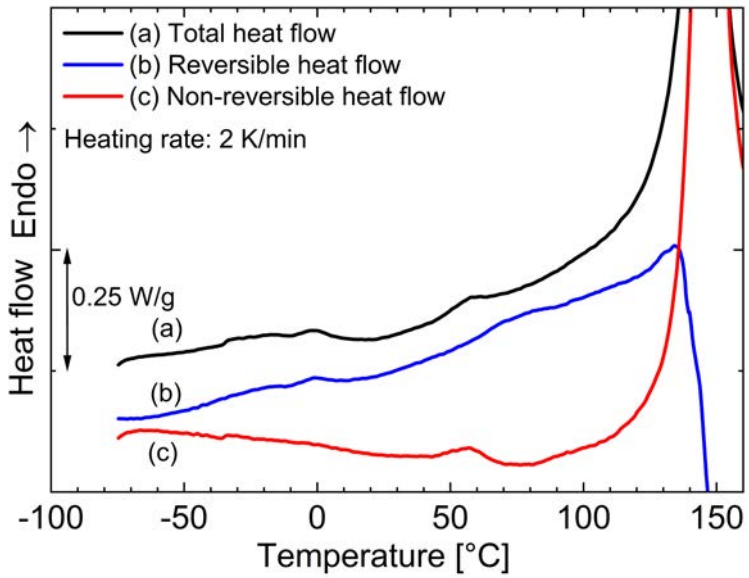

Figure 7.5: Modulated DSC thermogram of a P(VDF-TFE) film stretched at 110 °C during first heating.

In addition to the above features, the T_{mid} endothermic peak seen around 63 °C during the first heating disappears during the second heating in Figure 7.6. As secondary crystallization is a process that requires time, the absence of its corresponding melting endotherm during the second heating can be expected. Upon subsequent cooling and storage of the sample at room temperature for one week, we notice that the T_{mid} peak reappears. All these findings strengthen the argument that the T_{mid} transition is a result of secondary crystallization. However, looking at the DSC exotherm during cooling in Figure 7.7, we observe a clear peak at 58 °C corresponding to the T_{mid} endothermic peak seen during the first heating. Yet again, the second explanation of the T_{mid} transition as a result of secondary crystallization is also not completely valid.

In a third explanation found commonly in the literature, motions within the form II or α crystalline phase are attributed to this transition and it is referred to as the α_c relaxation [163]. A number of mechanisms have been proposed to describe it. These mechanisms can be commonly grouped as taking place in the surface of the crystals [201], at the interior [202] or a combination of both [164]. Nakagawa and Ishida [164] studied the relaxation time and the magnitude of this transition on the basis of a two-site

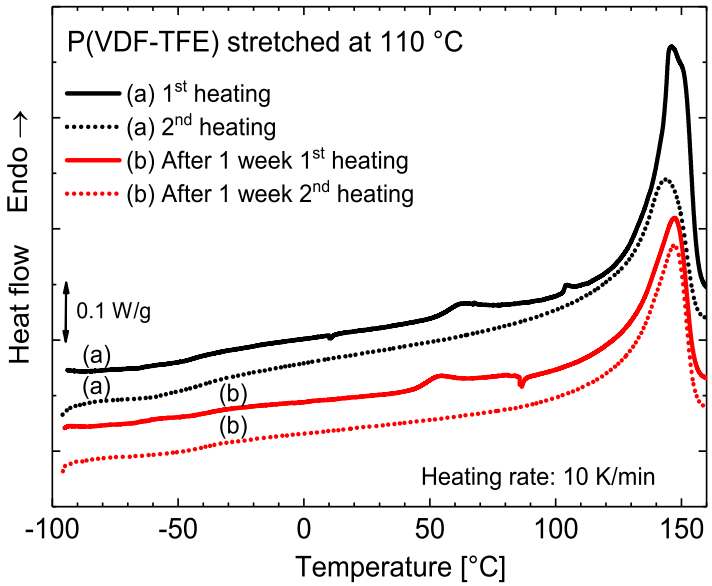

Figure 7.6: 1st- and 2nd-run DSC thermograms on P(VDF-TFE) stretched at 110 °C before (upper curves in black) and after (lower cures in red) storage at room temperature for one week.

model and concluded that this relaxation is attributed to molecular motions not only in the folds of the lamellar crystals, but also to those in the interior of the crystals. McBrierty *et al.* [203] added that the interpretation of Nakagawa and Ishida included also motions of the β' relaxation. These motions are assigned to the constrained amorphous chains. They proposed two models for α_c relaxation. The first model considers complete rotational oscillation motion of restricted amplitude about the main axis of crystalline chains. The model predicted that only about 37% of the crystalline chains rotate, while the others remain rigid. In the second model, complete rotation of the crystalline chains in the region of defects was considered. According to this model, only 5% of defects need to be present in the material, which is the case of H-H and T-T defects normally present on PVDF [204, 205].

Miyamato *et al.* [173] assumed that the molecular motions accompanying the α_c relaxation is due to the fluorine atoms in the TG^+TG^- chains of the non-polar α-phase (form II) crystals which either flip from up to down or *vice versa* ($TG^+TG^- \rightarrow G^+TG^-T$) as shown in Figure 7.8. This process is referred to as *conformational disorder (condis)*. The resulting change in the dipole moment across the molecular axis results in the experimentally observed α_c relaxation. They had also proposed two models by which the relaxation can take place within the crystalline regions. The difference between the models was with respect to the movement of defects. In the first model, molecular motion (*condis*) is accompanied by the movement of defects and in the second model, the defects remain stationary with molecular rearrangement around it. In this case, the *condis* starts at the surface of a lamella and propagates in a chain by a worm-like motion to the other surface.

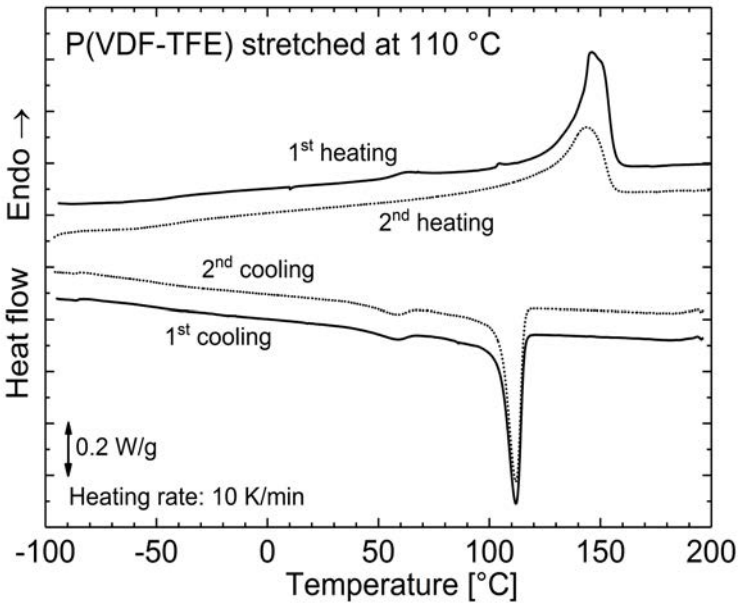

Figure 7.7: DSC thermograms of a P(VDF-TFE) film stretched at 110 °C during the 1st and 2nd heating and cooling cycles.

The concept of conformational disorder was supported by the works of Takashi *et al.* who showed that the molecules in form II crystals can have four different orientations depending on the direction of projection [206] and stated that the anti-phase domain structure suggested by Farmer *et al.* [207] favours up-to-down motion of α crystals [208]. They also reported from their X-ray diffraction results of PVDF a gradual change in the crystallographic axis along the *c*-direction above -3 °C of the α crystals (form II) with a temperature dependent up-and-down equilibrium above 97 °C [206, 209]. Later, based on previous dielectric results of Miyamato *et al.* and X-ray diffraction results of Takashi *et al.*, Loufkis and Wunderlich [195] adopted the same explanation to describe the T_{mid} transition observed between 47 and 77 °C on the DSC endotherms in their quenched α-PVDF samples [173, 206, 209]. They also showed that slow cooling from the melt freezes the up-to-down equilibrium associated with *condis* between 77 and 87 °C – observed as a DSC exotherm with a corresponding T_g-like relaxation step during heating. However, upon quenching, the *condis* peak was reported to shift to lower temperatures. Finally, subsequent heating was claimed to lead to un-freezing and re-organization of *condis* with an endothermic peak in the T_{mid} temperature range. It was stated that the endothermic T_{mid} peak can only be observed in quenched samples. Once the lower-temperature conformation relaxes with a *condis* reorganization, it cannot be re-introduced into the already grown crystals. Hence, the relaxation should be irreversible. Several other authors also agree with a *condis* relaxation (see *e.g.* Refs. [44, 45, 129, 162, 182, 187]). Frübing *et al.* associated the frequency-dependent (α_c) peaks in the dielectric spectra of P(VDF-HFP) (similar to the T_{mid} peaks of P(VDF-TFE) seen in Figure 7.2) to *condis* and found that the peaks disappeared after

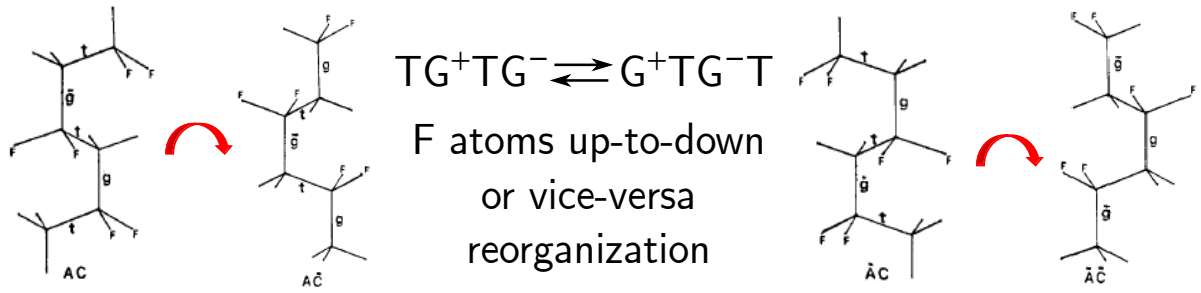

Figure 7.8: Conformational disorder process in α chains of PVDF. Adapted from the work of Loufakis and Wunderlich [195]. The letters A, $\overline{\text{A}}$, C and $\overline{\text{C}}$ refers to the orientation of the fluorine atom on the left, right, up and down direction, respectively.

stretching [45].

Even though the last explanation seems more convincing, certain aspects of the experimental results are still contradictory in themselves if we adopt the *condis* hypothesis. In Figure 7.1, we can clearly see that the endothermic peak is not only observed in quenched samples, but also in a non-annealed P(VDF-TrFE) sample and also as a step in a PVDF sample that was slowly cooled from the melt. In addition, as explained before, we see in Figures 7.6 and 7.7 that the process is reversible, as it re-appears in the DSC heating cycle after one week and as it is always present in the cooling cycle as an exotherm.

Apart from the above explanations, the interface effects should also be considered. As seen in the TSDC measurements in Figure 6.9, in the mid-temperature range between 30 and 80 °C, a depolarization peak is seen that can be assigned to the T_{mid} transition. The peak has been attributed to a Maxwell-Wagner Interface (MWI) polarization, which occurs as a result of injected charges trapped at the amorphous-crystalline (a-c) interfaces [177, 183]. Sasabe *et al.* was the first to identify this process and had labelled it as the α_{i} relaxation. Its existence was confirmed by several other authors such as Das-Gupta *et al.*, Mizutani *et al.*, Yamada *et al.* and Bamji *et al.* from their DRS and TSDC measurements on both α and β PVDF [172, 210, 211, 212, 213]. A brief review of the available literature regarding the T_{mid} peaks in TSDC can be found in the work of Doughty and Das-Gupta [214]. The injected space-charges at the a-c interface have various effects on the other properties of the polymer sample. Eberle and Eisenmenger reported that the MWI polarization can stabilize the crystallites in poled PVDF films [215]. The interfacial charge layers also play an important role behind the piezo- and pyro-electric activity of PVDF-based polymers as shown by several authors [184, 216, 217, 218]. From the above, it is clear that the interface effects need to be considered while an attempt is made to identify the origins of the T_{mid} transition.

7.3 Interrelated Origin(s) of the Mid-Temperature Transition - Hypothesis

Now, after a review of various references in the existing literature, we can actually see that some of the mechanisms proposed to explain the mid-temperature transition overlap. Even though the various authors used different terms or different ways of explaining, there are enough indications that the transition in question has interrelated origins. Furthermore, with the evidence gained from additional experiments, a new hypothesis can be formulated. Accordingly, the mid-temperature transition can be actually considered as an interrelated process where all the above-mentioned effects take place within a relevant temperature range [219].

Let us consider the amorphous-crystalline interphase where we have amorphous chains pinned at both sides to crystallites. These chain segments are usually known as tie molecules [186]. In addition, we have chain loops and cilia (*i.e.*, hair-like extensions) at the amorphous-crystalline interphase [65]. When the sample is below the mid-temperature transition temperature, as shown in the schematic illustrated in Figure 7.9(a), all these constrained amorphous chains are frozen. Above the glass transition, the "normal", almost un-constrained chains with random conformations (*i.e.*, those found inside a more or less continuous amorphous phase) unfreeze. However, the constrained amorphous phase (CAP) stuck between the crystallites still remains frozen. At the mid-temperature transition or just before it, the tie molecules along with the constrained amorphous phase unfreeze – leading to an upper glass-transition step. Upon further heating, the α crystals gain sufficient energy and also an additional degree of freedom to undergo conformational disorder ((b) in Figure 7.9). Then, when we continue to heat the sample, the imperfect crystals that might have formed either upon rapid quenching from the melt or during waiting (storage) periods will also melt (Figure 7.9(c)), which results in the endothermic peak that we see in the mid-temperature range of the DSC curves. The above changes in the crystalline, amorphous phase and their interphase result in the release of real or space charges from the amorphous-crystalline interface, observed as a MWI peak in TSDC measurements.

With the new hypothesis, we can predict the individual contributions of the above-mentioned mechanisms to the collective T_{mid} transition for different processing scenarios as shown in Table 7.1:

1. In films stretched at high temperatures, one would expect a low fraction of CAP and/or tie molecules, as the molecules can be easily oriented in a soft state - facilitated by the high temperature during stretching. The stabilization of the crystalline phase also hinders the formation of secondary crystals during storage. Here, the contribution would be expected to come mostly from conformational disorder, since it is present in all the VDF-based materials irrespective of the processing conditions (Figure 7.1). So, the T_{mid} transition is expected to be seen only as a small relaxation step in the

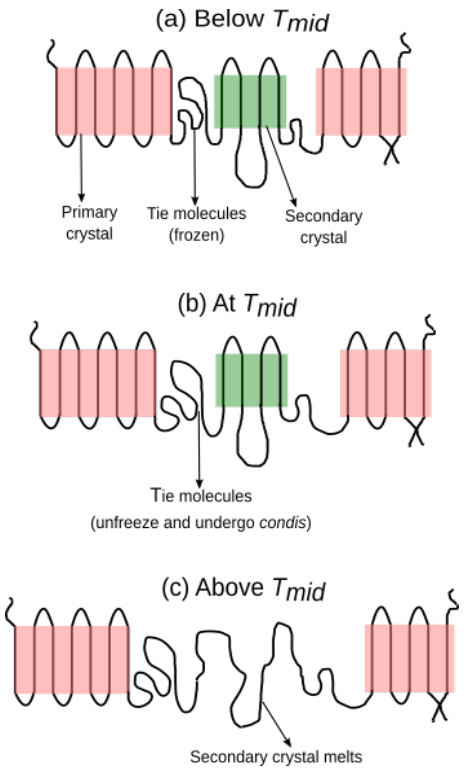

Figure 7.9: Schematic of the different processes presumably taking place together around T_{mid} at the amorphous-crystalline interphase of VDF-based homo-, co- and ter-polymers.

DSC endotherm.

2. In films annealed or slowly cooled from the melt, the fraction of amorphous-crystalline interphase would be the least, as annealing and slow cooling relieve and limit, respectively, constrained regions. In addition, annealing generally decreases the α phase fraction in VDF-based polymers [36, 220]. Thus, the contribution from *condis* would also be minimal, resulting in the weakest T_{mid} transition.

3. In films stretched at a low temperature, the lower stretching temperatures would prevent the complete $\alpha \rightarrow \beta$ phase transformation and also allow for a certain fraction of tie molecules/CAP to be present. This will permit for both conformational disorder to take place within the remaining form II/α crystalline regions and secondary crystals to be formed. However, the contribution from an upper glass-transition would be limited owing to the stretching. Hence, the former two processes can be expected to contribute to the bulk of the observed mid-temperature transition. Thus in DSC measurements, we would expect a small endothermic peak at T_{mid} .

4. In films that are quenched or non-annealed and un-stretched (e.g. drop-cast), the number of tie molecules would be the maximum. Also, the volume fraction of CAP would be higher resulting in a large *a-c* interphase area. This would lead to the observation of a strong $T_g(U)$ transition. In addition, the α-phase fraction (thermodynamically most favoured state) and the chances of secondary crystallization would be higher. This will result in a T_{mid} transition with strong contributions from all the different processes outlined before – manifesting itself as a strong endothermic DSC peak.

Table 7.1: Prediction of the type of the mid-temperature transition to be seen in DSC for different heat treatments.

Heat treatment	**No. of tie molecules/ Volume fraction of CAP**	$T_g(U)$	***Condis***	**Secondary crystallization**	T_{mid} **expected in DSC as**
Stretched (high temperature)	Low	↓	↑	↓	Relaxation step
Annealed/ slowly cooled	Least	↓	↑	↓	Weakest relaxation step
Stretched (low temperature)	Moderate	↓	↑	↑	Small endothermic peak
Quenched/ un-stretched/ non-annealed	High	↑	↑	↑	Large endothermic peak

The predictions of the hypothesis can be directly applied to the DSC curves shown in Figure 7.1. For example, in case of the samples stretched at high temperature such as a P(VDF-TFE) film stretched at 120 °C, we see that the mid-temperature transition looks like a relaxation-step. On the other hand, a P(VDF-TFE) film that was stretched at the lower temperature of 80 °C shows a small endothermic peak as predicted. Considering the case of an annealed and slowly cooled sample, the weakest relaxation is predicted as seen in the case of a PVDF or a P(VDF-TrFE-CFE) film. Finally, the DSC heating curves of a non-annealed P(VDF-TrFE) film, an un-stretched P(VDF-TFE) sample and a quenched P(VDF-TrFE-CFE) film all shown in Figure 7.1, exhibit a strong endothermic peak as listed in Table 7.1.

Figure 7.10 shows the dielectric spectra of an un-stretched P(VDF-TFE) film shown in Figure 7.2, but as a function of temperature instead of frequency. As seen in Figure 7.2, we observe both T_g and T_{mid} relaxation processes in the sample whose position shows a shift with temperature. Looking at the loss spectra, the T_{mid} process(es) already start(s) above 0 °C and, as the temperature increases, we see that the peak amplitude increases above 40 °C. From the proposed hypothesis, we know that the T_{mid} processes begin with the onset of the upper glass-transition process followed by *condis* relaxation. Hence, above 40 °C, we should have contributions from both of these processes, which can explain the

higher losses. Above 70 °C, we can see that the strength of the loss peaks is reduced, probably as a result of reduced contribution from an upper T_g process and the melting of secondary crystals. Hence, the primary contribution to T_{mid} should be from the *condis* process which continues up to the melting of α crystals [119]. This is also suggested by the gradual disappearance or reduction of loss peaks above 100 °C.

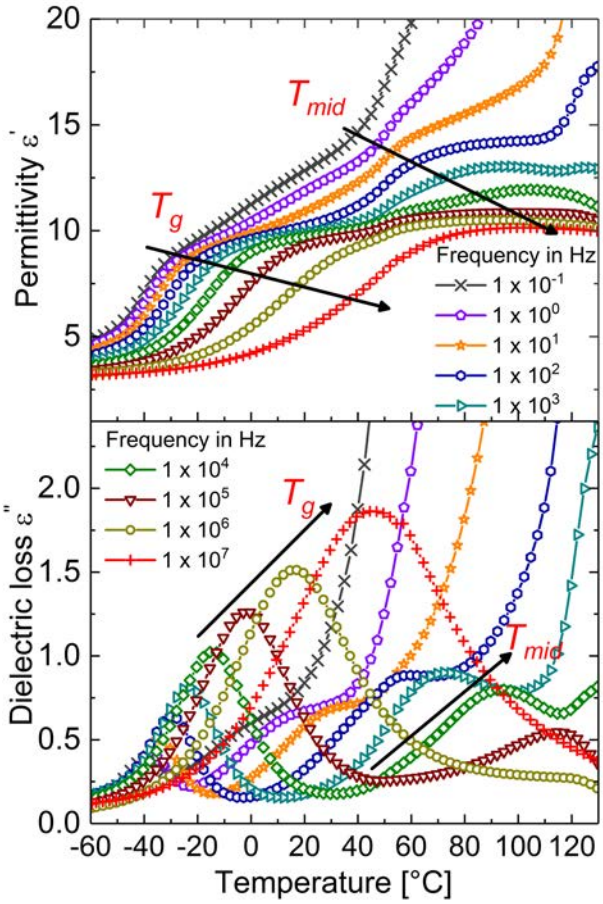

Figure 7.10: The permittivity and dielectric loss of an un-stretched P(VDF-TFE) film plotted as a function of temperature at fixed frequencies from 10^{-1} to 10^7 Hz.

7.4 Additional Evidence from Derivative Analysis of Dielectric Data

Derivative analysis of dielectric data can give additional information about the processes taking place in dielectric materials [74, 78] (Section 3.4.3.3). Hence these techniques were applied to the dielectric data of an un-stretched P(VDF-TFE) film shown in Figure 7.10. The results are depicted in Figure 7.11. In the derivative loss (ε''_{der}) curve starting with low temperature, we observe first the lower or conventional glass-transition, followed by the mid-temperature transition which manifests as a shoulder around 80 °C.

In the corresponding temperature coefficient of the permittivity ($\partial\,\varepsilon^{'}(T)/\partial\,T$) curve we observe the $T_g(L)$ peak at a lower temperature than that observed in the ε''_{der} curve. However, the main difference is seen in the mid-temperature region where we observe an additional transition occurring just before the T_{mid} transition. From the proposed hypothesis mentioned above, we can predict this transition to be a result of secondary crystals melting. Thus, it is shown that the melting endothermic process indeed occurs in a non-stretched sample and since it is usually masked by the *condis* relaxation, we do not observe it in the dielectric spectra. With the help of derivative techniques, it is possible to separate these individual processes taking place in the T_{mid} region. We also observe the Curie transition in the α_ε ($\partial\,\varepsilon^{'}(T)/\partial\,T$) curve around 125 °C, which is masked in Figure 7.10. Finally, the ε''_{der} curve in Figure 7.11 shows a peak around 137 °C just before melting of the primary crystals occur in the P(VDF-TFE) sample (*cf.* Figure 7.1). This peak could be a result of space-charge polarization due to the accumulation of real charges at the electrode-sample interface [83].

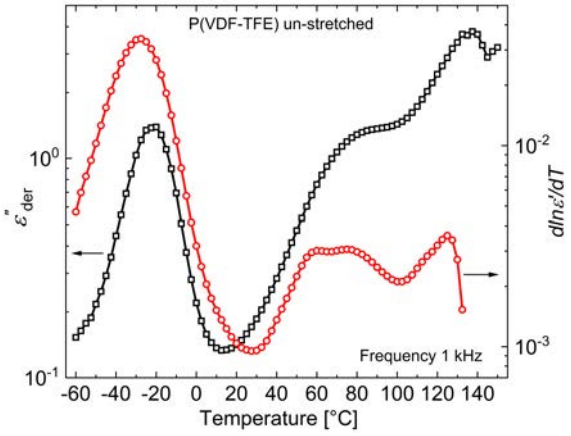

Figure 7.11: Isochronal representation of the "conduction-free" dielectric loss (ε''_{der}) along with the temperature coefficient of the permittivity $\partial\,\varepsilon^{'}(T)/\partial\,T = \alpha_\varepsilon$ of an un-stretched P(VDF-TFE) film at 1 kHz.

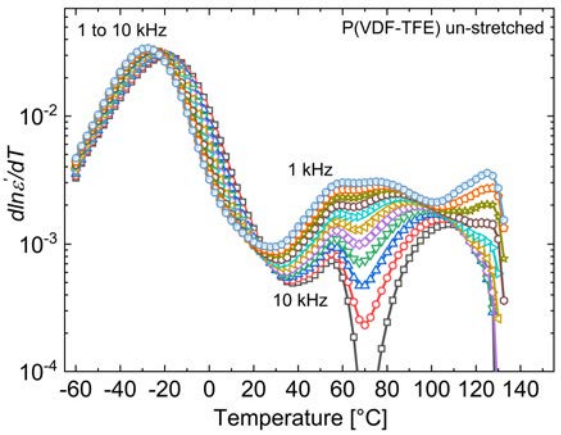

Figure 7.12: Temperature coefficient of the permittivity $\partial\,\varepsilon^{'}(T)/\partial\,T$ (α_ε) of an un-stretched P(VDF-TFE) film at fixed frequencies (10 data points per decade) between 10^3 and 10^4 Hz.

To check the frequency dependence of the temperature coefficient of the permittivity in the temperature regime, the α_ε curve recorded in the frequency range between 1 and 10 kHz is shown in Figure 7.12. The lower glass-transition peaks show a shift with frequency, typical of a relaxation process. In addition, we can clearly see that the structural transition seen at 55 °C is frequency-independent as expected and the conformational disorder relaxation process shows frequency-dependent response.

Similarly, looking at the heating and cooling curves of temperature dependent derivative α_ε of a melt-pressed PVDF film at a frequency of 1 kHz in Figure 7.13, we can observe the secondary crystallization melting peak during heating (40 °C) and its subsequent recrystallization peak during cooling, albeit a shift to higher temperature ($\approx$ 70 °C). The shift of the recrystallization peak to higher temperature is also

seen in the mDSC thermogram shown in Figure 7.14. This is different to the primary exothermic recrystallization peak which is usually found at a lower temperature than its corresponding melting endotherm (*cf.* Figure 7.7).

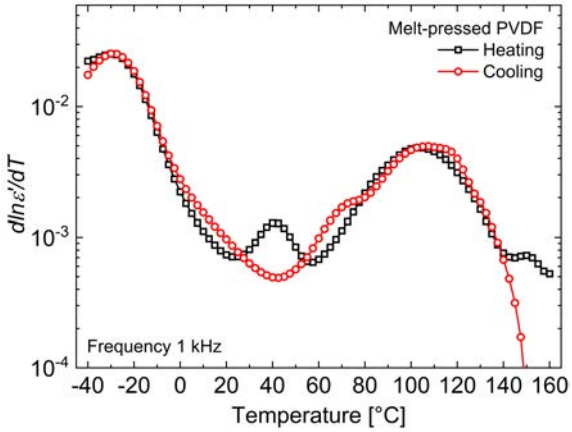

Figure 7.13: Temperature coefficient of the permittivity ($\partial\, ln\, \varepsilon'(T)/\partial\, T$) of a melt-pressed PVDF film during heating and subsequent cooling at a frequency of 1 kHz.

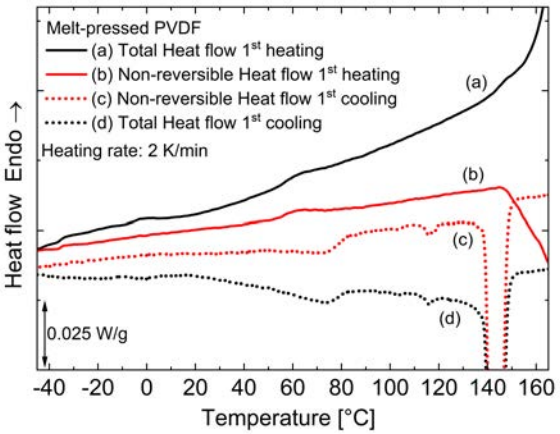

Figure 7.14: mDSC endotherms of a melt pressed PVDF film during first heating and cooling cycles.

In Figures 7.11 and 7.12 though we observe two main processes occurring in the T_{mid} region, we do not observe an upper glass-transition ($T_g(U)$) relaxation process. However, looking into the TSDC spectra of the 70/30 mol % un-stretched extruded P(VDF-TFE) sample in Figure 6.9, we definitely notice a shoulder around 0 °C that possibly points up to an $T_g(U)$ process. This is indeed confirmed from the presence of a step/peak at the same temperature in the total heat flow and reversible heat flow curves during heating and cooling cycles in a P(VDF-TFE) sample stretched at 110 °C as shown in Figure 7.15. The transition becomes weaker during the cooling cycles. In addition, the presence of an exothermic peak corresponding to the formation of secondary crystals is seen during the second cooling cycles in the heat flow/non-reversible heat flow curves. This indicates that indeed the secondary crystals are formed in a short span of time while cooling from the polymer melt. The reason for the absence of its corresponding melting endotherm during the second heating cycle is not clear yet. It can be speculated that the melting of the secondary crystals occurs over a broad temperature range and hence the process is not observed as a distinctive peak. The increase in the heat flow values above 40 °C up to the primary melting transition during the second heating cycle of the non-reversible heat flow curve supports this statement.

Nevertheless, it is clear that the formation of secondary crystals is influenced to a certain extent by the primary crystallization process. This can be understood by referring to Figure 7.16. The Figure shows the first heating/cooling cycles of a 70/30 mol% P(VDF-TFE) film previously stretched at 110 °C, heated up to 90 °C (solid black line) – just above the T_{mid} transition. The sample was then immediately

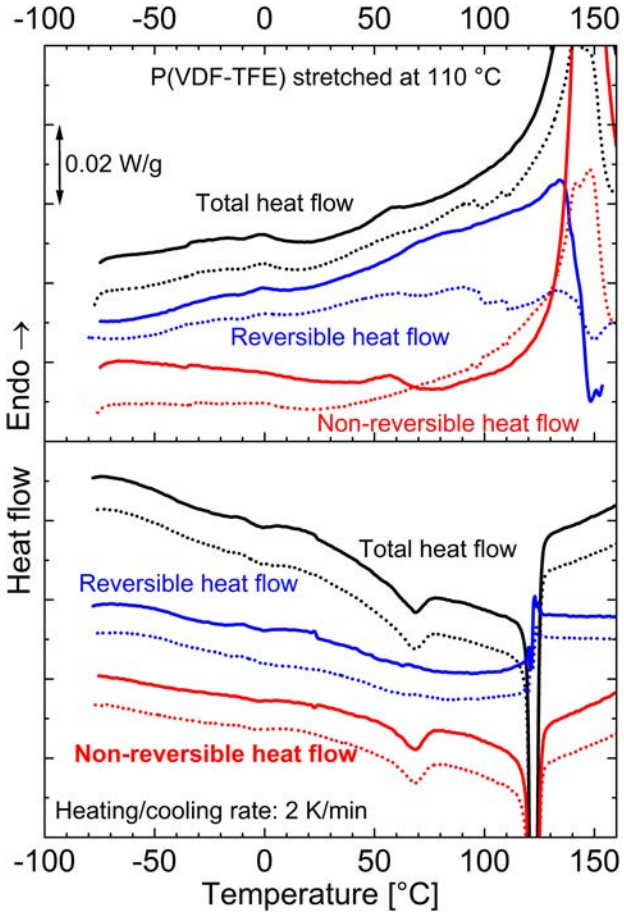

Figure 7.15: mDSC thermograms of a P(VDF-TFE) film stretched at 110 °C during subsequent heating and cooling cycles. Solid lines (—) denote 1st heating/cooling cycles and dotted lines (· · ·) denote 2nd heating/cooling cycles.

cooled down to -100 °C. Looking at the cooling curve of the sample, we notice the absence of T_{mid}, which appears in a similar sample cooled down from 200 °C (dotted dark blue line). In the case of the former sample, the thermal history is yet to be removed as the sample is heated to a temperature well below its primary melting point. The previously ordered secondary crystal molecular chains that exist in the amorphous/constrained amorphous regions while cooling down from 90 °C do not undergo immediate recrystallization. However, when cooled from its melt state where the molecules exist in a random coiled conformation [221], reorganization of crystalline morphology occurs. This in turn influences the amorphous phase and its interphase, thermodynamically allowing the formation of secondary crystals.

From the results shown above, it is possible to observe only some of the T_{mid} processes in a given experiment, since the individual processes often overlap or their contributions are not strong enough. However, since the T_{mid} transition is sensitive to processing, by choosing the right conditions it is possible to observe the individual processes in DRS using derivative techniques. Figures 7.17 and 7.18 show results

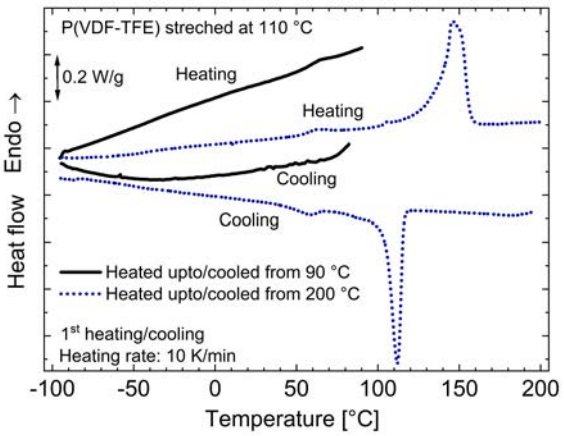

Figure 7.16: First and second heating/cooling thermograms of a stretched P(VDF-TFE) film heated to different temperatures during the first heating run.

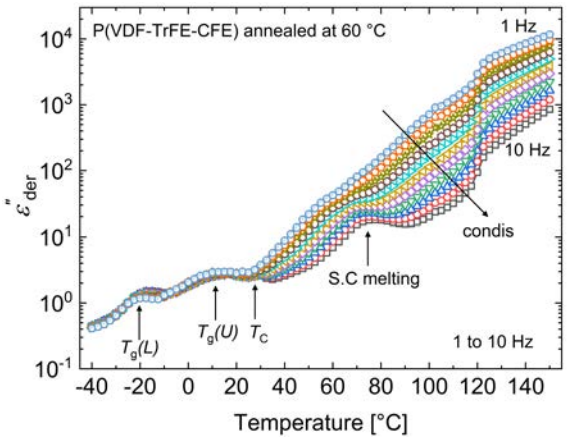

Figure 7.17: Conduction-free dielectric loss (ε''_{der}) of a P(VDF-TrFE-CFE) film annealed at 60 °C, measured fixed frequencies (10 data points per decade) between 10^0 and 10^1 Hz.

from derivative analysis of dielectric data from a P(VDF-TrFE-CFE) film annealed at 60 °C, measured at fixed frequencies. From the figures, in addition to the lower T_g around -20 °C and Curie transition around 30 °C (better seen in Figure 7.18), we can clearly identify the three different processes taking place in the mid-temperature region. This is possible in the terpolymer due to its low crystallinity and nano-crystalline regions [47, 48, 49], which leads to a high volume fraction of the constrained amorphous phase.

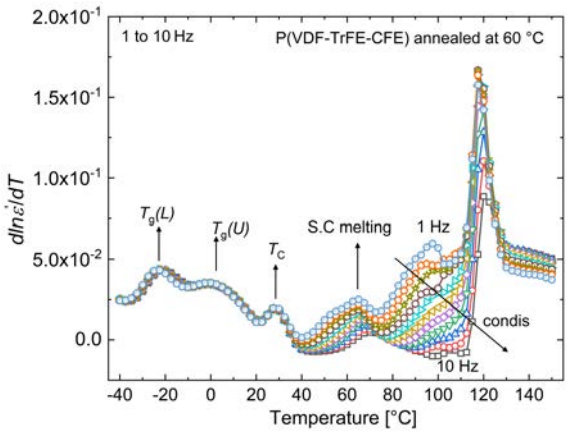

Figure 7.18: Temperature coefficient of the permittivity ($\partial ln\varepsilon'(T)/\partial T$) of a P(VDF-TrFE-CFE) film annealed at 60 °C, measured at fixed frequencies (10 data points per decade) between 10^0 and 10^1 Hz.

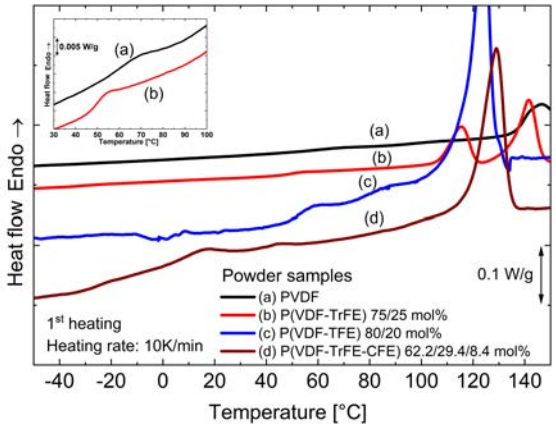

Figure 7.19: First heating thermogram recorded during DSC measurement on powder samples of various PVDF homo-, co- and ter-polymers. The figure inset shows the magnified curves of PVDF and P(VDF-TrFE) copolymer.

7.5 Nature of Mid-Temperature Transition

Previously, Nakajima suggested that the state/form of the material might have an influence on this transition [119]. It was stated that residual solvent might alter the amorphous locally, and this may affect the transitions occurring in the mid-temperature region. To investigate it further, DSC measurements on various PVDF and its related co- and ter-polymer powders were made. The contribution of residual solvent, if present, is minimum in the powder state of the sample. The results of the measurement are displayed in Figure 7.19. From the figure it is clear that T_{mid} is observed in all the samples between 30 and 80 °C (For PVDF and P(VDF-TrFE) samples, the transition is seen better in the inset of the figure). This confirms that mid-temperature transition is independent of the sample form (powder/film). As seen in the figure, the corresponding transition in a P(VDF-TrFE) is very weak and this might explain for the absence of the transition in the DSC measurements of similar P(VDF-TrFE) powder samples (Figure 13 in [119]). In addition, the employed heating rate has a direct influence on the strength and position of the signal recorded. This can be seen from the DSC endotherm of an un-stretched P(VDF-TFE) film shown in Figure 7.20. The heat-of-fusion of the mid-temperature transition(s) (area under the T_{mid} peak) and the temperature at which it is observed increases with increase in the heating rate. On the other hand, during cooling the transition shifts to lower temperatures with higher heat flow values. The behavior is similar to the shift/change in melting and recrystallization peaks as seen in the figure – commonly observed in semi-crystalline polymers [222]. This indicates the contribution from the melting of secondary crystals to the overall transition.

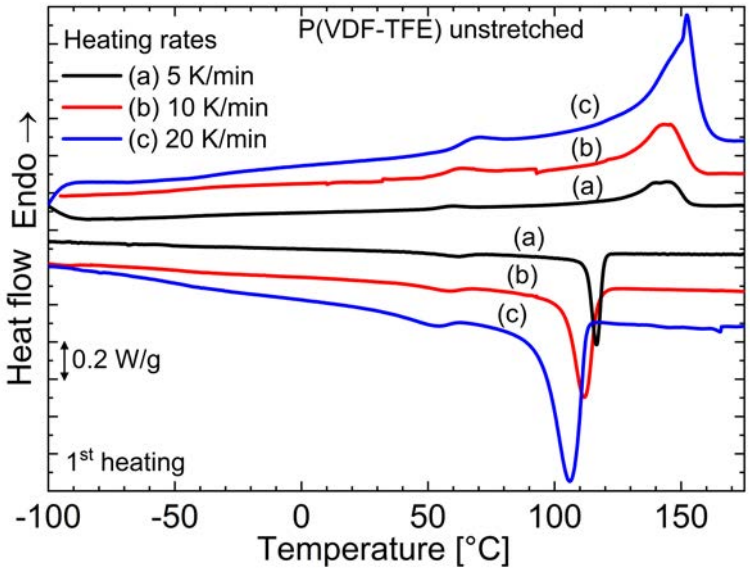

Figure 7.20: 1st heating DSC endotherm of an un-stretched 70/30 mol% P(VDF-TFE) film recorded using different heating rates.

8

Influence of Processing on Mid-Temperature Range and Other Transitions in PVDF-based Polymers

8.1 PVDF Homopolymer

PVDF homopolymer and other PVDF-based co- and ter-polymers have VDF as the main backbone molecule. The relative simple chemical structure of VDF consisting only of hydrogen and fluorine atoms attached to the carbon chains makes PVDF an ideal polymer to study in detail how preparation conditions influence the various mid-temperature range and other transitions.

8.1.1 Effect of Preparation Methods

Figure 8.1 shows the first heating DSC endotherm of differently prepared PVDF films. The mid-temperature transitions appear as predicted in Table 7.1. While the stretched and annealed samples show a weak T_{mid} in the form of a relaxation step in Figure 8.1a, samples which are quenched show a strong T_{mid} as observed in Figure 8.1b. The fact that T_{mid} is found in both PVDF and polyethylene based polymers which have a comparable chemical structure suggests that the transition is intrinsic to C-C backbone based organic semi-crystalline polymers [187, 223, 224, 225, 226].

8.1.2 Effects of Stretching and Crystalline Phases

We know that in DRS, an un-stretched PVDF film shows the presence of *condis* process in the form of frequency-dependent relaxation loss peaks above RT (Figure 6.1a). On the other hand, stretching removes this process as shown in Figure 8.2 (similar to the observation in a stretched P(VDF-TFE) sample in Figure 7.4). Looking at the derivative curves in Figure 8.3, we clearly observe the presence of a frequency-independent secondary crystallization (S.C) peak around 55 °C in the $\partial\, ln\, \varepsilon'(T)/\partial\, T$ plots and

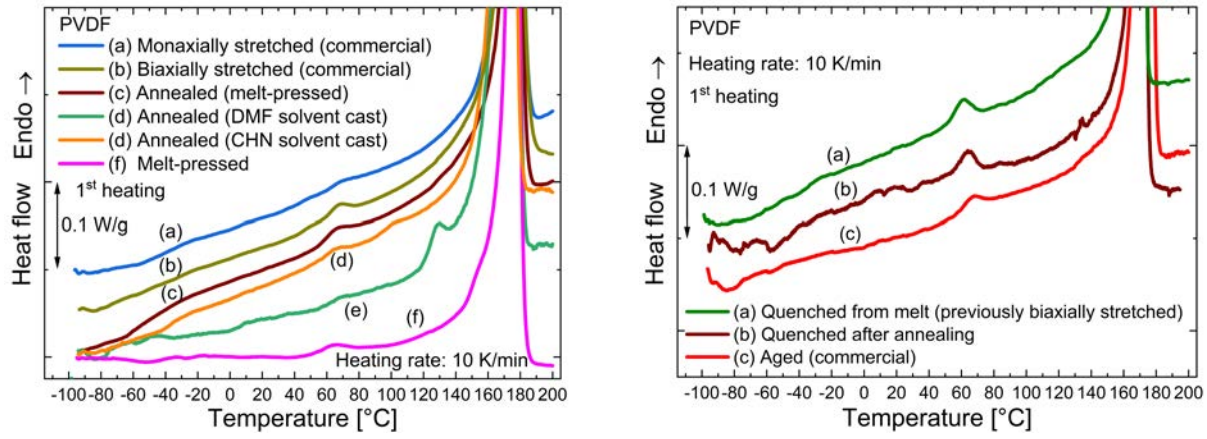

(a) **(b)**

Figure 8.1: First heating cycle during DSC measurement on PVDF films prepared by various methods where mid-temperature transition(s) is seen (a) as a step and (b) as a peak.

a corresponding step around the same temperature in $\varepsilon''_{\text{der}}$ of both the uniaxially and biaxially stretched PVDF films. In addition to it, we can still see traces of conformational disorder (*condis*) present in the biaxially stretched sample above the S.C peak in both the derivative curves in Figure 8.3b. The peaks are observed because a biaxially stretched sample not only predominantly consists of β crystals with a $T_{m>3}$ conformation (*cf.* Table 8.1) as result of the stretching process, but also still contains a considerable fraction of α crystals with the chains in the $TG^{+}TG^{-}$ conformation that contributes to the *condis* relaxation. A similar inference can be made from the RT WAXD spectra of a biaxially stretched sample in Figure 8.4. Hence, as predicted previously, *condis* relaxation also takes place in stretched samples which consists of a definite fraction of α phase (Table 7.1).

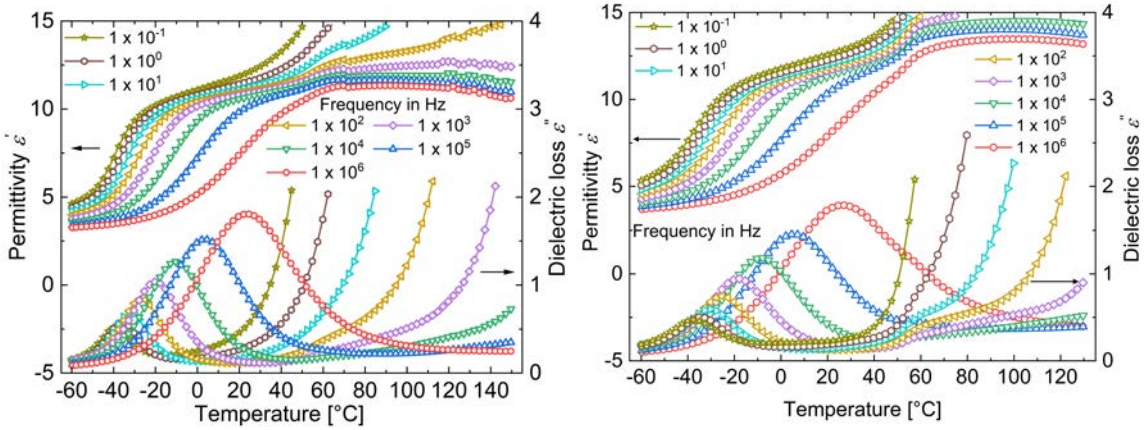

(a) Uniaxially stretched PVDF **(b)** Biaxially stretched PVDF

Figure 8.2: Dielectric spectra of a PVDF homopolymer which was (a) uniaxially stretched and (b) biaxially stretched, as a function of temperature at fixed frequencies from 10^{-1} to 10^{6} Hz.

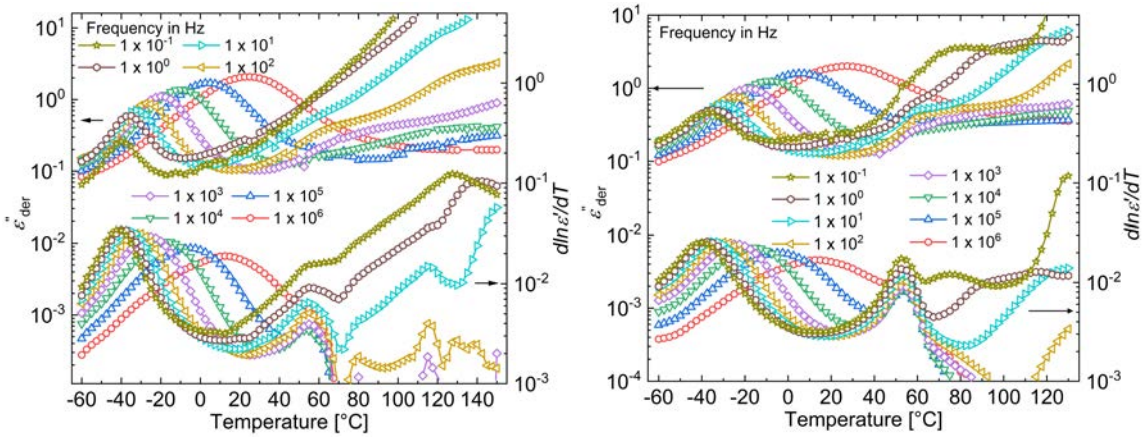

(a) Uniaxially stretched PVDF

(b) Biaxially stretched PVDF

Figure 8.3: Derivative curves $\varepsilon''_{\text{der}}$ and $\partial\, ln\, \varepsilon'(T)/\partial\, T$ (α_ε) obtained from the dielectric spectra of PVDF films (a) uniaxially stretched and (b) biaxially stretched.

Table 8.1: Fraction of $T_{m>3}$ and TG^+TG^- conformations in differently processed PVDF films.

PVDF homopolymer film	$T_{m>3}$ [%] **840 cm^{-1}**	TG^+TG^- [%] **763 cm^{-1}**
Uniaxially stretched	47	53
Biaxially stretched	56	44
Quenched from melt (biaxially stretched)	29	71
Drop-cast (DMF) at RT (non-annealed)	39	61
Drop-cast (DMF) at 110 °C	76	24
Drop-cast (CHN)	39	61

With respect to the uniaxially stretched sample, derivative analysis points out to the presence of a new frequency independent process around 120 °C as depicted in Figure 8.3a. This process also manifests around the same temperature range in the DSC endotherms and in the $\partial\, ln\, \varepsilon'(T)/\partial\, T$ (α_ε) derivative curves of a dimethyl formamide (DMF) evaporated PVDF film cast at 110 °C (Figures 8.1a and 8.5, respectively) and a cyclohexanone (CHN) evaporated PVDF sample cast at 80 °C (Figures 8.1a and 8.6b, respectively). Referring to the Table 8.1 and the Figure 8.4, we find that a DMF drop-cast film primarily crystallizes in an all-*trans* rich β phase [32] and CHN drop-cast sample crystallizes predominantly with non-polar α crystals [227, 228]. Since it appears at the same temperature range in both the β and α rich samples, it cannot be assigned to the melting of crystals belonging to a particular crystalline structure as previously documented [229].

The origin of this high-temperature peak between around 100 °C should be due to the melting of crystals formed at the annealing temperature which was 110 and 80 °C for DMF and CHN drop-cast samples, respectively [195]. This argument is strengthened from the derivative analysis of a CHN drop-cast PVDF

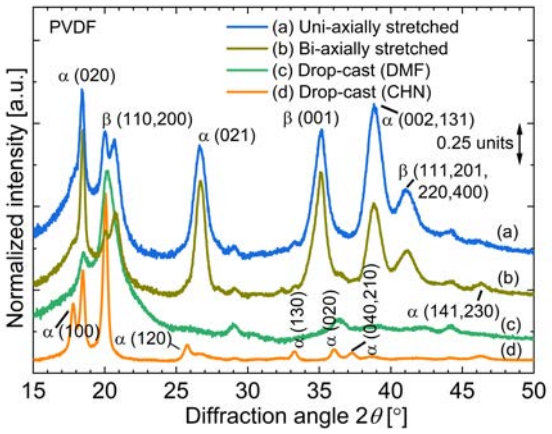

Figure 8.4: RT WAXD spectra of differently processed PVDF films.

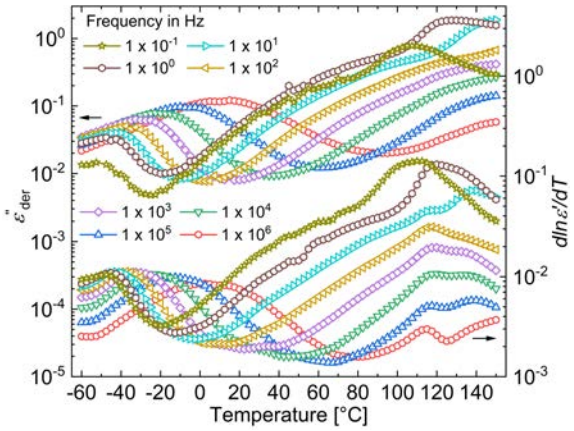

Figure 8.5: Derivative curves extracted from the dielectric spectra of a drop-cast PVDF homopolymer film prepared using DMF as the solvent, plotted as a function of temperature at fixed frequencies from 10^{-1} to 10^{6} Hz.

film shown in Figure 8.6. As expected, this structural transition is not visible in the $\varepsilon''_{\text{der}}$ curve depicted in Figure 8.6a, while we can see traces of it around 87.5 °C in the temperature coefficient of permittivity at high frequencies (Figure 8.6b). Hence, the α_ε curves between 10^5 and 10^6 Hz during heating followed by a subsequent cooling is plotted in Figure 8.7. Figure 8.7a clearly reveals the frequency-independent nature of this transition. The sample was heated up to a temperature of 140 °C – much lower than its main melting transition (*cf.* Figure 8.1a). During the cooling step, we can observe in Figure 8.7b that the corresponding transition occurring around 97.5 °C, implying recrystallization of the previously melt annealed crystals. From the above discussion, the transition seen at 115 °C in both the derivative curves of an uniaxially stretched PVDF in Figure 8.3a can probably be assigned to a similar melting transition due to possible heat treatment around this temperature.

Additional evidence for the presence of a second T_g can be found in the results of TSDC measurements on un-stretched and stretched PVDF films plotted in Figure 8.8. In a laboratory melt-pressed and a commercial extruded PVDF film (which were both not subjected to any stretching possess), a depolarization peak between −30 and −10 °C is seen. In 1970, Takamatsu and Fukada had already observed a similar peak at -10 °C in their TSDC measurements on PVDF films [178]. However, they could not identify the origin of this peak. Later, Abkowitz and Pfister had assigned this peak to the α_c relaxation process, which does not shift with heating rate and poling voltage [174]. Eliasson [179] had also associated the TSDC peak found at −20 °C with α_c process since the peak disappeared on stretching, similar to the observation in Figure 8.8. In addition, the peak was also affected by annealing. But, from DRS measurements on PVDF and other literature mentioned previously in Section 6.1, we know that the α_c relaxation is observed at a higher temperature above RT. Moreover, as mentioned previously, stretching

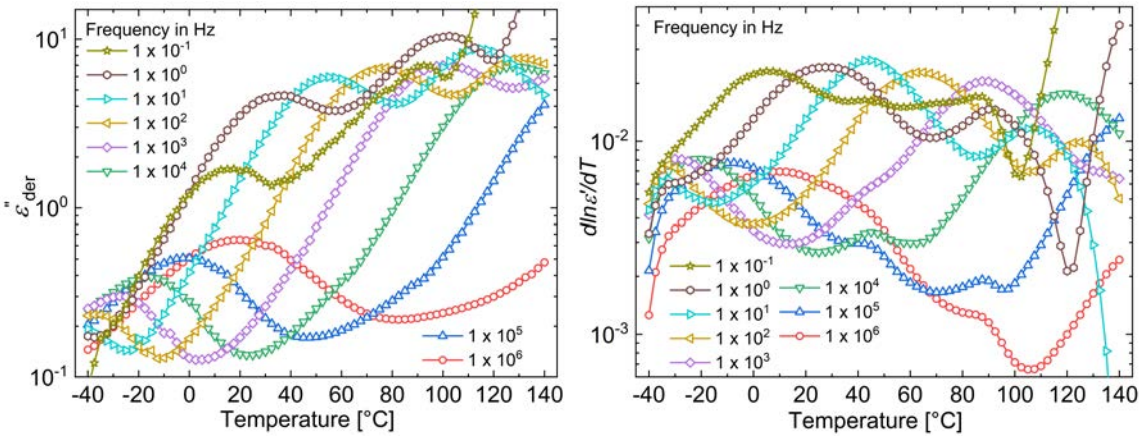

(a) **(b)**

Figure 8.6: Derivative curves (a) $\varepsilon''_{\mathrm{der}}$ and (b) $\partial\, ln\, \varepsilon'(T)/\partial\, T$ (α_ε) obtained from the dielectric spectra of a CHN drop-cast PVDF film.

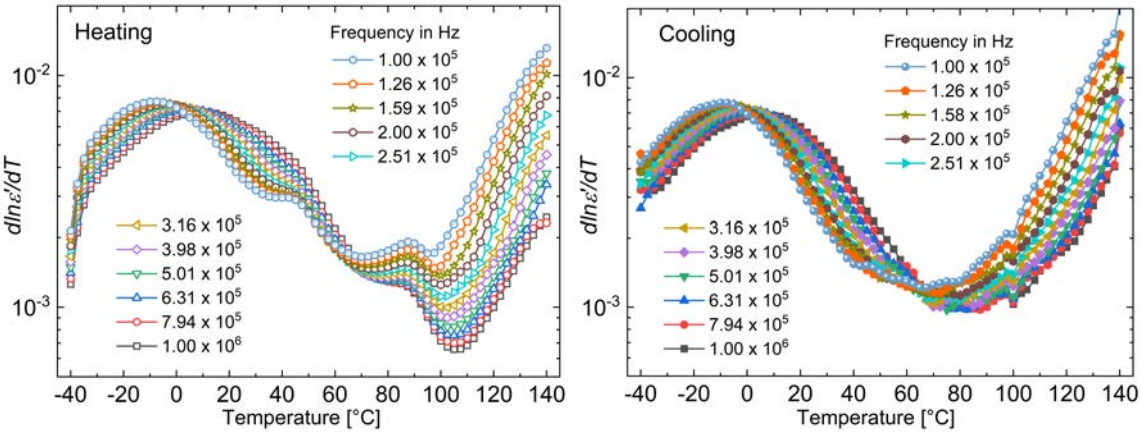

(a) Heating **(b)** Cooling

Figure 8.7: Temperature coefficient of permittivity $\partial\, ln\, \varepsilon'(T)/\partial\, T$ (α_ε) obtained from the dielectric spectra of a CHN drop-cast PVDF film during (a) heating and (b) subsequent cooling between 10^5 and 10^6 Hz (10 data points per decade).

can be expected to align the chains in the constrained amorphous regions and the tie-molecules in the a-c interphase, thus suppressing an $T_g(U)$ relaxation. Accordingly, Callens *et al.* identified this relaxation as $T_g(U)$ process, which they observed on γ-irradiated PVDF films at a temperature of $-23\,^{\circ}$C [190].

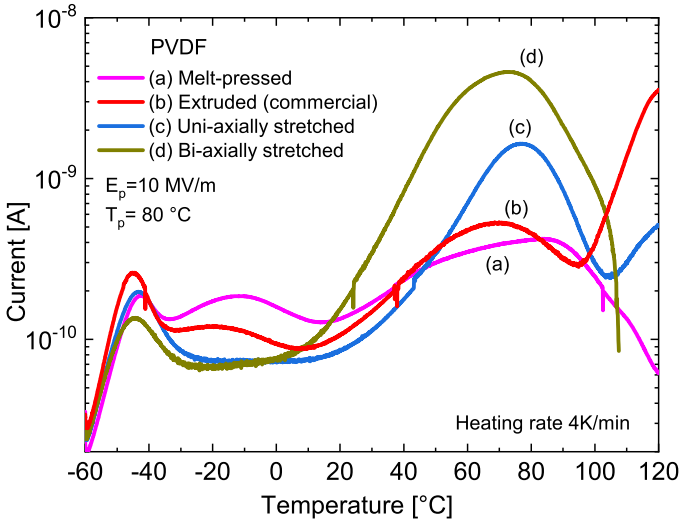

Figure 8.8: Depolarization spectra of unstretched and stretched PVDF films.

From the above observations, the depolarization peaks around $-10\,^{\circ}$C in a melt-pressed α PVDF and around $-17\,^{\circ}$C in an extruded commercial PVDF film can be associated with a second T_g process. It should be also mentioned that Oka and Koizumi [185] identified the relaxation around $-10\,^{\circ}$C in stretched samples containing both α and β phases. The role of ionic impurities in masking this transition was also clearly shown, which may explain why we do not observe this transition always in TSDC measurements.

Interestingly, an activation energy E_a of 0.93 eV was calculated by Abkowitz and Pfister for this relaxation process [174], which is comparable to the E_a value of space-charge peaks [213], the secondary crystallization process [230] and an upper glass-transition [190] estimated by other authors. Adding to it, Eliasson in a subsequent study poled α PVDF films at higher fields than previously used in [179] and observed a new peak at $0\,^{\circ}$C [231]. The depolarization peak seen in the previous study at $-20\,^{\circ}$C [179] (*cf.* Figure 8.8) was absent when poled at higher fields. The peak at $0\,^{\circ}$C similar to the $-20\,^{\circ}$C peak disappeared on stretching or annealing. From WAXD measurements it was concluded that the process of conversion of form II (α phase) into form I crystals (β phase), which happens *via* an intermediate conversion to II_p (polar form of α phase or δ phase) [31, 232, 233, 234, 235], has an effect on this peak – confirming its dipolar nature. On the other hand, the dependence on electrode material points to the possibility of contributions from space-charge. From the above observations, the multiple origins of T_{mid} process can be inferred.

8.1.3 Role of Annealing

Though the type of solvent plays as a major role in determining the end crystalline phases formed in PVDF, the temperature of crystallization also contributes to it. This can be demonstrated using DMF drop-cast films annealed at different temperatures during preparation. From Figure 8.9, we observe that a sample crystallized at RT (referred to as a non-annealed sample) shows strong paraelectric α crystalline peaks in comparison with a film annealed at 110 °C during the drop-casting process. Correlating the WAXD scans with the fraction of different crystalline phases calculated from FTIR spectra in Table 8.1, we find that a non-annealed (NA) sample even though was prepared using DMF as the solvent, still crystallizes with a major α phase. This directly has an effect on the mid-temperature transition as seen in Figure 8.10. As expected, a NA sample shows a clear T_{mid} between 60 and 80 °C due to the higher fraction of constrained amorphous phase (CAP) and α crystals present in the film. Comparatively, an annealed sample shows only a weak T_{mid} relaxation step in this temperature range.

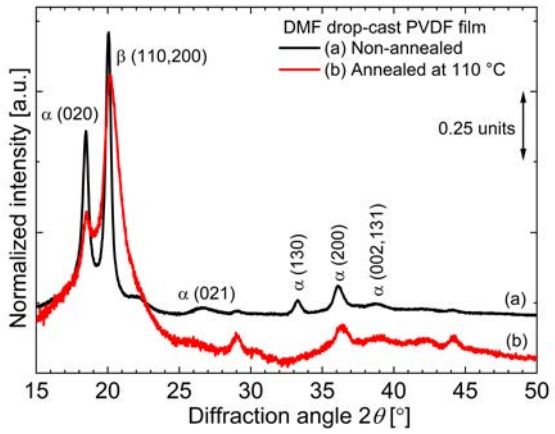

Figure 8.9: RT WAXD scan of drop-cast DMF films crystallized at different temperatures during sample preparation.

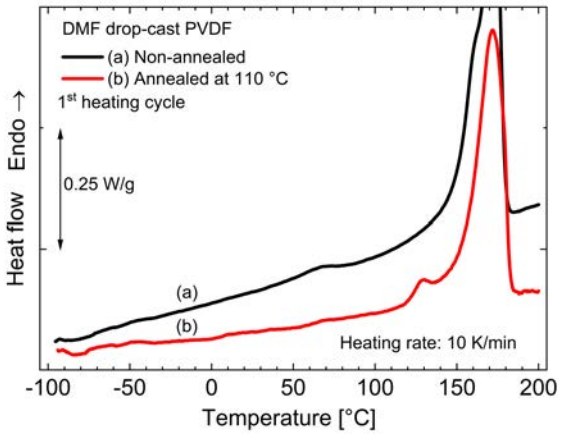

Figure 8.10: First DSC heating endotherm of films prepared by drop-casting PVDF from DMF at different temperatures.

8.1.4 Effect of Quenching

A biaxially oriented sample was heated above its melting point and then rapidly quenched in liquid nitrogen. The derivative curves obtained from the dielectric spectra of the quenched sample are displayed in Figure 8.11. Compared to the derivative analysis of dielectric spectra of the film before quenching plotted in Figure 8.3b, we can observe that the quenched film shows a strong *condis* relaxation. This is because the thermal history of the originally biaxially oriented sample is erased on melting and the quenching step leads to the increase of CAP along with a simultaneous increase of α phase (Table 8.1). This leads to a strong endothermic peak in DSC such as that shown in Figure 8.1b.

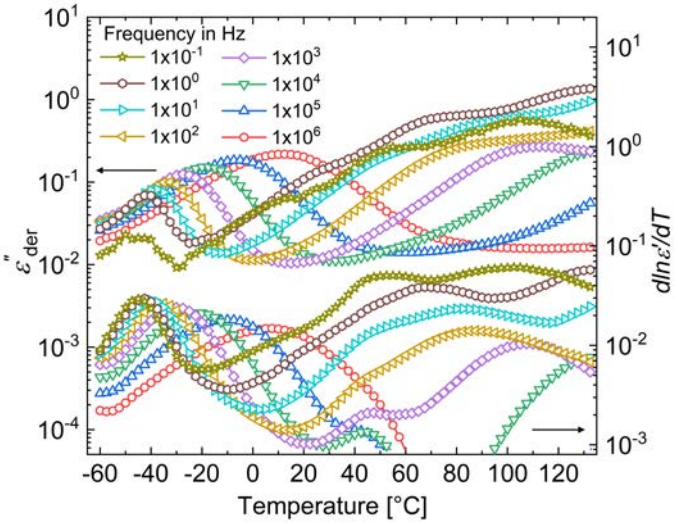

Figure 8.11: Derivative curves (a) ε''_{der} and (b) $\partial\, ln\, \varepsilon'(T)/\partial\, T$ (α_ε) obtained from the dielectric spectra of a biaxially PVDF film after quenching from melt.

8.2 P(VDF-TFE) Copolymers

8.2.1 Influence of Preparation Methods

The first heating DSC endotherms of a 80/20 mol% P(VDF-TFE) copolymer sample prepared using various methods are revealed in Figure 8.12. The processing conditions which result in a lower fraction of CAP lead to samples whose T_{mid} is seen as a step in the thermogram in Figure 8.12a, and those conditions which allow for a considerable amount of tie molecules and CAP to exist in the morphology results in the observation of an endothermic T_{mid} peak during the first heating cycle as seen in Figure 8.12b.

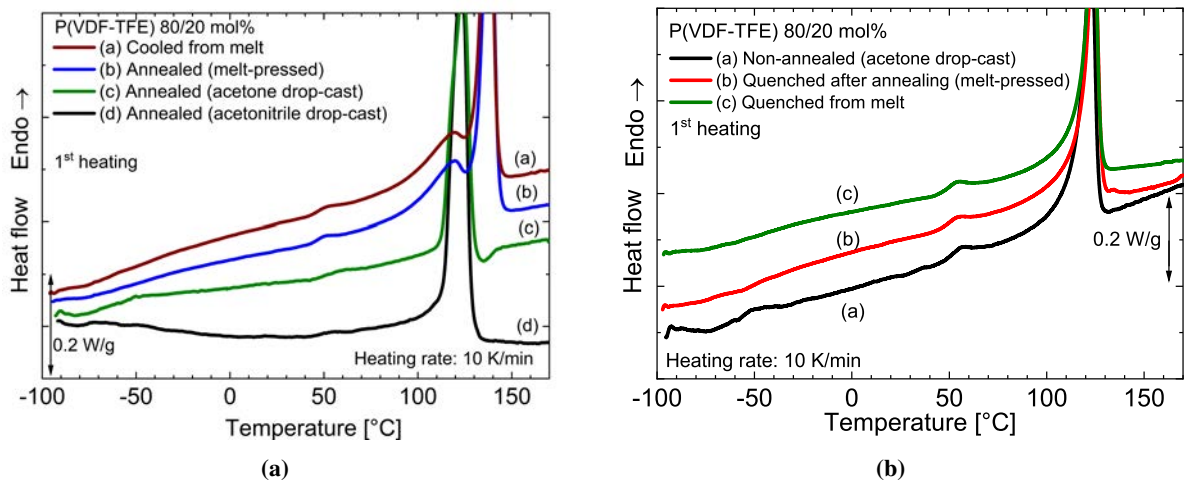

Figure 8.12: DSC thermograms of a P(VDF-TFE) 80/20 mol% copolymer prepared by various methods where mid-temperature transition(s) is seen (a) as a step and (b) as a peak.

Looking at Figure 8.13, during the first heating cycle, we observe that the melt-pressed samples show a higher melting point and the presence of a F-P transition (broad shoulder) just before the melting transition. In the case of drop-cast samples, it appears that the melting peak merges with the F-P transition. This can be confirmed by the presence of a shoulder between 115 and 120 °C during the first heating and separation of both the transitions during the second heating in an acetone drop-cast sample. The drop-cast samples were crystallized at a temperature of 110 °C, which may explain for the shift in T_m to lower temperatures. Table 8.2 summarizes the melting point, crystallinity and also the fraction of different crystalline conformations present in the different heat treated 80/20 mol% P(VDF-TFE) copolymers. Though the χ_c of the drop-cast samples is lower than the melt-pressed samples, FTIR measurements point out to an increase of α phase conformations. However, from Figure 8.12a, a weaker T_{mid} is observed in solvent-cast samples compared to that prepared using melt-pressing.

To investigate the effects of process-induced changes on T_{mid}, derivative analysis was performed on the dielectric data obtained from a melt-pressed and acetone drop-cast P(VDF-TFE) sample (annealed at 110 °C), whose results are plotted in Figure 8.14. It can be seen from the figure that both the melt-pressed (Figure 8.14a) and drop-cast samples (Figure 8.14b) show a strong conformational disorder relaxation. The shift of the melting transition to lower temperatures in drop-cast samples is also clearly seen in the derivative curves. While the drop-cast sample shows a frequency-independent peak around 110 °C (seen better in the $\partial\, ln\,\varepsilon'(T)/\partial\, T$ curve), the same is observed around 120 °C in a melt-pressed film. In addition, the presence of a weak shoulder between 100 and 110 °C in the temperature derivative curve of a melt-pressed sample, just before the melting transition, points out to the possible presence of a F-P transition.

Figure 8.14a shows the presence of an upper-T_g between -20 and 20 °C. Its existence is confirmed by the observation of a step in the mDSC total heat-flow curve and a corresponding enthalpy relaxation peak in the reversible heat-flow scan of a melt-pressed P(VDF-TFE) film shown in Figure 8.15. Similarly, in the TSDC depolarization curves displayed in Figure 8.16, a shoulder is observed in the same temperature range – seen clearer in the samples poled at higher temperatures, which can be assigned to $T_g(U)$.

Table 8.2: Summary of melting point T_m, crystallinity χ_c during first heating in DSC and the fraction of different crystalline conformations in melt-pressed and drop-cast P(VDF-TFE) copolymer films calculated from their characteristic FTIR absorption peaks using the method suggested by Gregorio and Cestari [148].

P(VDF-TFE) 80/20 mol% film	T_m [°C]	χ_c [%]	$T_{m>3}$ [%] **840 cm^{-1}**	TG^+TG^- [%] **763 cm^{-1}**
Cooled from melt (CM)	138.3	43	87	13
Melt-pressed and annealed	137.5	43	89	11
Annealed (acetone drop-cast)	124.1	31	79	21
Annealed (acetonitrile drop-cast)	122.7	38	82	18

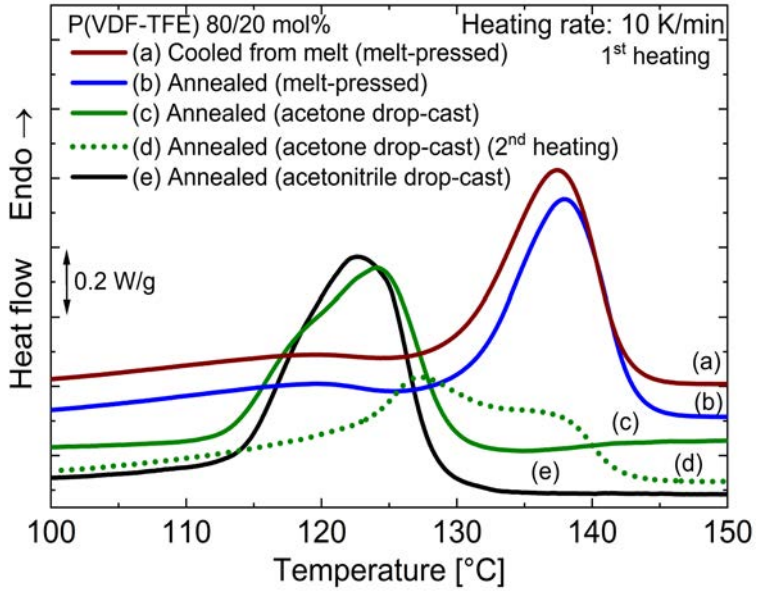

Figure 8.13: DSC thermograms of differently heat treated P(VDF-TFE) 80/20 mol% copolymer films during first heating run.

8.2.2 Influence of Stretching Temperature[1]

Figure 8.17 shows the first heating scans of a 70/30 mol% P(VDF-TFE) copolymer stretched at various temperatures from 80 to 120 °C. It is very interesting to observe the effects of the stretching process and the stretching temperature (T_s) on the shape of the T_{mid} transition. It changes from an endothermic peak, characteristic for a structural transition, into a relaxation step, as we move from sample 'S1' to 'S6'. This can be expected from the explanation provided in Section 7.3.

In the case of stretching at low temperatures, we have the situation where a high fraction of CAP and tie molecules can exist leading to a strong contribution to T_{mid} from the melting of secondary crystals (S.C). As the temperature increases, the material becomes soft and flexible. Consequently, the molecules in CAP can be effectively and efficiently oriented, limiting the chances for the growth of S.C. Hence, we observe a weak relaxation step at higher temperatures of stretching. Quantitatively, this can be seen in the change of the enthalpy values ΔH_{mid} for the T_{mid} transition from the un-stretched through the various stretched samples – as shown in Table 8.3. We notice that the enthalpy values steadily decrease from 'S1' to 'S6', thus illustrating how the mid-temperature transition can be modified by both the stretching itself and by the temperature at which the films are stretched. As stretching is also expected to change the a-c interface area, it may be used to control the MW polarization at the interface.

[1]Parts of this section are adapted from T. Raman Venkatesan *et al.*, "Influence of film stretching on crystalline phases and dielectric properties of a 70/30 mol% poly(vinylidenefluoride-tetrafluoroethylene) copolymer", *J. Adv. Dielect*, 10(5): 2050023 (10 pages), 2020 [140].

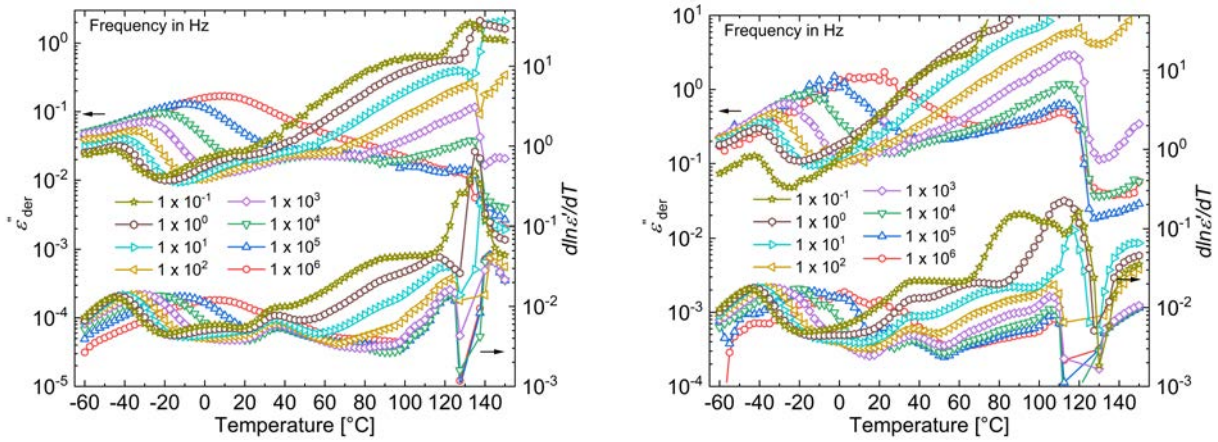

(a) Melt-pressed

(b) Annealed during drop-casting

Figure 8.14: $\varepsilon''_{\text{der}}$ and $\partial\, ln\, \varepsilon'(T)/\partial\, T$ curves obtained from derivative analysis of dielectric spectra on a (a) melt-pressed and (b) acetone drop-cast P(VDF-TFE) film (80/20 mol%).

Table 8.3: T_{mid} enthalpy (ΔH_{mid}) of an un-stretched and of several stretched P(VDF-TFE) copolymer films (at various temperatures as indicated).

P(VDF-TFE) 70/30 mol% copolymer	ΔH_{mid} [J/g]
S1 un-stretched	2.3
S2 stretched at 80 °C	2.2
S3 stretched at 90 °C	1.7
S4 stretched at 100 °C	1.2
S5 stretched at 110 °C	1.1
S6 stretched at 120 °C	0.9

8.3 P(VDF-TrFE) Copolymers

Figure 8.18 reveals T_{mid} transition as predicted by the proposed hypothesis (Table 7.1) in different processed P(VDF-TrFE)75/25 mol% films. Modulated DSC plot of a non-annealed sample (crystallized at RT) plotted in Figure 8.19 denotes the presence of an upper glass-transition around 0 °C – similar to that observed in a PVDF and P(VDF-TFE) sample.

8.3.1 Effect of Annealing

A non-annealed (NA) copolymer sample exhibits the strongest T_{mid} due to the presence of a higher fraction of CAP and α phase, while the annealed sample (annealed at 120 °C) shows a weak relaxation as annealing increases both the crystallinity and the fraction of polar all-*trans* conformation (Table 8.4). Derivative analysis of dielectric data clearly depicts the changes in individual T_{mid} processes with annealing. In Figure 8.20a, $\partial\, ln\, \varepsilon'(T)/\partial\, T$ curve reveals the sharp melting of secondary crystals around 50 °C along with a strong *condis* relaxation. The latter process is clearly noticeable in $\varepsilon''_{\text{der}}$ as well. On

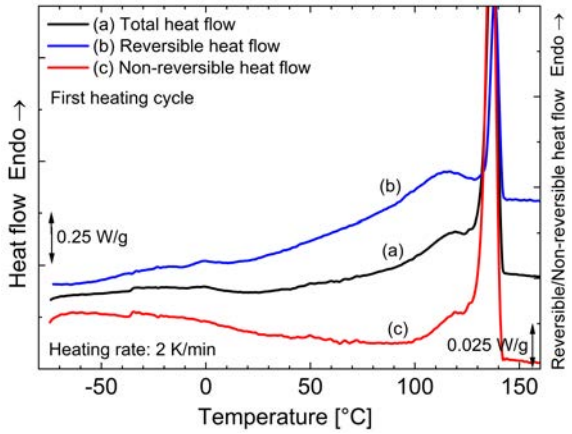

Figure 8.15: mDSC thermograms of a P(VDF-TFE) 80/20 mol% melt-pressed copolymer film during first heating cycle.

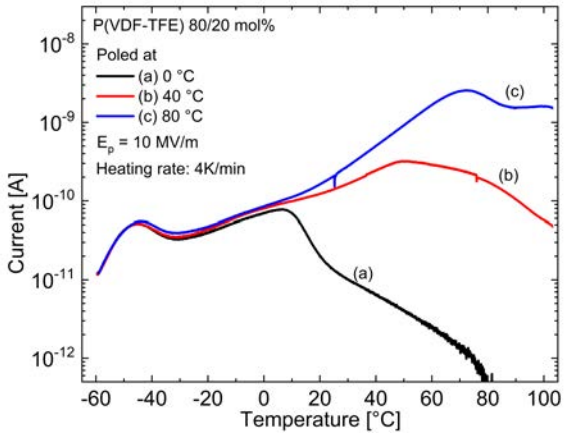

Figure 8.16: TSDC curves of a P(VDF-TFE) 80/20 mol% melt-pressed copolymer film poled at different temperatures with an electric field E_p of 10 MV/m.

the other hand, in an annealed sample whose derivative curves are displayed in Figure 8.20b, the melting of secondary crystals is indicated by a broad peak between 20 and 70 °C. In addition, we do not recognize a clear *condis* relaxation in both the derivative curves of an annealed sample.

Table 8.4: Summary of melting point T_m, crystallinity χ_c during first heating in DSC and the fraction of different crystalline conformations in non-annealed and annealed P(VDF-TrFE) 75/25 mol% copolymer films calculated from characteristic FTIR absorption peaks using the method suggested by Gregorio and Cestari [148].

P(VDF-TrFE) 75/25 mol% drop-cast film (acetonitrile)	T_m [°C]	χ_c [%]	$T_{m>3}$ [%] **840 cm^{-1}**	TG^+TG^- [%] **763 cm^{-1}**
Non-annealed	141.0	36	80	20
Annealed at 120 °C	141.1	56	88	12

8.3.2 Influence of Comonomer Ratio

In order to investigate whether the comonomer ratio had any influence on the mid-temperature transition, the heating thermograms of P(VDF-TrFE) copolymers with different ratios of VDF and TrFE are plotted in Figure 8.21. The samples were all measured as received in either powder or granular form without subjecting them to any processing which might other wise alter their crystalline phases. From the figure, we notice that all the samples show a T_{mid} transition in the form of a relaxation step. However, the T_{mid} does not seem to be affected by the change in TrFE ratio. On the other hand, a shift in T_C to lower temperatures with an increase in TrFE composition. The observation is consistent with previous results [129, 236]. This can be explained by the role of TrFE segments in reducing the interaction between VDF units, ultimately lowering the T_C according to the molar fraction added [25]. In the case of a 56/44 VDF/TrFE molar composition, the T_C peak merges with the T_{mid} step.

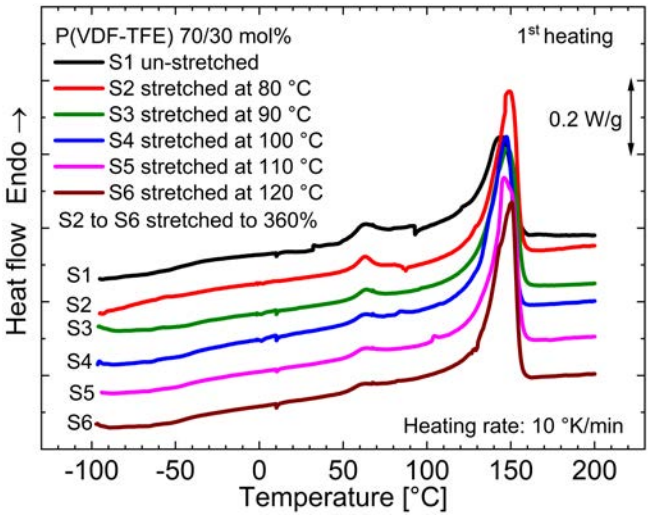

Figure 8.17: DSC thermograms of the un-stretched and stretched P(VDF-TFE) copolymer films as obtained during their first heating.

8.4 P(VDF-TrFE-CFE) Terpolymer

8.4.1 Effect of Annealing Temperature

8.4.1.1 Superposition of Curie and Mid-Temperature Transition[1]

The mid-temperature transition in different heat-treated P(VDF-TrFE-CFE) terpolymer films with a termonomer composition of 62.2/29.4/8.4 mol%, respectively, as seen during the first heating trace in DSC is depicted (red box) in Figure 8.22. The F-P transition of the terpolymer occurs in the vicinity of T_{mid} (generally observed as an endothermic peak between 10 and 20 °C) and is also affected by the processing conditions [49]. Hence, it has an influence on the mid-temperature range transitions. Especially, samples (a), (e) and (f) in the figure show a combined endothermic peak pertaining to both these transitions.

To understand the scenario better, the temperature coefficient of permittivity of the annealed sample at selected low frequencies is plotted in Figure 8.23. In addition to the glass-transition relaxation and Curie transition, we observe two additional processes above RT in the sample. The first process exhibits a small but definite shift with frequency. This can be identified with a possible upper glass transition. The second process occurring about 70 °C is frequency-independent and from the results of other PVDF-based homo- and co-polymers, can be assigned to secondary crystals melting. Due to the annealing procedure, these transitions are weak and only identified at low frequencies.

In a similar terpolymer annealed at a lower temperature of 60 °C (referred hereafter as partially-annealed sample) though we observe a superimposed peak in DSC (Figure 8.22), as mentioned previously

[1]Parts of this section are adapted from T. Raman Venkatesan *et al.*, "Tuning the Relaxor-Ferroelectric properties of Poly(vinylidene fluoride-trifluoroethylene-chlorofluoroethylene) Terpolymer by Thermally Induced Micro- and Nanostructures", under review in *Macromolecules*, 2022.

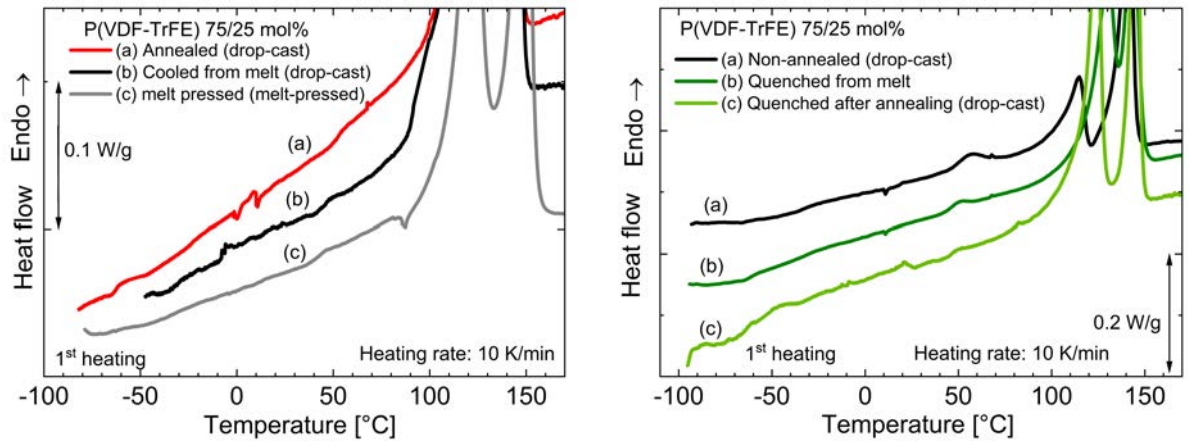

Figure 8.18: DSC thermograms recorded during first heating run on different heat-processed 75/25 mol % P(VDF-TrFE) films prepared by various methods where mid-temperature transition(s) is seen (a) as a step and (b) as a peak.

in Section 7.4, by using derivatives techniques it is possible to separate the individual processes, and it can be shown that the $T_g(U)$ process takes place before the terpolymer undergoes a transition to the paraelectric phase (*cf.* Figure 7.18). We do not observe a frequency shift associated with $T_g(U)$ in Figure 7.18. Nevertheless, the situation is more clearly seen in Figure 8.24 at higher frequencies, where we observe a shift in peak position as indicated by the arrow. The transition is reduced to a shoulder above 100 Hz, while the Curie transition is observed as a frequency independent peak around 30 °C. Hence, using derivative analysis, it is possible to separate these processes.

In Figure 8.22, similarly we observe a superimposed and a very asymmetrical endothermic peak for a non-annealed (NA) sample. In an attempt to separate and distinguish the individual processes, modulated DSC measurements with a lower heating rate of 2K/min was employed. The results obtained during first heating and cooling cycles of the terpolymer subjected to different annealing procedures are plotted in Figure 8.25. For a NA sample, during heating, we can observe that the superimposed endothermic peak seen at 58 °C in conventional DSC is split into two endothermic peaks in the irreversible heat-flow curve (dotted lines). While the first peak centred around 48.5 °C is only found in the irreversible heat flow curve, the second peak at 58 °C can be found in both the reversible (solid lines) and irreversible contributions to the total heat-flow. This suggests that the former peak can be assigned to the process of secondary crystals melting and the second peak can be assigned to the F-P transition [64]. The dielectric losses recorded on the non-annealed sample also confirm the same (Figure 8.26).

In Figure 8.26, between 40 and 60 °C, we can observe the two processes corresponding to the two endothermic peaks seen in the similar temperature range in Figure 8.25a. We know that at high frequencies, lower glass-transition process and F-P transition process combine to give a superimposed peak which shifts with temperature [49]. Accordingly, we notice that the second peak – initially showing a

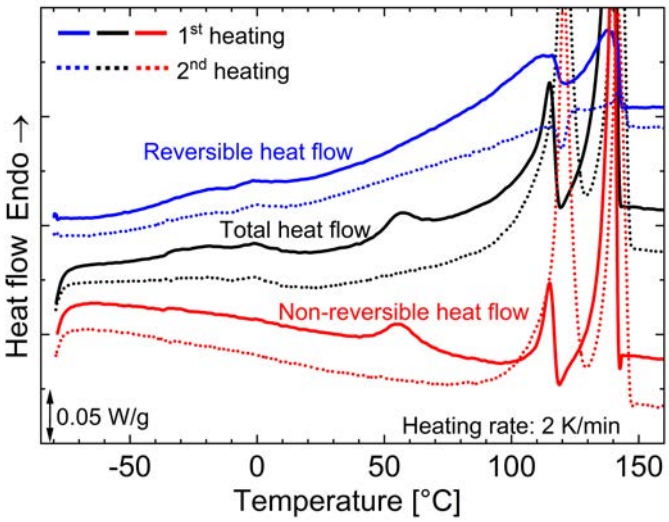

Figure 8.19: Modulated DSC traces measured on a non-annealed 75/25 mol% P(VDF-TrFE) sample during the first (—-) and second heating (· · ·) runs.

frequency-independent behavior after merging with the glass-transition peak gives rise to a combined peak. At the same time, we also note that the first peak remains as a frequency-independent shoulder even at very high frequencies, confirming the process of secondary crystals melting. With respect to a terpolymer film annealed at 60 °C (PA), as shown before in Figure 7.17, Curie transition already takes place before the observation of S.C melting. Hence, the first endotherm for a PA sample seen in Figure 8.25a (irreversible heat-flow) at 43 °C marks the T_C peak. However, irrespective of the annealing temperature, melting of the crystals formed due to storage always occurs at the same temperature around 48 °C as visualized in Figure 8.25a.

Upon cooling the heat-treated samples from temperatures above their melting points, the endothermic peaks in the T_{mid} can be separated as plotted in Figure 8.25b. Recrystallization of the secondary crystals occurs around 85 °C in the form of an exothermic peak on the irreversible heat-flow trace. On the other hand, paraelectric-to-ferroelectric transition occurs at lower temperatures around 16 °C – strongly observed in the reversible heat-flow curve, followed by the upper-glass transition.

From the above results, it can be inferred that annealing results in a shift of Curie temperature to lower temperatures and annealing at a higher temperature (120 °C, completely annealed) results in a higher shift than annealing at an intermediate temperature (60 °C). Accordingly, in a NA sample, T_C is observed after the S.C melt and *vice-versa* in the annealed samples. This has an influence on the relaxor-ferroelectric properties of the terpolymer, which is discussed in detail in Chapter 12.

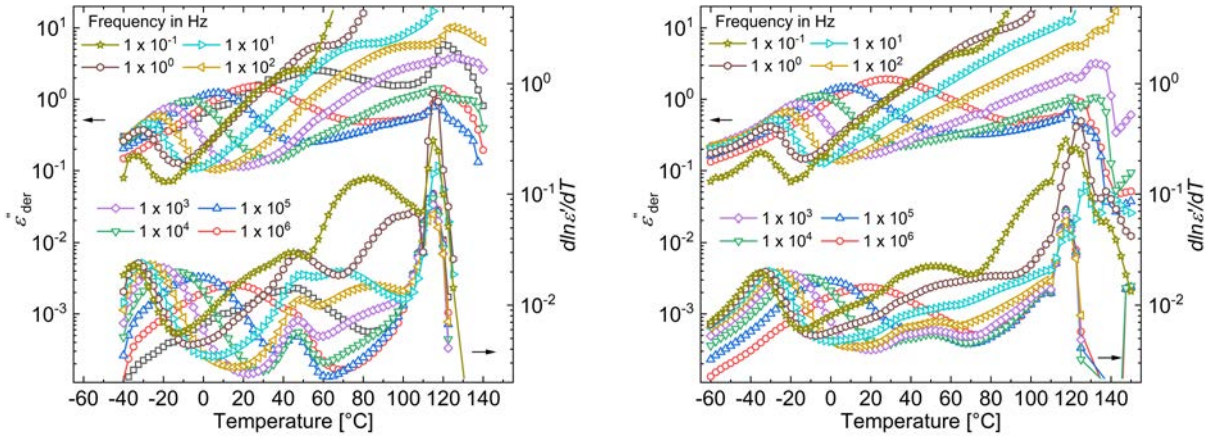

(a) Non-annealed

(b) Annealed

Figure 8.20: Derivative analysis curves ε_{der} and $\partial ln\,\varepsilon'(T)/\partial T$ from DRS measurements on a (a) Non-annealed and (b) Annealed acetonitrile drop-cast 75/25 mol% P(VDF-TrFE) film.

8.4.1.2 Influence on Upper-Glass Temperature

In addition to derivative analysis of dielectric relaxation spectra, TSDC being an electrical method allows even subtle effects to be detected, which increases resolution and detection sensitivity for the individual molecular processes. Hence, depolarization currents for the differently heat-treated samples were measured and the resulting TSDC spectra are shown in Figure 8.27.

In the figure, we observe the conventional glass transition at a temperature of $T_g \approx -27\,°C$ which appears as a peak in the non-annealed sample and as a shoulder in the annealed samples. The major difference is seen in the $T_g(U)$ peak found just above 0 °C in the annealed samples. The completely-annealed sample shows a clear peak around 5 °C which slightly moves to a higher temperature of 10 °C in the sample annealed at 60 °C. On the other hand, a non-annealed sample shows a broad peak at a much higher temperature of around 25 °C. Above the transition, we observe peaks in the temperature range of 25-30 °C which is due to poling in this temperature range [178]. In the non-annealed sample, the peak merges with the $T_g(U)$ peak. The non-annealed sample also shows a shoulder at 53 °C which might be an indication of an F-P transition. The latter peak is absent in the differently annealed samples – probably since it overlaps with the poling peak found in the F-P temperature range of the samples. Finally, above 60 °C, we observe space-charge peaks associated with MWI polarization [177] and their position depends on the respective sample and its poling conditions.

The shift of $T_g(U)$ on annealing can be also observed in the reversible heat-flow curves displayed in Figure 8.25a. A completely annealed sample shows a $T_g(U)$ step between -10 and 0 °C, which slightly shifts towards higher temperature in a PA sample. From TSDC results shown above, a NA sample is expected to possess a higher $T_g(U)$. In accordance, we see a gradual increase in heat-flow above 40 °C

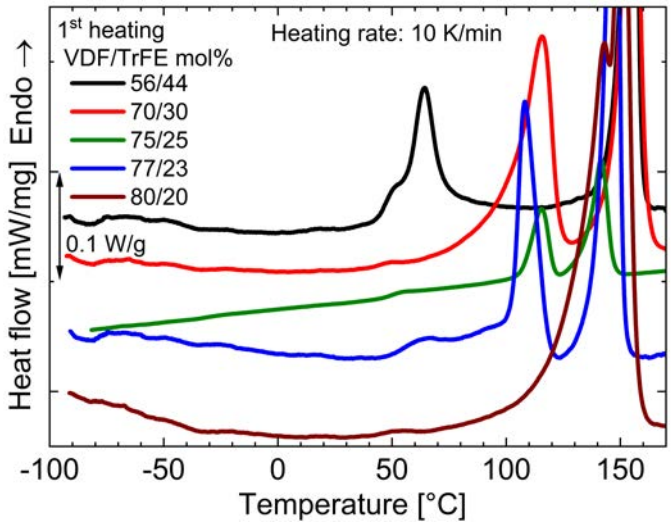

Figure 8.21: First heating endotherms of P(VDF-TrFE) copolymers with different ratios of VDF/TrFE.

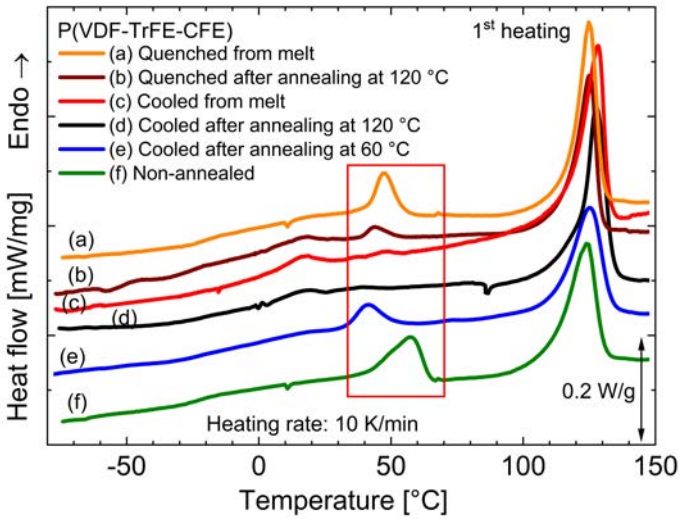

Figure 8.22: DSC first heating traces of a P(VDF-TrFE-CFE) terpolymer subjected to different heat treatments.

that merges with the endothermic F-P transition peak. However, we also observe a relaxation-like step in the $T_g(U)$ temperature range of the annealed samples. This suggests that in addition to changes in the fraction of CAP, annealing also induces other changes in the semi-crystalline structure that is responsible for this shift in $T_g(U)$ as discussed in detail in Section 12.4. Comparing the jump in heat-flow, the relaxation above 40 °C is stronger than that occurring at lower temperatures [177].

The effects of annealing on the overall mid-temperature transition are also clearly seen in Figure 8.25a (irreversible heat flow). The completely annealed sample (annealed at 120 °C) which has the least amount of tie molecules and the lowest CAP fraction exhibits only a small step/peak around 48 °C. This indicates that the major contribution comes from the *condis* transition . For the partially-annealed

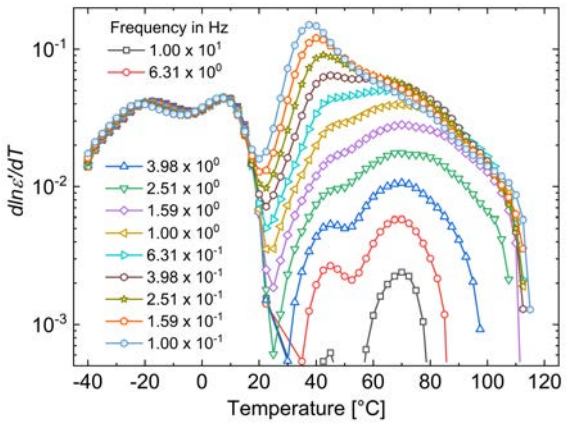

Figure 8.23: Temperature coefficient of permittivity α_ε of a P(VDF-TrFE-CFE) terpolymer annealed at 120 °C at fixed frequencies between 10^{-1} and 10^{1} Hz.

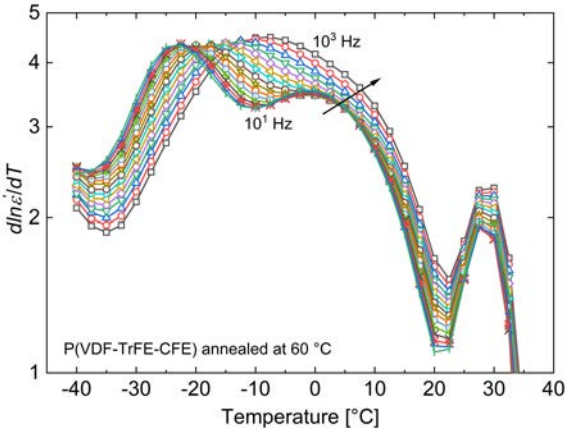

Figure 8.24: Temperature coefficient of permittivity α_ε of a P(VDF-TrFE-CFE) terpolymer annealed at 60 °C at fixed frequencies between 1 and 10^{3} Hz.

and non-annealed samples, a larger CAP volume fraction is expected, which facilitates the formation of secondary crystals, resulting in a stronger T_{mid} peak in the mDSC thermograms. An identical scenario can be observed in samples quenched from either annealed and melt state. In the case of a sample quenched from melt, T_C moves to a higher temperature than observed in slowly cooled samples (Section 9.8) and superimposes with the structural transition of S.C crystals melting as inferred from Figure 8.22.

8.5 Influence of Chemical Structure on T_{mid}

The observation of mid-temperature range transitions can be extended to other available PVDF-based co- and ter-polymers listed in Figure 8.28 (highlighted within red-box). This once again confirms that mid-temperature transition is a structure-related property of all PVDF-based polymeric materials. Irrespective of the type of PVDF-based polymer, each processing condition has a specific effect on the observed T_{mid} and influences the relative contribution of the individual processes to the overall observed transition. In addition, as inferred from the results presented in this chapter, variations within polymer systems are observed, indicating that the monomer and its molar composition also have an effect on the observed T_{mid}.

In general, PVDF homo- and P(VDF-TFE) co-polymers show a strong presence of T_{mid}. In the case of the homopolymer, this can be viewed in the light of thermodynamically preferred α phase. In a P(VDF-TFE) copolymer, though β phase is preferred, the chemical structure is similar to the homopolymer with a higher concentration of H-H and T-T defects. These 'TFE' defects can lead to localized constrained amorphous regions and can enhance a-c interface effects, explaining for the comparatively strong T_{mid} behavior observed. A similar scenario can be predicted for a P(VDF-HFP) copolymer which crystallizes

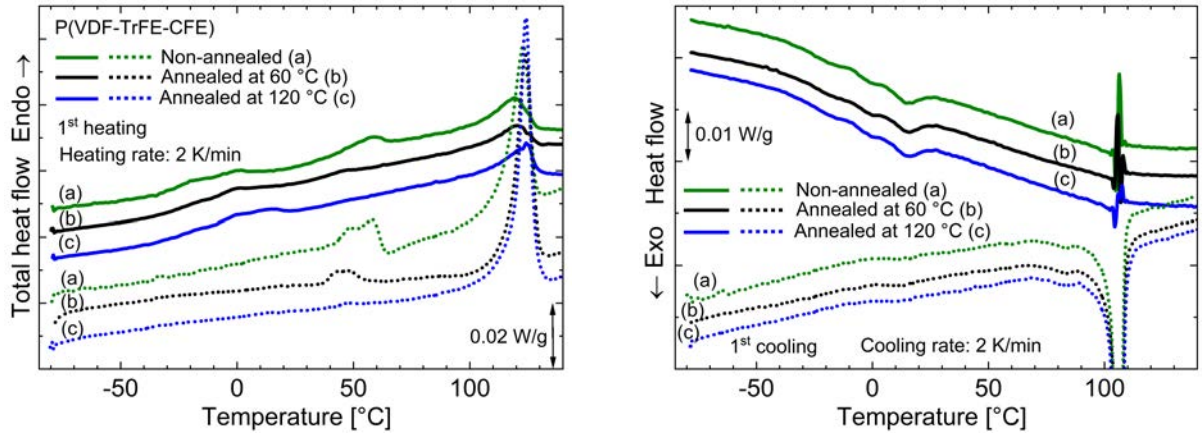

(a) **(b)**

Figure 8.25: Modulated DSC thermograms showing contributions from reversible heat-flow (—) and irreversible heat-flow (· · ·) as measured for a P(VDF-TrFE-CFE) terpolymer subjected to different heat-treatments during (a) first heating and (b) first cooling.

in a predominant α phase [44, 45] and shows a strong conformational disorder process.

On the other hand, P(VDF-TrFE) copolymers show the weakest T_{mid} among the PVDF family of materials studied in this work. A higher crystallinity with a predominant β crystalline structure can be attributed for this behavior. P(VDF-TrFE) based terpolymers by virtue of their F-P transition temperature lying in the vicinity of T_{mid}, most often show a combined endothermic peak during heating in DSC. It is necessary to use other techniques such as mDSC, TSDC and derivative analysis of dielectric spectra to separate the transitions.

8.6 Overview of Essential Observations

A summary of the most important observations of processing on T_{mid} and other transitions is tabulated in Table 8.5.

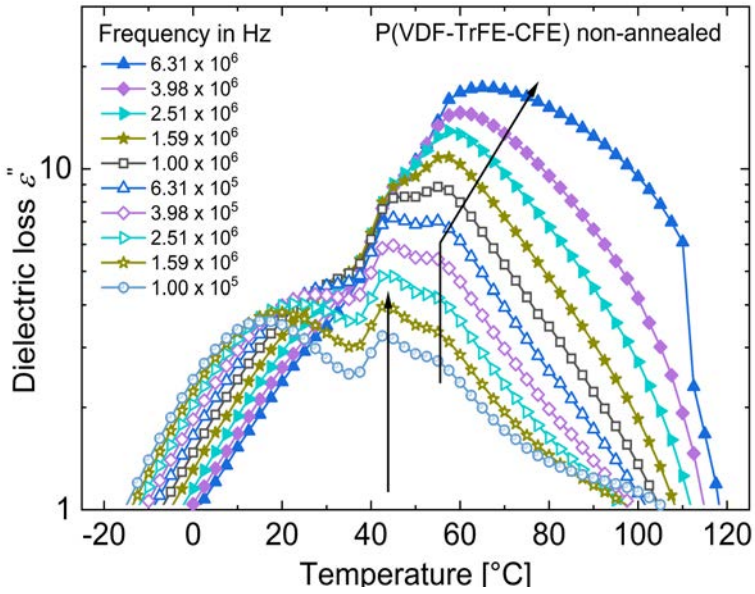

Figure 8.26: Dielectric losses of a non-annealed P(VDF-TrFE-CFE) terpolymer at selected frequencies between 10^5 to 10^7 Hz.

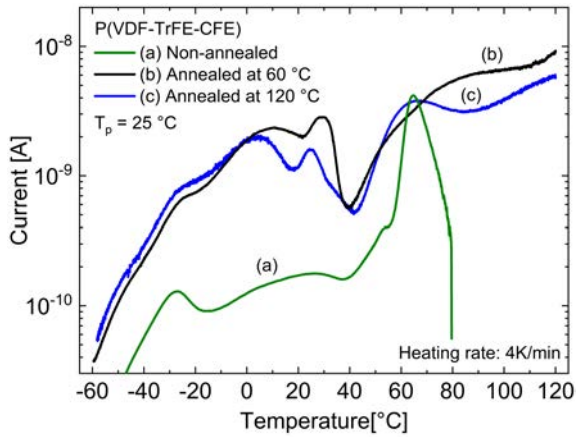

Figure 8.27: TSDC spectra of differently heat-treated P(VDF-TrFE-CFE) terpolymer films. The non-annealed sample was poled at $E_p = 5$MV/m and the annealed samples at $E_p = 10$MV/m for $t_p = 10$min.

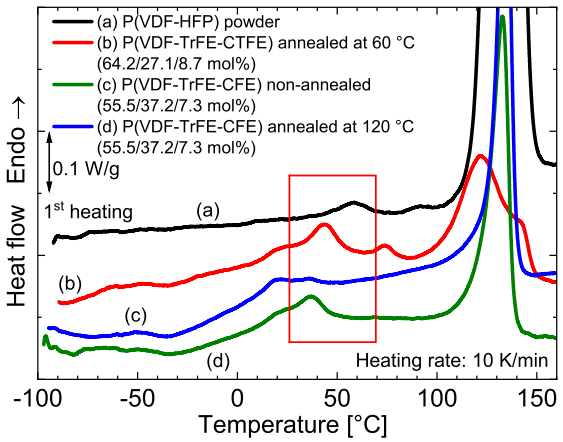

Figure 8.28: DSC 1st heating traces of other PVDF-based co- and ter-polymers.

Table 8.5: Overview of the important observations of processing on the transitions in PVDF-based polymers.

Process	Observation	Explanation
Overall T_{mid}	Strong in PVDF and P(VDF-TFE)	α phase thermodyamically favored and TFE units acting as defects, respectively
	In P(VDF-TFE), on stretching at low to higher temperature, shape changes from endothermic to relaxation-like step in DSC	change in fraction of Constrained Amorphous Phase (CAP)
	weak in P(VDF-TrFE)	β phase thermodyamically favored
	overlapping with Curie transition in P(VDF-TrFE-CFE)	lower T_{C} of terpolymers
$T_{\mathrm{g}}(U)$	detected between -20 and $+20\,^{\circ}\mathrm{C}$ in PVDF, P(VDF-TFE) and P(VDF-TrFE)	presence of CAP
	In P(VDF-TrFE-CFE) shifts with annealing	structure related changes on annealing
Condis	In PVDF, observed in stretched samples and samples prepared from CHN	presence of α phase
	In P(VDF-TrFE), present in non-annealed samples	higher fraction of CAP and α phase
T_{C}	In drop-cast P(VDF-TFE), merges with T_{m}	annealing temperature
	Higher ratio of TrFE, lower T_{C}	decrease in interaction between VDF units

8. INFLUENCE OF PROCESSING ON T_{MID} AND OTHER TRANSITIONS IN PVDF-BASED POLYMERS

9

Modifying Crystallinity and Morphology of PVDF-based Polymers by Means of Rapid Quenching

9.1 Introduction

In PVDF-based homo-, co- and ter-polymers which are semi-crystalline in nature, the morphology, type and fraction of different crystalline phases are strongly influenced by the processing methods. In laboratory conditions, polymer films are usually prepared by different methods such as drop-casting, melt-pressing, spin-coating, doctor blading, etc. [237, 238]. On the other hand, commercial films are prepared by extrusion technique, often involving rapid quenching of the polymer melt as it leaves the extruder die [239]. These films exhibit better structural homogeneity and lower DC conductivity [23, 240]. This could be seen as a result of controlling the crystallization kinetics during the quenching process. Hence, it would be advantageous to prepare such high-quality films in laboratory conditions by quenching the samples from the melt-state. In addition, studying the effects of rapid quenching on PVDF-based semi-crystalline polymers would be helpful to control the crystallinity and morphology of these materials.

9.2 State of the Art[1]

Nakagawa and Ishida performed various quenching experiments with PVDF as early as in 1973 [241]. In their study, form II (α) PVDF samples were quenched from their annealed (between 130 and 180 °C) and melt state. In addition, they also reannealed previously quenched samples. The specimens were characterized using specific volume measurements, DSC and electron microscopy. Measurements on quenched samples revealed that recrystallization of meta-stable crystals occurs during the heating step

[1] Parts of this section are adapted from T. Raman Venkatesan *et al.*, "Structure-Property Relationships in Three-Phase Relaxor-Ferroelectric Terpolymers", *Ferroelectrics*, 586(1), 60-81, 2022" [24].

in DSC. However, the crystallinity (χ_c) of the samples did not vary much due to quenching. A change in χ_c of only 15% was observed between the various samples which were either quenched or slowly cooled from their respective annealed or melt state.

Avrami equation of crystallization is used to describe isothermal crystallization in polymers [242, 243, 244]:

$$1 - X_t = \exp(-kt^n), \tag{9.1}$$

where X_t is the relative degree of crystallinity present at a given time (t), k is the overall crystallization rate constant containing individual contributions from nucleation and growth rate, and n is referred to as the Avrami parameter that depends on the nature of nucleation and growth geometry of the crystals. The crystallization rate k reaches a maximum at $(T_g + T_m)/2$ and an exponential decrease is seen as the sample temperature approaches its T_g and T_m [245].

The half crystallization time ($t_{1/2}$) is defined as the time required to reach half of the final crystallinity and can be calculated from k value using the below equation 9.2. In general, increasing in the crystallization temperature (T_{crys}) causes an increase in $t_{1/2}$ [245, 246, 247]

$$t_{1/2} = \left(\frac{\ln 2}{k}\right)^{1/2}. \tag{9.2}$$

Various studies on crystallization kinetics, microstructure and thermal behavior of PVDF samples have been done in the past [246, 248, 249, 250, 251]. These studies had estimated the Avrami exponent and half crystallization time ($t_{1/2}$) for the different crystallized PVDF specimens. A brief summary of their findings have been reported in the work of Silva *et al.* [247]. From previous studies and their own experiments, Silva *et al.* reported that crystallization at temperatures (T_{crys}) below 160 °C results in exclusively α PVDF. For crystallization at higher temperatures (above 160 °C), additional γ phase spherulites are also found. The γ crystallites were either directly formed from the melt or were transformed from α crystallites. In the case of Avrami parameter n, for samples crystallized at 150 °C a high n value of around 4 was determined, suggesting growth of spherulites with thermal-quenched induced nucleation (sporadic nucleation). On increasing the T_{crys} further, the α crystallization changes from thermal to athermal quench-induced nucleation (instantaneous nucleation). For γ crystallites, the crystallization morphology of the spherulites changes from fibrillar to lamellar with increasing T_{crys}.

On the other hand, the different annealing conditions had an effect on the melting behavior [241]. While samples annealed and then quenched had similar behavior as that of samples which were melt and then quenched, quench-reannealed specimens reported a different response depending upon whether they were annealed below or at/above their melting point (T_m). When samples were annealed below their T_m, new crystals are formed in regions of the amorphous phase where crystallization is permissible.

However since the crystallizable portion is limited owing to the presence of head-to-head defects, a marginal increase of χ_c of only 5 % is observed. In addition, the crystals which are formed during the melting step become more ordered. In the case of reannealing at or above their melting temperature, lamellar thickening occur in the already formed large crystals along with the melting of smaller crystals. Recrystallization of these smaller crystals occurs during the cooling process, leading to the observation of double endothermic peaks during subsequent heating.

The effects of quenching on the different crystalline phases in P(VDF-TrFE) based terpolymers were studied by Klein *et al.* [151] who reported that additional crystals were formed during quenching of a P(VDF-TrFE-CFE) terpolymer sample when it was crystallized at a temperature T_x and then quenched rapidly to RT. Such crystals that melt at lower temperatures than the crystals formed during isothermal crystallization have a higher fraction of polar all-*trans* conformations, enhancing terpolymer ferroelectricity. Consequently, the quenched terpolymers show larger hysteresis loops and smaller electrostrictive strains. As T_x was increased from 112 to 142 °C, the proportion of crystals formed during quenching increased. At T_x = 142 °C, it amounted to more than 90 % of the total number of crystals. At the same time, the absolute value of the electrostrictive strain decreased from −5.9 to −4.2 % in samples quenched after crystallization at 112 and 142 °C, respectively.

Gadinski *et al.* [116] had quenched P(VDF-TrFE-CTFE) samples from the melt in ice water (referred to as TerQ) and studied the influence of rapid quenching on the crystalline phases that govern the dielectric hysteresis behavior. They observed that the quenched samples show higher fractions of all-*trans* conformations when compared to slowly melt-cooled samples (referred to as TerAC) and to samples annealed at 90 °C (cooled from the melt before annealing and cooling down to RT; referred to as TerSCAn). In addition, quenching resulted in the CTFE terpolymer exhibiting a SHL with a lower saturation polarization (P_s) and a higher remanent polarization (P_r), *i.e.*, opposite to the DHLs with a higher P_s value and a lower P_r value observed on the two slowly cooled samples. The differences were explained as a result of the changes in the crystalline phases during quenching.

In the case of quenching, the terpolymer is reported to form two roughly equivalent fractions, one rich in TrFE (ferroelectric) and poor in CTFE, and the other one *vice-versa* (paraelectric-like or relaxor-ferroelectric). On application of an electric field, the existing FE regions are aligned and the R-F regions are irreversibly converted into FE regions, which results in SHLs observed for the quenched samples. In the case of the slowly cooled TerAC and TerSCAn samples, the slow crystallization times allow for a sufficient number of CTFE groups to be included in the crystalline structure so that we find a dominant R-F phase in the terpolymer. In addition, a significant fraction of a paraelectric (PE) phase with non-polar TG^+TG^- conformations are formed [54, 116]. Hence, on application of an electric field, the paraelectric regions undergo a reversible transformation into the polar FE phase (PE → FE) during

which the molecular chains adopt all-*trans* conformations and the R-F regions undergo an irreversible R-F $\rightarrow$ FE transformation [116, 150]. The former transformation leads to the observed DHL behavior.

9.3 In-House Quenching Setup

Usually in studies where the samples are quenched, the samples are heated to a temperature above their melting points in a hot-plate or oven and then thrown into ice-water, liquid nitrogen or water [186, 241]. This step involves a time-delay between the melting and quenching steps during which the sample already starts to crystallize and undergoes changes from its melt-state. This time-delay can be avoided by carrying out the quenching process *in-situ* without having to remove the sample from the heating equipment. For this purpose, an in-house quenching setup as shown in Figure 9.1 was fabricated and used. The sample to be quenched is placed in an active cell between two metal plates of a sample holder inside a measurement chamber, similar to the assembly in a DRS setup. Hence, the setup can be used for dielectric measurements by connecting with an impedance analyzer and also used for TSDC measurements in conjunction with an electrometer. The sample holder is connected to a vertical pneumatic moving arm to mount the sample. In addition, two horizontal retractable arms on either side of the sample can be used to hold the samples under pressure during heating. The sample holder is held under vacuum in a dry nitrogen gas atmosphere. The heating and cooling of the samples are controlled by a Novocontrol Quatro cryosystem. The quenching medium (liquid nitrogen) is placed below the measurement chamber. After heating of the sample film above its melting point for several minutes, the quenching operation starts with the opening of the flap located at the bottom of the measurement chamber. This is followed by the downward movement of the sample holder directly into the quenching medium. The sample reaches the temperature of the quenching medium (liquid nitrogen) very quickly within a few seconds as shown in Figure 9.2 (sample quenched from 0 °C).

9.4 Quenching Procedure

In this study, PVDF homopolymer (melt-pressed), P(VDF-TFE) 80/20 mol% (melt-pressed), P(VDF-TrFE) 75/25 mol% (drop-cast) and P(VDF-TrFE-CFE) 62.2/29.4/8.4 mol% (drop-cast) films were quenched either from their melt- or annealed-state in liquid nitrogen. For comparison, films which were slowly air-cooled from their melt- or annealed-state were used. In the case of PVDF, the samples were melt at 200 °C for 30 min and the other PVDF-based co- and terpolymers were melt at a temperature of 180 °C for 30 minutes above their melting-points to erase their thermal history before rapidly quenching them in liquid nitrogen. For the annealing step, all the samples were cooled quickly from their melt-temperature to 120 °C. The samples were annealed for a duration of 30 min before quenching them in liquid nitrogen.

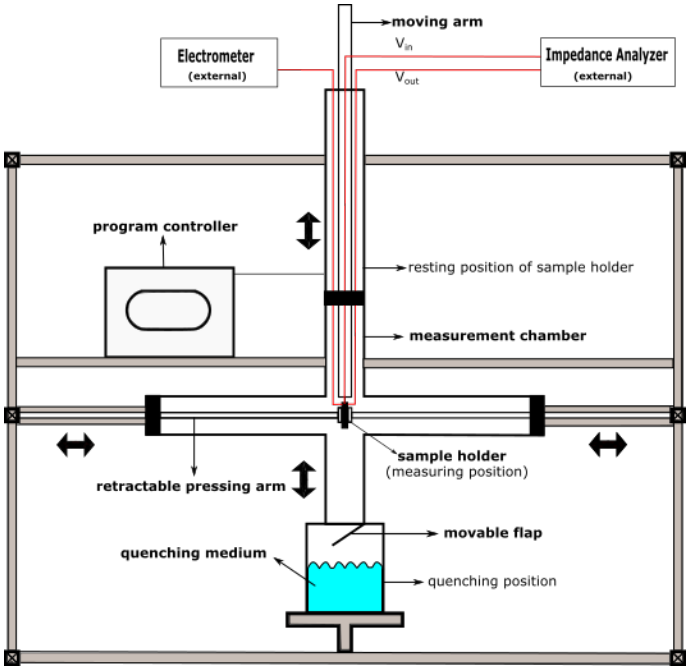

Figure 9.1: Schematic of in-house quenching setup used for rapid quenching of polymer films.

9.5 Effect of Quenching on Melt-pressed PVDF Homopolymer Films

Figure 9.3 and Table 9.1 shows the RT FTIR spectra of quenched PVDF films compared with that of slow-cooled samples. From the characteristic wavelengths associated with the different crystalline conformations we observe that PVDF films primarily crystallize in α phase with the presence of some β crystals. Though Silva *et al.* had reported the presence of γ crystals when crystallized above 160 °C [247], we do not observe a definite peak at 506 cm^{-1} assigned to γ phase (Section 5.5). From this we can infer that crystallization from the melt (slow-cooled or quenched) shows different behavior than crystallization at temperatures near its melting point.

Table 9.1 shows the fraction of β and α phase crystals present in the different heat treated PVDF films estimated based on the method by Gregorio and Cestari [148] (Section 5.5). From the table we can observe that samples quenched from melt (QM) do not show much difference in the fraction of β and α crystals when compared to a sample cooled from melt (CM). Since annealing is shown to stabilize the α phase [241, 247], we see an increase of the paraelectric phase α crystals in a sample slowly cooled after annealing (CA) when compared to a CM sample. On the other hand, quenching a sample after annealing (referred to as QA) shows an increase in the amount of β crystals as seen by the increase in the strength of the shoulder at 840 cm^{-1} in Figure 9.3.

The effects of quenching on the crystalline morphology can be understood by analyzing the data from WAXD scans. Figure 9.4 shows the RT WAXD scans of the different heat treated samples between

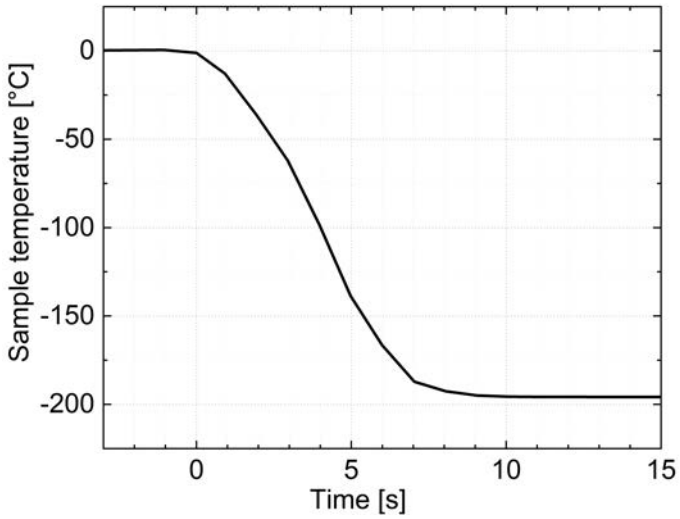

Figure 9.2: Plot of sample temperature *vs.* time since the commencement of the quenching operation.

Table 9.1: Fraction of different crystalline conformations in quenched and slow-cooled PVDF films calculated from characteristic FTIR absorption peaks using the method suggested by Gregorio and Cestari [148].

PVDF melt-pressed film	$T_{m>3}$ **[%] 840 cm^{-1}**	TG^+TG^- **[%] 763 cm^{-1}**
Cooled from melt (CM)	35	65
Quenched from melt (QM)	31	69
Cooled after annealing (CA)	27	73
Quenched after annealing (QA)	38	62

15 and 30° corresponding to the crystals present perpendicular to the chain axis [138, 151]. We can observe that quenching of the PVDF films results in the suppression and amorphous broadening of the α peaks near $2\theta = 25.7°$ and 27.9°. Accordingly, an overall decrease of crystallinity is observed in the quenched samples as shown in Table 9.2. Though from FTIR we see an increase in the fraction of α in CA samples on comparison with CM samples, they show a lower crystallinity than melt-cooled samples. This might be due to the fact that CA samples were quickly cooled from their melt state to the annealing temperatures which would have resulted in less nucleation of crystals in the samples when compared to CM samples which were gradually cooled to RT from their melt temperature. Preparation of samples from the melt state also leads to higher coherence length L_c of α crystals located in the (100) crystalline plane than annealed samples.

Overall, the crystallinity of the samples and coherence length of the α crystals in the perpendicular direction of the chain axis are reduced. These changes can be observed in the images obtained under a polar microscope as shown in Figure 9.5. In the case of a CM film slowly cooled from the melt-state, we have large spherulites (sample spherulite highlighted in yellow in Figure 9.5a) with a wide distribution

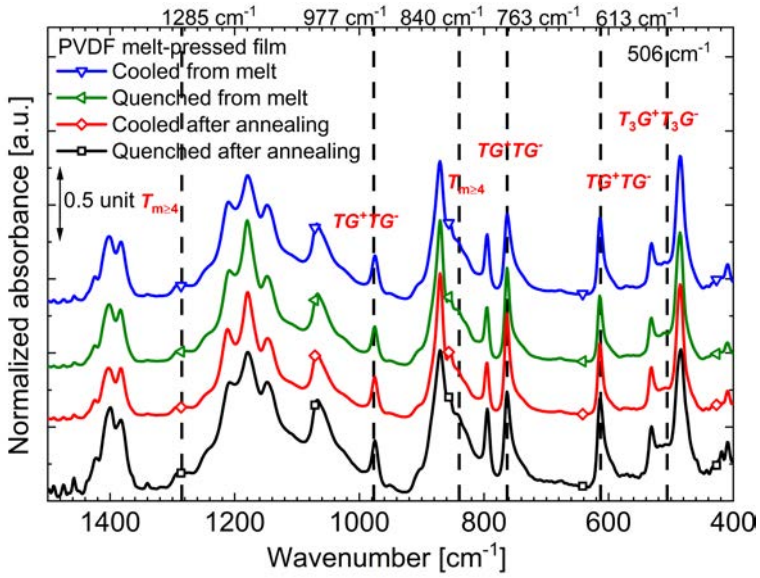

Figure 9.3: RT FTIR spectra of a melt-pressed PVDF homopolymer films subjected to different heat treatment. Symbols are added to the continuously measured spectra in order to facilitate their identification.

of the spherulite size suggesting sporadic nucleation [247]. In the case of a QA sample, it was first quenched (dry nitrogen gas) from the melt to 120 °C leading to a presence of few larger crystals (sample spherulite highlighted in yellow in the Figure 9.5b) due to thermal-quench induced sporadic nucleation. The annealing step at 120 °C stabilizes the growth of α crystals. Finally, quenching of the sample in liquid nitrogen leads to the growth of large number of smaller crystallites (highlighted in red in Figure 9.5b) with a more uniform size distribution (instantaneous athermal-quench induced crystallization) during which the crystallization rate reaches a maximum at $(T_m + T_g)/2$ [245].

Table 9.2: Summary of peak position, coherence length L_c of α crystals near the (100) and (120) planes and total crystallinity of the PVDF films subjected to various heat-treatments.

PVDF melt-pressed film	Lattice indices	Peak Position [°]	Coherence Length L_c [nm]	Crystallinity χ_c[%]
Cooled from melt	(100)	17.7	23.2	55
	(120)	25.7	18.7	
Quenched from melt	(100)	17.7	26.7	37
Cooled after annealing	(100)	17.7	10.1	40
	(120)	25.7	15.5	
Quenched after annealing	(100)	17.8	18.8	32
	(120)	25.7	8.0	

In addition to the crystalline phases and their morphology, the thermal properties of PVDF homopolymer films are actively modified as a result of quenching process. Figure 9.6 shows the 1st heating DSC

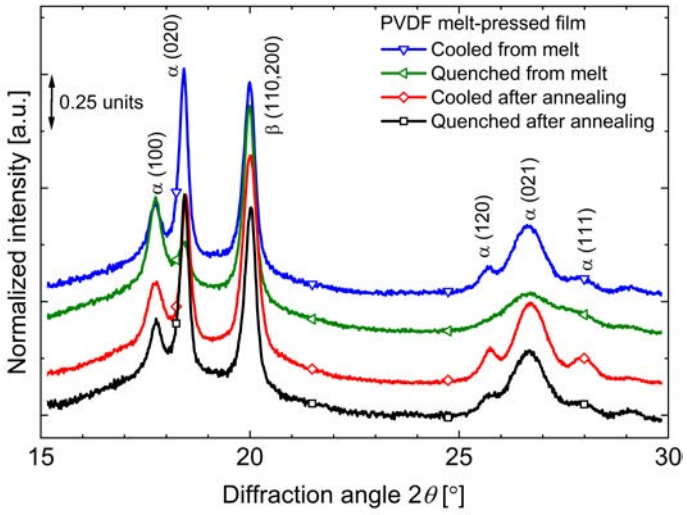

Figure 9.4: RT WAXD scans of melt-pressed PVDF homopolymer films subjected to different heat treatments. Symbols are added to the continuously measured diffraction in order to facilitate their identification.

endotherm of quenched and slow-cooled PVDF films. The changes in mid-temperature transition accompanying the quenching process have already been discussed in Section 8.1.4. With respect to the main melting peak, as listed in Table 9.3, quenched samples (both quenched from melt and annealed state) show a small shift to lower temperatures (1^{st} heating). However, no change in crystallinity is seen between the samples.

Table 9.3: Melting-point T_m, enthalpy of melting ΔH_m and crystallinity χ_c of different heat-treated PVDF films as seen during first and second heating run in DSC. A ΔH_∞ value of 104.6 J/g for 100 % PVDF was used.

PVDF melt-pressed film	heating cycle	T_m [°C]	ΔH_m [J/g]	χ_c [%]
Cooled from melt (CM)	1^{st}	173.4	54.8	52
	2^{nd}	173.0	51.2	49
Quenched from melt (QM)	1^{st}	172.1	54.7	54
	2^{nd}	171.4	58.8	56
Cooled after annealing (CA)	1^{st}	175.3	56.3	55
	2^{nd}	175.4	53.5	51
Quenched after annealing (QA)	1^{st}	172.8	57.1	56
	2^{nd}	171.8	57.7	55

Finally, changes in crystallinity are seen within the samples during the second heating cycle. As shown in Table 9.3, in slowly cooled samples, χ_c decreases slightly during the second heating run, while it generally increases in the case of the quenched samples. In the case of slowly cooled samples, when the films were heated and held at either the melt or annealed state, as specified above, form meta-stable crystals. Since during the DSC procedure samples are melt and immediately cooled down, less meta-

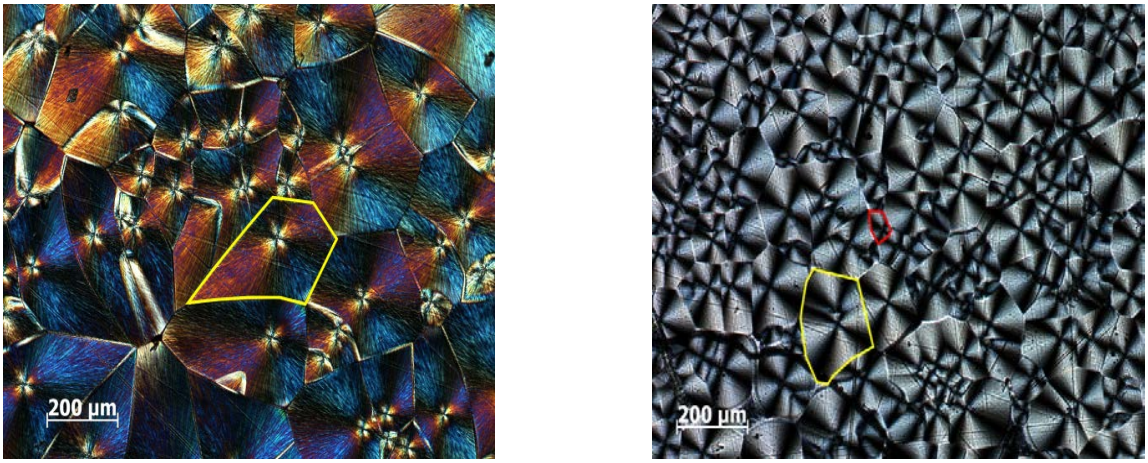

(a) (b)

Figure 9.5: Images of a PVDF film (a) slowly cooled from the melt and a PVDF film (b) quenched after annealing obtained under a polar microscope.

stable crystals could be formed during the cooling cycle which results in a small decrease of crystallinity compared to the thermally treated state. In the case of the quenched samples, during the cooling cycle as the thermal history is erased, crystallization of previously amorphous regions takes place and contributes to the increase in χ_c.

9.6 Effect of Quenching on Melt-pressed P(VDF-TFE) 80/20 mol% Copolymer Films

The RT FTIR spectra of a P(VDF-TFE) copolymer film with a VDF/TFE molar ratio of 80/20, respectively, cooled from its melt state is shown in Figure 9.7. The copolymer shows peaks predominantly at wavelengths assigned to the polar and ferroelectric β phase. In addition to it, we see a certain presence of non-polar paraelectric α and weakly polar γ phases. Particularly, the presence of γ phase is seen in the WAXD scan of a P(VDF-TFE) 80/20 mol% copolymer, irrespective of its heat-treatment. In Figure 9.8, in addition to the β crystalline peak at $2\theta = 19.8^\circ$ with a lattice spacing (d) of 4.48 Å, we observe an additional peak at $2\theta = 19.3^\circ$ with a d value of 4.61 Å. This peak corresponds to the γ phase crystals [135, 252]. Bargain *et al.* had observed a similar peak in solvent-cast 72/28 mol% P(VDF-TrFE) copolymer films which were subjected to consecutive annealing treatment from 87 to 103 °C [138] and they had assigned it to the so-called defective ferroelectric phase (DFE). According to their research, ferroelectric phase during cooling from the annealed paraelectric state does not completely return back to its all-*trans* conformation. Some of the chain segments crystallize with *gauche* conformations resulting in the formation of DFE. A similar phenomenon can be expected to occur in the melt-pressed P(VDF-TFE) films used in this work since they were all re-annealed before either slowly cooling down to RT or

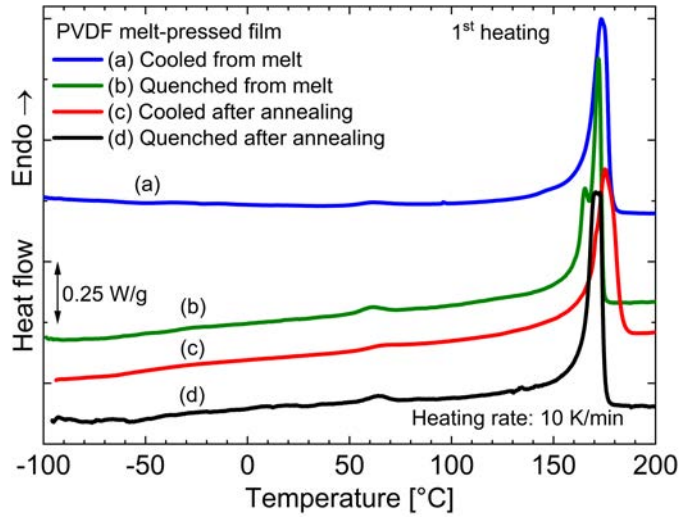

Figure 9.6: DSC endotherm of different heat-treated PVDF homopolymer films as seen during 1st heating run.

quenched in liquid nitrogen. This should have resulted in the formation of *gauche* containing γ phase in the crystalline structure of the heat-treated films in comparison to the initial films prior to the treatment prepared by melt-pressing. In a melt-pressed sample we observe only the presence of the β phase peak at $2\theta = 19.7^\circ$ as depicted in Figure 9.9.

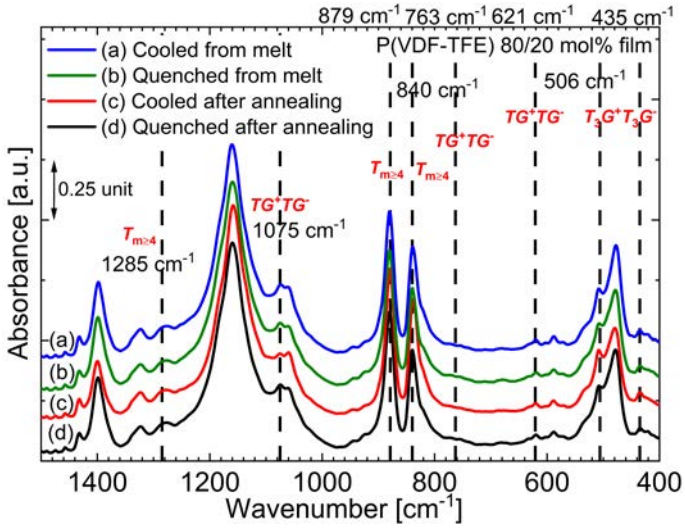

Figure 9.7: RT FTIR spectra of a P(VDF-TFE) 80/20 mol% copolymer films subjected to different heat treatments.

Quenching does not seem to affect the FTIR peak intensities qualitatively. The fraction of β and α phases, relative to each other, present in the various thermally treated samples are quantified in Table 9.4. Quenching process seems to slightly increase the α phase in the copolymer films, similar to that observed in melt-quenched PVDF homopolymer films. This can be confirmed by looking at the

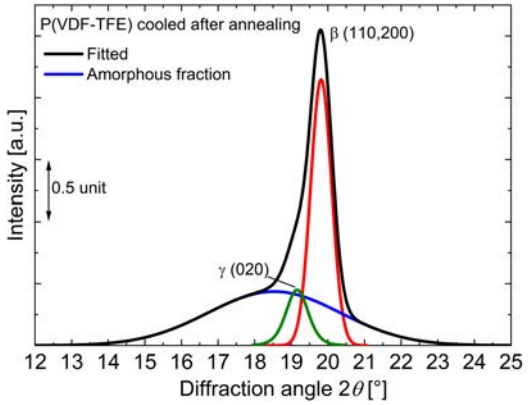

Figure 9.8: RT WAXD scan of a P(VDF-TFE) 80/20 mol% copolymer film slowly cooled after annealing at 120 °C.

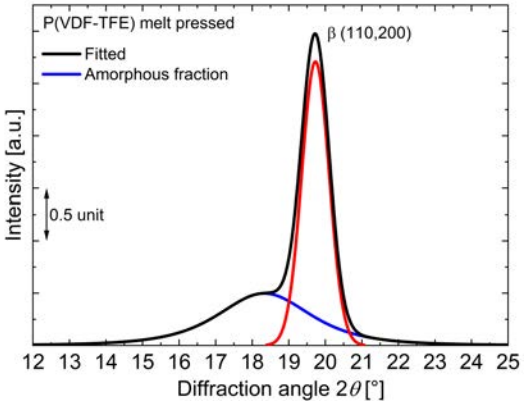

Figure 9.9: RT WAXD scan of a P(VDF-TFE) 80/20 mol% melt-pressed film which was used for the heat-treatment procedures.

RT WAXD scans of the quenched samples in comparison to the slowly cooled specimens as shown in Figure 9.10. Quenching results in the suppression of β phase peaks in P(VDF-TFE) copolymer films, especially those above $2\theta = 30°$, which correspond to crystals that lie on planes parallel to the chain axis (intrachain order) [138, 151]. In the case of the transmission recorded around $2\theta = 35.1°$, the crystalline peak disappears after quenching and we observe only amorphous halo around this region in the quenched samples. As expected, the crystallinity of the quenched samples are reduced (Table 9.5).

Table 9.4: Fraction of different crystalline phases in quenched and slow-cooled 80/20 mol% P(VDF-TFE) films calculated from characteristic FTIR absorption peaks using the method suggested by Gregorio and Cestari [148].

P(VDF-TFE) melt-pressed film 80/20 mol%	$T_{m>3}$ **[%] 840 cm^{-1}**	TG^+TG^- **[%] 763 cm^{-1}**
Cooled from melt (CM)	87	13
Quenched from melt (QM)	84	16
Cooled after annealing (CA)	89	11
Quenched after annealing (QA)	85	15

In order to study the effect of quenching on the thermal properties DSC scans were performed on the specimens, whose results are displayed in Figure 9.11. Clear differences are observed between the melting behavior of quenched and cooled samples. While the slowly cooled samples show two endothermic peaks at high temperatures, the melt quenched (QM) sample only shows a single transition at an intermediate temperature between the two endotherms observed in the slowly cooled samples. In the case of an annealed and quenched (QA) sample, similar to a QM sample also shows a large melting endotherm at 124 °C, followed by an additional melting peak around 134 °C.

To know more about this phenomenon, DRS on a melt and slowly cooled sample was made and the dielectric spectra as a function of temperature at different frequencies is shown in Figure 9.12. Just above

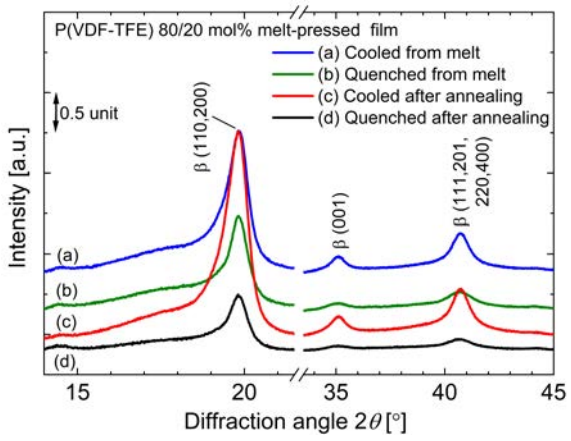

Figure 9.10: RT WAXD scans of P(VDF-TFE) copolymer films subjected to quenching procedure compared with that of samples which were slowly cooled from melt.

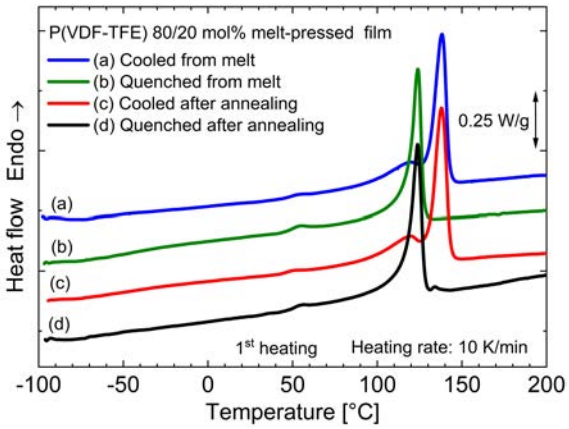

Figure 9.11: DSC endotherm of different heat-treated P(VDF-TFE) copolymer films as seen during 1st heating run.

Table 9.5: Melting-point T_m, enthalpy of melting ΔH_m of different thermally-treated P(VDF-TFE) films as seen during first heating and cooling run in DSC. The table also lists χ_c values calculated from DSC (1st heating run using ΔH_m and $\Delta H_{F\text{-}P}$ values, ΔH_∞ = 104.6 J/g for 100 % crystalline PVDF used) and WAXD.

P(VDF-TFE) 80/20 mol% melt-pressed film	T_m [°C] DSC	ΔH_m [J/g] DSC	χ_c [%] DSC	χ_c [%] WAXD
Cooled from melt (CM)	138.3	44.8	43	35
	135.0	40.4	39	[-]
Quenched from melt (QM)	124.0	34.1	33	25
	133.6	39.8	38	[-]
Cooled after annealing (CA)	137.5	33.3	43	35
	125.3	38.3	37	[-]
Quenched after annealing (QA)	124.0	33.4	32	19
	131.6	38.7	37	[-]

the temperature where we observe the lower DSC endotherm in slowly cooled samples (around 120 °C in Figure 9.11), we observe a frequency-independent peak at 129.5 °C in the real part of permittivity. This points out to a structural or phase transition process. The presence of this peak is also seen in the dielectric loss spectra at about 132 °C. Since the losses are higher at low frequencies due to the contribution from conductivity in Figure 9.12, the conduction-free dielectric loss (ε''_{der}) factor is plotted along with the temperature coefficient of permittivity $\partial\, ln\, \varepsilon'(T)/\partial\, T = \alpha_\varepsilon$ in Figure 9.13. From the figure, it is clear that the process is frequency-independent and above this peak the sample begins to melt. Based on results from a similar composition, it can be identified with a ferroelectric-to-paraelectric/Curie transition commonly found in PVDF-based copolymers [15, 16]. Lovinger *et al.* were the first to detect a Curie transition in P(VDF-TFE) copolymers [15]. The authors had also observed that rapidly quenched

samples show a single melting endotherm at 126 °C in their P(VDF-TFE) samples with a VDF/TFE molar ratio of 81/19 [16]. Hence, it is clear that quenching reduces the melting transition temperature (T_m) to lower temperatures. From Figure 9.13, we can also see the contribution of different processes to T_{mid}. While in the conduction-free loss derivative we observe the conformational disorder process, in the $\partial ln\varepsilon'(T)/\partial T$ curve we observe the structural process of secondary crystals melting.

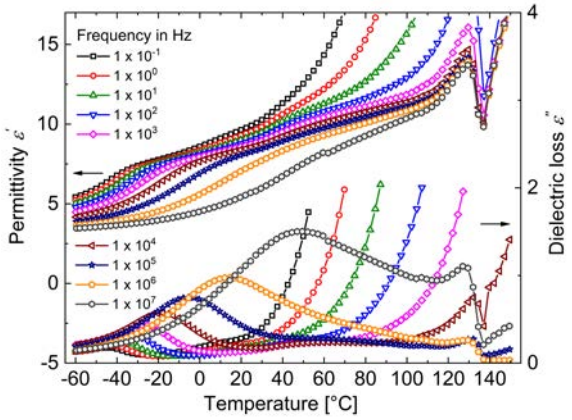

Figure 9.12: Dielectric spectra of a P(VDF-TFE) 80/20 mol% copolymer film slowly cooled sample from the melt plotted as a function of temperature at fixed frequencies.

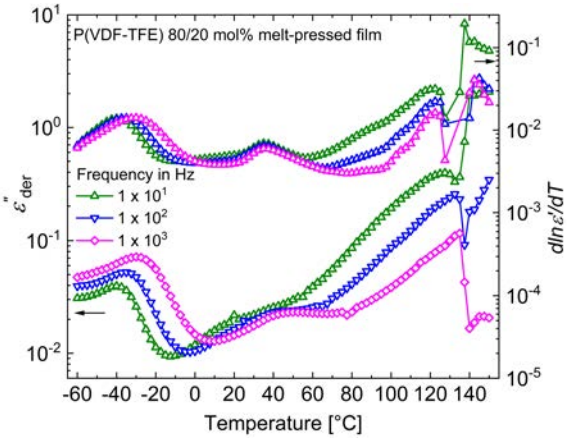

Figure 9.13: Conduction-free dielectric loss (ε''_{der}) along with the temperature coefficient of the permittivity $\partial ln\varepsilon'(T)/\partial T = \alpha_\varepsilon$ of a P(VDF-TFE) 80/20 mol% melt-pressed film slowly cooled from melt derived from the dielectric spectra measured at frequencies from 10^1 to 10^3 Hz.

With respect to the fraction of β phase in the quenched samples as seen in Table 9.4, the values doe not change much compared to slowly cooled samples. This suggests that the F-P transition process is superimposed with the melting transition in the quenched samples. This is confirmed in the second heating endotherm of a QM sample as shown in Figure 9.14 where we observe dual peaks corresponding to both T_C and T_m, respectively, as opposed to the first heating where only a single endotherm is visible. A similar behavior was also exhibited by an AQ sample. Initially, no clear T_C was detected in P(VDF-TFE) copolymers [253]. This is because the TFE unit stabilizes the *trans* conformation of the copolymer [207] and results in the shift of T_C to move very close to its melting temperature (T_m) [22]. This is further demonstrated in the second heating run of a slowly cooled P(VDF-TFE) film in Figure 9.15 where the F-P transition no more appears as a separate endotherm as seen during first heating and merges with the melting-transition – visible only as a small shoulder. In addition, during both cooling cycles we only observe a single exothermic peak around 105 °C. However, by using a slower heating rate it is possible to separate the transitions during the cooling step as shown in the inset of Figure 9.15 [16].

Returning back to the dual melting peak in a QA sample, from Figure 9.16 we see that the F-P transition is observed during the second heating at 127 °C followed by the melting peak which appears

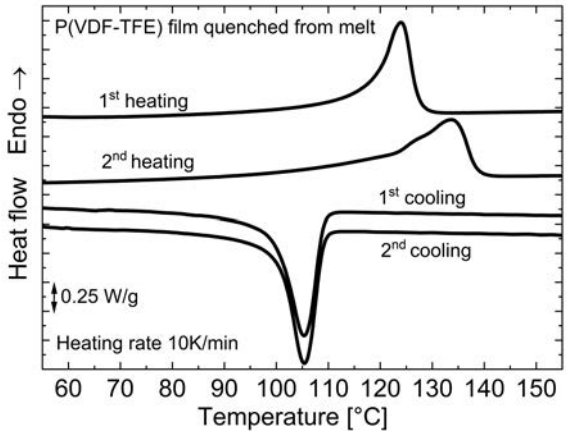

Figure 9.14: DSC endotherm of a P(VDF-TFE) 80/20 mol % film which was quenched from melt during 1st and 2nd heating/cooling cycles.

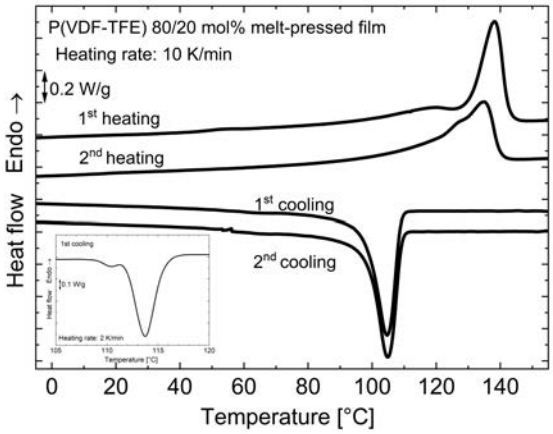

Figure 9.15: DSC endotherm of a P(VDF-TFE) 80/20 mol % film slowly cooled from melt during 1st and 2nd heating/cooling cycles. Inset shows the 1st cooling cycle at a lower heating rate of 2 K/min.

around the same temperature where the smaller peak appears during the first heating. This confirms that majority of the crystals are formed during quenching, which melt at a lower temperature than reorganized crystals. This is similar to the observation by Klein *et al.* [151]. As seen from Table 9.5, changes in χ_c observed during the second heating run in the various thermally treated P(VDF-TFE) films are similar to those observed in PVDF samples. We also observe a decrease in χ_c for quenched P(VDF-TFE) films similar to that observed in quenched PVDF homopolymer samples (Table 9.2).

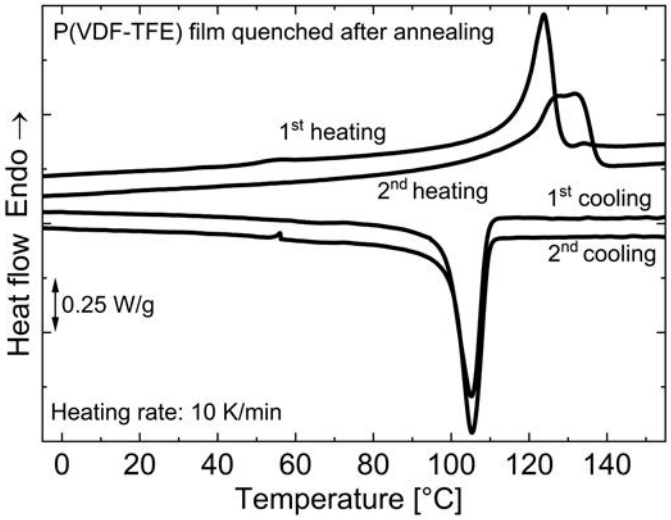

Figure 9.16: DSC endotherm of a P(VDF-TFE) 80/20 mol % film which was quenched from melt during 1st and 2nd heating/cooling cycles.

9.7 Effect of Quenching on Drop-Cast P(VDF-TrFE) 75/25 mol % Copolymer Films

Previously, various studies have employed the use of quenched P(VDF-TrFE) films [252, 254, 255, 256, 257]. Lee *et al.* [257] reported that spin-coated films which were quenched from the melt in ice or liquid-nitrogen show preferential chain orientation near the normal to the planar surface with 'face-on' lamellar crystals. These films were reported to have lower ferroelectric properties than cast or annealed films. Similarly, annealing at temperatures higher than T_m were shown to produce P(VDF-TrFE) films with poor polarization properties owing to the lower χ_c [258, 259]. Contrarily, Li *et al.* stated that annealing the copolymer samples above their melting point resulted in a higher χ_c [260] and Singh *et al.* [255] pointed out that faster cooling rates lead to a 30% increase in polarization of P(VDF-TrFE) films. Hence, exclusive studies relating the effect of quenching on the crystalline phase morphology, phase transitions would help to better predict the ferroelectric and subsequent polarization properties of P(VDF-TrFE) copolymers, which are the most widely used PVDF-based copolymers. Accordingly, they were subjected to quenching procedures and their results are discussed below.

The RT FTIR spectra of a 75/25 mol % P(VDF-TrFE) copolymer shows similar features as that of a P(VDF-TFE) copolymer. The crystalline regions consist of a rich all-*trans* conformation (β phase) resonated by the strong peaks at 1285, 879 and 842 cm^{-1} in Figure 9.17. Though they show very weak absorbance at characteristic wavelengths attributed to α phase with a TG^+TG^- conformation at 840 and 506 cm^{-1}, still the presence of it in the crystalline morphology is confirmed by the peak at 1075 cm^{-1}. In addition, peaks at 506 and 435 cm^{-1} also indicate the presence of $T_3G^+T_3G^-$ conformation crystallizing in γ phase. Hence, the method of Osaki *et al.* was used to calculate the relative fraction of each phase in the different thermally-treated copolymer samples [157] and the results are tabulated in Table 9.6.

In the case of a CM sample, cooling from the melt to RT results in roughly equal amount of β and γ phases in the copolymer. However, when the same sample is cooled from 200 to 120 °C and annealed at this temperature, the resultant film predominantly consists of β crystals. These findings are in line with those observed by Tahiro *et al.* [236] on a 73/27 mol % P(VDF-TrFE) copolymer. It was reported that annealing the sample below 125 °C increases the all-*trans* conformation. While quenching from the melt only slightly changes the polar β fraction, quenching from the annealed state results in a large decrease of *trans* segments with a corresponding increase of *gauche* containing α and γ crystals when compared to their corresponding slowly-cooled samples.

Looking at the RT WAXD scans made on the differently treated P(VDF-TrFE) films in Figure 9.18, we do not observe any major changes in peak shape. Only a difference in the shape of amorphous halo around the (110,200) family of planes is observed. These correspond to changes in the overall crystallinity of the sample. Quenched samples show a lower χ_c than the slowly cooled samples as one

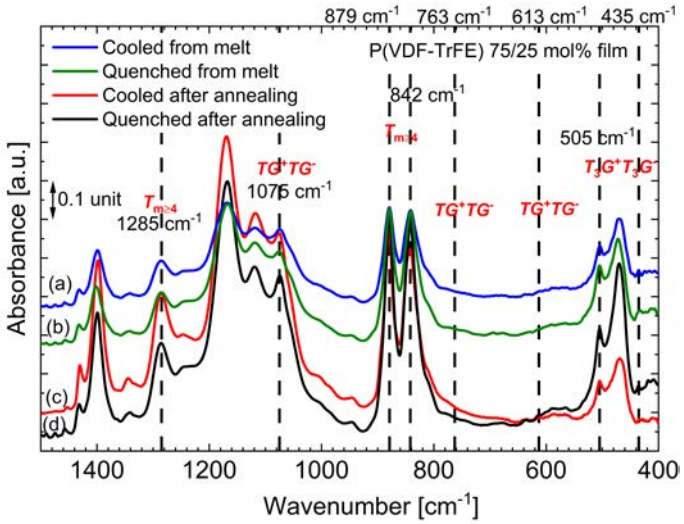

Figure 9.17: RT FTIR spectra of P(VDF-TrFE) 75/25 mol % copolymer films subjected to different heat treatments.

Table 9.6: Fraction of different crystalline phases in 75/25 mol % P(VDF-TrFE) copolymer films subjected to quenching in comparison with films slowly cooled from melt (Based on method suggested by Osaki *et al.* [51, 157]).

P(VDF-TrFE) 75/25 mol % drop-cast copolymer	$T_{m>3}$ **[%] 1285 cm^{-1}**	TG^+TG^- **[%] 613 cm^{-1}**	$T_3G^+T_3G^-$ **[%] 506 cm^{-1}**
Cooled from melt (CM)	38	12	50
Quenched from melt (QM)	35	12	53
Cooled after annealing (CA)	74	2	24
Quenched after annealing (QA)	42	9	49

would expect (Table 9.7). From the Long period L_p value calculated from Small Angle X-ray Diffraction (SAXD), which gives an estimation of the overall crystalline size distribution, we see that quenched samples show smaller L_p values comparing to the slowly cooled samples owing to the very little time available for crystallization during rapid quenching.

DSC endotherms recorded during the first heating cycle of P(VDF-TrFE) samples with different thermal histories are shown in Figure 9.19. While the melting transition temperatures are similar for the various samples, the F-P transition temperatures for the quenched samples are higher than slowly cooled samples. Previously, although a similar behavior was observed in both samples quenched in ice or liquid nitrogen [254], the reason behind this shift in T_C is not clear. It can be speculated that the decrease in L_p values observed from SAXD measurements on quenched samples (Table 9.7) may have a role in increasing the F-P transition temperature.

Table 9.8 lists the various thermal parameters observed during the first and second heating runs of DSC. In accordance with the results observed from WAXD, we see a decrease in χ_c for the quenched

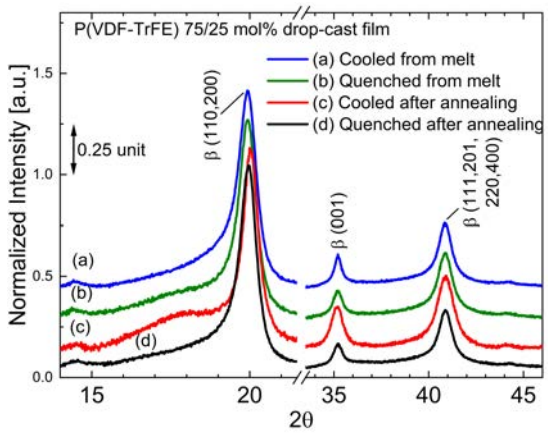

Figure 9.18: RT WAXD scans of P(VDF-TrFE) copolymer films either quenched or slowly cooled from their respective melt and annealed states.

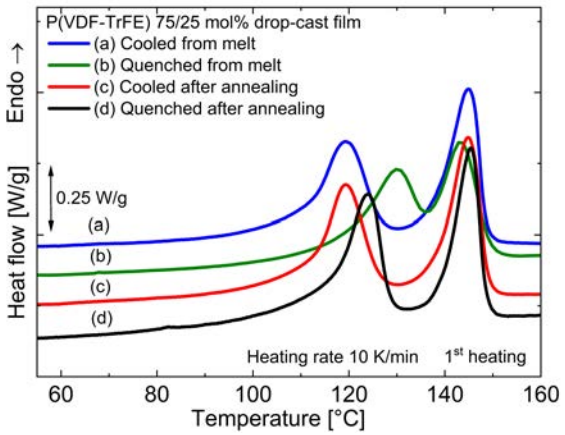

Figure 9.19: DSC endotherms of differently heat-treated P(VDF-TrFE) copolymer films recorded during the first heating run.

Table 9.7: Summary from crystallinity calculated from peak WAXD fitting and Long period L_p calculated from SAXD of thermally treated P(VDF-TrFE) copolymer films.

P(VDF-TrFE) 75/25 mol % drop-cast copolymer	χ_c [%]	L_p [nm]
Cooled from melt (CM)	39	45.0
Quenched from melt (QM)	35	29.0
Cooled after annealing (CA)	40	45.5
Quenched after annealing (QA)	38	45.0

samples during first heating. As expected, an increase of χ_c during the second heating run of a previously quenched film from the melt is observed. However, the contrary is observed in a QA sample, which may be due to experimental errors. A similar behavior of a decrease in χ_c during the second heating is recorded in slowly-cooled samples as observed in the case of PVDF homopolymer and P(VDF-TFE) copolymer. Finally, we observe that once the thermal history of the sample is erased at the end of the first heating cycle after the sample is heated to 200 °C, the T_C of the quenched sample becomes comparable to that of the other samples during the second heating run.

9.8 Effect of Quenching on Drop-Cast 62.2/29.4/8.4 mol % P(VDF-TrFE-CFE) Terpolymer Films

Terpolymer films due to their low crystallinity, smaller crystalline size offer a high amorphous-crystalline interphase area which can be further modified by quenching. From Figure 9.20 which shows the RT FTIR scans and Table 9.9 which tabulates the fraction of different crystalline phases calculated from the intensity of absorption at characteristic wavelengths of the different quenched and cooled samples, we

Table 9.8: Melting point T_m and Curie-transition temperature $T_{F\text{-}P}/T_c$ along with their respective enthalpies observed during the first and second heating cycles of DSC measurements on different thermal treated P(VDF-TrFE) films. The table also summarizes the total crystallinities (using $\Delta H_m + \Delta H_{F\text{-}P}$ and $\Delta H_\infty = 91.45$ J/g for 100 % P(VDF-TrFE)) estimated in these samples.

P(VDF-TrFE) 75/25 mol % drop-cast copolymer	Heating cycle	T_m [°C]	ΔH_m [J/g]	$T_{F\text{-}P}$ [°C]	$\Delta H_{F\text{-}P}$ [J/g]	χ_c [%]
Cooled from melt (CM)	1 st	145.0	27.2	119.4	31.3	64
	2 nd	143.5	24.0	120.2	28.1	57
Quenched from melt (QM)	1 st	142.8	21.3	129.8	24.6	51
	2 nd	146.8	24.4	124.6	28.4	58
Cooled after annealing (CA)	1 st	144.9	33.9	119.4	27.7	67
	2 nd	143.2	24.4	121.0	31.9	62
Quenched after annealing (QA)	1 st	145.3	21.6	124.0	25.4	51
	2 nd	143.1	19.4	120.5	20.7	44

can infer that quenching from the melt increases the β fraction and quenching after annealing increases the γ fraction. On comparison with slowly cooled samples, new *upbeta* crystals are formed when the sample is quenched from the melt and more *trans* containing segments are induced in the existing α crystals when the sample is quenched after annealing. From the WAXD scan displayed in in Figure 9.21, the effect of quenching is seen more in a QM sample than a QA sample. While both the quenched samples result in an increase of the amorphous halo at the base of the paraelectric peak at $2\theta = 18.2°$ (near (110,200) family of planes), a QM sample shows a broader reflection in comparison to a QA sample. However, the weak juxtaposition ferroelectric peak corresponding to (111, 201, 220, 400) family of planes practically remains unaffected by the different heat treatments.

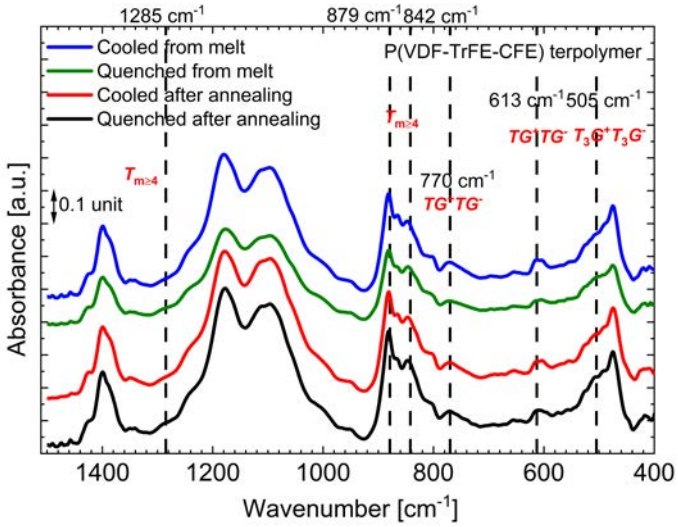

Figure 9.20: RT FTIR spectra of a 62.2/29.4/8.4 mol % P(VDF-TrFE-CFE) terpolymer film subjected to different heat treatments.

Table 9.9: Fraction of different crystalline phases in P(VDF-TrFE-CFE) terpolymer films subjected to different thermal treatments calculated from FTIR based on the method suggested by Osaki *et al.* [51, 157].

P(VDF-TrFE-CFE) 62.2/29.4/8.4 mol % drop-cast terpolymer	$T_{m>3}$ **[%] 1285 cm^{-1}**	TG^+TG^- **[%] 613 cm^{-1}**	$T_3G^+T_3G^-$ **[%] 505 cm^{-1}**
Cooled from melt (CM)	15	31	54
Quenched from melt (QM)	20	27	53
Cooled after annealing (CA)	19	30	51
Quenched after annealing (QA)	18	27	55

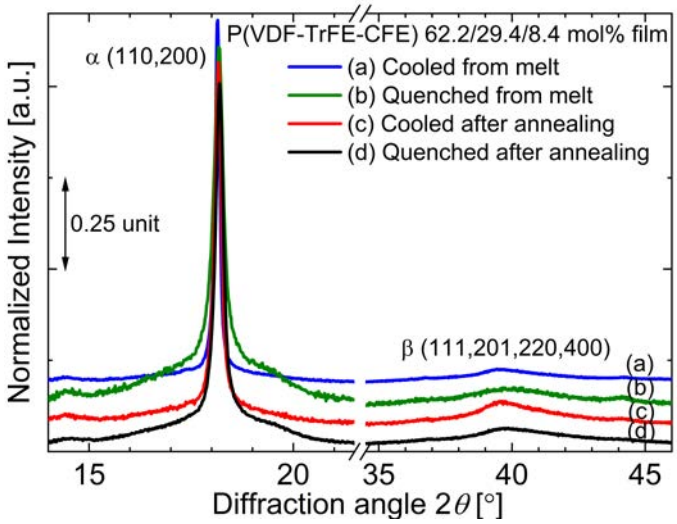

Figure 9.21: RT WAXD scans of P(VDF-TrFE-CFE) terpolymer films with various thermal histories.

Table 9.10: Summary of crystallinity calculated from peak WAXD fitting and Long period L_p calculated from SAXD of heat-treated P(VDF-TrFE-CFE) films.

P(VDF-TrFE-CFE) 62.2/29.4/8.4 mol % drop-cast terpolymer	χ_c **[%]**	L_p **[nm]**
Cooled from melt (CM)	20	60.0
Quenched from melt (QM)	15	24.5
Cooled after annealing (CA)	20	60.0
Quenched after annealing (QA)	15	25.0

The overall long period L_p of the crystals and crystallinity decrease in the quenched samples as shown in Table 9.10. As seen from the table, the values are almost the same for the cooled or quenched samples irrespective of the state it was cooled/quenched from. This should be due to the fact that the annealing temperature of 120 °C is very close to the T_m of the terpolymer, as seen from the DSC endotherms in Figure 9.22. Quenching marginally reduces the T_m of the films.

The major impact of quenching is seen on the Curie and mid-temperature range transitions. Quenching obviously enhances T_{mid} as discussed previously (Section 8.4). In the case of a QM sample, it appears

that the T_C seems to have superimposed with the T_{mid} peak as we observe only one endothermic peak at 47 °C. The corresponding high $\Delta H_{F\text{-}P}$ value shown in Table 9.11 suggests it is a superimposed peak. Gadinski *et al.* [116] identified the corresponding endothermic peak in both quenched and slow-cooled CTFE-based terpolymer samples as FE→PE (Curie) transition. To investigate further about the nature of the endothermic peak, DSC heating and cooling curves of a QM sample during the first and second cycles were recorded and are displayed in Figure 9.23. We know that in DSC, the peak/step corresponding to T_{mid} is absent during the second heating cycle (Section 7.2). Looking at the second heating endotherm here, we observe only one peak below the melting transition around 17 °C, which can be assigned to a F-P transition based on DSC endotherms of the other samples during first heating (Figure 9.22). Hence, similar to the case of a QM P(VDF-TrFE) sample, on quenching, T_C moves to a higher temperature in a P(VDF-TrFE-CFE) terpolymer. Further, as seen from FTIR and WAXD studies on a QA sample, we do not observe much changes in the crystalline composition compared with a CA sample. Hence, we observe an identical T_C in Figure 9.22, inferring the superposition of F-P and mid-temperature range transitions in a QM sample. In accordance with WAXD measurements, results from DSC also point to the decrease in χ_c on quenching (Table 9.11).

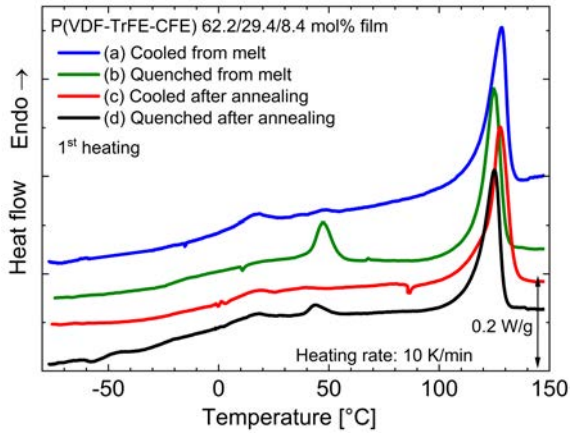

Figure 9.22: DSC endotherms of differently heat-treated P(VDF-TrFE-CFE) terpolymer films recorded during the first heating run.

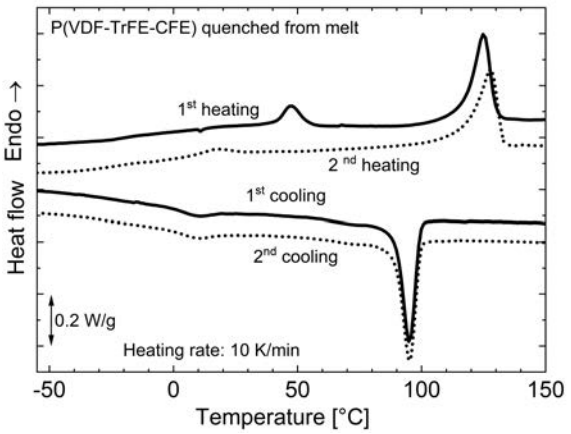

Figure 9.23: DSC endotherms of a P(VDF-TrFE-CFE) terpolymer film quenched from the melt as seen during the first and second heating runs.

The difference between the Curie-transition temperature in a QM and a QA terpolymer sample can be also visualized in their respective dielectric permittivity spectra plotted in Figure 9.24. A QM sample by virtue of its superposition with the mid-temperature transitions shows a single composite peak maximum around 40 °C. With a QA sample, we observe two permittivity steps around 20 and 45 °C associated with F-P and T_{mid} transition(s), respectively.

To summarize the effect of quenching on PVDF-based homo- and other related co- and terpolymers, it can be stated that quenching from the melt or annealed state both result in decrease of the overall

Table 9.11: Melting point T_m and Curie-transition temperature $T_{F\text{-}P}/T_c$ along with their respective enthalpies and calculated crystallinities observed during the first and second heating cycles of DSC measurements on different thermal treated P(VDF-TrFE-CFE) drop-cast films. For the calculation of χ_c both ΔH_m and $\Delta H_{F\text{-}P}$ values were used and a ΔH_∞ of 91.45 J/g for 100 % P(VDF-TrFE) was used.

P(VDF-TrFE-CFE) 62.2/29.4/8.4 mol % drop-cast terpolymer	Heating cycle	T_m [°C]	ΔH_m [J/g]	$T_{F\text{-}P}$ [°C]	$\Delta H_{F\text{-}P}$ [J/g]	χ_c [%]
Cooled from melt (CM)	1 st	128.3	20.8	18.7	1.6	25
	2 nd	126.5	18.7	17.6	1.9	23
Quenched from melt (QM)	1 st	124.9	20.1	47.3 [a]	3.9	26
	2 nd	127.8	22.2	17.4	1.7	26
Cooled after annealing (CA)	1 st	127.7	20.7	16.4	1.0	24
	2 nd	129.1	18.0	19.0	1.4	21
Quenched after annealing (QA)	1 st	125.1	17.4	16.2	1.4	22
	2 nd	127.6	20.5	17.7	1.7	24

[a] superimposed with T_{mid}

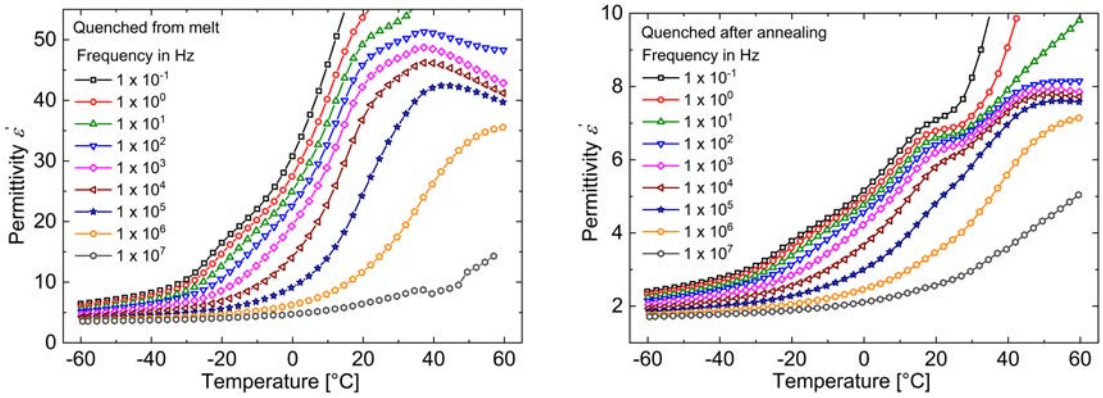

(a) Quenched from melt

(b) Quenched after annealing

Figure 9.24: Dielectric permittivity ε' of a P(VDF-TrFE-CFE) terpolymer film (a) quenched from the melt and (b) quenched after annealing, plotted as a function of temperature at selected frequencies.

crystallinity of the samples. In addition, as seen from the coherence length and long period values from X-ray diffraction experiments, rapid quenching generally results in a smaller crystalline structure due to less time available for crystallization. From these findings it can be inferred that quenched samples possess a higher amorphous-crystalline interphase area which in turn governs the various mid-temperature range transitions. While PVDF homopolymer films show a small decrease of polar fraction on quenching from melt, the samples quenched after annealing show a larger decrease of non-polar α phase consisting of TG^+TG^- conformation. A 80/20 mol % P(VDF-TFE) copolymer on the other hand shows a small decrease of polar $T_{m>3}$ conformations (thermodynamically most favoured state) on quenching from both melt or annealed state. Adding to it, quenching shifts the melting transition to lower temperatures in these copolymer films. Similarly, a 75/25 mol % P(VDF-TrFE) copolymer on quenching shows a reduction of β phase fraction with a subsequent increase in *gauche* containing conformations.

Contrary to the observation in PVDF copolymers, a P(VDF-TrFE-CFE) which predominantly consists of $TG^{+}TG^{-}$ and $T_3G^{+}T_3G^{-}$ conformations show an increase of *trans* structures on quenching. In both P(VDF-TrFE) copolymer and P(VDF-TrFE-CFE) terpolymer, quenching generally increases the Curie-transition temperature. Overall, quenching can be used as an effective technique to modify the three phases in semi-crystalline PVDF-based polymers – crystalline and amorphous phase, along with their interphase. The effects of quenching can be exploited for fine tuning specific application relevant properties.

10

Influence of Film Stretching on Crystalline Phases and Dielectric Properties of a 70/30 mol% Poly(Vinylidenefluoride-Tetrafluoroethylene) Copolymer[1]

10.1 Previous Studies on P(VDF-TFE) Copolymer

Even though initial studies on P(VDF-TFE) were done as early as in the 1960s [34], it was only after the discovery of piezoelectricity in PVDF in 1969 [11] that their ferroelectric and dielectric properties were investigated [261, 262]. P(VDF-TFE) received much attention in the 1980s mainly due to the work of Lovinger *et al.*, who studied the influence of the TFE comonomer as well as that of the copolymer composition on structural phase transitions and dielectric properties [15, 16, 263]. Further contributions by Murata, Koizumi and Hagino led to a better understanding of dielectric and thermal behavior for copolymers with varying amounts of TFE [253, 264, 265]. The influence of crystallization and polarization conditions on the properties of P(VDF-TFE) was investigated by Tasaka and Miyata [266], and by Kulk and Hilczer [267]. Tashiro *et al.* studied the structural changes in ferroelectric phase transitions by means of X-ray diffraction, infrared and Raman spectroscopy [220, 268]. Seminal studies on applications, on the functionalization of P(VDF-TFE), and on intramolecular dipole-dipole interactions were done by Tournut [38] and by Kochervinskii *et al.* [135].

As already mentioned in Chapter 9 (Section 9.6), initially, in analogy to PVDF, no clear Ferroelectric-to-Paraelectric (F-P) Curie transition could be observed on P(VDF-TFE) [253], which was attributed to its similar chemical structure with form-II PVDF (α phase) including head-to-head defects. Later, however, the presence of a Curie temperature (T_C) with a typical phase change from the polar β phase

[1]Parts of this Chapter are adapted from T. Raman Venkatesan *et al.*, "Influence of film stretching on crystalline phases and dielectric properties of a 70/30 mol% poly(vinylidenefluoride-tetrafluoroethylene) copolymer", *J. Adv. Dielect*, 10(5): 2050023 (10 pages), 2020 [140].

to the non-polar α phase with alternating *trans* and *gauche* conformation (TG^+TG^-) was observed by Lovinger *et al.* [15, 16, 263] and also by several other authors [135, 264, 265], which makes P(VDF-TFE) similar to P(VDF-TrFE) in terms of the observed dielectric, thermal and phase behavior. In general, as with TrFE, the addition of TFE into the VDF chains forces the copolymer chains to adopt a polar all-*trans* zig-zag conformation (β-PVDF or form I) [34]. However, the crystalline phases and the thermal transitions including T_C depend on the TFE content [22]. When the TFE content is $\leq$ 7 mol %, the α phase is predominant. When TFE content is in the range of ∼8-28 mol %, the copolymer has a majority of β phase, and between ∼29 and 65 mol % of TFE, a mixture of both β and α phases is found. Finally, with $\geq$ 66 mol % of TFE, the copolymer assumes a non-polar phase similar to polytetrafluoroethylene (PTFE) [263]. Thus, the properties of P(VDF-TFE) strongly depend on the TFE co-monomer content.

Though the ferroelectricity of P(VDF-TFE) is similar to that of P(VDF-TrFE), the TFE unit stabilizes the *trans* conformation of the copolymer chains to a higher extent (about twice as much) than the TrFE unit, *i.e.*, a smaller fraction of TFE is needed in comparison to TrFE in order to achieve a stable β phase which leads to the highest ferroelectricity in the copolymer [207]. As a result, it is more difficult to bring about a change from the *trans* to the *gauche* conformation in P(VDF-TFE). This causes the T_C to move very close to the melting point (T_m) in comparison to P(VDF-TrFE) with a similar VDF content. However, TFE units are considered to have a higher thermal mobility than TrFE units. This is also supported by the small thermal hysteresis found on P(VDF-TFE). The higher thermal mobility of TFE units that are adjacent to VDF units facilitate the *trans-gauche* conformational change. So, the overall Curie transition occurs at a lower temperature than in P(VDF-TrFE). The smaller dipole moments of the VDF-TFE chains also play an important role in reducing the F-P transition temperature [22].

10.2 Samples and Experiments

Free-standing P(VDF-TFE) films with a VDF/TFE ratio of 70/30 mol % that had been produced by means of melt extrusion (F2ME, Russia) were used for the experiments. The thickness of the films was in the range of 100-200 µm. Extruded films had been stretched to a ratio of 3.6 in the longitudinal direction (*i.e.*, the direction of extrusion; uniaxial stretching) at temperatures from 80 to 120 °C, in temperature intervals of 10 °C (samples 'S2' to 'S6'). For comparison, un-stretched P(VDF-TFE) films (sample 'S1') were also studied.

10.3 Crystalline Phases Deducted in FTIR Spectroscopy

Room-temperature (RT) FTIR spectra of an un-stretched and a stretched P(VDF-TFE) copolymer films (stre -tched at various temperatures) are shown in Figure 10.1 along with the main characteristic wavelengths assigned to the different crystalline fractions in the copolymer (*cf.* Tables 5.4 and 5.5). Looking

at the spectrum for an un-stretched P(VDF-TFE) sample (S1) in Figure 10.1, we see that it shows characteristic peaks for both α and β phases implying the coexistence of both phases at RT [135]. It also reveals the existence of a certain amount of γ phase crystals (with $T_3G^+T_3G^-$ chain conformation) that are clearly identified by the characteristic peak at 506 cm^{-1}. Upon stretching, we notice that the peaks which correspond to the α phase either disappear or are at least reduced significantly. At the same time, we observe an increase in the absorption of β phase peaks, which confirms the conversion of the non-polar α phase into the polar β phase. In addition, at higher stretching temperatures, there is a decrease in the intensity of the α peaks at 485 cm^{-1} and a parallel increase in the absorption of the γ phase band at 506 cm^{-1}, indicating that some of the α phase is converted into γ phase.

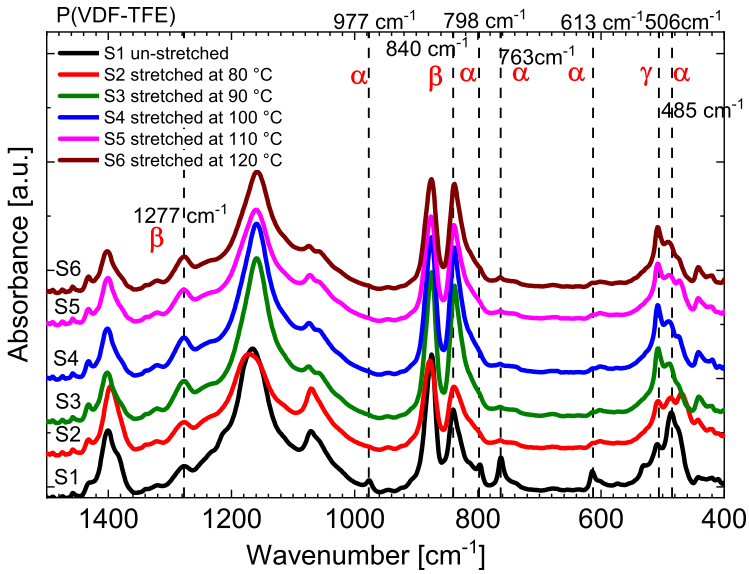

Figure 10.1: FTIR spectra of P(VDF-TFE) copolymer films stretched at various temperatures along with the spectrum of an un-stretched P(VDF-TFE) copolymer.

Using the method suggested by Gregorio and Cestari [148], the fractions of the crystalline β and α phases, relative to each other in un-stretched and stretched samples are tabulated in Table 10.1. We observe that the un-stretched sample shows mainly the β phase, but with a significant amount of α phase. Upon stretching, there is an increase in β phase content with a corresponding decrease in α phase content. Thus, stretching P(VDF-TFE) films has a similar effect as stretching α PVDF, forcing polymer chains to assume the all-*trans* conformation. For increasing values of T_s, up to 90 °C, there is a continuous increase of the β phase. However, with a further increase in the stretching temperature T_s, no appreciable effect is seen on the β phase fraction. When comparing the different crystalline fractions in P(VDF-TFE) 70/30 mol % films to those in extruded (un-stretched) P(VDF-TrFE) films with a similar VDF-comonomer ratio (*cf.* Table 5.6), we find that only P(VDF-TFE) films stretched at high temperatures show a comparable

β phase content, while the un-stretched sample has a much smaller β phase fraction [111], which can be understood from the similar molecular comformations and crystalline structures of P(VDF-TFE) and the PVDF, but with a higher number of head-to-head defects in the copolymer.

Table 10.1: Fraction of the different crystalline phases in the un-stretched and stretched P(VDF-TFE) copolymer films.

P(VDF-TFE) 70/30 mol % copolymer	β fraction [%]	α fraction [%]
S1 un-stretched	63	37
S2 stretched at 80 °C	78	22
S3 stretched at 90 °C	88	12
S4 stretched at 100 °C	88	12
S5 stretched at 110 °C	85	15
S6 stretched at 120 °C	86	14

10.4 Changes in Crystalline Phases and Morphology as Observed in WAXD Scans

Figure 10.2 shows RT WAXD scans obtained on P(VDF-TFE) films that were stretched at various temperatures and on an un-stretched sample. The diffraction peaks are fitted with the Pearson VII function and labelled according to the respective crystallographic planes and crystalline phases as identified by Kochervinskii *et al.* [21, 44, 135]. In an un-stretched film, we find peaks associated with both α and β phases analogous to those observed in FTIR (Figure 10.1).

Upon stretching, we observe that the peaks assigned to the non-polar paraelectric α phase disappear, with a corresponding increase in the intensity of the polar ferroelectric β phase peaks. In particular, the α phase peak found on sample 'S1' at $2\theta = 18.4°$ with an inter-planar distance/lattice constant of $d = 4.82\ Å$, associated with the (020) plane, reduces to a shoulder in the stretched samples 'S2'-'S6' and resembles the amorphous halo usually observed in P(VDF-TrFE) samples [54]. It is associated with an anti-ferroelectric or paraelectric state [15, 135]. Additionally upon stretching, the peak at $2\theta = 35.8°$ ($d = 2.51\ Å$) which results from the (200) crystallographic plane of the paraelectric phase crystals and is found in 'S1', disappears – with a simultaneous appearance of the β phase peak at $2\theta = 35.0°$ ($d = 2.56\ Å$). For samples 'S2' to 'S6', there are no significant differences between the diffraction peaks after stretching at various temperatures.

As stated earlier, according to Bargain *et al.* [138], it is not possible to calculate the coherence length 'L_c' from the Full Width at Half Maximum (FWHM) of an observed diffraction peak when the peak is the juxtaposition of several Bragg peaks – as seen in the case of the peaks at $2\theta = 20.3°$ ($d = 4.44\ Å$) and $2\theta = 41.0°$ ($d = 2.21\ Å$). Yet, it is reasonable to compare the changes in the FWHM of the diffraction peaks assigned to the ferroelectric- and paraelectric-phase crystals in the WAXD patterns of the various

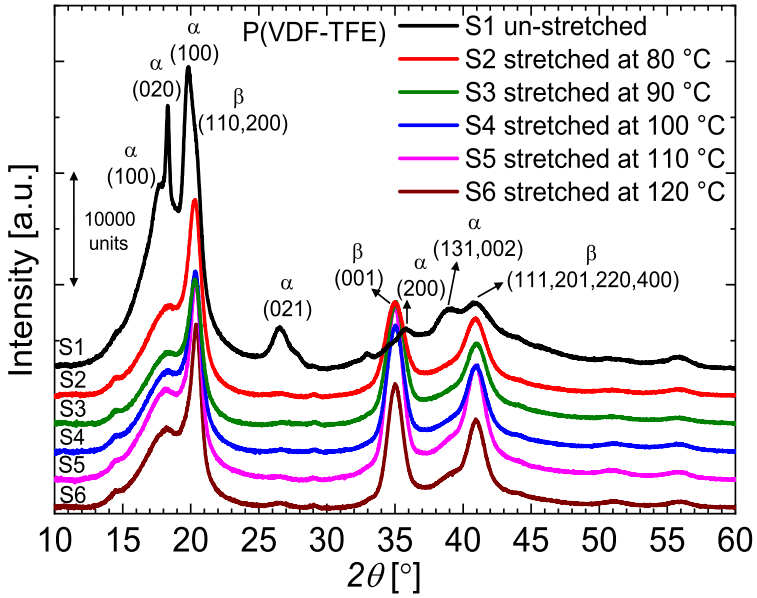

Figure 10.2: WAXD at room temperature for an un-stretched and stretched P(VDF-TFE) copolymer films which were stretched at various temperatures as indicated.

P(VDF-TFE) samples to qualitatively predict the change in the coherence length of the particular phase in the samples. The measured FWHM values are listed in Table 10.2.

Table 10.2: Full width at half maximum (FWHM) of the various diffraction peaks in the un-stretched and stretched P(VDF-TFE) copolymer films.

P(VDF-TFE)	**Full width at half maximum (FWHM) [$\AA$]**		
70/30 % copolymer	**20.3°**	**35.0°**	**41.0°**
S1 un-stretched	1.10	[-]	2.19
S2 stretched at 80 °C	1.10	1.77	1.55
S3 stretched at 90 °C	0.95	1.64	1.45
S4 stretched at 100 °C	0.91	1.47	1.44
S5 stretched at 110 °C	0.83	1.38	1.34
S6 stretched at 120 °C	0.82	1.40	1.29

At first, let us consider the reflections at 20.3° which correspond to the inter-chain order of the crystals perpendicular to the chain axis [136, 137, 138, 139]. Initially, though stretching does not induce a change in FWHM, an increase of the stretching temperature (T_s) results in decrease of FWHM, pointing out to the increase in L_c of ferroelectric crystals. The FWHM of the ferroelectric peaks at 2θ = 35.0° and 41.0° that are associated with the intra-chain crystalline order along the chain axis also undergoes changes on stretching. While the process of stretching gives rise to the peak at 35.0°, it results in the reduction of FWHM value of the 41.0° peak. In addition, lowering of FWHM values with increasing T_s in both the peaks indicate that stable crystals are formed along the chain axis.

From the above-mentioned FWHM values of the Bragg diffraction peaks, it can be inferred that stretching causes a decrease in the fraction of non-polar paraelectric crystals and a corresponding increase in the polar ferroelectric crystalline content (both perpendicular to and along the chain axis). In addition, stretching at high temperatures stabilizes the ferroelectric crystals in the P(VDF-TFE) films – an observation that is supported by the decreasing FWHM values of the relevant peaks.

10.5 Effect of Stretching on Thermal Properties

DSC thermograms taken during the first heating cycle for the un-stretched and stretched P(VDF-TFE) copolymer samples are plotted in Figure 8.17. We can clearly identify three transitions in both the un-stretched and the stretched samples. The first transition is seen as a step at lower temperatures between –50 and –30 °C associated with micro-Brownian motions of amorphous chain segments [16, 44]. The glass-transition temperature (T_g) is calculated to be around –45 °C and thus, very close to that of the PVDF homopolymer with a T_g of around –40 °C [16, 163]. At higher temperatures, we can identify the mid-temperature transition between 50 and 70 °C. The changes in T_{mid} as a result of stretching have been discussed previously in Section 8.2.2. The change in shape of T_{mid} from that of an endothermic peak to a relaxation-step on stretching can be better visualized by comparing the mDSC plots shown in Figures 10.3 and 10.4. The non-reversible heat flow curve of the un-stretched S1 sample reveals a strong endothermic peak around 60 °C with an enthalpy value of 1.3 J/g, while the stretched sample 'S5' exhibits a weaker endothermic peak in the same temperature range with a lower enthalpy value of 1.0 J/g. Hence, a lower amount of secondary crystals are formed in stretched samples, especially in those stretched at high temperatures. At the same time, we see a relaxation step between 60 and 80 °C in the reversible heat flow contribution of both the samples that can be inferred as the contribution from *condis* relaxation.

Returning back to the DSC plot in Figure 8.17, the third transition at higher temperatures indicates the melting of the crystals (melting point 'T_m') in the copolymer [253, 265]. T_m values are between 146 to 150 °C, in a similar range as the melting points of P(VDF-TrFE) films with comparable VDF-comonomer ratios [49]. The crystallinities (χ_c) of the various copolymer samples calculated from the areas under crystalline and amorphous peaks in WAXD scans and from heat-of-fusion values in DSC traces are listed in Table 10.3, respectively. A heat-of-fusion value of 104.6 J/g for 100 % crystalline PVDF [146] was used. As expected, we observe an increase in the sample crystallinity upon stretching, because stretching helps to align imperfect crystals and to remove constrained regions [22]. Further, an increase in stretching temperature (T_s) causes a marginal increase in χ_c. Thus, the soft state of the copolymer at high temperatures tend to facilitate the stretching process and stabilize the crystalline phase.

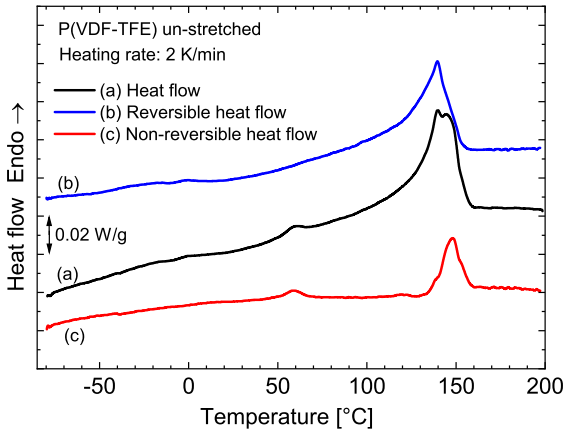

Figure 10.3: 1st heating mDSC trace of an un-stretched P(VDF-TFE) copolymer.

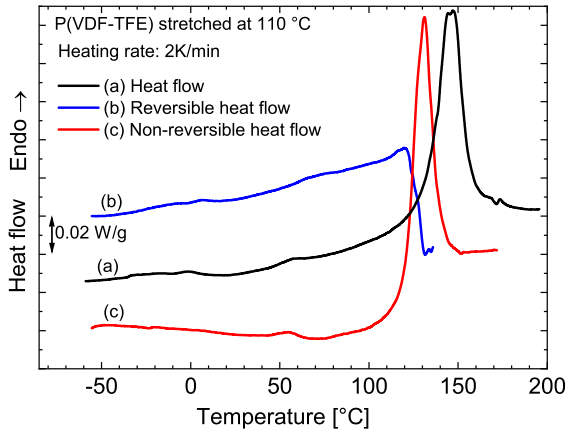

Figure 10.4: 1st heating mDSC trace of a P(VDF-TFE) copolymer stretched at 110 °C (S5).

Table 10.3: Crystallinity (χ_c) of an un-stretched and of several stretched P(VDF-TFE) copolymer films (at various temperatures as indicated) calculated from WAXD and DSC.

P(VDF-TFE)	χ_c **[%]**	
70/30 mol % copolymer	**WAXD**	**DSC**
S1 un-stretched	15	29
S2 stretched at 80 °C	33	39
S3 stretched at 90 °C	35	42
S4 stretched at 100 °C	33	44
S5 stretched at 110 °C	37	43
S6 stretched at 120 °C	36	46

10.6 Dielectric Properties as Observed in DRS and DMA

The dielectric spectra of an un-stretched P(VDF-TFE) sample (S1) as previously elaborated in Section 7.2 show presence of a lower-glass transition and *condis* relaxational processes (*cf.* Figure 6.3). Stretching removes the peaks associated with *condis*, allowing us to visualize the structural transition of secondary crystals (S.C.) melting (Figure 7.4). In addition to it, a third frequency-independent process is detected around 110 °C in the permittivity plot displayed in Figure 10.5. Based on the previously mentioned literature in Section 10.1 and dielectric and thermal measurements on a 80/20 mol % P(VDF-TFE) sample summarized in Section 9.6, this transition can be identified with a F-P transition. The transition along with the S.C. melting process can be better observed in permittivity coefficient derivative curve plotted in Figure 10.6. The presence of conformational disorder relaxation is also revealed in the ε''_{der} curves of the stretched 'S2' sample. Based on the above observations, the dual endothermic peaks seen between 140 and 150 °C in Figures 10.3 and 10.4 can be assigned to the Curie and melting transition, respectively. Since the F-P transition in the copolymer occurs very close to its melting point, it merges

with the melting transition at higher heating rates as observed in Figure 8.17 [264]. The Curie transition of P(VDF-TFE) occurs at a lower temperature than that of P(VDF-TrFE) (T_C is about 15 °C lower) with a similar VDF monomer content (*cf.* Figure 6.4) for reasons already explained in Section 10.1 above.

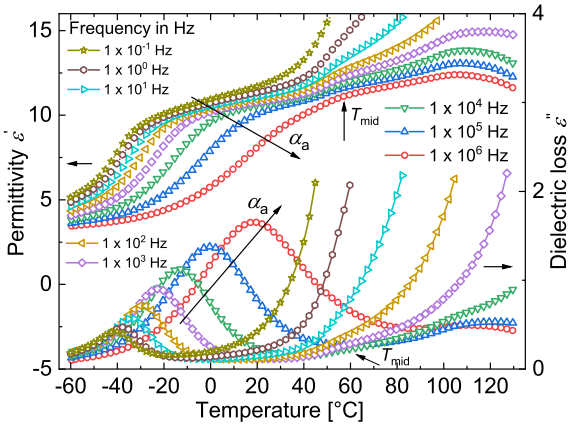

Figure 10.5: The permittivity and dielectric loss of a P(VDF-TFE) film stretched at 80 °C (S2) plotted as a function of temperature at fixed frequencies from 10^{-1} to 10^{7} Hz.

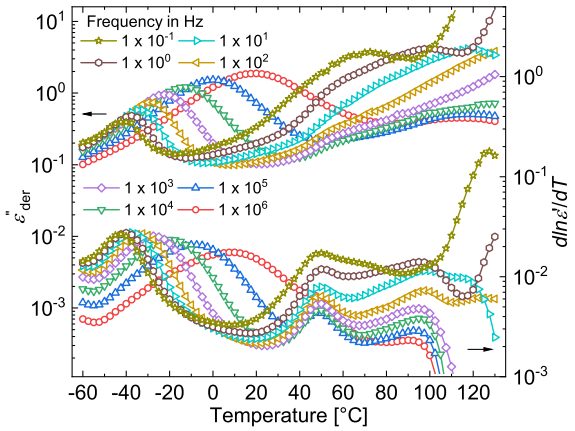

Figure 10.6: Conduction-free dielectric loss (ε''_{der}) and temperature coefficient of permittivity $\partial \ln \varepsilon'(T)/\partial T$ (α_ε) of a P(VDF-TFE) film stretched at 80 °C (S2).

As the contribution from various processes to the T_{mid} transition is limited in a stretched sample, the Curie transition is more clearly visible (Figure 10.5) than in an un-stretched sample (Figure 7.10) where the F-P transition is masked by the *condis* peaks that shift to higher temperature with increasing frequency. The effect of the stretching temperature on the dielectric properties of the P(VDF-TFE) films can be seen from the dielectric dissipation factor ($\tan\delta$) of the different samples – as shown in Figure 10.7. The glass-transition relaxation peaks (α_a) show no change in intensity for samples stretched at various temperatures. This finding shows that the stretching temperature has no influence below the glass transition of the samples. Apparently, the T_{mid} transition in the stretched samples is not distinctively observed in the dissipation-factor plot. On the other hand, an increase in T_s causes a suppression in the intensity of the Curie transition, which is found in the form of a shoulder in the higher temperature range of the spectra as shown in the inset of Figure 10.7. As stretching at higher temperatures stabilizes the ferroelectric β phase in the copolymer, as seen from the WAXD curves of Figure 10.2, the losses associated with the ferroelectric-to-paraelectric transition are also reduced.

Dynamic mechanical analysis (DMA) can be used to complement dielectric studies for observing processes connected with the various relaxations and transitions in dielectric materials. Figure 10.8 shows the elastic modulus and the mechanical loss factor tan δ on a P(VDF-TFE) film stretched at 80 °C. At the low-temperature end, we see a drop in elastic modulus with a corresponding loss peak. From

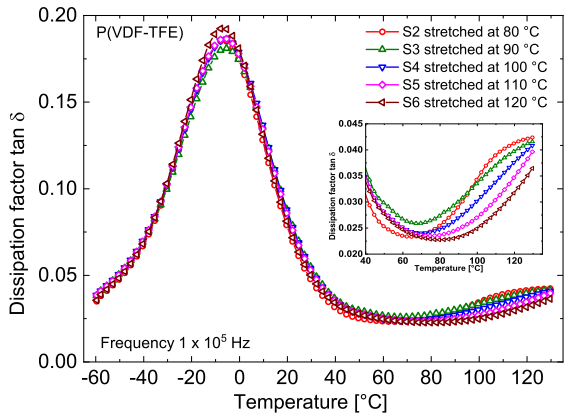

Figure 10.7: Dielectric dissipation factor tan δ of stretched P(VDF-TFE) samples as a function of temperature at a frequency of 10^5 Hz.

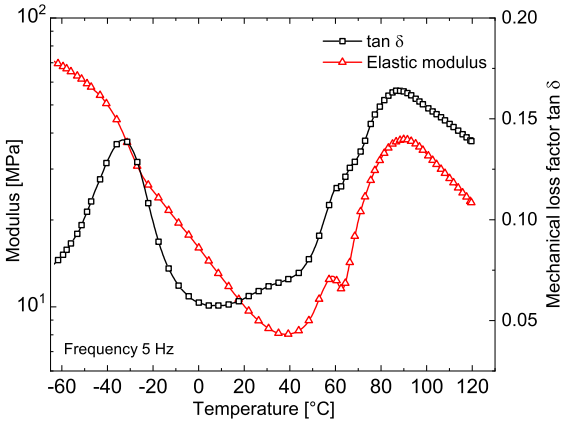

Figure 10.8: Elastic modulus (red, triangles) and mechanical loss factor tan δ (black, squares) of a P(VDF-TFE) copolymer sample stretched at 80 °C – both as functions of temperature at a measuring frequency of 5 Hz.

a comparison with the dielectric loss spectrum of the same sample in Figure 10.5, the peak is easily assigned to the glass transition.

Around 60 °C, we identify a modulus peak that is accompanied by a shoulder in the mechanical-loss curve at exactly the same temperature where we observe a permittivity step in Figure 10.5. The peak is clearly the manifestation of the T_{mid} transition. Hence, as seen from temperature-dependent permittivity measurements, stretching at low temperature did not remove all the tie molecules and constrained regions. It is to be noted that DMA measurements by Frübing *et al.* yielded loss peaks around 40 °C that are associated with the T_{mid} transition, but that were previously only explained as a result of the melting of secondary crystals [45]. Finally, around 90 °C, we see the F-P transition peak in both the modulus and the loss curves – at the same temperature as observed in the derivative plots of Figure 10.6. Hence, the existence of a F-P transition in P(VDF-TFE) copolymers is also confirmed from the DMA measurements.

Overall, Stretching of P(VDF-TFE) films, similar to stretching of PVDF films, induces a higher fraction of β phase crystals in the sample with a corresponding decrease in α phase as indicated by the results of FTIR and WAXD. Increase in stretching temperature does not have a major influence on the fraction of the different crystalline phases. However, the stability of ferroelectric crystals seems to be improved from the decrease in FWHM values of WAXD peaks in both parallel and perpendicular directions to the chain axis. The reduction of dielectric losses associated with Curie transition at higher stretching temperatures also points out to the same.

Stretching though seems to remove the contribution from *condis* relaxation, seen by the absence of frequency-dependent peaks in the mid-temperature region of dielectric relaxation spectra, its presence in

stretched samples can be clearly seem from the derivative analysis of DRS results and mDSC thermograms. In addition, the influence of stretching temperature on T_{mid} follows the hypothesis proposed in Chapter 7. At low temperatures of stretching, T_{mid} is observed in the form of an endothermic peak in DSC and as the stretching temperature increases, the transition is marked by a relaxation-like step.

11

Non-Linear Dielectric Spectroscopy for Detecting and Evaluating Structure-Property Relations in a P(VDF-TrFE-CFE) Relaxor-Ferroelectric Terpolymer[1]

11.1 Motivation to Study Non-Linear Dielectric Spectroscopy

As shown previously in Chapter 6, conventional Dielectric Relaxation Spectroscopy (DRS) and Thermally Stimulated Depolarization (TSDC) were employed to study relaxations and transitions in P(VDF-TrFE-CFE) [48, 49, 136, 177]. However, recording and evaluating the complex non-linear dielectric permittivities ε_2^* and ε_3^* of P(VDF-TrFE-CFE) can provide more information about relaxations and transitions that cannot be clearly seen in more conventional ε_1^* measurements. In particular, Non-Linear Dielectric Spectroscopy (NLDS) may help us to better understand the mid-temperature transition, especially the contribution from Maxwell-Wagner interface (MWI) polarization, which had been observed during TSDC measurements [81, 177]. Hence, in this study, NLDS measurements were performed on spin-coated and annealed P(VDF-TrFE-CFE) films, and for comparison also on annealed P(VDF-TrFE) copolymer films that show typical ferroelectric properties.

[1]Parts of this chapter are adapted from T. Raman Venkatesan *et al.*, "Non-Linear Dielectric Spectroscopy for Detecting and Evaluating Structure-Property Relations in a P(VDF-TrFE-CFE) Relaxor-Ferroelectric Terpolymer", *Appl. Phys. A*, 127: 756 (10 pages), 2021 [83].

11.2 Sample Preparation and Measurement Techniques

A P(VDF-TrFE-CFE) terpolymer resin from Piezotech-Arkema with a 62.2/29.4/8.4 molar ratio of VDF/TrFE/CFE, respectively, was used. For the NLDS experiments, P(VDF-TrFE-CFE) films with thicknesses between 1.7 and 3.6 µm were prepared by means of spin-coating. The samples were annealed at a temperature of 120 °C either immediately after spin-coating or before the NLDS runs for 4 or 1 hour(s), respectively. Spin-coated P(VDF-TrFE) films were prepared in a similar manner. The average thickness of the film was around 3.2 µm. The copolymer samples were annealed at 120 °C for one hour before the NLDS measurements.

For short-circuit TSDC measurements, free-standing ter- and copolymer films coated on both sides with aluminum electrodes of 60 nm thickness were used. The films were prepared by drop casting polymer solutions with the same concentrations as used for spin-coating (Section 4.2). The thickness of the free-standing ter- and copolymer films was 137 and 20 µm, respectively. For the TSDC measurements, a Keithley 6578 electrometer was used to pole the samples at a temperature T_p = 40 °C with a DC field E_p of 10 MV/m for a time period t_p = 10 min before cooling them down to −60 °C, which is lower than the glass-transition temperature of both the terpolymer and the copolymer [49]. The depolarization currents were measured while heating the sample at a rate of 4 K/min. Conventional DRS measurements were also made on free-standing terpolymer films in vacuum by means of a Novocontrol Alpha dielectric analyzer. Dielectric-hysteresis measurements were performed by use of a Sawyer-Tower circuit on spin-coated films. The dielectric displacement D was recorded as a function of the electric field E applied in the form of triangular voltage signals with a frequency of 10 Hz.

11.3 Order of Phase Transition in P(VDF-TrFE-CFE) Terpolymer

Figure 11.1a shows the real and imaginary parts of ε or ε_1 (0^{th}-order non-linear permittivity) of an annealed P(VDF-TrFE-CFE) terpolymer film, plotted as a function of temperature during heating and subsequent cooling measured at a frequency of 1 kHz. Looking at the heating curve, we can see that the real part of the permittivity (ε_1') shows a maximum at the F-P transition temperature (around 27 °C) with a peak value of 63. The corresponding loss peak ε'' (imaginary part of the permittivity) with a peak value above 5 is found around 15 °C.

In order to compare the dielectric behaviour of the R-F terpolymer with that of a typical ferroelectric material, the dielectric spectra of a P(VDF-TrFE) ferroelectric copolymer with a VDF/TrFE ratio of 75/25 (similar to the VDF/TrFE ratio in the terpolymer) are plotted as functions of temperature in Figure 11.1b. We can see that during the heating scan, the copolymer shows a maximum permittivity (ε_1') of 35, which is lower than the value in the terpolymer investigated here. We also observe that the copolymer

shows a very high T_C of approximately 128 °C. It should be noted that the T_C value of a P(VDF-TrFE) copolymer depends on the VDF/TrFE ratio and can vary between 60 and 135 °C [36] – values that are higher than the transition temperature of the terpolymer studied here.

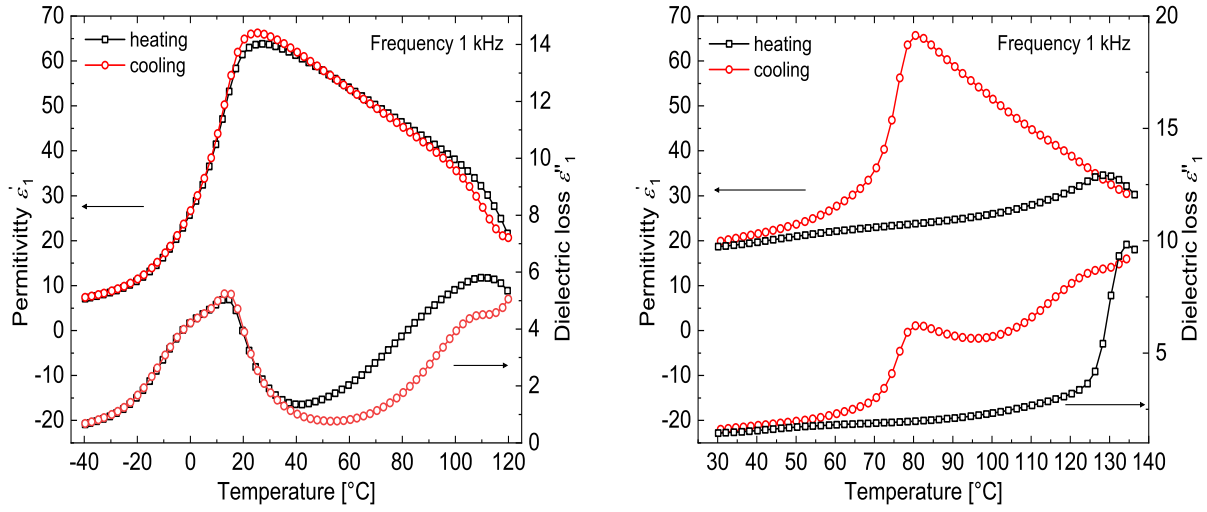

(a) P(VDF-TrFE-CFE) **(b)** P(VDF-TrFE)

Figure 11.1: Real and imaginary parts of the first-order permittivity ε_1' in unpoled and annealed (a) P(VDF-TrFE-CFE) and (b) P(VDF-TrFE) copolymer as functions of temperature during heating and subsequent cooling measured at a frequency of 1 kHz.

As mentioned in Section 3.4.7.1, it is possible to determine the order of the F-P phase transition from the sign of ε_3 (real part) in the paraelectric phase. In Figure 11.2a, we observe a change in the sign of ε_3' from positive to negative when the terpolymer passes through the temperature region of the F-P transition, which implies that the R-F terpolymer undergoes a second-order transition. The second-order of the F–P transition is also confirmed by the results shown in Figure 11.1a where ε_1' does not exhibit any significant thermal hysteresis during cooling. On the other hand, we observe that a ferroelectric P(VDF-TrFE) copolymer with a VDF/TrFE ratio of 75/25 mol % shows a first-order transition as evident from the positive sign of ε_3' in the paraeletric phase (*cf.* Figure 11.2b) and from the presence of a thermal hysteresis in Figure 11.1b.

11.4 Other Transitions and Relaxations in P(VDF-TrFE-CFE) Terpolymer

One major advantage of NLDS is that the state of polarization of the material under investigation can be directly revealed from the sign of ε_2' (Section 3.4.7.1). From Equation 3.41, we expect that for the terpolymer ε_2' (real part) should be zero (even-order permittivity) in the paraelectric phase, as a dielectric material in its non-polarized paraelectric state must behave as an ideal capacitor. In Figure 11.3, though

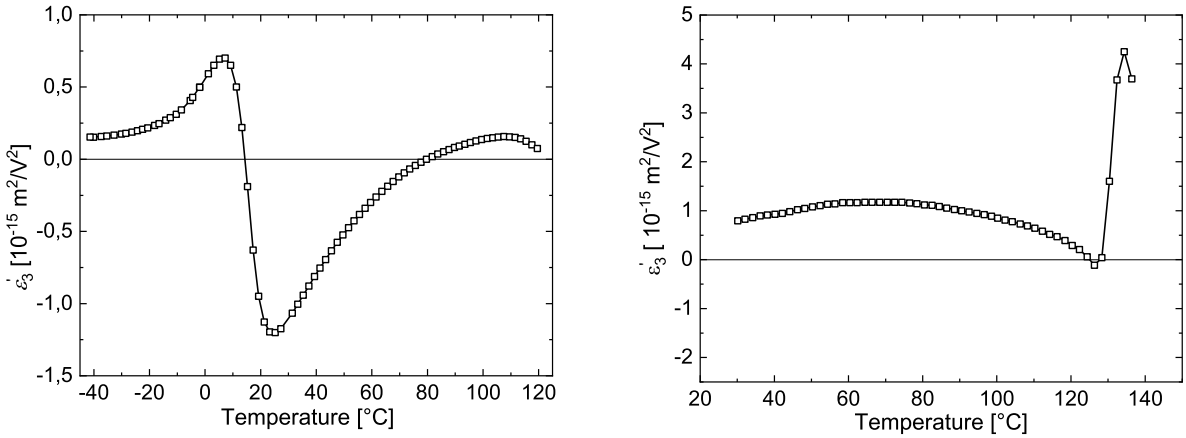

(a) P(VDF-TrFE-CFE)

(b) P(VDF-TrFE)

Figure 11.2: The real part of the third-order permittivity ε_3' at a frequency of 1 kHz in annealed and unpoled (a) P(VDF-TrFE-CFE) terpolymer sample and (b) P(VDF-TrFE) copolymer sample measured as a function of temperature during heating.

ε_2' becomes 0 at 11 °C (T_C), which is lower than the corresponding value obtained from ε_1' measurement (Figure 11.1a), we clearly see that the terpolymer's ε_2' adopts negative or non-zero values even in the paraelectric phase. In particular, new peaks are observed around 30 and 80 °C during heating as well as cooling.

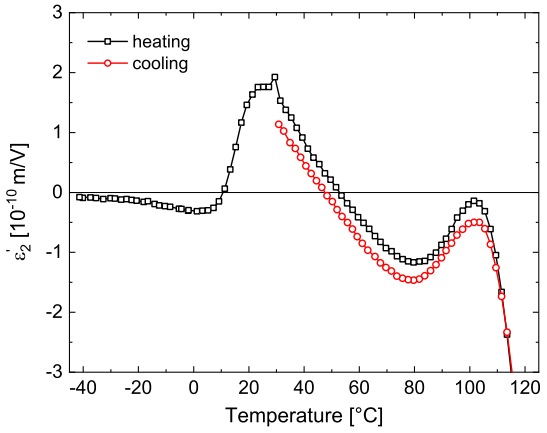

Figure 11.3: Real part of the second-order permittivity (ε_2') in an unpoled and annealed P(VDF-TrFE-CFE) terpolymer at a frequency of 1 kHz as a function of temperature during heating and subsequent cooling.

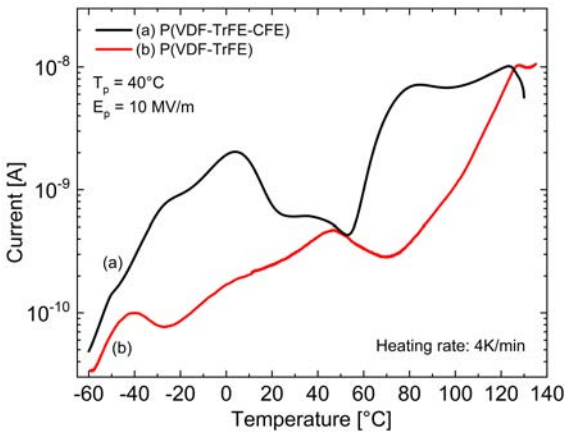

Figure 11.4: TSDC spectra of a P(VDF-TrFE-CFE) terpolymer and P(VDF-TrFE) copolymer film poled with $E_p = 10$ MV/m for $t_p = 10$ min.

While the depolarization current is measured in short-circuit TSDC experiments, the voltage decay is often recorded in open-circuit measurements that are better suited for detecting charge motion during discharge processes. Therefore, the various transitions and relaxations occurring in a polar sample can

be precisely seen in short-circuit TSDC experiments during heating at a constant heating rate. On the TSDC curve of the terpolymer shown in Figure 11.4, we can clearly observe a shoulder around 40 °C and a peak around 85 °C. The two features can be associated with the ε_2' peaks found at the same temperature ranges in Figure 11.3.

Similar TSDC and NLDS measurements were also carried out on the reference P(VDF-TrFE) copolymer – as shown in Figures 11.4 and 11.5, respectively. In Figure 11.4, the copolymer TSDC curve shows a peak around 40 °C, but no peak can be identified around 80 °C. In Figure 11.5, we do not observe the peak around 40 °C that had been revealed in the TSDC measurement of the copolymer, and the ε_2' value is essentially zero in the ferroelectric phase – as expected for a non-poled sample. However, when heating the copolymer above 110 °C, ε_2' becomes positive, just below the Curie-transition temperature T_C, and during cooling, the curve is shifted to lower temperatures. In the paraelectric phase, the copolymer sample shows non-zero ε_2' values in a similar manner as the terpolymer sample.

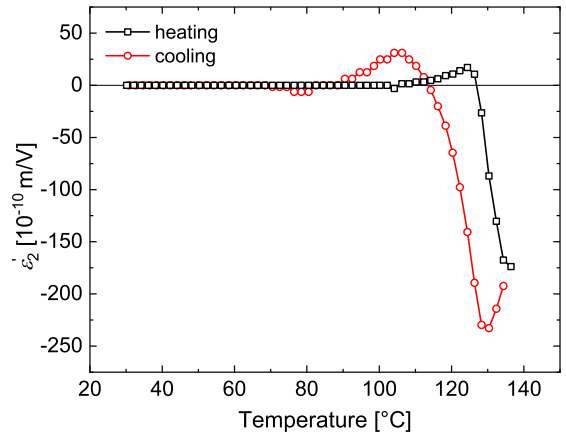

Figure 11.5: Real part of the second-order permittivity ε_2' of an unpoled and annealed P(VDF-TrFE) copolymer at a frequency of 1 kHz as a function of temperature during heating and subsequent cooling.

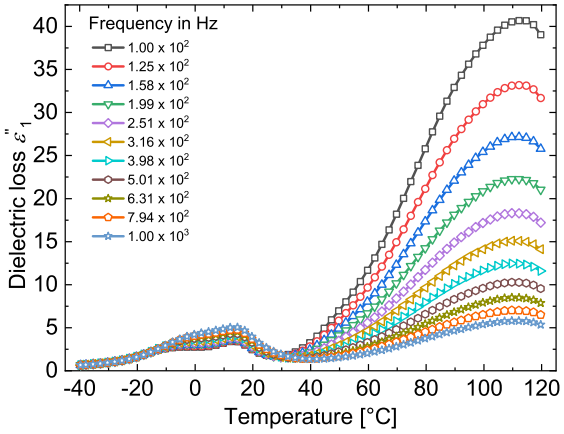

Figure 11.6: Dielectric losses ε_1'' of an annealed and unpoled P(VDF-TrFE-CFE) terpolymer as a function of temperature during heating – measured at 11 distinct frequencies between 100 Hz and 1 kHz as indicated.

The peak around 30-40 °C found in NLDS (ε_2') and TSDC measurements on the co- and the terpolymer is assigned to the mid-temperature (T_{mid}) transition with contribution from MWI polarization process – as discussed earlier in Section 7.2) [81, 119]. In case of the terpolymer, the nano-crystalline regions lead to a much larger a-c interface area than in the copolymer [48] with its larger crystallites. The different nanostructure results in a much stronger T_{mid} process in the terpolymer [81] that is readily seen in ε_2' measurements. Due to the proximity of the F-P transition to the T_{mid} process in the terpolymer, the T_{mid} transition cannot usually be seen as a distinct phenomenon in conventional dielectric experiments. As NLDS measurements are more sensitive, they allow us to resolve the process much better. The value of ε_2 depends on the spontaneous polarization of the sample [89]. Since MWI polarization can contribute

to spontaneous polarization, we observe non-zero ε_2 values in the paraelectric phase of the terpolymer (*cf.* Figure 11.3). Though T_{mid} transition is not discernible in Figure 11.5, earlier remanent-polarization measurements on thin P(VDF-TrFE) copolymer films with the same composition revealed a clear non-zero polarization peak in the T_{mid} range during cooling – even after the initial polarization had been lost [86, 119], probably as a result of surface and interface effects that are predominant in ultra-thin films. From the TSDC results shown in Figure 11.4 and from other experiments [49, 119], the presence of a T_{mid} process in P(VDF-TrFE) samples is obvious.

Looking again at the dielectric-loss curves shown in Figure 11.1a, we can observe a high-temperature peak around 110 °C in the terpolymer, both during heating and during cooling. It is also seen in the real part of the permittivity as a shoulder. In order to study the frequency dependence of the peak, the dielectric loss during heating has been measured at multiple frequencies. In Figure 11.6, we can see that the position of the high-temperature peak shows no frequency dependence – just like a structural transition such as the Curie or the melting transition. Since the melting point of the terpolymer is about 128.5 °C, as determined previously in DSC experiments [49], the attribution of the peak to melting can be ruled out, and it is clear that the F-P transition occurs at a much lower temperature.

Though the peak position does not depend on frequency, the peak amplitude shows a strong frequency dependence. In the temperature range from 50 to 120 °C, the dielectric loss is roughly proportional to the reciprocal frequency. Such a frequency dependence is expected when the dielectric loss is essentially caused by charge-transport phenomena [269]. In addition, the temperature at which the transition is seen changes from sample to sample. For a similar annealed terpolymer film, the transition is seen as a shoulder in the permittivity around 90 °C [24], about 20 °C lower than observed in the ε_1' plot in Figure 11.1a. This further supports the explanation of electrode polarization and thus, the peak found at 80 °C in the ε_2' measurement (Figure 11.3) should be associated with this phenomenon. The peak is not only observed on the terpolymer, but also in the loss plot of the P(VDF-TrFE) copolymer during cooling (*cf.* Figure 11.1b), but at a slightly higher temperature.

In order to shed more light on the high-temperature peak, dielectric-hysteresis measurements at selected temperatures were carried out. Results for the terpolymer are depicted in Figure 11.7 where, around RT, we can see that the terpolymer shows its characteristic slim hysteresis loop [48, 270]. In the paraelectric phase above 20 °C, we notice a steady drop in the electric-displacement values up to 80 °C. However, at 100 °C and above, the loop becomes elliptical indicating an increase in capacity and conductivity of the sample.

Since non-linear permittivities can give information about the ferroelectric state of the sample, complementing the results obtained from dielectric hysteresis measurements, the remanent polarization ratio $\varepsilon_2/3\varepsilon_0^2\varepsilon_1^3$ is plotted as a function of temperature for a poled and annealed terpolymer sample in Figure 11.8. The plot shows a minimum at approximately 30 °C due to the mid-temperature transition. Upon

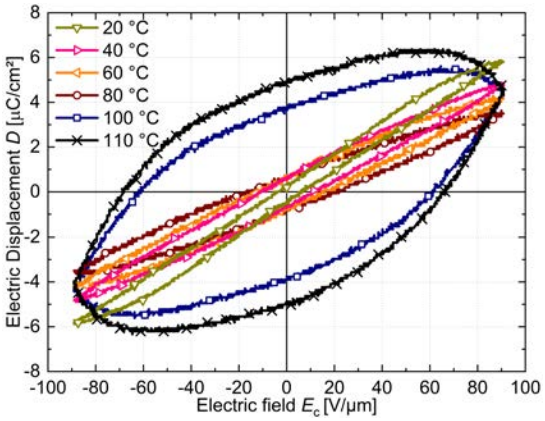

Figure 11.7: Electric-displacement-*versus*-electric-field hysteresis curves of an annealed and poled P(VDF-TrFE-CFE) terpolymer film at different temperatures as indicated. Symbols have been added to the continuously measured curves to facilitate their identification.

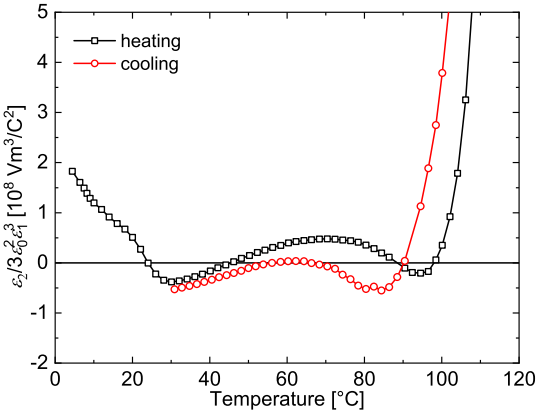

Figure 11.8: Ratio $\varepsilon_2/3\varepsilon_0^2\varepsilon_1^3$ (which is proportional to the remanent polarization in the sample) as a function of temperature during heating and cooling for an annealed P(VDF-TrFE-CFE) terpolymer poled at 4 °C.

further heating, we observe yet another minimum in the high-temperature peak range around 100 °C, followed by a steep increase in P_r ratio. Both observations, *i*.e., an elliptical hysteresis curve and an irregular P_r curve above 100 °C, indicate that the high-temperature peak observed in the permittivity measurements has its origin in real charges at the electrode-sample interface [271, 272] – an explanation that is supported by the shift in the polarization curve during cooling within the high-temperature range, as seen in Figure 11.8.

In addition, we find from ε_1'' measurements at different frequencies (Figure 11.6) that the peak is stronger at lower frequencies (< 1 kHz) and gradually disappears at higher frequencies, which is expected in the case of electrode/space-charge polarization processes, as the charges cannot follow the faster electric-field variations at higher frequencies [271]. Furthermore, previous TSDC measurements on a similar terpolymer poled at different electric fields show that the position of the peak seen around 85 °C changes (*cf.* Figure 11.4) and that the peak does not seem to depend on poling conditions, which means that there is no distinct dipolar motion behind the process [273]. The onset of melting in the same temperature range (Figure 8.22) increases conductivity in the sample, facilitates motion of real charges towards the electrodes, and thus induces electrode polarization.

The results of dielectric-hysteresis and remanent-polarization measurements on the P(VDF-TrFE) copolymer are shown in Figures 11.9 and 11.10, respectively. From Figure 11.9, we see that as the temperature increases, not only the maximum displacement D_{max} (as also found on the terpolymer), but also its remanent value D_r (related to the remanent polarization P_r) decreases. In particular between 100 and 110 °C, the displacement decreases drastically. The decrease in D_r can be explained with the gradual

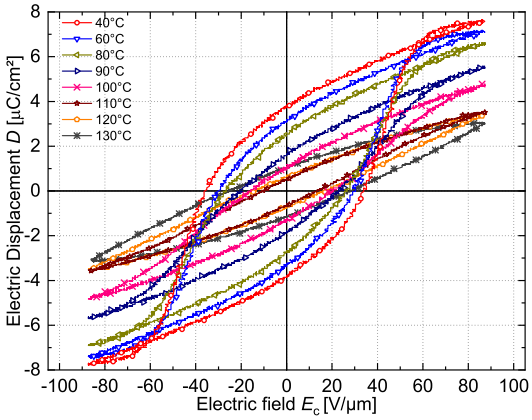

Figure 11.9: Electric-displacement-*versus*-electric-field hysteresis curves of an annealed and poled P(VDF-TrFE) copolymer film at different temperatures as indicated. Symbols have been added to the continuously measured curves to facilitate their identification.

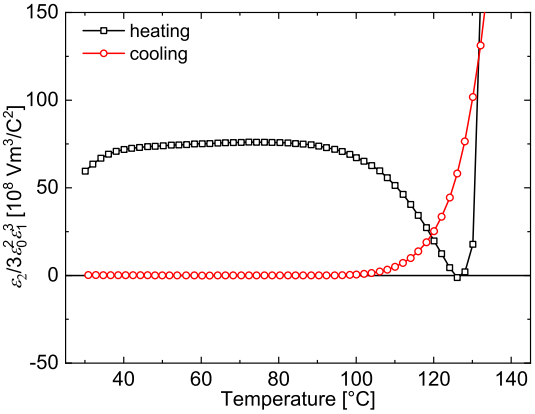

Figure 11.10: Ratio $\varepsilon_2/3\varepsilon_0^2\varepsilon_1^3$ (which is proportional to the remanent polarization in the sample) as a function of temperature during heating and cooling for an annealed P(VDF-TrFE) copolymer poled at RT.

decrease of the crystallinity in the copolymer at increasing temperatures [138]. At 120 °C, we see that the loop stops shrinking. At 130 °C, however, the recorded hysteresis loop is bigger than that observed at 120 °C with a higher D_r, but a lower D_{max}.

Comparing D_r in Figure 11.9 with the $\varepsilon_2/3\varepsilon_0^2\varepsilon_1^3$ ratio in Figure 11.10, we see that the polarization remains stable up to 100 °C. Above 100 °C, we observe a sharp decrease in P_r similar to that observed for its corresponding hysteresis curves, and as the temperature increases further, P_r drops to zero at the T_C. At 130 °C, we observe a steep rise in the polarization, as also observed in the high-temperature range of the terpolymer, which confirms that the growth of the hysteresis loop of the copolymer in the same temperature range (*cf.* Figure 11.9) is due to an electrode polarization that increases the overall sample capacitance. The elliptical shape of the hysteresis loop points out to the same phenomenon. It should be mentioned that new crystals have been observed to be formed in the paraelectric phase of the same copolymer [138], which can also contribute to the increase of capacitance. The resulting charge migration could lead to a much stronger growth of P_r in the copolymer (as observed above 130 °C in Figure 11.10) than in the terpolymer above 100 °C (Figure 11.8). The other difference observed in the copolymer in Figure 11.10, when compared to the corresponding plot of the terpolymer, is that P_r drops to zero upon cooling, which indicates that all the electrode polarization has been lost. Real charges which are responsible for the electrode polarization observed in both the co- and the ter-polymer can exist in the sample due to impurities or defects introduced during preparation or processing. Hence, the method of preparation, the choice of solvents, etc. play important roles for the presence of the observed charges.

12

Effects of Thermal Processing on the Relaxor-Ferroelectric Properties of P(VDF-TrFE-CFE) Films[1]

12.1 Effects of Annealing on P(VDF-TrFE-CFE) Terpolymers

Recently, it was found that thermal history has an effect on crystalline phases and morphology in a P(VDF-TrFE-CFE) terpolymer [54]. This in turn affects the R-F properties of this class of PVDF-based materials, especially its F-P temperature [49]. On the other hand, ferroelectric materials are known to feature significantly enhanced electromechanical effects and dielectric permittivities near their respective F-P transition temperatures [33]. Hence, further detailed investigations on the terpolymer via Dielectric Relaxation Spectroscopy (DRS) in combination with the evaluation of dielectric-hysteresis loops were performed with the aim of better understanding the impact of the annealing temperatures on the applications-relevant R-F properties of P(VDF-TrFE-CFE) terpolymer films.

12.2 Sample Preparation and Experiments

A P(VDF-TrFE-CFE) terpolymer resin with a monomer ratio of 62.2/29.4/8.4 mol % (Piezotech-Arkema) was employed in this study. Samples were prepared from a solution of 10 wt % terpolymer in acetone. The spin-coated samples that were used for DRS and dielectric hysteresis measurements were between 1.7 and 3.6 µm in thickness and the drop-cast films were 40 to 60 µm thick (used for DRS, DSC/mDSC, WAXD and TSDC measurements). The dielectric displacement D was recorded as a function of the electric field E applied in the form of triangular voltage signals with a frequency of 10 Hz.

[1] Parts of this chapter are adapted from T. Raman Venkatesan *et al.*, "Tuning the Relaxor-Ferroelectric properties of Poly(vinylidene fluoride-trifluoroethylene-chlorofluoroethylene) Terpolymer by Thermally Induced Micro- and Nanostructures", under review in *Macromolecules*, 2022.

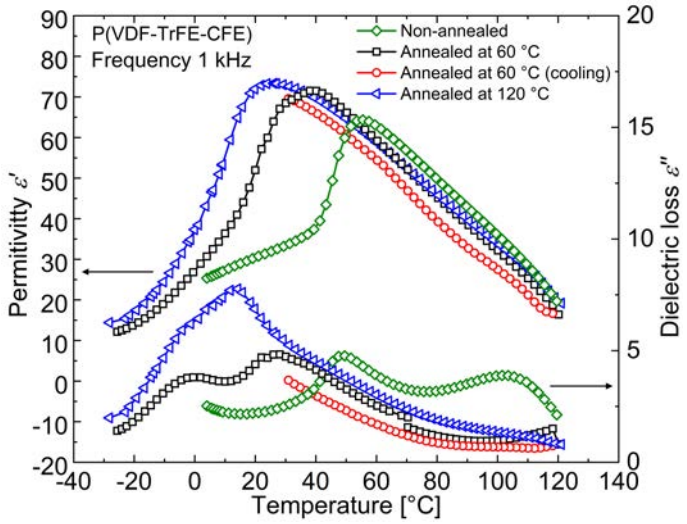

Figure 12.1: Dielectric spectra (real and imaginary parts of the complex permittivity) observed on P(VDF-TrFE-CFE) terpolymer films subjected to different heat treatments.

For the heat treatment, one set of terpolymer films was not subjected to any thermal processing, and the other sets were annealed either at 60 °C (referred to as partial-temperature annealing) or at 120 °C (referred to as high-temperature annealing) for time periods between 1 and 4 hours and then slowly cooled down to RT.

12.3 Dielectric Relaxation Spectra, Calorimetry Scans and *D-E* Hysteresis Loops on Differently Heat-Treated Samples

The dielectric spectrum of a non-annealed terpolymer is plotted together with the DRS spectra of terpolymer samples partially annealed at an intermediate temperature or fully annealed at a high temperature in Figure 12.1. For the terpolymer annealed at an intermediate temperature, the spectrum has also been recorded during cooling. From the figure, a clear difference is observed in the Curie transition of the different samples. In case of the non-annealed sample, the Curie transition (T_C) occurs at a temperature of 55.5 °C (ε'), which is almost 30 °C higher than for the fully annealed terpolymer sample and still more than 17 °C higher than on the terpolymer film annealed at an intermediate temperature (T_C = 38 °C (ε')) – *i.e.*, annealing shifts the Curie transition to lower temperatures. Furthermore, the high-temperature dielectric-loss peak around 100 °C on the non-annealed sample is removed as a result of heat treatments at high or partial temperatures. The loss peak associated with electrode polarization disappears after intermediate- or high-temperature annealing [83].

The thermal behavior of free-standing, non-annealed or annealed, terpolymer films can be observed in Figure 12.2 that consists of DSC traces during first heating. At temperatures below 0 °C, we observe

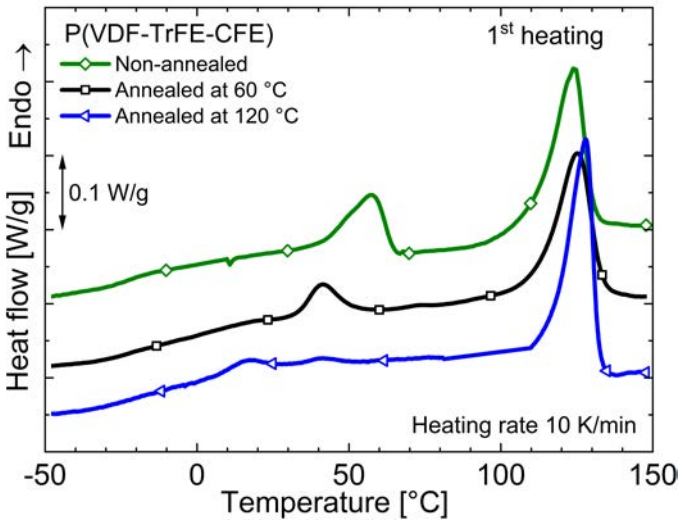

Figure 12.2: Differential Scanning Calorimetry thermograms of differently heat-treated P(VDF-TrFE-CFE) terpolymer films during first heating. Symbols are added to the continuously measured curves in order to facilitate their identification.

the glass-transition step for all terpolymer samples. A glass-transition temperature (T_g) of around $-18\,^\circ$C is found for all three samples. While the non-annealed (NA) sample shows an endothermic melting peak at 124.5 °C (T_m), the annealed films show slightly higher T_m values around 126–128 °C. The major difference is observed in the Curie-transition temperatures T_C. As seen from Figure 12.2, the NA terpolymer exhibits a higher T_C around 58 °C. On the other hand, annealing reduces the Curie temperature T_C to 41.5 and 18 °C in the samples annealed at 60 and 120 °C, respectively. The results are consistent with those observed in DRS experiments.

For the design and the optimization of device applications, it is essential to understand the effects of annealing on the dielectric polarization in the terpolymer. Consequently, dielectric hysteresis measurements were made on spin-coated sample films. Figure 12.3 exhibits the dielectric *D-E* hysteresis loops of a non-annealed terpolymer film at selected temperatures from -30 to $+50\,^\circ$C. We see that the NA sample shows practically no dielectric hysteresis below 20 °C. Then, the loop starts to open up and to become more non-linear, as the sample reaches ambient temperatures. At 30 °C, a ferroelectric-like hysteresis loop with a high remanent displacement D_r (≈ 1.7 μC/cm^2) and a high coercive field E_c (≈ 27 V/μm) becomes visible. As the temperature increases further approaching T_C, the curve becomes narrow – resembling that of a relaxor-ferroelectric material. A maximum saturation displacement (D_{sat}) of around 5 μC/cm^2 is recorded at 50 °C for the applied maximum electric field of 90 V/μm. Upon further heating up to 60 °C, the shape of the loops do not change.

Now, the terpolymer sample that has been annealed at a partial temperature of 60 °C was cooled down to $-30\,^\circ$C (*i.e.*, below the T_g of the terpolymer). The hysteresis loops were again measured up to 110 °C

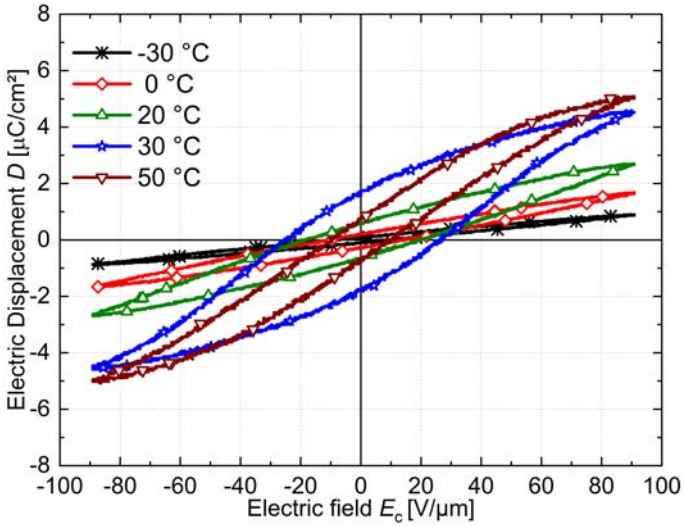

Figure 12.3: Dielectric hysteresis loops of a non-annealed P(VDF-TrFE-CFE) terpolymer film at different temperatures.[1]

and are plotted in Figure 12.4. Below T_g (Figure 12.4a), we observe no hysteresis, since the dipoles are completely frozen in the glassy state of the terpolymer. The elliptical shape of the hysteresis curve, which persists until the samples reach their glass-transition temperature around $-20\,^{\circ}\mathrm{C}$, is indicative for the contribution from the sample capacitance to the overall polarization. Above T_g, the hysteresis curves start to be non-linear and are no longer elliptical. At $0\,^{\circ}\mathrm{C}$, we now observe the effect of annealing, as the sample shows a clear hysteresis (blue curve with stars) that had been absent in the neat sample at $0\,^{\circ}\mathrm{C}$ (*cf.* Figure 12.3).

Inspecting Figure 12.4b, it can be noticed that a temperature increase above $0\,^{\circ}\mathrm{C}$ results in ferroelectric-like hysteresis loops in the PA sample up to $20\,^{\circ}\mathrm{C}$ – similar to the hysteresis in the non-annealed sample (Figure 12.3). Again, when the sample is heated to a temperature in the vicinity of T_C (Table 12.1), it reveals a typical relaxor-ferroelectric hysteresis. Looking closely at the hysteresis loop for $30\,^{\circ}\mathrm{C}$, we find that the displacement is almost reduced to zero upon removal of the electric field, *i.e.*, exhibits a double hysteresis loop (DHL) (Section 5.1). In Figure 12.4c, we observe that the DHL disappears when the temperature of an partially-annealed (PA) sample rises above its Curie temperature, since the terpolymer is now in its paraelectric state. Above $50\,^{\circ}\mathrm{C}$ (Figures 12.4c and 12.4d), the hysteresis curve becomes elliptical in shape due to the increases in sample capacitance and conductivity. At the end of the hysteresis measurements at increasing temperatures the PA sample was annealed once more at $120\,^{\circ}\mathrm{C}$ (not shown in the figure).

If we look at the dielectric spectra during cooling of a PA terpolymer after the additional annealing at $120\,^{\circ}\mathrm{C}$ (red coloured curve with circles in Figure 12.1), we notice that the curve quite closely

[1] Symbols are added to all continuously measured hysteresis curves in this chapter in order to facilitate their identification.

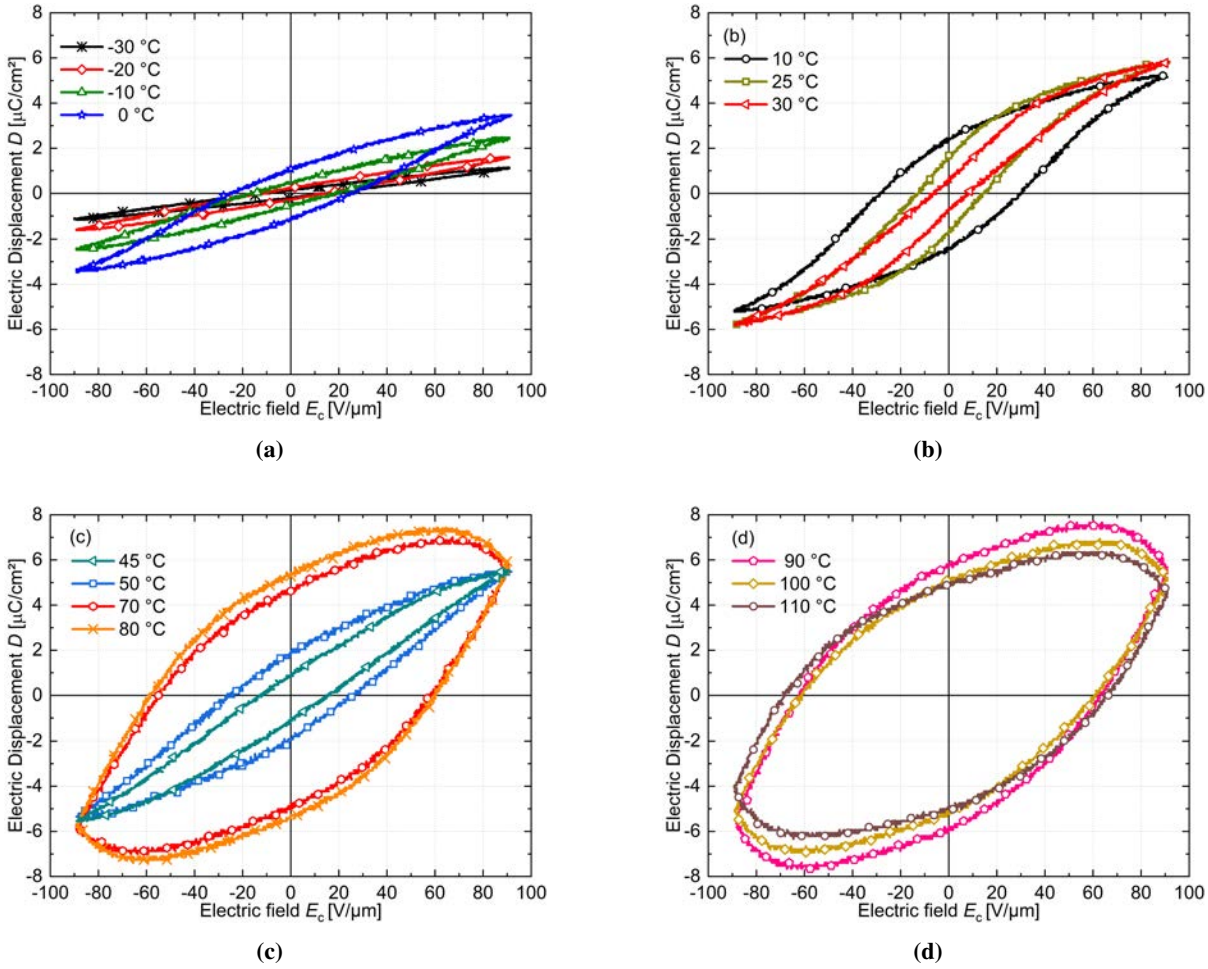

Figure 12.4: Dielectric hysteresis curves of a partially-annealed P(VDF-TrFE-CFE) terpolymer measured at temperatures from −30 to +110 °C.

resembles that of the sample that had initially been annealed at the high temperature of 120 °C (black curve consisting of square symbols) indicating that the partially-annealed (PA) sample has been completely annealed during the experiment that included a step-by-step heat treatment up to a temperature of 120 °C. Figure 12.5 shows the hysteresis curves of a completely-annealed terpolymer sample at selected temperatures as it is being cooled down from its annealed state. As shown in Figure 12.5a, the sample capacitance is greatly reduced below 100 °C as a result of annealing. However, the shape of the curves remains elliptical until the temperature is reduced to temperatures near T_C (*cf.* Table 12.1), accompanied by a continuous increase in the observed displacement (D) values. At 20 °C, a clear R-F hysteresis loop is observed. As the temperature is reduced further to values below RT (Figure 12.5b), the annealed sample continues to exhibit slim curves until about 0 °C, below which the hysteresis loops become broader and resemble those of an FE polymer – with a decrease in displacement D, and increase in remanent displacement (D_r) and coercive field (E_c).

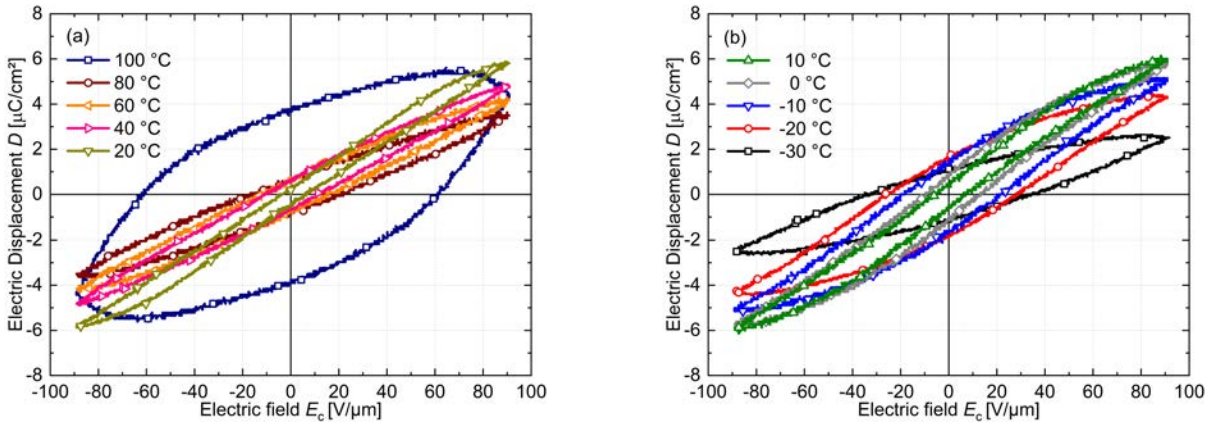

(a) **(b)**

Figure 12.5: Dielectric hysteresis curves of a completely-annealed P(VDF-TrFE-CFE) terpolymer measured while cooling from $+100$ to $-30\,^{\circ}$C.

A similar observation has been reported before on uniaxially stretched P(VDF-TrFE-CFE) films below $0\,^{\circ}$C [115]. While the decrease in D should be a result of the overall reduced mobility of the dipoles at low temperatures, the increase in D_r and E_c should be due to the increase in the ferroelectric nature of the terpolymer that results from the higher T_g of CFE molecules when compared to VDF and TrFE molecules. As the terpolymer crystallinity is in general low, the amorphous phase and its associated a-c interface should play important roles in the overall mobility and hence also the polarization response of the sample.

Though a P(CFE) homopolymer has not been synthesised and characterized, a reasonable assessment of its T_g and thus the contribution of CFE molecules to the overall glass-transition process of the terpolymer can be estimated by examining a P(CTFE) homopolymer which has a chemical structure close to that of P(CFE). A T_g of approximately $45\,^{\circ}$C has been reported for P(CTFE) [274]. The amorphous phase of CFE molecules should also have a higher T_g than VDF and TrFE, the T_g values of which are found close to -40 and $-12\,^{\circ}$C, respectively [49, 129]. Consequently, during poling in the low temperature range below $0\,^{\circ}$, the VDF-TrFE molecules can still respond to the applied field and thus exhibit a broad ferroelectric hysteresis loop. However, at temperatures lower than $-20\,^{\circ}$C – below the overall T_g of the terpolymer – the curve becomes again elliptical due to the restricted motion of both VDF-TrFE and CFE chain segments.

12.4 Influence of Annealing on the Terpolymer Behavior

The shift of the Curie transition from higher to lower temperatures upon annealing of the terpolymer can be explained as follows: Depending on its composition, the terpolymer can show different electrome-

Table 12.1: Essential parameters of P(VDF-TrFE-CFE) terpolymer samples kept at RT or annealed at 60 or 120 °C from DRS, DSC and WAXD measurements (near (200,110) family of planes.

P(VDF-TrFE-CFE) terpolymer	ε'_{max} [-] DRS at 1 kHz	T_C [°C] from ε'^a	ε''^a	DSC[b]	FWHM [Å] WAXD	d [Å] WAXD	χ_c[%] WAXD
Non-annealed (NA)	64	55	49.5	58	0.93	4.55	15
Annealed at 60 °C (PA)	71	38	28	41.5	0.37	4.87	18
Annealed at 120 °C (CA)	73	26	14	18	0.19	4.89	20

[a] DRS (at 1 kHz)
[b] Except for the CA sample, the samples show a superimposed T_C peak in DSC experiments

chanical properties from that of a ferroelectric polymer and instead behave as a relaxor-ferroelectric (R-F) polymer [47, 51, 270, 275]. Though Xia *et al.* demonstrated that only 4 % of the CFE termonomer is sufficient to generate the characteristic slim hysteresis curves that are typical for R-F materials [51], Klein *et al.* varied the CFE content between 0 and 9 % and found that the terpolymer was completely converted into an R-F material and showed maximum electromechanical properties only for a CFE content of about 8.5 % [52]. However, both Xia *et al.* and Klein *et al.* used only samples that had been annealed at 120 °C. Bao *et al.* varied the annealing temperature of a terpolymer with a CFE content of 8.2 % and found that when the sample had been annealed at temperatures lower than 110 °C, it could exhibit a ferroelectric phase in addition to the paraelectric/relaxor-ferroelectric phase at RT [136]. The same behavior can also be deduced from the WAXD results in Figure 12.6. The non-annealed terpolymer reveals the presence of a definite ferroelectric (FE) phase with a peak around $2\theta = 19.5°$ near the (110,200) family of planes [54, 136].

While the non-annealed sample shows only a broad amorphous shoulder around $2\theta = 18°$, we observe a sharp relaxor-ferroelectric (R-F) peak in the annealed terpolymer films with a smaller Full Width at Half Maximum (FWHM) compared to that of the ferroelectric peak in the non-annealed sample, which indicates an increase of the coherence length (L_c) in the crystals. The FWHM values of the different terpolymer samples are listed in Table 12.1. It is also obvious that thermal treatment can improve the crystallinity in the terpolymer. Looking at the WAXD peaks, while a total crystallinity (χ_c) of 18 % and 20 % was calculated for the samples annealed at 60 and 120 °C, respectively, the NA sample has a lower χ_c value of 15 %. The annealing temperature also has an influence on the lattice constant (d) between the crystalline planes of the terpolymer (Table 12.1). Thus, the NA terpolymer shows a d spacing of 4.55 Å, which is closer to the value observed on a pure P(VDF-TrFE) copolymer [54], and clearly indicates that the NA sample crystallizes with a predominant ferroelectric structure. Upon annealing, we notice an increase in d values for both annealed samples, indicating a higher inclusion of CFE molecules in the crystalline structure – in agreement with its R-F behavior.

Though the WAXD spectrum of the partially-annealed (PA) sample is similar to that of the sample

Table 12.2: Essential parameters of P(VDF-TrFE-CFE) terpolymer samples kept at RT or annealed at 60 or 120 °C from FTIR, TSDC and dielectric hysteresis.

P(VDF-TrFE-CFE) terpolymer	β [%] FTIR	α [%] FTIR	γ [%] FTIR	$T_g(U)$ [°C] TSDC	D_{sat} [μC/cm²] (both at 10 Hz)	E_c [MV/m] (both at 10 Hz)
Non-annealed (NA)	28	20	52	25	5.1 (at 50 °C)	10.5 (at 50 °C)
Annealed at 60 °C (PA)	23	24	53	10	5.8 (at 30 °C)	9.0 (at 30 °C)
Annealed at 120 °C (CA)	19	30	51	5	6.1 (at 10 °C)	7.0 (at 10 °C)

annealed at 120 °C, Figure 12.6 shows a d value of 4.87 Å for the PA sample and also a β-phase fraction of 23 % from FTIR measurements (Table 12.2). This result suggests that localized regions that are rich in CFE and others that mainly consist of P(VDF-TrFE) can co-exist within the same crystallite [115, 116, 136]. Hence, the effect of CFE in reducing the interaction between the P(VDF-TrFE) chains is limited (pinning effect). When we compare the fractions of different phases in samples that underwent different thermal treatments, we observe that annealing leads to a decrease of the polar ferroelectric β-phase with a simultaneous increase in the non-polar α-phase. However, the fraction of the weakly polar $T_3G^+T_3G^-$ molecular conformation that forms the largest crystalline phase in the terpoymer remains almost unchanged. Thus upon annealing, the fraction of the ferroelectric crystals are reduced with a simultaneous increase of R-F regions in the terpolymer, which in turn lowers the T_C of the annealed terpolymers, similar to the effect observed when adding CFE chains to the P(VDF-TrFE) copolymer.

The crystallinity and the fraction of different crystalline micro- and nano-structures have a direct influence on the polarization behavior of heat-treated terpolymer films, which can be seen from the maximum electric displacement (D_{sat}) values and from the coercive fields (E_c) recorded on the individual terpolymers at temperatures in the range of their T_C. The respective values are tabulated in Table 12.2: A sample annealed at 120 °C shows the highest D_{sat} and also the highest χ_c among the differently thermally processed samples. Such a sample also shows the lowest E_c due to the lowest fraction of β phase. On the other hand, a non-annealed terpolymer shows the lowest D_{sat} and the highest E_c values owing to its lower χ_c and higher content in β phase, respectively, when compared to the other two samples. A PA sample exhibits intermediate D_{sat} and E_c values as expected.

From all the above results, it is also clear that high temperatures above 100 °C are required for the samples to be completely annealed. The statement is supported by the findings of Liu *et al.* who annealed a terpolymer with a CTFE molar ratio of 8% from 60 to 140 °C and studied its morphological evolution with temperature and its effects on the electrical and mechanical sample properties [276]. Liu *et al.* also concluded that the higher the annealing temperature, the more homogeneous is the growth of worm-like nano-crystalline domains which contribute to higher R-F activity. This indicates that even terpolymers with high CFE content, which exhibit excellent R-F properties, can possess significant amounts of ferroelectric regions – unless they are completely annealed.

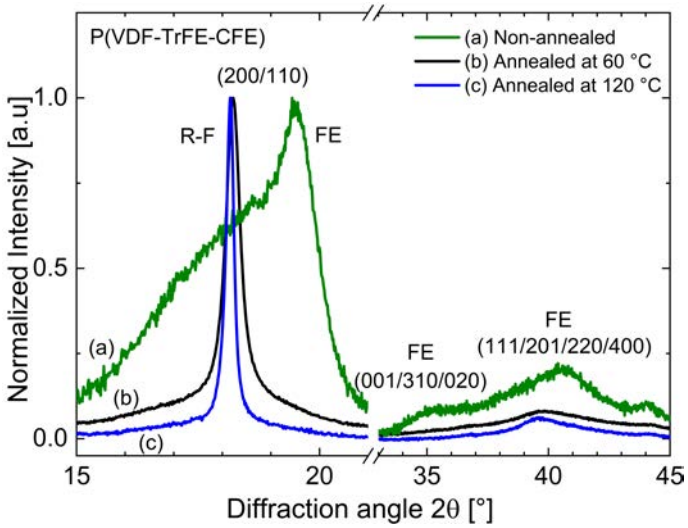

Figure 12.6: WAXD patterns obtained at room temperature on different thermally treated P(VDF-TrFE-CFE) terpolymer films near the (110, 200) reflexes.

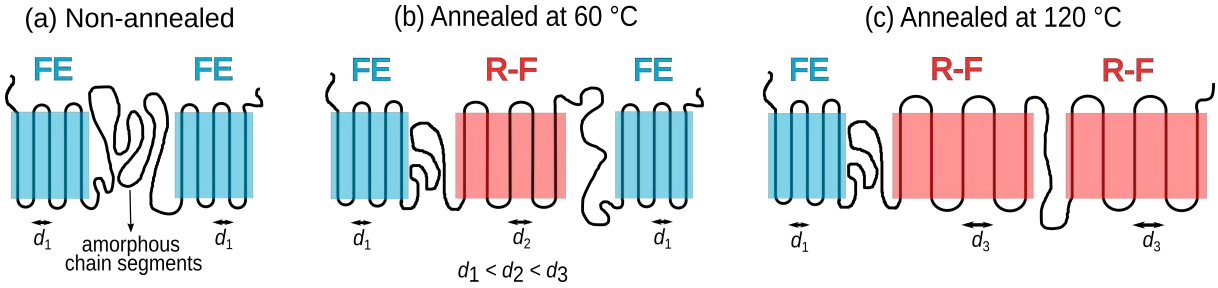

Figure 12.7: Schematic representation of the respective crystalline structures in differently heat-treated terpolymer samples. FE – ferroelectric regions, R-F – relaxor-ferroelectric regions.

A schematic cartoon of the possible changes in the crystalline structure of the terpolymer as a result of different heat treatments is presented in Figure 12.7. As stated above, the NA sample mostly has ferroelectric (FE) P(VDF-TrFE) chains in its crystalline structure with a lattice constant d_1. Hence, the majority of the polymer chains containing CFE are excluded from the crystallites and are found in the amorphous phase. In the case of a PA sample, the annealing process leads to the inclusion of a certain number of CFE groups into the crystal structure with an increased lattice constant d_2. Complete annealing of the sample at higher temperature leads to further inclusion of CFE groups in the crystallites and thus, results in relaxor-ferroelectric crystalline regions with the highest lattice spacing d_3 and crystallinity χ_c.

12.5 Comparison of Electric-displacement-*versus*-Electric-field Hysteresis Loops in Differently Annealed Terpolymer Films

In order to compare the polarization of the differently heat-treated terpolymer films at various temperatures, the hysteresis curves of the samples at six selected temperatures are shown in Figure 12.8a–f, respectively. At $-20\,^{\circ}\mathrm{C}$ – near the conventional glass transition of the terpolymers – a ferroelectric hysteresis loop is solely found for a completely annealed sample. At $0\,^{\circ}\mathrm{C}$, the non-annealed sample shows an almost linear response to the applied electric field – typical for a pure paraelectric material. According to Table 12.1, the non-annealed sample has the lowest crystallinity (χ_c) and also the smallest crystallites (highest FWHM values) of all samples, *i.e.*, the total number of dipoles that can contribute to the polarization is a minimum. In addition, the sample temperature ($0\,^{\circ}\mathrm{C}$) is below its respective $T_g(U)$ (*cf.* Table 12.2) so that the dipoles in the constrained amorphous phase (CAP), in the crystallites and in the a-c interface regions remain frozen. Such conditions lead to a rather small polarization response in the NA sample at the relatively low temperature of $0\,^{\circ}\mathrm{C}$. For the completely-annealed (CA, at $120\,^{\circ}\mathrm{C}$) terpolymer sample, the temperature is at the onset of its $T_g(U)$, and the higher fraction of bulkier CFE groups in the crystalline structure reduces the co-operative interactions between the ferroelectric P(VDF-TrFE) domains, which limits its polarization response and yields a very slim hysteresis loop. For the partially-annealed (PA) sample, the temperature of $0\,^{\circ}\mathrm{C}$ is below its $T_g(U)$, resulting in the absence of a proper hysteresis loop in this case. However, since the temperature is approaching near the $T_g(U)$ temperature range of the sample, we observe a broad loop similar to the situation of the CA sample at $-20\,^{\circ}\mathrm{C}$.

At $+20\,^{\circ}\mathrm{C}$ (Figure 12.8c), both annealed samples are above their respective $T_g(U)$ temperatures, and the Curie temperature of a completely-annealed (CA) terpolymer (T_C) lies in the experimental temperature range. Since R-F materials exhibit high permittivities near their respective Curie temperatures T_C [33], we observe the highest D_s and the lowest D_r values for a CA terpolymer sample at this temperature. In comparison to the typical R-F curve recorded at $0\,^{\circ}\mathrm{C}$ and up to $10\,^{\circ}\mathrm{C}$ (Figure 12.5b), the sample now shows DHL behavior at high electric fields. A PA terpolymer sample, however, starts to yield a hysteresis loop with ferroelectric characteristics above its $T_g(U)$, which can be explained with a lower fraction of CFE molecules in a PA sample, limiting pinning and allowing the dipoles within a FE P(VDF-TrFE) domain to interact with each other. Further facilitated by the moderate crystallinity (Table 12.1), a sufficient number of dipoles can rotate in the applied electric field. Hence, the PA sample shows relatively higher E_c and D_r values. Though the hysteresis loop of the non-annealed terpolymer starts to open up at this temperature, the linear contribution of the capacitance to the overall displacement still dominates below $T_g(U)$.

As the temperature is raised to $30\,^{\circ}\mathrm{C}$, *i.e.*, close to its $T_g(U)$, the non-annealed (NA) sample reveals a clear hysteresis – as shown in Figure 12.8d. Due to its lowest fraction of CFE groups within the

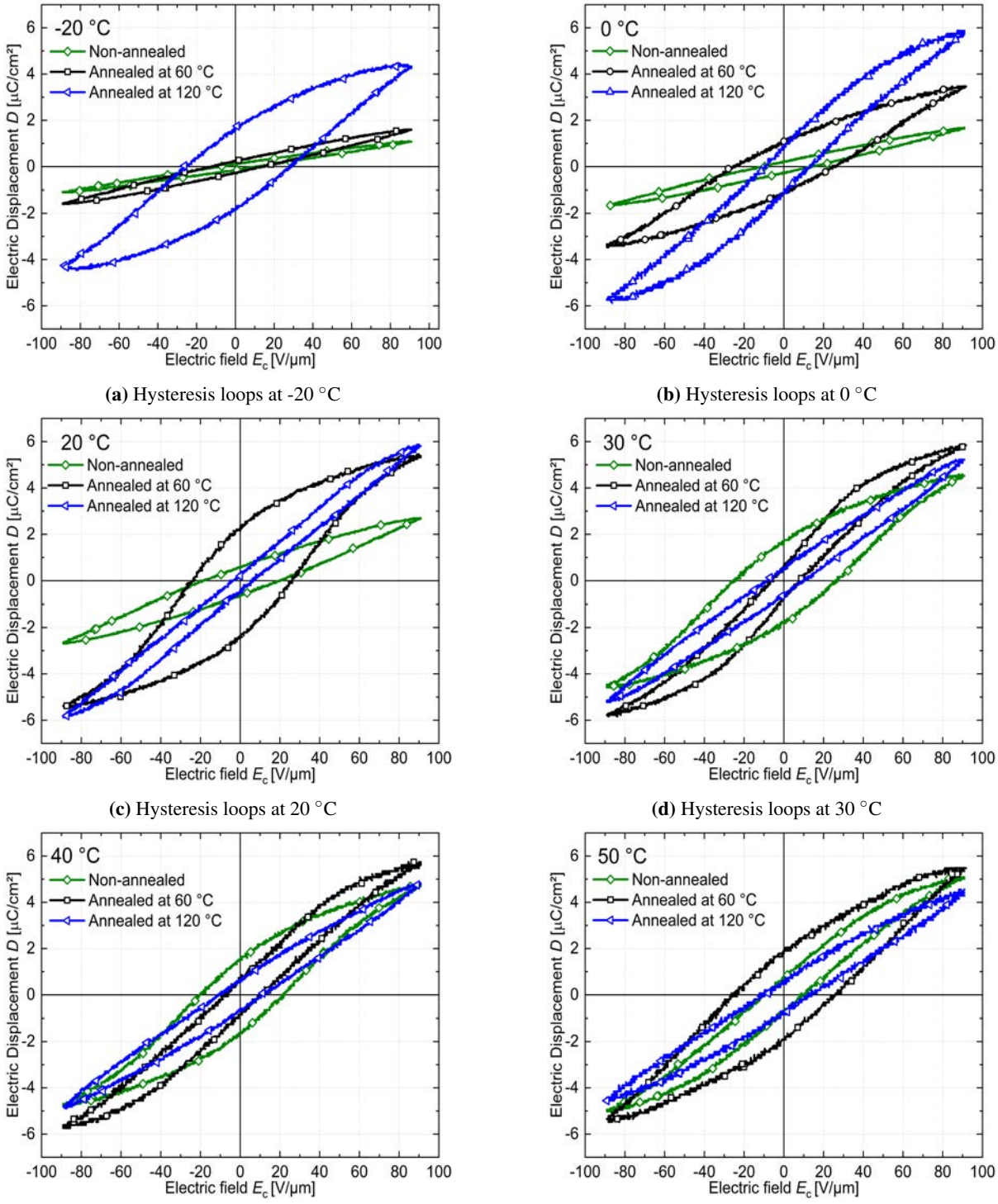

(a) Hysteresis loops at -20 °C

(b) Hysteresis loops at 0 °C

(c) Hysteresis loops at 20 °C

(d) Hysteresis loops at 30 °C

(e) Hysteresis loops at 40 °C

(f) Hysteresis loops at 50 °C

Figure 12.8: Hysteresis curves of differently heat-treated P(VDF-TrFE-CFE) terpolymer films measured at various temperatures.

crystalline phase, the NA sample exhibits typical ferroelectric behavior, and its lower crystallinity χ_c (in comparison with a PA sample) results in a lower D_r value. The CA sample on the other hand exhibits an elliptical curve indicating its paraelectric state at and above this temperature. Here, the hysteresis loop of a PA sample changes from ferroelectric-like behavior at 20 °C to R-F characteristics at 30 °C with a DHL, since the temperature of the experiment lies in the range of its T_C – similar to the situation of a CA terpolymer at 20 °C (Figure 12.8c).

At 40 °C, the hysteresis curves of the differently heat-treated samples are again easy to distinguish due their quite different crystalline structures and dielectric characteristics. The PA sample exhibits an increase in its capacitance above its T_C – as deduced from the more elliptical shape of its hysteresis loop. Even though the respective loop is elliptical, the polarization values are still high due to the superposition of the other mid-temperature-range processes in this temperature range that is very close to its T_C.

The single composite peak present around 40 °C in the heating DSC thermogram of Figure 12.2 and the ε' peak around 38 °C (*cf.* Figure 12.1) support our explanation. Since the onset of a *condis* process can result in an enhanced chain mobility, which has been shown to stabilize and improve other ferroelectric properties [129], it can also lead to the hysteresis behavior found for the PA sample. A similar explanation may also be adopted for the completely-annealed sample, which still shows a high D_r value – in spite of an overall elliptical hysteresis behavior. The NA sample on the other hand starts to show R-F-like hysteresis loops as the temperature is approaching its T_C and finally at 50 °C (Figure 12.8f), we observe a proper slim hysteresis loop. Both the PA and CA samples show elliptical loops in their paraelectric state as expected.

From Figure 12.8 and the above explanation, it is clear that the differently heat-treated terpolymer samples all show dielectric hysteresis loops roughly in the temperature range between their upper glass transition at $T_g(U)$ and their Curie transition at T_C. As mentioned before, the upper glass transition at $T_g(U)$ enhances the molecular mobility of the constrained amorphous phase (CAP) and its associated crystalline phase, allowing the dipoles in the terpolymer to be switched in an external electric field. More importantly, all three differently heat-treated terpolymers exhibit both ferroelectric-like and R-F hysteresis loops – depending on their respective crystalline structures and on the temperatures at which the dielectric-hysteresis behavior is measured.

Figure 12.9 shows how the real part of the dielectric permittivity and the remanent electric displacement of the differently heat-treated P(VDF-TrFE-CFE) terpolymer films depend on temperature – along with the temperature ranges (colored stripes) in which the different characteristic shapes (FE-like, R-F SHL or R-F DHL) of the hysteresis loops are observed. The temperature range in which hysteresis loops are observed decreases from the non-annealed (NA) samples to the intermediately (PA) and the completely (CA) annealed ones – in accordance with their respective $T_g(U)$ and T_C transition temperatures.

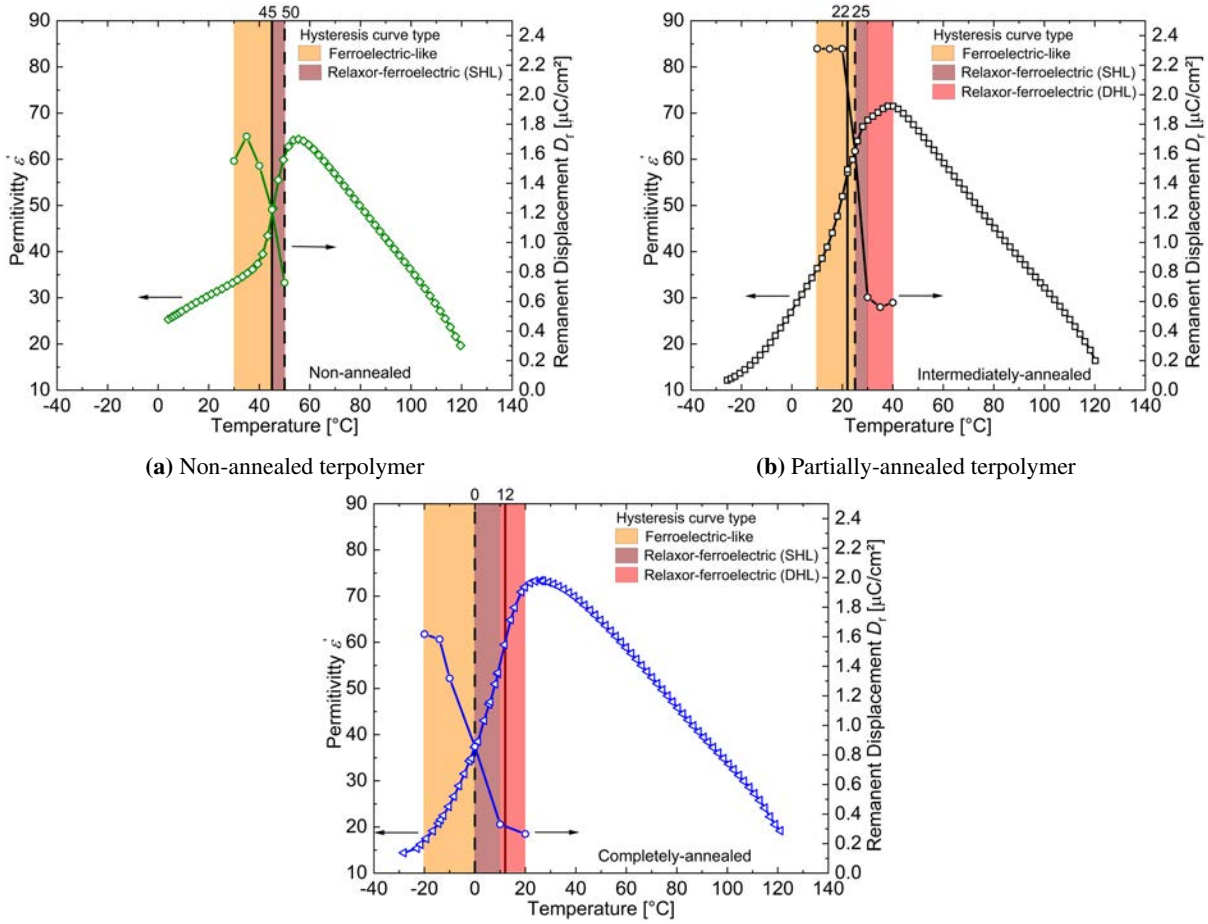

(a) Non-annealed terpolymer

(b) Partially-annealed terpolymer

(c) Completely-annealed terpolymer

Figure 12.9: Temperature dependencies of the permittivity ε' and the remanent displacement (D_r) for differently heat-treated P(VDF-TrFE-CFE) terpolymers. Further details about the dashed (minimum dD_r/dT) and solid (maximum $d\varepsilon'/dT$) lines are found in the text.

We also notice a common feature with respect to the evolution of hysteresis loops with temperature: Initially, in the temperature range around $T_g(U)$, the differently heat-treated terpolymers tend to show a ferroelectric-like hysteresis with a high D_r value. Then, as the temperature of a sample increases, a big drop in its D_r value is observed at a certain temperature, the loop shrinks and shows R-F behavior with a single-hysteresis-loop (SHL). Finally, in the vicinity of their Curie transition, the annealed samples exhibit double-hysteresis loops (DHLs).

Among all the differently heat-treated samples, a non-annealed terpolymer sample mostly exhibits ferroelectric-like hysteresis loops due to the high VDF-TrFE fraction in its crystalline structure which also explains the absence of DHLs. This emphasizes that in addition to the strength of the applied electric field, the mobility and fraction of CFE units within the crystalline structure plays an important role for the observed DHL loops. Consequently, for the annealed samples, the higher concentration of CFE groups

in their crystalline structure provokes a similar occurrence of FE-like and R-F hysteresis curves (both SHLs and DHLs).

Figure 12.9 also shows the temperature at which the rate of decrease in the remanent displacement D_r (T_d, dashed line) and the rate of increase in the dielectric permittivity (T_p, solid line) reaches a maximum for each of the three differently heat-treated terpolymer samples. While a ΔT of about 10 °C between T_d and T_p is found for on CA samples, the difference is very small for NA and PA terpolymer films. As expected, T_d (*i.e.*, the temperature of the lowest dD_r/dT value) in all three sample types is observed near the transition temperature at which the hysteresis loop changes from ferroelectric-like to relaxor-ferroelectric behavior ($T_{FE\rightarrow R\text{-}F}$). This behavior is similar to that observed in P(VDF-TrFE) with low VDF content [114]. In low-VDF-content P(VDF-TrFE) copolymers, it was also found that the D_r values drop to zero at T_p and that the material enters its paraelectric state. However, the scenario is different in annealed terpolymers where we observe R-F hysteresis loops at temperatures higher than T_p as shown in Figure 12.9.

The transition temperature $T_{FE\rightarrow R\text{-}F}$ should depend on the fraction of CFE in the amorphous phase. As discussed before, terpolymers show ferroelectric hysteresis loops at temperatures where the mobility of CFE molecules is restricted (Section 12.3). It has also been shown before that higher CTFE percentages in a P(VDF-CTFE) copolymer lead to higher glass-transition temperatures T_g [277]. A similar behavior can be expected for the influence of the CFE-termonomer fraction on the overall T_g values, as an increase in CFE groups in the amorphous phase also produces an increase in the temperature limit up to which their mobility is limited. Hence, a non-annealed terpolymer which has a higher amount of VDF-TrFE in its crystalline structure (*i.e.*, a higher CFE content in its amorphous phase) should exhibit a higher $T_{FE\rightarrow R\text{-}F}$ transition temperature than the annealed samples – as confirmed by Figure 12.9.

12.6 Remanent Polarization as Measured Using Non-Linear Dielectric Spectroscopy

As mentioned in Section 3.4.7.2, the remanent polarization (P_r) can also be determined in non-linear permittivitiy measurements. The ratio $\varepsilon_2/3\varepsilon_0^2\varepsilon_1^3$ is plotted *vs.* temperature in Figure 12.10 for the different heat-treated samples. The figure includes the curves from neat un-poled samples not subjected to any electrical treatment and other samples subjected to hysteresis measurements prior to the determination of non-linear permittivties (refered to as 'poled' sample). The differences between un-poled and poled samples are clearly visible. In case of un-poled samples, the polarization is reduced to zero near their respective T_C. On the other hand, the poled samples show a non-zero polarization in their paraelectric phase. Especially, the CA poled sample shows a peak at 30 °C corresponding to mid-temperature transition (T_{mid}).

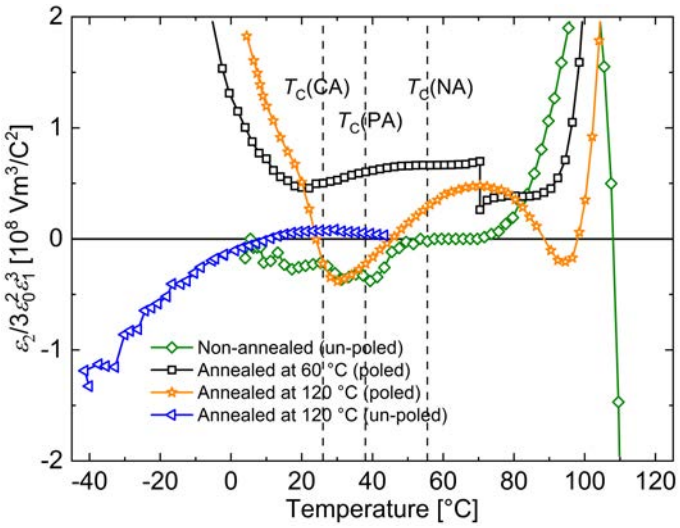

Figure 12.10: Ratio $\varepsilon_2/3\varepsilon_0^2\varepsilon_1^3$ proportional to the remanent polarization as a function of temperature during heating for a non-annealed (NA), a partially annealed (PA) and a completely annealed (CA) P(VDF-TrFE-CFE) terpolymer.

The observation of a clear peak in a poled sample implies that the major contribution to T_{mid} comes from Maxwell-Wagner interface polarization due to the release of charges from the a-c interface that were injected during poling (similar to that in TSDC). The poled PA sample shows a broad shoulder in this temperature range. Within the non-poled samples, as contributions from some of the mid-temperature processes are higher in the case of a non-annealed sample, the effect of T_{mid} transition is better seen in this sample. Indications of electrode-polarization are seen in all samples above 80 °C where we observe elliptical loops in the dielectric hysteresis (Figures 12.4d and 12.5a).

12.7 Suitability of Terpolymers for Memory Applications

The rapid increase in the market of organic electronic devices [278] has led to a demand for applications with better performance, higher reliability and easier fabrication. P(VDF-TrFE) copolymers have been the workhorse materials for such devices that can be used for non-volatile memory storage applications [92, 257, 279, 280, 281] and as ferroelectric field-effect transistors [92, 282]. This is due to their excellent polarization stability and the large remanent polarization they can possess. However, they suffer from the drawback that a high activation energy is required for polarization switching, thereby requiring high operating voltages [283, 284]. In addition, they take relatively longer times for the polarization switching [285, 286]. On the other hand, the more recently developed P(VDF-TrFE) based terpolymers offer lower switching voltages on account of its lower E_c and a high electrical energy density with faster discharge rates [287]. These make them very attractive for utilization in ferroelectric random access memory (FeRAM) devices with a low operating voltage and high reading/writing speeds [288].

The polarization of a P(VDF-TrFE-CFE) terpolymer depends on the annealing conditions and on the temperature at which the polarization is measured. From the application point of view, it is desirable to determine the stability of polarization and optimum conditions for poling the terpolymer. Non-linear permittivity measurements serve as an attractive tool to determine the $\varepsilon_2/3\varepsilon_0^2\varepsilon_1^3$ ratio, which is proportional to the P_r. This allows us to determine the polarization stability and retention time of the samples after poling in a non-destructive way. Since the state of polarization can be assessed by reading the sign of second order permittivity (Section 3.4.7.1), the unpoled and poled state could be assigned as '0' and '1' to describe the polarization state in a memory device. Non-linear permittivity measurements were employed to access the polarization behavior and stability of different heat-treated P(VDF-TrFE-CFE) terpolymers in order to determine the optimum poling conditions. Spin-coated samples with top and bottom electrodes were used for poling and measuring the ε_1 and ε_2 values.

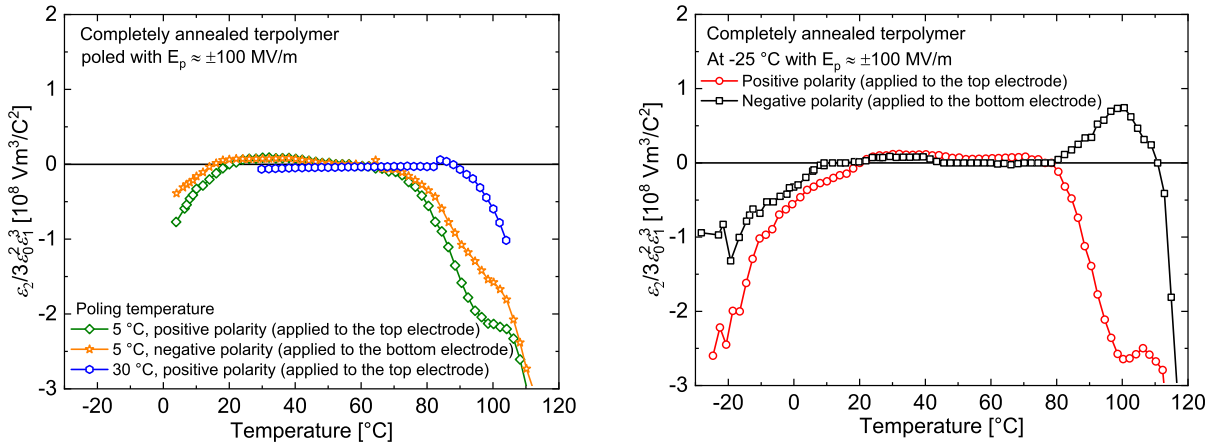

(a) poled at 5 and 30 °C

(b) poled at −25 °C

Figure 12.11: $\varepsilon_2/3\varepsilon_0^2\varepsilon_1^3$ ratio (proportional to the remanent polarization in the sample) plotted as a function of temperature during heating for a completely-annealed P(VDF-TrFE-CFE) terpolymer poled at different temperatures.

12.7.1 Influence of Poling Temperature

At RT, the completely annealed sample does not show any P_r (*cf.* Figure 12.8), since the sample is in its paraelectric state. Hence, when the completely-annealed sample is poled at RT, the $\varepsilon_2/3\varepsilon_0^2\varepsilon_1^3$ ratio is close to zero as plotted in Figure 12.11a. However, when the temperature is lowered to temperatures below their $T_g(U)$, they can be expected to show a P_r polarization as observed in Figure 12.5b. Accordingly, the CA samples were poled around 5 and −25 °C and the $\varepsilon_2/3\varepsilon_0^2\varepsilon_1^3$ ratio was measured as a function of temperature. The results are displayed in Figure 12.11. It is to be mentioned that there is a small offset imposed in the measurement due to the lock-in amplifier, since highly sensitive gain ranges are used to

amplify the signals. Hence, it is not possible to compare the absolute values of the calculated ratio of different samples.

When poled around 5 °C, the sample is polarized in both the positive and negative directions as inferred from a definite $\varepsilon_2/3\varepsilon_0^2\varepsilon_1^3$ value at this temperature. Since negative voltage was applied using the bottom electrode, the current was measured from the top electrode, which explains for the similar sign of the curve as that of a positively poled sample. As the poling temperature lies in the range where the CA sample shows relaxor-ferroelectric hysteresis curves (Figure 12.9), the observed $\varepsilon_2/3\varepsilon_0^2\varepsilon_1^3$ value is still low. Since high P_r values are desired in memory applications, the CA sample was poled at −25 °C, in the temperature region where ferroelectric behavior was previously observed (Figure 12.9). The temperature is just near the conventional T_g of the terpolymer sample. Yet, from Figure 12.11b we observe a definite $\varepsilon_2/3\varepsilon_0^2\varepsilon_1^3$ value for both the polarities – higher than that observed at 5 °C. This denotes that at this temperature, the dipoles can still rotate under high electric fields. However, to be used in memory applications, the annealed terpolymer needs to be cooled down below RT. On the other hand, looking at Figure 12.8d, a non-annealed terpolymer due to the higher fraction of ferroelectric phase shows a higher P_r than the partially-annealed and completely-annealed samples. As a result, it is more suitable for RT memory applications.

12.7.2 Stability of Polarization

To investigate the stability of polarization, after poling the sample at the experimental temperature, the $\varepsilon_2/3\varepsilon_0^2\varepsilon_1^3$ ratio was measured as a function of time. In Figure 12.12, the annealed sample was poled at 5 and −25 °C. In accordance with the observation in Figure 12.11, we see the presence of a small polarization in the sample polarized at 5 °C. Due to the offset introduced by the setup, the sign of the measured ratio for the positively poled sample is positive. However, we can detect a stable polarization for the entire measurement time of about 4.5 hours (partially shown up to 2.5 hr in Figure 12.12).

The CA sample poled at −25 °C was initially poled with a negative polarity and the ratio was measured for a time period of 35 min after the removal of the field. Then the sample was once again poled, this time with a positive voltage and the stability of the $\varepsilon_2/3\varepsilon_0^2\varepsilon_1^3$ ratio was monitored for another 100 min. Initially, a drop in the ratio is observed before the value becomes stable within a few minutes. On switching the polarity, the sign of the ratio changes but the values are stable for the remaining measurement time.

Figure 12.13 shows the $\varepsilon_2/3\varepsilon_0^2\varepsilon_1^3$ retention behavior of a non-annealed sample poled at RT with opposite polarities. When poled with a negative voltage on the top electrode, we observe an initial polarization of about 1.7×10^8 Vm^3/C^2 that steadily decreases to a value of 1.0×10^8 Vm^3/C^2 at 100 min after the removal of field. This accounts for about 60 % of the original value. On poling with a positive voltage on the top electrode, the value decreases to 12 % of its initial value after about 145 min.

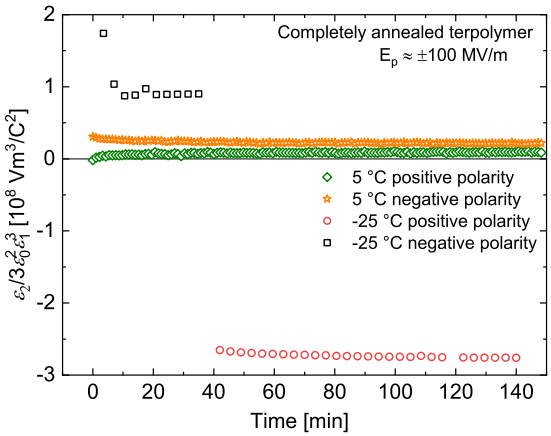

Figure 12.12: $\varepsilon_2/3\varepsilon_0^2\varepsilon_1^3$ ratio of an annealed terpolymer measured as a function of time after poling at 5 and $-25\,^{\circ}$C with both polarities.

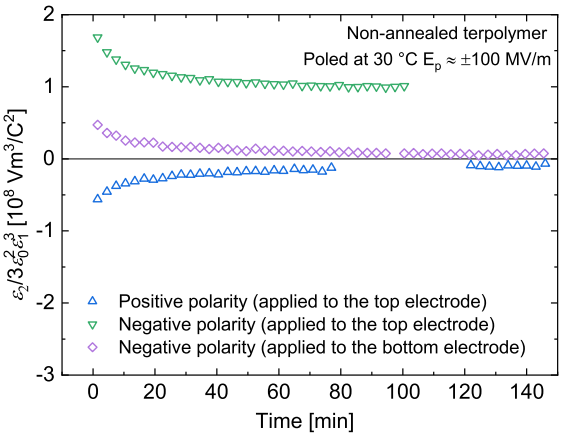

Figure 12.13: Temporal development of $\varepsilon_2/3\varepsilon_0^2\varepsilon_1^3$ ratio of a non-annealed terpolymer after poling at room-temperature with both polarities.

This is unexpected since from the hysteresis curve in Figure 12.8d we observe a similar P_r value for both the polarities. A possible explanation for this behavior is the partial breakdown of the sample due to poling at high voltages. Accordingly, when the sample is poled with a negative voltage on the bottom electrode, we have a similar behavior.

On comparing the polarization behavior and stability of the completely annealed and non-annealed samples, we can conclude that annealed samples need to be poled at low temperatures below RT in order to polarize them, while the latter samples exhibit a stable polarization at RT. Thus, non-annealed sample are better suitable for RT memory devices. With respect to the polarization retention, $\varepsilon_2/3\varepsilon_0^2\varepsilon_1^3$ *vs.* time measurements indicate that both the annealed and non-annealed films exhibit a stable polarization for several minutes.

To summarize, it is clear that the polarization behavior of the terpolymer at various temperatures is profoundly affected by the thermal processing conditions which modify the crystalline and amorphous structures in the annealed materials. Thus, in view of the temperature of operation at which the terpolymer will be used in an application, it is of paramount importance to select optimal processing parameters for each specific situation. Irrespective of temperature, due to the higher crystallinity and the larger crystallites, annealed samples always show superior R-F behavior compared to non-annealed material.

13

Conclusions and Outlook[1]

13.1 Conclusions

The effects of chemical, thermal and mechanical treatments on the semi-crystalline three-phase structure, and morphology of poly(vinylidene fluoride) (PVDF)-based homo-, co- and ter-polymers, which influence the ferroelectric and relaxor-ferroelectric properties have been studied. The main impact of the treatments is seen on the mid-temperature transition (T_{mid}). In the past, different explanations – some complementary and some contradictory have been proposed to explain this transition. In this work, from a detailed literature review and additional experiments, a new hypothesis that assumes multiple origins has been proposed and outlined in order to explain this mysterious transition. During heating from a low temperature, the process starts with an upper glass-transition ($T_{\mathrm{g}}(U)$) in the Constrained Amorphous Phase (CAP), followed by a conformational disorder (*condis*) relaxation involving the flipping of fluorine atoms in α crystals. On further heating, secondary crystals that had formed as a result of storage or quenching will melt. The resultant changes in the three-phase structure causes real charges trapped in the amorphous-crystalline (a-c) interface to be released, observed as Maxwell-Wagner interface polarization peaks in thermally stimulated depolarization current (TSDC) traces.

The individual contribution of each of the processes to the overall T_{mid} is dictated by the processing conditions. Subjecting the polymers to heat-treatment such as annealing or slow-cooling from the melt, and stretching them at high temperatures limits the fraction of CAP/tie/cilia molecules in the final sample. This reduces the contribution from $T_{\mathrm{g}}(U)$ and the formation of secondary crystals leading to a weak T_{mid} to be observed. On the other hand, conditions such as quenching from the melt, stretching at low temperatures or not subjecting the sample to any heat treatment allow for a higher fraction of CAP and

[1]Parts of this chapter are adapted from T. Raman Venkatesan *et al.*, "Non-Linear Dielectric Spectroscopy for Detecting and Evaluating Structure-Property Relations in a P(VDF-TrFE-CFE) Relaxor-Ferroelectric Terpolymer", *Appl. Phys. A*, 127: 756 (10 pages), 2021 [83] and T. Raman Venkatesan *et al.*, "Tuning the Relaxor-Ferroelectric properties of Poly(vinylidene fluoride-trifluoroethylene-chlorofluoroethylene) Terpolymer by Thermally Induced Micro- and Nanostructures", under review in *Macromolecules*, 2022.

higher number of tie or cilia molecules to exist. On storage, imperfect secondary crystals can also be formed. All these lead to a higher contribution from $T_g(U)$ and secondary crystals melting process, ultimately resulting in a strong T_{mid}. Since *condis* takes place in α crystals that exist in smaller ratios even in samples where β phase formation is preferred, it is always observed irrespective of the processing conditions.

The strength of the T_{mid} processes depends also on the chemical structure of the monomers to a certain extend. As α phase is the thermodynamically preferred phase in PVDF, a strong T_{mid} is observed. On the other hand, poly(vinylidene fluoride-tetrafluoroethylene) (P(VDF-TFE)) which crystallizes with a predominant β crystalline structure also shows an enhanced T_{mid}. This can be viewed in the light of its chemical structure that resembles PVDF with a higher percentage of head-to-head and tail-to-tail defects. Similarly, a poly(vinylidene fluoride-trifluoroethylene-cholofluoroethylene) (P(VDF-TrFE-CFE)) terpolymer by virtue of its lower crystallinity (χ_c) and smaller crystalline size shows a higher a-c interface area, ultimately manifesting in a stark T_{mid} process. In the case of a poly(vinylidene fluoride-trifluoroethylene) (P(VDF-TrFE)) copolymer, the presence of a stable β structure with a higher crystallinity leads to the observation of a weak T_{mid}. As the different mid-temperature processes occur within a narrow temperature range and the relative contribution of each process varies, they often are superimposed or suppressed. Hence, it is difficult to observe these samples separately in dielectric or thermal experiments. However, by analyzing the dielectric data using derivative techniques, it has been demonstrated that these processes can be observed individually. The different mid-temperature transition processes have an impact on several properties of the PVDF-based polymers such as their piezo- and pyro-electric activity.

Rapid quenching of polymer films from their melt or annealed state has been performed and the resultant changes in crystalline morphology, phases and thermal transitions have been analyzed. As pointed out from Wide-Angle X-ray Diffraction (WAXD) and Differential Scanning Calorimetry (DSC) scans, both types of quenched samples exhibit a lower χ_c and a smaller crystalline size due to the less time available for crystallization. In general, quenching from the melt does not induce a major change in the crystalline phases. While in PVDF homopolymer and structurally similar P(VDF-TFE) copolymer, rapid quenching of the films from the melt state leads to a small increase in non-polar α crystals, the contrary is observed in the case of P(VDF-TrFE) and P(VDF-TrFE-CFE) films where a small increase of polar β phase is recorded in Fourier Transform InfraRed (FTIR) spectroscopy.

The main difference is seen in between the annealed samples that have been either subjected to rapid quenching or slow cooling. Annealing at 120 °C stabilizes the α phase in PVDF homopolymer. However, quenching from this state leads to a definite increase in the polar β crystals. On the other hand, annealing P(VDF-TrFE) films at the same temperature favors the growth of β crystals and quenching from this state promotes the formation of weakly polar γ crystals. Quenching also has an effect on the

thermal properties in a 80/20 mol% P(VDF-TFE) copolymer as indicated by the lowering of its melting point by about 15 °C. This results in the superposition of the Curie and melting transitions. In the case of P(VDF-TrFE) and P(VDF-TrFE-CFE) samples, quenching increases the Curie temperature. These results point out that all the three-phases in semi-crystalline PVDF-based materials can be modified by quenching.

In another study, P(VDF-TFE) films with a 70/30 molar ratio of VDF/TFE have been subjected to stretching at different temperatures, and the resulting effects on crystalline phases and dielectric properties have been looked into. FTIR and WAXD studies show that the un-stretched sample contains both the non-polar paraelectric α phase and the polar ferroelectric β phase at room temperature. Stretching forces the major part of the crystalline fraction to assume the all-*trans* β conformation with a corresponding reduction in the paraelectric α phase — similar to that observed after suitable stretching of α PVDF films. Moreover, WAXD measurements point to a reduction in the Full Width at Half Maximum (FWHM) values become with increasing stretching temperature (T_s) in the parallel and perpendicular directions to the molecular chain axis, indicating stabilization of the ferroelectric crystals.

Dielectric Relaxation Spectroscopy (DRS) measurements reveal the presence of a Curie transition and the dissipation factor $\tan\delta$ plot reveals a reduction in the losses associated with the transition at high temperatures with an increase in the stretching temperature – reinforcing the findings from WAXD measurements. Further, an increase in T_s facilitates the stretching process and results in an increase in χ_c of the samples. The impact of stretching is clearly seen from the DRS and DSC results. Though stretching removes $T_g(U)$, the presence of a structural transition due to the melting of secondary crystals and a *condis* relaxation is confirmed from the derivative plots. In an un-stretched sample and samples stretched at a low T_s, an endothermic peak in DSC indicates the T_{mid} due to the strong contribution from all the mid-temperature processes. As the T_s increases, the main contribution comes from *condis* indicated by a step in the heating curve.

As non-linear dielectric spectroscopy (NLDS) can reveal additional information that normally cannot be identified in conventional DRS, it has been employed to study transitions and relaxations in P(VDF-TrFE-CFE) relaxor-ferroelectric (R-F) terpolymers. In order to complement the NLDS results, related techniques such as TSDCs and dielectric hysteresis measurements have been utilized. For comparing and highlighting the differences between a relaxor-ferroelectric and a ferroelectric polymer, reference measurements have been performed on a P(VDF-TrFE) copolymer with a comparable VDF/TrFE ratio as that found in the terpolymer. Several noteworthy results have been obtained, and they may shed new light on the large range of possible structure-property relations in complex polymers.

The sign of ε_3' (2^{nd}-order non-linear permittivity) changes from positive to negative at the Ferroelectric-to-Paraelectric (F-P) transition temperature, which reveals that the R-F terpolymer undergoes a second-order transition, while the ferroelectric P(VDF-TrFE) copolymer shows a positive sign throughout, which

indicates a first-order transition. As the remanent polarization vanishes in the paraelectric phase irrespective of the order of the transition, the value of ε_2' should be zero above the respective F-P transition temperature. However, measurements on both the co- and the ter-polymer revealed non-zero values in the paraelectric state. Especially for the terpolymer, new peaks were observed in the paraelectric state at 30 and 80 °C.

The peak at 30 °C in the terpolymer is associated with the mid-temperature transition. Though the peak was absent in ε_2'-*versus*-temperature measurements on the P(VDF-TrFE) copolymer, it is indeed observed in TSDC experiments and other previous measurements. The peak at 80 °C found in ε_2' measurement is related to the high-temperature peak observed around 100 °C on the terpolymer in conventional dielectric-loss (ε_1'' or ε'') measurements, which shows frequency-independent nature at lower frequencies – similar to that of a structural transition. However, the amplitude of the peak is inversely proportional to frequency, indicating that the dielectric loss may originate from charge motions. Evaluating the ratio $\varepsilon_2/3\varepsilon_0^2\varepsilon_1^3$ which is proportional to the remanent polarization in a given sample, it has been shown that the high-temperature peak is a result of the space-charge/electrode polarization at the metal-electrode/sample interface – in close agreement with electrical-hysteresis measurements. A similar origin can be deduced for the shift in the ε_2' values of the copolymer above 110 °C.

Thermal annealing has been demonstrated as an effective method to modify the relaxor-ferroelectric properties in a P(VDF-TrFE-CFE) terpolymer with a VDF/TrFE/CFE ratio of 62.2/29.4/8.4 mol% by means of DRS and dielectric-hysteresis measurements. Other techniques such as DSC, WAXD, TSDCs and FTIR spectroscopy have been used to shed additional light on the results from the DRS and hysteresis-loop experiments. While one set of samples have not been subjected to any subsequent heat treatment, the other two sample sets have been annealed at two different temperatures (60 and 120 °C, respectively).

The main impact of annealing is seen in the Curie transition of the terpolymer. While a terpolymer annealed at 120 °C (completely annealed) shows the lowest Curie-transition temperature (T_C) around 25 °C, its non-annealed or less annealed counterparts show much higher T_C values above RT. Samples annealed at 60 °C (partially annealed) exhibit an intermediate T_C between the values for a non-annealed and a completely annealed film. The above shift in T_C is a result of the variations in the ferroelectric-phase content across and between the different samples. In the case of a non-annealed terpolymer, the existence of a significant fraction of ferroelectric regions could be shown in FTIR and WAXD experiments. As a result of annealing, the ferroelectric regions are converted into relaxor-ferroelectric regions, which in turn reduces the respective Curie-transition temperature. Additionally, annealing the terpolymer at high temperatures above 100 °C is necessary to bring about the necessary changes in the crystalline structure and make it completely relaxor-ferroelectric in nature.

Thermal treatment also has an effect on the mid-temperature (T_{mid}) transition of the terpolymer. This is clearly seen in the shift of the so-called upper glass-transition peak at $T_{\text{g}}(U)$ (one of the processes occurring in the mid-temperature region) in the depolarization traces – in a similar fashion as the shift of the F-P peak in DRS. In DSC thermograms taken during the first heating of a sample, except for the completely-annealed sample, the transition is superimposed with the F-P transition. However, using a lower heating rate, the respective processes can be separated, allowing us to independently observe both transitions.

Both the Curie-transition temperature and the mid-temperature transition(s), have a direct impact on the dielectric displacement behavior and the hysteresis loops of the terpolymer at different temperatures. Hence, the dielectric displacement in the terpolymer is strongly affected by the annealing conditions. In general, the differently heat-treated terpolymer samples begin to show hysteresis loops above their respective upper glass-transition temperatures where the loops are ferrolectric-like. As the temperature increases, the FE-like loops gradually shrink and then reveal R-F behavior. Further, near their respective T_{C}s, the hysteresis curves show a double-hysteresis loops – similar to anti-ferroelectric materials. Finally, above their respective T_{C}, the samples reveal elliptical $D-E$ loops in their paraelectric state. Annealed terpolymers (annealed at 60 or at 120°C) show higher polarizability than the non-annealed films, which probably is a consequence of their higher crystallinity, as evident from WAXD scans.

To access the applicability of terpolymers for possible use in non-volatile memory-storage devices where a stable remanent polarization is required, $\varepsilon_2/3\varepsilon_0^2\varepsilon_1^3$ ratio has been measured. In addition, different polarities and poling temperatures have been used to determine the suitable poling conditions. Both the non-heat treated and treated terpolymer films exhibit a stable polarization for several minutes. A definite polarization was detected in the non-annealed and annealed samples for the total measured time of 2.5 hr and 4.5 hr, respectively. With respect to the poling temperature, a non-annealed sample could be poled at RT conditions owing to its higher Curie temperature, while a completely annealed terpolymer needs to be cooled to lower temperatures where they exhibit a more ferroelectric behavior. From comparing the above result with the dielectric hysteresis measurements, it can be inferred that non-annealed samples are more suitable to be used in memory-applications at ambient temperatures as they also show a higher P_{r}, as a result of a strong ferroelectric phase present in the sample.

The results presented in this study shed new insights into the preparation/processing modified structure-property relationships in PVDF-based polymers, where these different treatments such as annealing, quenching and stretching become important factors for effective process control with the aim of optimizing properties for specific applications.

13.2 Outlook

Further experiments can aid in understanding more about the intriguing three-phase PVDF-based semi-crystalline polymers and how their properties can be modified by their fabrication and processing conditions.

- Temperature dependent WAXD measurements in the mid-temperature transition range could help to further understand the changes in the crystalline structure due to conformational disorder and melting of secondary crystals. Similarly, detailed Dynamical Mechanical Analysis (DMA) can allow us to monitor the changes in mechanical properties during T_{mid} and also above this temperature range. This can provide additional information about the effects of T_{mid} on the application performance.
- Since the partially-annealed P(VDF-TrFE-CFE) terpolymer shows a balance between ferroelectric and relaxor-ferroelectric regions, they could offer a combination of both properties that can be exploited in memory-applications. In this regard, $\varepsilon_2/3\varepsilon_0^2\varepsilon_1^3$ ratio measurements on these samples could be carried out.

References

[1] R. Gerhard. From electrode charges on dielectric elastomers to trapped charges and electric dipoles in electrets and ferroelectrets: fundamental and applications-relevant aspects of diversity in electroactive polymers. In Y. Bar-Cohen and F. Vidal, editors, *Electroactive Polymer Actuators and Devices (EAPAD) 2016*, page 97980T, 2016. (and references therein) doi:10.1117/12.2218300.

[2] M.V. Bennett. Who found electric fish first? In *3rd Mediterranean Conference of Neuroscience*, Alexandria, Egypt, 2009. Frontier. doi:10.3389/conf.neuro.01.2009.16.068.

[3] R. Gerhard. Piezoelectricity and Electrostriction. In F. Carpi, editor, *Electromechanically Active Polymers*, pages 489–567. Springer International Publishing, Cham, 2016. doi:0.1007/978-3-319-31767-0_21-1.

[4] W. Gilbert. *De magnete, magneticisque corporibus, et de magno magnete tellure; Physiologia nova, plurimis argumentis, experimentis demonstrata*. Petrus Short, London, 1600. English translation by Thompson S.P. (On the magnet, magnetick bodies also, and on the great magnet the earth a new physiology, demonstrated by many arguments and experiments) available at http://www.gutenberg.org/ebooks/33810 (open access).

[5] O. Heaviside. Electromagnetic induction and its propagation. electrization and electrification. natural electrets. *The Electrician*, 15:230–231, 1885.

[6] Sessler. G.M., editor. *Electrets*. Topics in Applied Physics. Springer Berlin Heidelberg, Dordrecht, 1987. doi:10.1007/3-540-17335-8.

[7] S. B. Lang. Pyroelectricity: From Ancient Curiosity to Modern Imaging Tool. *Phys. Today*, 58(8):31–36, 2005. doi:10.1063/1.2062916.

[8] J. Curie and P. Curie. Développement par compression de l'électricité polaire dans les cristaux hémièdres à faces inclinées (development of polar electricity through compression in hemihedral crystals at inclined faces). *Bulletin de minéralogie*, 3(4):90–93, 1880.

[9] J. Valasek. The early history of ferroelectricity. *Ferroelectrics*, 2(1):239–244, 1971. doi:10.1080/00150197108234098.

[10] E. Fukada. History and recent progress in piezoelectric polymers. *IEEE Trans. Ultrason. Ferroelectr. Freq. Control*, 47(6):1277–1290, 2000. doi:10.1109/58.883516.

[11] H. Kawai. The Piezoelectricity of Poly (vinylidene Fluoride). *Jpn. J. Appl. Phys.*, 8(7):975, 1969. doi:10.1143/JJAP.8.975.

[12] W. Heywang, K. Lubitz, and W. Wersing. *Piezoelectricity: Evolution and Future of a Technology*. Springer Series in Materials Science. Springer Berlin Heidelberg, 2008. isbn:978-3-540-68680-4.

[13] R. Gerhard, S. Bauer, and X. Qiu. Charge-spring model for predicting the piezoelectric response of dielectric materials: Considering tetragonality extends validity to ferroelectric crystals. In *2016 IEEE Conference on Electrical Insulation and Dielectric Phenomena (CEIDP)*, pages 81–84, Toronto, ON, Canada, 2016. doi:10.1109/CEIDP.2016.7785500.

[14] Q. M. Zhang. Giant Electrostriction and Relaxor Ferroelectric Behavior in Electron-Irradiated Poly(vinylidene fluoride-trifluoroethylene) Copolymer. *Science*, 280(5372):2101–2104, 1998. doi:10.1126/science.280.5372.2101.

[15] A. J. Lovinger. Ferroelectric transition in a copolymer of vinylidene fluoride and tetrafluoroethylene. *Macromolecules*, 16(9):1529–1534, 1983. doi:10.1021/ma00243a021.

[16] A. J. Lovinger, G. E. Johnson, H. E. Bair, and E. W. Anderson. Structural, dielectric, and thermal investigation of the Curie transition in a tetrafluoroethylene copolymer of vinylidene fluoride. *J. Appl. Phys.*, 56(9):2412–2418, 1984. doi:10.1063/1.334303.

[17] S-G. Lu, H. Xiong, A. Wei, X. Li, and Q. Zhang. Electrocaloric and electrostrictive effect of polar P(VDF–TrFE–CFE) terpolymers. *J. Adv. Dielect*, 03(02):1350015, 2013. doi:10.1142/S2010135X1350015X.

[18] T. Furukawa. Structure and Properties of Ferroelectric Polymers. *Key Eng. Mater*, 92-93:15–30, 1994. doi:10.4028/www.scientific.net/KEM.92-93.15.

[19] T. Furukawa. Ferroelectric properties of vinylidene fluoride copolymers. *Phase Transit.*, 18(3-4):143–211, 1989. doi:10.1080/01411598908206863.

[20] R. G. Kepler and R. A. Anderson. Ferroelectric polymers. *Adv. Phys.*, 41(1):1–57, 1992. doi:10.1080/00018739200101463.

[21] V. V. Kochervinskii. The structure and properties of block poly(vinylidene fluoride) and systems based on it. *Russ. Chem. Rev.*, 65(10):865, 1996. doi:10.1070/RC1996v065n10ABEH000328.

[22] H. S. Nalwa. *Ferroelectric polymers : chemistry, physics, and applications*. New York : M. Dekker, Inc, 1995. isbn:978-0-8247-9468-2.

[23] T. Furukawa. Structure and functional properties of ferroelectric polymers. *Adv. Colloid Interface Sci.*, 71(Supplement C):183–208, 1997. doi:10.1016/S0001-8686(97)90017-8.

[24] Thulasinath Raman Venkatesan, Michael Wübbenhorst, and Reimund Gerhard. Structure-property relationships in three-phase relaxor-ferroelectric terpolymers. *Ferroelectrics*, 586(1):60–81, 2022. doi:10.1080/00150193.2021.2014260.

[25] Q. Li and Q. Wang. Ferroelectric Polymers and Their Energy-Related Applications. *Mater. Chem. Phys.*, 217(11):1228–1244, 2016. doi:10.1002/macp.201500503.

[26] P. Martins, A.C. Lopes, and S. Lanceros-Mendez. Electroactive phases of poly(vinylidene fluoride): Determination, processing and applications. *Prog. Polym. Sci.*, 39(4):683–706, 2014. doi:10.1016/j.progpolymsci.2013.07.006.

[27] J. C. Scott and L. D. Bozano. Nonvolatile memory elements based on organic materials. *Adv. Mater.*, 19(11):1452–1463, 2007. doi:10.1002/adma.200602564.

[28] S. Bauer and F. Bauer. Piezoelectric Polymers and Their Applications. In W. Heywang, K. Lubitz, and W. Wersing, editors, *Piezoelectricity*, pages 157–177. Springer, Berlin, Heidelberg, 2008. doi:10.1007/978-3-540-68683-5_6.

[29] G. M. Sessler. Piezoelectricity in polyvinylidenefluoride. *J. Acoust. Soc. Am.*, 70(6):1596–1608, 1981. doi:10.1121/1.387225.

[30] A. J. Lovinger. Annealing of poly(vinylidene fluoride) and formation of a fifth phase. *Macromolecules*, 15(1):40–44, 1982. doi:10.1021/ma00229a008.

[31] D. K. Das-Gupta and K. Doughty. Corona charging and the piezoelectric effect in polyvinylidene fluoride. *J. Appl. Phys.*, 49(8):4601–4603, 1978. doi:10.1063/1.325441.

[32] K. Tashiro, H. Tadokoro, and M. Kobayashi. Structure and piezoelectricity of poly(vinylidene fluoride). *Ferroelectrics*, 32(1):167–175, 1981. doi:10.1080/00150198108238688.

[33] Q. M. Zhang, J. Zhao, T. Shrout, N. Kim, L. E. Cross, A. Amin, and B. M. Kulwicki. Characteristics of the electromechanical response and polarization of electric field biased ferroelectrics. *J. Appl. Phys.*, 77(6):2549–2555, 1995. doi:10.1063/1.358785.

[34] J. B. Lando and W. W. Doll. The polymorphism of poly(vinylidene fluoride). I. The effect of head-to-head structure. *J. of Macromol. Sci. B*, 2(2):205–218, 1968. doi:10.1080/00222346808212449.

[35] T. Furukawa, M. Date, E. Fukada, Tajitsu Y., and A. Chiba. Ferroelectric behavior in the copolymer of vinylidenefluoride and trifluoroethylene. *J. Appl. Phys.*, 19(2):L109, 1980. doi:10.1143/JJAP.19.L109.

[36] K. J. Kim, G. B. Kim, C. L. Vanlencia, and J. F. Rabolt. Curie transition, ferroelectric crystal structure, and ferroelectricity of a VDF/TrFE (75/25) copolymer 1. The effect of the consecutive annealing in the ferroelectric state on curie transition and ferroelectric crystal structure. *J. Polym. Sci. B Polym. Phys.*, 32(15):2435–2444, 1994. doi:10.1002/polb.1994.090321501.

[37] G. A. Samara and F. Bauer. The effects of pressure on the β molecular relaxation and phase transitions of the ferroelectric copolymer p(vdf0.7trfe0.3). *Ferroelectrics*, 135(1):385–399, 1992. doi:10.1080/00150199208230040.

[38] C. Tournut. New copolymers of vinylidene fluoride. *Macromol. Symp.*, 82(1):99–109, 1994. doi:10.1002/masy.19940820112.

[39] B. Ameduri. From Vinylidene Fluoride (VDF) to the Applications of VDF-Containing Polymers and Copolymers: Recent Developments and Future Trends. *Chem. Rev.*, 109(12):6632–6686, 2009. doi:10.1021/cr800187m.

[40] Z. Chen, L. Christensen, and J. R. Dahn. Large-volume-change electrodes for Li-ion batteries of amorphous alloy particles held by elastomeric tethers. *Electrochem. Commun.*, 5(11):919–923, 2003. doi:10.1016/j.elecom.2003.08.017.

[41] C. Tournut. *Modern Fluoropolymers: High Performance Polymers for Diverse Applications*. Wiley, 1997. isbn:978-0-471-97055-2.

[42] X. Lu, A. Schirokauer, and J. Scheinbeim. Giant electrostrictive response in poly (vinylidene fluoride-hexafluoropropylene) copolymers. *IEEE Trans. Ultrason. Ferroelectr. Freq. Control*, 47(6):1291–1295, 2000. doi:10.1109/58.883517.

[43] A. C. Jayasuriya, A. Schirokauer, and J. I. Scheinbeim. Ferroelectric behavior in solvent cast poly(vinylidene fluoride/hexafluoropropylene) copolymer films. *Appl. Surf. Sci.*, 175-176(Supplement C):386 – 390, 2001. doi:10.1016/S0169-4332(01)00130-1.

[44] V. V. Kochervinskii, I. A. Malyshkina, G. V. Markin, N. D. Gavrilova, and N. P. Bessonova. Dielectric relaxation in vinylidene fluoride–hexafluoropropylene copolymers. *J. Appl. Polym. Sci.*, 105(3):1101–1117, 2007. doi:10.1002/app.26145.

[45] P. Frübing, F. Wang, and M. Wegener. Relaxation processes and structural transitions in stretched films of polyvinylidene fluoride and its copolymer with hexafluoropropylene. *Appl. Phys. A*, 107(3):603–611, 2012. doi:10.1007/s00339-012-6838-1.

[46] A. Odajima, Y. Takase, T. Ishibashi, and K. Yuasa. Irradiation effects on the ferroelectric phase transition of vinylidene fluoride and trifluoroethylene copolymers. *Conf. Proc. of 5th International Symposium on Electrets,*, pages 642–647, 1985. doi:10.1109/ISE.1985.7341550.

[47] T. C. Chung and A. Petchsuk. Synthesis and Properties of Ferroelectric Fluoroterpolymers with Curie Transition at Ambient Temperature. *Macromolecules*, 35(20):7678–7684, 2002. doi:10.1021/ma020504c.

[48] F. Bauer, E. Fousson, Q. M. Zhang, and L. M. Lee. Ferroelectric copolymers and terpolymers for electrostrictors: synthesis and properties. *IEEE Trans. Dielectr. Electr. Insul.*, 11:293–298, 2004. doi:10.1109/TDEI.2004.1285900.

[49] T. Raman Venkatesan, A. A. Gulyakova, P. Frübing, and R. Gerhard. Relaxation processes and structural transitions in Poly(vinylidene fluoride-trifluoroethylene-chlorofluoroethylene) relaxor-ferroelectric terpolymers as seen in dielectric spectroscopy. *IEEE Trans. Dielectr. Electr. Insul.*, 25(6):2229–2235, 2018. doi:10.1109/TDEI.2018.007440.

[50] C. Ang and Z. Yu. Ferroelectric, electroactive, and dielectric-relaxation behavior of fluoropolymers. *Adv. Mater.*, 16(12):979–982, 2004. doi:10.1002/adma.200306036.

[51] F. Xia, Z.-Y. Cheng, H.S. Xu, H.F. Li, Q.M. Zhang, G.J. Kavarnos, R.Y. Ting, G. Abdul-Sadek, and K.D. Belfield. High Electromechanical Responses in a Poly(vinylidene fluoride-trifluoroethylene-chlorofluoroethylene) Terpolymer. *Adv. Mater.*, 14(21):1574–1577, 2002. doi:10.1002/1521-4095(20021104)14:21<1570::AID-ADMA1570>3.0.CO;2-N.

[52] R. J. Klein, F. Xia, Q. M. Zhang, and F. Bauer. Influence of composition on relaxor ferroelectric and electromechanical properties of poly(vinylidene fluoride-trifluoroethylene- chlorofluoroethylene). *J. Appl. Phys.*, 97(9):094105, 2005. doi:10.1063/1.1882769.

[53] F. Bauer. Relaxor fluorinated polymers: novel applications and recent developments. *IEEE Trans. Dielectr. Electr. Insul.*, 17(4), 2010. (and references therein). doi:10.1109/TDEI.2010.5539681.

[54] T. Raman Venkatesan, P. Frübing, and R. Gerhard. Influence of composition and preparation on crystalline phases and morphology in poly(vinylidene fluoride-trifluoroethylene-chlorofluoroethylene) relaxor-ferroelectric terpolymer. In *2018 IEEE 2nd International Conference on Dielectrics (ICD)*, pages 1–4, 2018. doi:10.1109/ICD.2018.8468492.

[55] G. S. Buckley, C. M. Roland, R. Casalini, A. Petchsuk, and T. C. Chung. Electrostrictive properties of poly(vinylidenefluoride- trifluoroethylene-chlorotrifluoroethylene). *Chem. Mater.*, 14(6):2590–2593, 2002. doi:10.1021/cm0116471.

[56] T. C. Chung, A. Petchsuk, and G. W. Taylor. Ferroelectric polymers with large electrostriction; based on semicrystalline VDF/TrFE/CTFE terpolymers. *Ferroelectr. Lett.*, 28(5-6):135–143, 2001. doi:10.1080/07315170108202957.

[57] S. K Nayak, S. N Yadav, and S. Mohanty. *Fundamentals of Plastics Testing*. Springer, 2010. isbn:978-81-8486-566-8.

[58] P. R. Griffiths, J. A. De Haseth, and J. D. Winefordner. *Fourier Transform Infrared Spectrometry*. Chemical Analysis: A Series of Monographs on Analytical Chemistry and Its Applications. Wiley, 2007. isbn:978-0-47-010629-7.

[59] Fourier transform infrared spectrometer (FTIR). http://osmania.ac.in/cfrd/Equip-FTIR.html. Accessed: 2017-11-21.

[60] Bruker application note, ATR-a versatile tool for FT-IR spectroscopy. https://www.bruker.com/fileadmin/user_upload/8-PDF-Docs/OpticalSpectrospcopy/FT-IR/ALPHA/AN/AN79_ATR-Basics_EN.pdf. Accessed: 2017-11-21.

[61] Bragg's law. http://hyperphysics.phy-astr.gsu.edu/hbase/quantum/bragg.html. Accessed: 2021-11-30.

[62] B. B. He, U. Preckwinkel, and K. L. Smith. Comparison between conventional and two-dimensional XRD. *Adv. X-Ray Anal.*, 46:37–42, 2003. http://www.icdd.com/resources/axa/VOL46/V46_05.pdf.

[63] Investigation of polymers with differential scanning calorimetry, July 2017. DSC Lab manual. https://polymerscience.physik.hu-berlin.de/docs/manuals/DSC.pdf.

[64] J. L. Lutkenhaus, K. McEnnis, A. Serghei, and T. P. Russell. Confinement Effects on Crystallization and Curie Transitions of Poly(vinylidene fluoride-co-trifluoroethylene). *Macromolecules*, 43(8):3844–3850, 2010. doi:10.1021/ma100166a.

[65] M. Neidhöfer, F. Beaume, L. Ibos, A. Bernès, and C. Lacabanne. Structural evolution of PVDF during storage or annealing. *Polymer*, 45(5):1679–1688, 2004. doi:10.1016/j.polymer.2003.12.066.

[66] R. J. Meredith. *Engineers' Handbook of Industrial Microwave Heating*. Number 25 in Energy Engineering. Institution of Engineering and Technology, London, 1998. isbn:0-85296-916-3.

[67] P. Frübing. Dielectric spectroscopy, June, 2011. Advanced lab experiments. http://canopus.physik.uni-potsdam.de/teaching/PolymSciMaPro/DielSpec.pdf.

[68] P. Mehrotra, B. Chatterjee, and S. Sen. EM-wave biosensors: A review of RF, Microwave, mm-Wave and Optical Sensing. *Sensors*, 19(5), 2019. doi:10.3390/s19051013.

[69] L.D. Landau and E.M. Lifshitz. *Statistical Physics: Volume V*, volume 5. Elsevier Science, 1978. isbn:978-0-0805-7046-4.

[70] F. Kremer and A. Schönhals. *Broadband Dielectric Spectroscopy*. Springer Berlin Heidelberg, 2002. isbn:978-3-642-56120-7.

[71] C. J. F. Böttcher and P. Bordewijk. *Theory of electric polarization*, volume 2. Elsevier Science Limited, 1978. isbn:978-0-4444-1579-0.

[72] P. J. W. Debye. *Polar molecules*. New York: Chemical Catalogue Co., 1927.

[73] A.A. Lukichev. Relaxation function for the non-Debye relaxation spectra description. *Chem. Phys.*, 428:29–33, 2014. doi:10.1016/j.chemphys.2013.10.021.

[74] M. Wübbenhorst and J. van Turnhout. Analysis of complex dielectric spectra. I. One-dimensional derivative techniques and three-dimensional modelling. *J. Non-Cryst. Solids*, 305(1):40–49, 2002. doi:10.1016/S0022-3093(02)01086-4.

[75] A. Brather. Numerisch einfache Bezichungen zwischen Verlust- und Speicherkomponente des dynamischen dielektrischen Faktors. *Colloid Polym. Sci.*, 257(5):467–477, 1979. doi:10.1007/BF01626224.

[76] P. A. M. Steeman and J. van Turnhout. A numerical Kramers-Kronig transform for the calculation of dielectric relaxation losses free from Ohmic conduction losses. *Colloid Polym. Sci.*, 275(2):106–115, 1997. doi:10.1007/s003960050059.

[77] J. van Turnhout. Extended abstracts europhys. conf. on macromolecular physics. In *EPS Geneva*, pages 24–30, Hamburg, Germany, 1983.

[78] J. van Turnhout and M. Wübbenhorst. Analysis of complex dielectric spectra. II: Evaluation of the activation energy landscape by differential sampling. *J. Non-Cryst. Solids*, 305(1):50–58, 2002. doi:10.1016/S0022-3093(02)01120-1.

[79] P. A. M. Steeman and J. van Turnhout. Fine Structure in the Parameters of Dielectric and Viscoelastic Relaxations. *Macromolecules*, 27(19):5421–5427, 1994. doi:10.1021/ma00097a023.

[80] M. Wübbenhorst, E. M. Van Koten, J. C. Jansen, W. Mijs, and J. van Turnhout. Dielectric relaxation spectroscopy of amorphous and liquid-crystalline side-chain polycarbonates. *Macromol. Rapid Commun.*, 18(2):139–147, 1997. doi:10.1002/marc.1997.030180211.

[81] T. Raman Venkatesan and R. Gerhard. Origin of the mid-temperature transition in vinylidenefluoride-based ferro-, pyro- and piezoelectric homo-, co- and ter-polymers. *Mater. Res. Express*, 7(6):065301, 2020. doi:10.1088/2053-1591/ab842c.

[82] R. Richert and M. Yang. Solvation dynamics of molecular glass-forming liquids in confinement. *J. Condens. Matter Phys.*, 15(11):S1041, 2003. doi:10.1088/0953-8984/15/11/326.

[83] T. Raman Venkatesan, D. Smykalla, B. Ploss, M. Wübbenhorst, and R. Gerhard. Non-linear dielectric spectroscopy for detecting and evaluating structure-property relations in a P(VDF-TrFE-CFE) relaxor-ferroelectric terpolymer. *Appl. Phys. A*, 127(10):756, 2021. doi:10.1007/s00339-021-04876-0.

[84] M. E Lines and A. M. Glass. *Principles and applications of ferroelectrics and related materials*. Oxford university press, 2001. doi:10.1093/acprof:oso/9780198507789.001.0001.

[85] B. Heiler and B. Ploss. Dielectric nonlinearities of P(VDF-TrFE). In *Proceedings of 8th International Symposium on Electrets (ISE 8)*, pages 662–667, Paris, France, 1994. doi:10.1109/ISE.1994.514848.

[86] D. Nordheim, S. Hahne, and B. Ploss. Nonlinear dielectric properties and polarization in thin ferroelectric P(VDF-TrFE) copolymer films. *IEEE Trans. Dielectr. Electr. Insul.*, 19(4):1175–1180, 2012. doi:10.1109/TDEI.2012.6259986.

[87] B. Ploss and B. Ploss. Influence of poling and annealing on the nonlinear dielectric permittivity of P(VDF-TrFE) copolymers. *IEEE Trans. Dielectr. Electr. Insul.*, 5(1):91–95, 1998. doi:10.1109/94.660777.

[88] L. E. Cross. Relaxorferroelectrics: An overview. *Ferroelectrics*, 151(1):305–320, 1994. doi:10.1080/00150199408244755.

[89] S. Ikeda, H. Kominami, K. Koyama, and Y. Wada. Nonlinear dielectric constant and ferroelectric-to-paraelectric phase transition in copolymers of vinylidene fluoride and trifluoroethylene. *J. Appl. Phys.*, 62:3339–3342, 1987. doi:10.1063/1.339294.

[90] T. Furukawa. Recent advances in ferroelectric polymers. *Ferroelectrics*, 104(1):229–240, 1990. doi:10.1080/00150199008223826.

[91] S. Ikeda, H. Suzuki, K. Koyama, and Y. Wada. Second-Order Dielectric Constant of a Copolymer of Vinylidene Fluoride and Trifluoroethylene (52:48 Mole Ratio). *Polym. J.*, 19(6):681–686, 1987. doi:10.1295/polymj.19.681.

[92] D. Nordheim. *Dielectric non-linearities of P(VDF-TrFE) single and multilayers for memory applications*. doctoral thesis, Faculty of Science, Universität Potsdam, 2018. http://nbn-resolving.de/urn:nbn:de:kobv:517-opus4-421778.

[93] M. Wübbenhorst, X. Zhang, and T. Putzeys. Polymer Electrets and Ferroelectrets as EAPs: Characterization. In F. Carpi, editor, *Electromechanically Active Polymers: A Concise Reference*, pages 591–623. Springer International Publishing, Cham, 2016. doi:10.1007/978-3-319-31530-0_26.

[94] H. Frei and G. Grutzinger. Uber das freiwerden elektrischer energie beim aufschmelzen des elektreten. *Zeitschrift für Physik*, 37:720–724, 1936.

[95] G. Groetzinger and H. Kretsch. Über die permanente polarisation des elektreten. *Zeitschrift für Physik*, 103(5):337–349, 1936. doi:10.1007/BF01340195.

[96] J. van Turnhout. *Thermally stimulated discharge of polymer electrets: a study on nonisothermal dielectric relaxation phenomena*. Elsevier Scientific Pub. Co., 1975. isbn:978-0444412904.

[97] G. Collins and B. Long. A thermally stimulated current/relaxation map analysis of the relaxation processes in aromatic polyester, liquid crystal polymer film. *J. Appl. Polym. Sci.*, 53(5):587–608, 1994. doi:10.1002/app.1994.070530511.

[98] S.H. Carr. Chapter 5 - thermally stimulated discharge current analysis of polymers. In D. A. Seanor, editor, *Electrical Properties of Polymers*, pages 215–239. Academic Press, 1982. doi:10.1016/B978-0-12-633680-1.50010-9.

[99] W. Eisenmenger and M. Haardt. Observation of charge compensated polarization zones in polyvinylindenfluoride (PVDF) films by piezoelectric acoustic step-wave response. *Solid State Commun.*, 41(12):917–920, 1982. doi:10.1016/0038-1098(82)91235-2.

[100] B. Dickens, E. Balizer, A. S. DeReggi, and S. C. Roth. Hysteresis measurements of remanent polarization and coercive field in polymers. *J. Appl. Phys.*, 72(9):4258, 1992. doi:10.1063/1.352213.

[101] M. Wegener. Polarization-electric field hysteresis of ferroelectric PVDF films: Comparison of different measurement regimes. *Rev. Sci. Instrum.*, 79(10):106103, 2008. doi:10.1063/1.2972169.

[102] C. B. Sawyer and C. H. Tower. Rochelle Salt as a Dielectric. *Phys. Rev.*, 35(3):269–273, 1930. doi:10.1103/PhysRev.35.269.

[103] G. Zhu, Z. Zeng, L. Zhang, and X. Yan. Polarization fatigue in ferroelectric vinylidene fluoride and trifluoroethylene copolymer films. *Appl. Phys. Lett.*, 89(10):102905, 2006. doi:10.1063/1.2340080.

[104] Ferroelectrics investigation. http://www.gdp.pwr.edu.pl/pliki/physics_%20of_dielectrics/electric_permitivity/Ferroelectrics_LFCS.pdf. Accessed: 2021-12-07.

[105] L Reimer. Scanning electron microscopy: Physics of image formation and microanalysis, second edition. *Measurement Science and Technology*, 11(12):1826–1826, 2000.

[106] Microscope configuration. https://www.olympus-lifescience.com/en/microscope-resource/primer/techniques/polarized/configuration/. Accessed: 2021-12-09.

[107] M. Pashkevich. *Ultrafast light-induced magnetization dynamics in Co/garnet heterostructures*. doctoral thesis, University of Białystok, 2014.

[108] T. Raman Venkatesan. Influence of preparation conditions on the dielectric and electromechanical properties of poly(vinylidene fluoride-trifluoroethylene-chlorofluoroethylene) relaxor-ferroelectric terpolymers. *Applied Condensed Matter Physics, Institute of Physics and Astronomy, University of Potsdam*, pages 22–23, July, 2017. Master Internship report.

[109] T. Furukawa, M. Date, and E. Fukada. Hysteresis phenomena in polyvinylidene fluoride under high electric field. *J. Appl. Phys.*, 51(2):1135–1141, 1980. doi:10.1063/1.327723.

[110] G. T. Davis, M. G. Broadhurst, A. J. Lovinger, and T. Furukawa. Hysteresis in copolymers of vinylidene fluoride and trifluoroethylene. *Ferroelectrics*, 57(1):73–84, 1984. doi:10.1080/00150198408012753.

[111] Q. D. Nguyen, T. Raman Venkatesan, W. Wirges, and R. Gerhard. Non-uniform polarization profiles in P(VDF-TrFE) copolymer films after cyclical poling. In *2019 IEEE International Symposium on Applications of Ferroelectrics (ISAF)*, pages 1–4, Lausanne, Switzerland, 2019. doi:10.1109/ISAF43169.2019.9034937.

[112] K. Ohwada and Y. Tomita. Experiment and theory of $Pb(In_{1/2}Nb_{1/2})O_3$: Antiferroelectric, ferroelectric, or relaxor state depending on perovskite b-site randomness. *J. Phys. Soc. Japan*, 79(1):011012, 2010. doi:10.1143/JPSJ.79.011012.

[113] A. Chauhan, S. Patel, R. Vaish, and C. R. Bowen. Anti-ferroelectric ceramics for high energy density capacitors. *Materials*, 8(12):8009–8031, 2015. doi:10.3390/ma8125439.

[114] Y. Takahashi, H. Kodama, M. Nakamura, T. Furukawa, and M. Date. Antiferroelectric-Like Behavior of Vinylidene Fluoride/Trifluoroethylene Copolymers with Low Vinylidene Fluoride Content. *Polym J*, 31(3):263–267, 1999. doi:10.1295/polymj.31.263.

[115] L. Yang, X. Li, E. Allahyarov, P. L. Taylor, Q.M. Zhang, and L. Zhu. Novel polymer ferroelectric behavior via crystal isomorphism and the nanoconfinement effect. *Polymer*, 54(7):1709–1728, 2013. doi:10.1016/j.polymer.2013.01.035.

[116] M. R. Gadinski, Q. Li, G. Zhang, X. Zhang, and Q. Wang. Understanding of relaxor ferroelectric behavior of poly(vinylidene fluoride–trifluoroethylene–chlorotrifluoroethylene) terpolymers. *Macromolecules*, 48(8):2731–2739, 2015. doi:10.1021/acs.macromol.5b00185.

[117] N. Tsutsumi, K. Okumachi, K. Kinashi, and W. Sakai. Re-evaluation of the origin of relaxor ferroelectricity in vinylidene fluoride terpolymers: An approach using switching current measurements. *Sci. Rep.*, 7(1):15871, 2017. doi:10.1038/s41598-017-16017-w.

[118] L. Yang, B. A. Tyburski, F. Domingues Dos Santos, M. K. Endoh, T. Koga, D. Huang, Y. Wang, and L. Zhu. Relaxor ferroelectric behavior from strong physical pinning in a poly(vinylidene fluoride- *co* -trifluoroethylene- *co* -chlorotrifluoroethylene) random terpolymer. *Macromolecules*, 47(22):8119–8125, 2014. doi:10.1021/ma501852x.

[119] T. Raman Venkatesan, M. Wübbenhorst, B. Ploss, X. Qiu, T. Nakajima, T. Furukawa, and R. Gerhard. The Mystery Behind the Mid-Temperature Transition(s) in Vinylidenefluoride-based Homo-, Co- and Terpolymers – Has the Puzzle Been Solved? *IEEE Trans. Dielectr. Electr. Insul.*, 27(5):1446–1464, 2020. doi:10.1109/TDEI.2020.008865.

[120] V. Sencadas, S. Lanceros-Méndez, R. Sabater i Serra, A. Andrio Balado, and J. L. Gómez Ribelles. Relaxation dynamics of poly(vinylidene fluoride) studied by dynamical mechanical measurements and dielectric spectroscopy. *Eur. Phys. J. E*, 35(5):41, 2012. doi:10.1140/epje/i2012-12041-x.

[121] I.O. Pariy, A.A. Ivanova, V.V. Shvartsman, D.C. Lupascu, G.B. Sukhorukov, M.A. Surmeneva, and R.A. Surmenev. Poling and annealing of piezoelectric Poly(Vinylidene fluoride) micropillar arrays. *Mater. Chem. Phys.*, 239:122035, 2020. doi:10.1016/j.matchemphys.2019.122035.

[122] W. Heywang, K. Lubitz, and W. Wersing, editors. *Piezoelectricity: evolution and future of a technology*. Number 114 in Springer series in materials science. Springer, Berlin, 2008. ISBN: 978-3-540-68680-4 978-3-540-68683-5.

[123] A. G. Kolbeck. Aging of piezoelectricity in poly(vinylidene fluoride). *J. Polym. Sci. Polym. Phys. Ed.*, 20(11):1987–2001, 1982. doi:10.1002/pol.1982.180201102.

[124] B. Elling, R. Danz, and P. Weigel. Reversible pyroelectricity in the melting and crystallization region of polyvinylidene fluoride. *Ferroelectrics*, 56(1):179–186, 1984. doi:10.1080/00150198408221368.

[125] D. DeRossi, A. S. DeReggi, M. G. Broadhurst, S. C Roth, and G. T. Davis. Method of evaluating the thermal stability of the pyroelectric properties of polyvinylidene fluoride: Effects of poling temperature and field. *J. Appl. Phys.*, 53:7, 1982. doi:10.1063/1.330078.

[126] G. E. Johnson, L. L. Blyler, G. R. Crane, and C. Gieniewski. Thermal piezoelectric stability of poled uniaxially-and biaxially-oriented poly(vinylidene fluoride. *Ferroelectrics*, 32(1):43–47, 1981. doi:10.1080/00150198108238672.

[127] T. T. Wang. Aging behavior of piezoelectric poly(vinylidene fluoride) films irradiated by γ rays. *J. Polym. Sci. B Polym. Lett. Ed.*, 19(6):289–293, 1981. doi:10.1002/pol.1981.130190602.

[128] L. L. Blyler, G. E. Johnson, and N. M. Hylton. Characterization of biaxially-oriented polyvinylidene fluoride-film for transducer applications. *Ferroelectrics*, 28(1):303–306, 1980. doi:10.1080/00150198008227094.

[129] G. Teyssèdre and C. Lacabanne. Study of the thermal and dielectric behavior of P(VDF-TrFE) copolymers in relation with their electroactive properties. *Ferroelectrics*, 171(1):125–144, 1995. doi:10.1080/00150199508018427.

[130] B.A. Tuttle and D.A. Payne. The effects of microstructure on the electrocaloric properties of Pb (Zr, Sn, Ti) O_3 ceramics. *Ferroelectrics*, 37(1):603–606, 1981. doi:10.1080/00150198108223496.

[131] Y.V. Sinyavsky and V.M. Brodyansky. Experimental testing of electrocaloric cooling with transparent ferroelectric ceramic as a working body. *Ferroelectrics*, 131(1):321–325, 1992. doi:10.1080/00150199208223433.

[132] A. S. Mischenko, Q. Zhang, J. F. Scott, R. W. Whatmore, and N. D. Mathur. Giant electrocaloric effect in thin-film $PbZr_{0.95}Ti_{0.05}O_3$. *Science*, 311(5765):1270–1271, 2006. doi:10.1126/science.1123811.

[133] B. Neese, B. Chu, S-G. Lu, Y. Wang, E. Furman, and Q. M. Zhang. Large electrocaloric effect in ferroelectric polymers near room temperature. *Science*, 321(5890):821–823, 2008. doi:10.1126/science.1159655.

[134] B. Neese, S. G. Lu, B. Chu, and Q. M. Zhang. Electrocaloric effect of the relaxor ferroelectric poly(vinylidene fluoride-trifluoroethylene-chlorofluoroethylene) terpolymer. *Appl. Phys. Lett.*, 94(4):042910, 2009. doi:10.1063/1.3077189.

[135] V. V. Kochervinskii, N. V. Kozlova, A. Y. Khnykov, M. A. Shcherbina, S. N. Sulyanov, and K. A. Dembo. Features of structure formation and electrophysical properties of poly(vinylidene fluoride) crystalline ferroelectric polymers. *J. Appl. Polym. Sci.*, 116(2):695–707, 2010. doi:10.1002/app.31044.

[136] H-M. Bao, J-F. Song, J. Zhang, Q-D. Shen, C-Z. Yang, and Q. M. Zhang. Phase Transitions and Ferroelectric Relaxor Behavior in P(VDF-TrFE-CFE) Terpolymers. *Macromolecules*, 40(7):2371–2379, 2007. doi:10.1021/ma0628001.

[137] A. J. Lovinger. Ferroelectric polymers. *Science*, 220(4602):1115–1121, 1983. doi:10.1126/science.220.4602.1115.

[138] F. Bargain, P. Panine, F. Domingues Dos Santos, and S. Tencé-Girault. From solvent-cast to annealed and poled poly(VDF- co -TrFE) films: New insights on the defective ferroelectric phase. *Polymer*, 105:144–156, 2016. doi:10.1016/j.polymer.2016.10.010.

[139] F. Bargain, D. Thuau, P. Panine, G. Hadziioannou, F. Domingues Dos Santos, and S. Tencé-Girault. Thermal behavior of poly(VDF-ter-TrFE-ter-CTFE) copolymers: Influence of CTFE termonomer on the crystal-crystal transitions. *Polymer*, 161:64–77, 2019. doi:10.1016/j.polymer.2018.11.064.

[140] T. Raman Venkatesan, A. A. Gulyakova, and R. Gerhard. Influence of film stretching on crystalline phases and dielectric properties of a 70/30 mol% poly(vinylidenefluoride-tetrafluoroethylene) copolymer. *J. Adv. Dielect.*, 10(05):2050023, 2020. doi:10.1142/S2010135X2050023X.

[141] P. Scherrer. Bestimmung der inneren Struktur und der Größe von Kolloidteilchen mittels Röntgenstrahlen. In *Kolloidchemie Ein Lehrbuch*, pages 387–409. Springer Berlin Heidelberg, Berlin, Heidelberg, 1912. doi:10.1007/978-3-662-33915-2_7.

[142] H. P. Klug and L.E. Alexander. *X-Ray Diffraction Procedures: For Polycrystalline and Amorphous Materials, 2nd Edition*. Wiley Publishing, 1974.

[143] S. Kavesh and J. M. Schultz. Meaning and measurement of crystallinity in polymers: A Review. *Polym. Eng. Sci.*, 9(5):331–338, 1969. doi:10.1002/pen.760090504.

[144] N. Doebelin and R. Kleeberg. *Profex*: a graphical user interface for the Rietveld refinement program *BGMN*. *J. Appl. Crystallogr.*, 48(5):1573–1580, 2015.

[145] V. B. F. Mathot and M. F. J. Pijpers. Heat capacity, enthalpy and crystallinity of polymers from DSC measurements and determination of the DSC peak base line. *Thermochim. Acta*, 151:241–259, 1989. doi:10.1016/0040-6031(89)85354-7.

[146] B. Wunderlich. Appendix - ATHAS Table of Thermal Properties of Linear Macromolecules. In B. Wunderlich, editor, *Thermal Analysis*, pages 417–431. Academic Press, 1990. doi:10.1016/B978-0-12-765605-2.50012-1.

[147] J. Clements, G.R. Davies, and I.M. Ward. A broad-line nuclear magnetic resonance study of a vinylidene fluoride/trifluoroethylene copolymer. *Polymer*, 33(8):1623–1629, 1992. doi:10.1016/0032-3861(92)91058-A.

[148] R. Gregorio Jr. and M. Cestari. Effect of crystallization temperature on the crystalline phase content and morphology of poly(vinylidene fluoride). *J. Polym. Sci. B Polym. Phys.*, 32(5):859–870, 1994. doi:10.1002/polb.1994.090320509.

[149] S. Harstad, N. D'Souza, N. Soin, A. A. El-Gendy, S. Gupta, V. K. Pecharsky, T. Shah, E. Siores, and R. L. Hadimani. Enhancement of β-phase in PVDF films embedded with ferromagnetic Gd_5Si_4 nanoparticles for piezoelectric energy harvesting. *AIP Adv.*, 7(5):056411, 2017. (and references therein) doi:10.1063/1.4973596.

[150] S. Zhang, B. Chu, B. Neese, K. Ren, X. Zhou, and Q. M. Zhang. Direct spectroscopic evidence of field-induced solid-state chain conformation transformation in a ferroelectric relaxor polymer. *J. Appl. Phys.*, 99(4):044107, 2006. doi:10.1063/1.2169659.

[151] R. J. Klein, J. Runt, and Q. M. Zhang. Influence of Crystallization Conditions on the Microstructure and Electromechanical Properties of Poly(vinylidene fluoride-trifluoroethylene-chlorofluoroethylene) Terpolymers. *Macromolecules*, 36(19):7220–7226, 2003. doi:10.1021/ma034745b.

[152] K. J. Kim, N. M. Reynolds, and S. L. Hsu. Spectroscopic analysis of the crystalline and amorphous phases in a vinylidene fluoride/trifluoroethylene copolymer. *Macromolecules*, 22(12):4395–4401, 1989. doi:10.1021/ma00202a001.

[153] F. Wang, A. Lack, Z. Xie, P. Frübing, W. Wirges, and R. Gerhard. Ionic liquids induce crystalline β phase and ferroelectric polarization in sub-micrometer films of poly(vinylidene fluoride) (pvdf).

In *2011 Annual Report Conference on Electrical Insulation and Dielectric Phenomena*, pages 710–713, 2011. (and references therein) doi:10.1109/CEIDP.2011.6232755.

[154] A. Salimi and A. A. Yousefi. Conformational changes and phase transformation mechanisms in pvdf solution-cast films. *J. Polym. Sci. B Polym. Phys.*, 42(18):3487–3495, 2004. doi:10.1002/polb.20223.

[155] S. L. Hsu, F.J. Lu, D. A. Waldman, and M. Muthukumar. Analysis of the crystalline phase transformation of poly (vinylidene fluoride). *Macromolecules*, 18(12):2583–2587, 1985. doi:10.1021/ma00154a038.

[156] N. Betz, A. Le Moël, E. Balanzat, J. M. Ramillon, J. Lamotte, J. P. Gallas, and G. Jaskierowicz. A FTIR study of PVDF irradiated by means of swift heavy ions. *J. Polym. Sci. B Polym. Phys.*, 32(8):1493–1502, 1994. doi:10.1002/polb.1994.090320821.

[157] S. Osaki and Y. Ishida. Effects of annealing and isothermal crystallization upon crystalline forms of poly (vinylidene fluoride). *J. Polym. Sci.: Poly. Phys.*, 13(6):1071–1083, 1975. doi:10.1002/pol.1975.180130602.

[158] K. Tashiro, M. Kobayashi, and H. Tadokoro. Vibrational spectra and disorder-order transition of poly (vinylidene fluoride) form III. *Macromolecules*, 14(6):1757–1764, 1981. doi:10.1021/ma50007a028.

[159] M. Benz and W. B. Euler. Determination of the crystalline phases of poly(vinylidene fluoride) under different preparation conditions using differential scanning calorimetry and infrared spectroscopy. *J. Appl. Polym. Sci.*, 89(4):1093–1100, 2003. doi:10.1002/app.12267.

[160] H. Xu, G. Shanthi, V. Bharti, Q. M. Zhang, and T. Ramotowski. Structural, Conformational, and Polarization Changes of Poly(vinylidene fluoride-trifluoroethylene) Copolymer Induced by High-Energy Electron Irradiation. *Macromolecules*, 33(11):4125–4131, 2000. doi:10.1021/ma9919561.

[161] H. Xu, Z.-Y. Cheng, D. Olson, T. Mai, Q. M. Zhang, and G. Kavarnos. Ferroelectric and electromechanical properties of poly(vinylidene-fluoride–trifluoroethylene–chlorotrifluoroethylene) terpolymer. *Appl. Phys. Lett.*, 78(16):2360–2362, 2001. doi:10.1063/1.1358847.

[162] Y. Nabata. Molecular Motion in Form II Poly(vinylidene Fluoride). *Jpn. J. Appl. Phys*, 29(Part 1, No. 12):2782–2788, 1990. doi:10.1143/JJAP.29.2782.

[163] H. Sasabe, S. Saito, M. Asahina, and H. Kakutani. Dielectric relaxations in poly(vinylidene fluoride). *J. Polym. Sci. A-2 Polym. Phys.*, 7(8):1405–1414, 1969. doi:10.1002/pol.1969.160070810.

[164] K. Nakagawa and Y. Ishida. Dielectric relaxations and molecular motions in poly(vinylidene fluoride) with crystal form II. *J. Polym. Sci. A-2 Polym. Phys*, 11(8):1503–1533, 1973. doi:10.1143/JJAP.29.2782.

[165] A. Peterlin and J. (Holbrook) Elwell. Dielectric constant of rolled polyvinylidene fluoride. *J. Mater. Sci.*, 2(1):1–6, 1967. doi:10.1007/BF00550045.

[166] E. Tuncer, M. Wegener, and R. Gerhard(-Multhaupt). Distribution of relaxation times in α-phase polyvinylidene fluoride. *J. Non-Cryst. Solids*, 351(33-36):2917–2921, 2005. doi:10.1016/j.jnoncrysol.2005.03.055.

[167] A. Bello, E. Laredo, and M. Grimau. Distribution of relaxation times from dielectric spectroscopy using monte carlo simulated annealing: Application to $\alpha-$PVDF. *Phys. Rev. B*, 60:12764–12774, 1999. doi:10.1103/PhysRevB.60.12764.

[168] R. Ranko and Y. Min. Solvation dynamics of molecular glass-forming liquids in confinement. *J. Phys. Condens. Matter*, 15(11):S1041–S1050, 2003. doi:10.1088/0953-8984/15/11/326.

[169] A Callens, R De Batist, and L Eersels. Relaxational behaviour of polyvinylidene fluoride. *Il Nuovo Cimento B (1971-1996)*, 33(1):434–446, 1976. doi:10.1007/BF02722512.

[170] G. Teyssèdre and C. Lacabanne. Compositional variation of the glass transition and the associated dielectric relaxation in copolymers of vinylidene fluoride and trifluoroethylene. *Polymer*, 36(19):3641–3648, 1995. doi:10.1016/0032-3861(95)93765-E.

[171] H. Kakutani. Dielectric absorption in oriented poly(vinylidene fluoride). *J. Polym. Sci. A-2 Polym. Phys.*, 8(7):1177–1186, 1970. doi:10.1002/pol.1970.160080712.

[172] D. K. Das-Gupta and K. Doughty. Dielectric relaxation spectra of poled polyvinylidene fluoride. *Ferroelectrics*, 28(1):307–310, 1980. doi:10.1080/00150198008227095.

[173] Y. Miyamoto, H. Miyaji, and K. Asai. Anisotropy of dielectric relaxation in crystal form II of poly(vinylidene fluoride). *J. Polym. Sci.: Poly. Phys.*, 18(3):597–606, 1980. doi:10.1002/pol.1980.180180318.

[174] M. Abkowitz and G. Pfister. Combined ac and dc thermocurrent measurements to study molecular relaxation and electrical phenomena in polyvinylidene fluoride films. *J. Appl. Phys.*, 46(6):2559–2573, 1975. doi:10.1063/1.321933.

[175] J. Menegotto, L. Ibos, A. Bernes, P. Demont, and C. Lacabanne. Dielectric relaxation spectra in ferroelectric P(VDF-TrFE) copolymers. *Ferroelectrics*, 228(1):1–22, 1999. doi:10.1080/00150199908226122.

[176] L. E. Cross. Relaxorferroelectrics: An overview. *Ferroelectrics*, 151(1):305–320, 1994. doi:10.1080/00150199408244755.

[177] T. Raman Venkatesan, A. A. Gulyakova, P. Frübing, and R. Gerhard. Electrical polarization phenomena, dielectric relaxations and structural transitions in a relaxor-ferroelectric terpolymer investigated with electrical probing techniques. *Mater. Res. Express*, 6(12):125301, 2019. doi:10.1088/2053-1591/ab5352.

[178] T. Takamatsu and E. Fukada. Thermal Change of Depolarization Current in Polymer Electrets. *Polym. J.*, 1(1):101–106, 1970. doi:10.1295/polymj.1.101.

[179] S. Eliasson. On TSD in PVDF in the temperature range $-60\,^{\circ}$C to $165\,^{\circ}$C I. *J. Phys. D: Appl. Phys.*, 18(2):275–282, 1985. doi:10.1088/0022-3727/18/2/015.

[180] T. Raman Venkatesan, D. Smykalla, B. Ploss, M. Wübbenhorst, and R. Gerhard. Tuning the relaxor-ferroelectric properties of poly(vinylidene fluoride-trifluoroethylene-chlorofluoroethylene) terpolymer by thermally induced micro- and nanostructures. under review, 2022.

[181] J-F. Capsal, E. Dantras, and C. Lacabanne. Molecular mobility interpretation of the dielectric relaxor behavior in fluorinated copolymers and terpolymers. *J. Non-Cryst. Solids*, 363:20–25, 2013. doi:10.1016/j.jnoncrysol.2012.12.008.

[182] G. Teyssedre, A. Bernes, and C. Lacabanne. Influence of the crystalline phase on the molecular mobility of PVDF. *J. Polym. Sci. B Polym. Phys.*, 31(13):2027–2034, 1993. doi:10.1002/polb.1993.090311316.

[183] D. Rollik, S. Bauer, and R. Gerhard(-Multhaupt). Separate contributions to the pyroelectricity in poly(vinylidene fluoride) from the amorphous and crystalline phases, as well as from their interface. *J. Appl. Phys.*, 85(6):3282–3288, 1999. doi:10.1021/ma00243a021.

[184] R. M. Faria, A. Jorge, and O. N. Oliveira. A novel space-charge effect in thermally stimulated current measurements on β-PVDF. *J. Phys. D: Appl. Phys.*, 23(3):334–337, 1990. doi:10.1088/0022-3727/23/3/011.

[185] Y. Oka and N. Koizumi. Effects of Impurity Ions on Electrical Properties of Poly(vinylidene fluoride). *Polym. J.*, 14(11):869–876, 1982. doi:10.1295/polymj.14.869.

[186] C. Leonard, J.L. Halary, L. Monnerie, and F. Micheron. DSC studies on the transitions in poly(vinylidenefluoride) and some related copolymers. *Polym. Bull.*, 11(2), 1984. doi:10.1007/BF00258030.

[187] G. Teyssedre, M. Grimau, A. Bernes, J. J. Martinez, and C. Lacabanne. α-Relaxation/retardation mode in semicrystalline polymers with flexible chains. *Polymer*, 35(20):4397–4403, 1994. doi:10.1016/0032-3861(94)90098-1.

[188] S. Wietzke, C. Jansen, M. Reuter, T. Jung, J. Hehl, D. Kraft, S. Chatterjee, A. Greiner, and M. Koch. Thermomorphological study of the terahertz lattice modes in polyvinylidene fluoride and high-density polyethylene. *Appl. Phys. Lett.*, 97(2):022901, 2010. doi10.1063/1.3462312.

[189] C. Lacabanne, D. Chatain, T. El Sayed, D. Broussoux, and F. Micheron. Transitions in poly(vinylidene fluoride) by thermally stimulated techniques. *Ferroelectrics*, 30(1):307–314, 1980. doi:10.1080/00150198008209528.

[190] A. Callens, L. Eersels, and R. De Batist. Low-temperature TSD measurements on γ-irradiated polyvinylidene fluoride. *J. Mater. Sci.*, 12(7):1361–1375, 1977. doi:10.1007/BF00540850.

[191] M. Abkowitz, W. M. Prest, D. J. Luca, and G. Pfister. Thermocurrent spectra of γ-phase-containing PVF2 films. *Appl. Phys. Lett.*, 34(1):19–22, 1979. doi:10.1063/1.90582.

[192] R. F. Boyer. Glassy transitions in semicrystalline polymers. *J. Polym. Sci.: Polymer Symposia*, 50(1):189–242, 1975. doi:10.1002/polc.5070500114.

[193] J. B. Enns and R. Simha. Transitions in semicrystalline polymers. I. poly(vinyl Fluoride) and poly(vinylidene fluoride). *J. of Macromol. Sci. B*, 13(1):11–24, 1977. doi:10.1080/00222347708208750.

[194] A. Torres, J. Jiménez, B. Vega, and J. A. De Saja. Thermally stimulated depolarization currents in PVDF-α a dipolar interaction approach to β and γ transitions. *J. Mater. Sci.*, 22(5):1623–1629, 1987. doi:10.1007/BF01132383.

[195] K. Loufakis and B. Wunderlich. Thermal analysis of the conformational disorder in semicrystalline poly(vinylidene fluoride) and poly(trifluoroethylene). *Macromolecules*, 20(10):2474–2478, 1987. doi:10.1021/ma00176a026.

[196] G. E. Roberts and E. F. T. White. Relaxation Processes in Amorphous Polymers. In R. N. Haward, editor, *The Physics of Glassy Polymers*, pages 153–222. Springer Netherlands, Dordrecht, 1973. doi:10.1007/978-94-010-2355-9_4.

[197] R. G. Kepler and R. A. Anderson. On the origin of pyroelectricity in polyvinylidene fluoride. *J. Appl. Phys.*, 49(9):4918–4921, 1978. doi:10.1063/1.325526.

[198] J. M. Schultz, J. S. Lin, R. W. Hendricks, R. R. Lagasse, and R. G. Kepler. Temperature-dependent small-angle x-ray scattering from poly(vinylidene fluoride). *J. Appl. Phys.*, 51(10):5508, 1980. doi:10.1063/1.327468.

[199] S. Kavesh and J. M. Schultz. Lamellar and interlamellar structure in melt-crystallized polyethylene. I. Degree of crystallinity, atomic positions, particle size, and lattice disorder of the first and second kinds. *J. Polym. Sci. A-2 Polym. Phys.*, 8(2):243–276, 1970. doi:10.1002/pol.1970.160080205.

[200] H. Marand, A. Alizadeh, R. Farmer, R. Desai, and V. Velikov. Influence of Structural and Topological Constraints on the Crystallization and Melting Behavior of Polymers. 2. Poly(arylene ether ether ketone). *Macromolecules*, 33(9):3392–3403, 2000. doi:10.1021/ma9913562.

[201] Y. Ishida and K. Yamafuji. Frequency dependence of dielectric crystalline dispersion in oxidized polyethylene. *Kolloid-Z. u. Z. Polymere*, 202(1):26–33, 1965. doi:10.1007/BF01497182.

[202] K. Yamafuji. Theory of dielectric crystalline dispersion in high polymers. *Kolloid-Z.u.Z.Polymere*, 195(2):111–122, 1964. doi:10.1007/BF01503658.

[203] V. J. McBrierty, D. C. Douglass, and T. A. Weber. Nuclear magnetic relaxation and molecular motion in poly(vinylidine fluoride). *J. Polym. Sci.: Poly. Phys.*, 14(7):1271–1286, 1976.

[204] A. Peterlin and J.D. Holbrook. Dielectric behavior of polyvinylidene fluoride. *Kolloid-Z. u. Z. Polymere*, 203(1):68–69, 1965. doi:doi.org/10.1007/BF01499933.

[205] S. Osaki, S. Uemura, and Y. Ishida. Effects of a static electric field upon dielectric properties of poly(vinylidene fluoride) and poly(vinyl fluoride). *J. Polym. Sci. A-2 Polym. Phys.*, 9(4):585–594, 1971. doi:10.1002/pol.1971.160090402.

[206] Y. Takahashi, Y. Matsubara, and H. Tadokoro. Mechanisms for crystal phase transformations by heat treatment and molecular motion in poly(vinylidene fluoride). *Macromolecules*, 15(2):334–338, 1982. doi:10.1021/ma00230a026.

[207] B. L. Farmer, A. J. Hopfinger, and J. B. Lando. Polymorphism of poly(vinylidene fluoride): potential energy calculations of the effects of head-to-head units on the chain conformation and packing of poly(vinylidene fluoride). *J. Appl. Phys.*, 43(11):4293–4303, 1972. doi:10.1063/1.1660919.

[208] Y. Takahashi and K. Miyaji. Long-range order parameters of form II of poly(vinylidene fluoride) and molecular motion in the α_c relaxation. *Macromolecules*, 16(11):1789–1792, 1983. doi:10.1021/ma00245a019.

[209] Y. Takahashi. Packing Disorder in Form II of Poly(vinylidene fluoride): Influence of Elongation and Annealing Temperature. *Polym. J.*, 15(10):733–742, 1983. doi:10.1295/polymj.15.733.

[210] T. Mizutani, T. Yamada, and M. Ieda. Thermally stimulated currents in polyvinylidene fluoride. I. Unstretched alpha -form PVDF. *J. Phys. D: Appl. Phys.*, 14(6):1139–1147, 1981. doi:10.1088/0022-3727/14/6/022.

[211] S. S. Bamji, K. J. Kao, and M. M. Perlman. Piezoelectricity and pyroelectricity of polyvinylidene fluoride corona-poled at elevated temperature. *J. Polym. Sci.: Poly. Phys.*, 18(9):1945–1954, 1980. doi:10.1002/pol.1980.180180907.

[212] S. S. Bamji and M. M. Perlman. Piezoelectricity of uniaxially stretched poly(vinylidene fluoride) corona poled at elevated temperature. *J. Polym. Sci.: Poly. Phys.*, 19(9):1365–1369, 1981. doi:10.1002/pol.1981.180190908.

[213] T. Yamada, T. Mizutani, and M. Ieda. Thermally stimulated currents in polyvinylidene fluoride. II. Effects of stretching. *J. Phys. D: Appl. Phys.*, 15(2):289–297, 1982. doi:10.1088/0022-3727/15/2/014.

[214] D. Doughty and D. K. Das-Gupta. On the origins of space charge TSDC peaks in polyvinylidene fluoride. *J. Phys. D: Appl. Phys.*, 19(2):L29–L32, 1986. (and references therein) doi:10.1088/0022-3727/19/2/004.

[215] G. Eberle and W. Eisenmenger. Thermal depolarization of PVDF: anomaly at 180 °C. *IEEE Trans. Electr. Insul.*, 27(4):768–772, 1992. doi:10.1109/14.155795.

[216] P. Huo and P. Cebe. Dielectric relaxation of poly(phenylene sulfide) containing a fraction of rigid amorphous phase. *J. Polym. Sci. B Polym. Phys.*, 30(3):239–250, 1992. doi:10.1002/polb.1992.090300303.

[217] R. G. Kepler and R. A. Anderson. Piezoelectricity in polymers. *Crit. Rev. Solid State Mater. Sci.*, 9(4):399–447, 1980. doi:10.1080/10408438008243576.

[218] E. Bihler, G. Neumann, G. Eberle, and W. Eisenmenger. Influence of charge injection on the formation of remanent polarization in P(VDF-TrFE) copolymers. In *1990 IEEE Annual Conference on Electrical Insulation and Dielectric Phenomena*, pages 140–145, Pocono Manor, PA, USA, 1990. doi:10.1109/CEIDP.1990.201333.

[219] M. Eguchi. XX. *On the permanent electret. London, Edinburgh Dublin Philos. Mag. J. Sci.*, 49(289):178–192, 1925. doi:10.1080/14786442508634594.

[220] K. Tashiro and M. Kobayashi. Structural phase transition in ferroelectric fluorine polymers: X-ray diffraction and infrared/Raman spectroscopic study. *Phase Transit.*, 18(3-4):213–246, 1989. doi:10.1080/01411598908206864.

[221] V.R. Gowariker, N.V. Viswanathan, and J. Sreedhar. *Polymer Science*. R. F. Boyer Library Collection. Wiley, 1986. isbn:978-0-85226-307-5.

[222] C. J. G. Plummer and H. H. Kausch. The effect of melting point distributions on DSC melting peaks. *Polym. Bull.*, 36(3):355–360, 1996. doi:10.1007/BF00319237.

[223] R. Mutter, W. Stille, and G. Strobl. Transition regions and surface melting in partially crystalline polyethylene: A raman spectroscopic study. *J. Polym. Sci. B Polym. Phys.*, 31(1):99–105, 1993. doi:10.1002/polb.1993.090310113.

[224] J.J. Martinez and C. Lacabanne. Thermally-stimulated creep spectroscopy in the study of physicochemical ageing of LDPE. *Thermochim. Acta*, 226:51–64, 1993. doi:10.1016/0040-6031(93)80206-P.

[225] B. G. Sumpter, D. W. Noid, and B. Wunderlich. Computer experiments on the internal dynamics of crystalline polyethylene: Mechanistic details of conformational disorder. *J. Chem. Phys.*, 93(9):6875–6889, 1990. doi:10.1063/1.458921.

[226] R. Popli, M. Glotin, L. Mandelkern, and R. S. Benson. Dynamic mechanical studies of α and β relaxations of polyethylenes. *J. Polym. Sci. Polym. Phys. Ed.*, 22(3):407–448, 1984. doi:10.1002/pol.1984.180220306.

[227] D. C. Bassett, editor. *Developments in Crystalline Polymers—1*. Polymer Science and Technology Series. Springer Netherlands, 1982. doi:10.1007/978-94-009-7343-5.

[228] A. Salimi and A. A. Yousefi. Conformational changes and phase transformation mechanisms in PVDF solution-cast films. *J. Polym. Sci. B Polym. Phys.*, 42(18):3487–3495, 2004. doi:10.1002/polb.20223.

[229] E. Benedetti, S. Catanorchi, A. D'Alessio, G. Moggi, P. Vergamini, M. Pracella, and F. Ciardelli. FTIR-Microspectroscopy and DSC Studies of Poly(vinylidene fluoride). *Polym. Int.*, 41(1):35–41, 1996. doi:10.1002/(SICI)1097-0126(199609)41:1<35::AID-PI579>3.0.CO;2-T.

[230] A. Callens, R. De Batist, and L. Eersels. Relaxational behaviour of polyvinylidene fluoride. *Il Nuovo Cimento B*, 33:443–446, 1976. doi:10.1007/BF02722512.

[231] S. Eliasson. On TSD in PVDF in the temperature range -60 to 165 °C. II. *J. Phys. D: Appl. Phys.*, 19(10):1965–1972, 1986. doi:10.1088/0022-3727/19/10/022.

[232] G. T. Davis, J. E. McKinney, M. G. Broadhurst, and S. C. Roth. Electric-field-induced phase changes in poly(vinylidene fluoride). *J. Appl. Phys.*, 49(10):4998–5002, 1978. doi:10.1063/1.324446.

[233] G. R. Davies and H. Singh. Evidence for a new crystal phase in conventionally poled samples of poly(vinylidene fluoride) in crystal form II. *Polymer*, 20(6):772–774, 1979. doi:10.1016/0032-3861(79)90253-2.

[234] N. C. Banik, P. L. Taylor, and A. J. Hopfinger. Field-induced phase transitions in phase-II poly(vinylidene fluoride). *J. Appl. Phys.*, 37(1):49–50, 1980. doi:10.1063/1.91843.

[235] H. Dvey-Aharon, P. L. Taylor, and A. J. Hopfinger. Dynamics of the field-induced transition to the polar α phase of poly(vinylidene fluoride). *J. Appl. Phys.*, 51(10):5184–5187, 1980. doi:10.1063/1.327422.

[236] K. Tashiro, R. Tanaka, K. Ushitora, and M. Kobayashi. Annealing effect on ferroelectric phase transitional behavior of vinylidene fluoride-trifluoroethylene copolymers: An interpretation based on the concept of domain and trans-gauche conformational disorder. *Ferroelectrics*, 171(1):145–162, 1995. doi:10.1080/00150199508018421.

[237] M. O'Kane. Solution-processing techniques: A comparison. https://www.ossila.com/pages/solution-processing-techniques-comparison#DoctorBlading. Accessed: 2021-09-28.

[238] E. B. Mano and L. A. Durao. Review of laboratory methods for the preparation of polymer films. *J. Chem. Educ.*, 50(3):228, 1973. doi:10.1021/ed050p228.

[239] J. A. Brydson. *Plastics Materials*. Butterworth-Heinemann, 1999. isbn:978-0-08-051408-6.

[240] N. Meng, R. Mao, W. Tu, X. Zhu, R. M. Wilson, E. Bilotti, and M. J. Reece. Processing and characterization of free standing highly oriented ferroelectric polymer films with remarkably low coercive field and high remnant polarization. *Polymer*, 100:69–76, 2016. doi:10.1016/j.polymer.2016.08.017.

[241] K. Nakagawa and Y. Ishida. Annealing effects in poly(vinylidene fluoride) as revealed by specific volume measurements, differential scanning calorimetry, and electron microscopy. *J. Polym. Sci. A-2 Polym. Phys.*, 11(11):2153–2171, 1973. doi:10.1002/pol.1973.180111107.

[242] M. Avrami. Kinetics of phase change. I general theory. *J. Chem. Phys.*, 7(12):1103–1112, 1939. doi:10.1063/1.1750380.

[243] M. Avrami. Kinetics of phase change. II transformation-time relations for random distribution of nuclei. *J. Chem. Phys.*, 8(2):212–224, 1940. doi:10.1063/1.1750631.

[244] M. Avrami. Granulation, phase change, and microstructure kinetics of phase change. III. *J. Chem. Phys.*, 9(2):177–184, 1941. doi:10.1063/1.1750872.

[245] V. Sencadas, C. M. Costa, J. L. Gómez Ribelles, and S. Lanceros-Mendez. Isothermal crystallization kinetics of poly(vinylidene fluoride) in the α-phase in the scope of the Avrami equation. *J. Mater. Sci.*, 45(5):1328–1335, 2010. doi:10.1007/s10853-009-4086-3.

[246] C. Mancarella and E. Martuscelli. Crystallization kinetics of poly(vinylidene fluoride). *Polymer*, 18(12):1240–1242, 1977. doi:10.1016/0032-3861(77)90286-5.

[247] M.P. Silva, V. Sencadas, G. Botelho, A.V. Machado, A.G. Rolo, J.G. Rocha, and S. Lanceros-Mendez. α- and γ-PVDF: Crystallization kinetics, microstructural variations and thermal behaviour. *Mater. Chem. Phys.*, 122(1):87–92, 2010. doi:10.1016/j.matchemphys.2010.02.067.

[248] J. Liu, Z. Qiu, and B-J. Jungnickel. Crystallization and morphology of poly(vinylidene fluoride)/poly(3-hydroxybutyrate) blends. III. Crystallization and phase diagram by differential scanning calorimetry. *J. Polym. Sci. B Polym. Phys.*, 43(3):287–295, 2005. doi:10.1002/polb.20274.

[249] H-J. Chiu. Spherulitic Morphology and Crystallization Kinetics of Poly(vinylidene fluoride)/Poly(vinyl acetate) Blends. *J. Polym. Res.*, 9(3):169–174, 2002. doi:10.1023/A:1021387524243.

[250] Z. Qiu, C. Yan, J. Lu, and W. Yang. Miscible Crystalline/Crystalline Polymer Blends of Poly(vinylidene fluoride) and Poly(butylene succinate-co-butylene adipate): Spherulitic Morphologies and Crystallization Kinetics. *Macromolecules*, 40(14):5047–5053, 2007. doi:10.1021/ma070255y.

[251] W. Fan and S. Zheng. Miscibility and crystallization behavior in blends of poly(methyl methacrylate) and poly(vinylidene fluoride): Effect of star-like topology of poly(methyl methacrylate) chain. *J. Polym. Sci. B Polym. Phys.*, 45(18):2580–2593, 2007. doi:10.1002/polb.21264.

[252] S. Nayak, H. T. Ng, and A. Pramanick. Enhanced dielectric permittivity and relaxor behavior in thermally annealed P(VDF-TrFE) copolymer films. *Appl. Phys. Lett.*, 117(23):232903, 2020.

[253] N. Koizumi, J. Hagino, and Y. Murata. Dielectric behavior of copolymers of vinylidene fluoride and tetrafluoroethylene. *Ferroelectrics*, 32:141–147, 1981. doi:10.1080/00150198108238685.

[254] N. Alves, P.R.O. Ruiz, A.E. Job, O.N. Oliveira, and J.A. Giacometti. Thermal treatment effects on phase transitions in P(VDF-TrFE). In *1999 IEEE 10th International Symposium on Electrets (ISE 10). Proceedings (Cat. No.99 CH36256)*, pages 347–350, Athens, Greece, 1999. doi:10.1109/ISE.1999.832058.

[255] D. Singh, A. Garg, and Deepak. Cooling rate controlled microstructure evolution and reduced coercivity in P(VDF–TrFE) devices for memory applications. *Org. Electron.*, 15(1):82–90, 2014. doi:10.1016/j.orgel.2013.10.024.

[256] J. F. Legrand. Structure and ferroelectric properties of P(VDF-TrFE) copolymers. *Ferroelectrics*, 91(1):303–317, 1989. doi:10.1080/00150198908015747.

[257] J. S. Lee, A. A. Prabu, and K. J. Kim. Annealing effect upon chain orientation, crystalline morphology, and polarizability of ultra-thin P(VDF-TrFE) film for nonvolatile polymer memory device. *Polymer*, 51(26):6319–6333, 2010. doi:10.1016/j.polymer.2010.10.053.

[258] Y. J. Park, S. J. Kang, C. Park, K. J. Kim, H. S. Lee, M. S. Lee, U-In Chung, and I. J. Park. Irreversible extinction of ferroelectric polarization in P(VDF-TrFE) thin films upon melting and recrystallization. *Appl. Phys. Lett.*, 88(24):242908, 2006. doi:10.1063/1.2207831.

[259] D. Mao, M.A. Quevedo-Lopez, H. Stiegler, B.E. Gnade, and H.N. Alshareef. Optimization of poly(vinylidene fluoride-trifluoroethylene) films as non-volatile memory for flexible electronics. *Org. Electron.*, 11(5):925–932, 2010. doi:10.1016/j.orgel.2010.02.012.

[260] W. Li, L. Yu, Y. Zhu, D. Hua, J. Wang, L. Luo, and J. Zhang. Annealing effect on poly(vinylidene fluoride/trifluoroethylene) (70/30) copolymer thin films above the melting point. *J. Appl. Polym. Sci.*, 116(2):663–667, 2010. doi:10.1002/app.31631.

[261] N. Murayama, T. Oikawa, T. Katto, and K. Nakamura. Persistent polarization in poly(vinylidene fluoride). II. Piezoelectricity of poly(vinylidene fluoride) thermoelectrets. *J. Polym. Sci. Pol. Phys.*, 13(5):1033–1047, 1975. doi:10.1002/pol.1975.180130515.

[262] J. C. Hicks, T. E. Jones, and J. C. Logan. Ferroelectric properties of poly(vinylidene fluoride-tetrafluoroethylene). *J. Appl. Phys.*, 49(12):6092–6096, 1978. doi:10.1063/1.324528.

[263] A. J. Lovinger, Don D. Davis, R. E. Cais, and J. M. Kometani. Compositional variation of the structure and solid-state transformations of vinylidene fluoride/tetrafluoroethylene copolymers. *Macromolecules*, 21(1):78–83, 1988. doi:110.1021/ma00179a017.

[264] Y. Murata and N. Koizumi. Curie Transition in Copolymers of Vinylidene Fluoride and Tetrafluoroethylene. *Polym. J.*, 17(9):1071–1074, 1985. doi:10.1295/polymj.17.1071.

[265] Y. Murata. Curie Transition in Poled and Unpoled Copolymer of Vinylidene Fluoride and Tetrafluoroethylene. *Polym. J.*, 19(3):337–346, 1987. doi:10.1295/polymj.19.337.

[266] S. Tasaka and S. Miyata. Effects of crystal structure on piezoelectric and ferroelectric properties of copoly(vinylidenefluoride-tetrafluoroethylene). *J. Appl. Phys.*, 57(3):906–910, 1985. doi:10.1063/1.334691.

[267] J. Kulk and B. Hilczer. Effect of crystallization and polarization conditions on the properties of P(VDF/TFE) (0.98/0.02) copolymer foil. *Ferroelectrics*, 109(1):291–296, 1990. doi:10.1080/00150199008211428.

[268] K. Tashiro, H. Kaito, and M. Kobayashi. Structural changes in ferroelectric phase transitions of vinylidene fluoride-tetrafluoroethylene copolymers: 2. Normal-modes analysis of the infra-red and Raman spectra at room temperature. *Polymer*, 33(14):2929–2933, 1992. doi:10.1016/0032-3861(92)90078-B.

[269] S. Uemura. Low-frequency dielectric behavior of poly(vinylidene fluoride). *J. Polym. Sci. Polym. Phys. Ed.*, 12(6):1177–1188, 1974. doi:10.1002/pol.1974.180120612.

[270] F. Bauer. Review on the properties of the ferrorelaxor polymers and some new recent developments. *Appl. Phys. A*, 107(3):567–573, 2012. doi:10.1007/s00339-012-6831-8.

[271] K. C. Kao. Electric Polarization and Relaxation. In *Dielectric Phenomena in Solids*, chapter 2, pages 58 – 77. Academic Press, San Diego, 2004. doi:10.1016/B978-012396561-5/50012-8.

[272] E. Riande and R. Diaz-Calleja. Physical fundamentals of dielectrics. In *Electrical Properties of Polymers*, chapter 1. New York: M. Dekker, Inc, New York, 2004.

[273] T. Raman Venkatesan. Relaxation processes and structural transitions in poly(vinylidenefluoride-trifluoroethylene-chlorofluoroethylene) relaxor-ferroelectric terpolymers. Master's thesis, Joint Polymer-Science Program at FU, HU and TU Berlin, and U Potsdam, 2017.

[274] L. Mandelkern, G.M. Martin, and F.A. Quinn. Glassy state transitions of poly-(chlorotrifluoroethylene), poly-(vinylidene fluoride), and their copolymers. *J. Res. Natl. Bur. Stan.*, 58(3):137, 1957.

[275] Y. Liu, K. Ren, H. F. Hofmann, and Q. Zhang. Electrostrictive polymers for mechanical energy harvesting. In Y. Bar-Cohen, editor, *Smart Structures and Materials 2004: Electroactive Polymer Actuators and Devices (EAPAD)*, page 17, San Diego, CA, 2004. doi:10.1117/12.547133.

[276] Q. Liu, C. Richard, and J-F. Capsal. Control of crystal morphology and its effect on electromechanical performances of electrostrictive P(VDF-TrFE-CTFE) terpolymer. *Eur. Polym. J.*, 91:46–60, 2017. doi:10.1016/j.eurpolymj.2017.03.046.

[277] A. Singh, P. K. Soni, T. Shekharam, and A. Srivastava. A study on thermal behavior of a poly(VDF-CTFE) copolymers binder for high energy materials. *J. Appl. Polym. Sci.*, 127(3):1751–1757, 2013. doi:10.1002/app.37780.

[278] Organic electronics market by material type (semiconductor, dielectric, conductor, substrate), by application (display, battery, lighting, conductive ink, memory, organic photovoltaics, sensor, organic RFID), and by region forecast to 2028. `https://www.emergenresearch.com/industry-report/organic-electronics-market`. Accessed: 2021-11-22.

[279] H. F. Wong, S. M. Ng, W. Zhang, Y. K. Liu, P. K. J. Wong, C. S. Tang, K. K. Lam, X. W. Zhao, Z. G. Meng, L. F. Fei, W. F. Cheng, D. Nordheim, W. Y. Wong, Z. R. Wang, B. Ploss, J-Y. Dai, C. L. Mak, A. T. S. Wee, and C. W. Leung. Modulating magnetism in ferroelectric polymer-gated perovskite manganite films with moderate gate pulse chains. *ACS Appl. Mater. Interfaces*, 12(50):56541–56548, 2020. doi:10.1021/acsami.0c14172.

[280] Z. Hu, M. Tian, B. Nysten, and A. M. Jonas. Regular arrays of highly ordered ferroelectric polymer nanostructures for non-volatile low-voltage memories. *Nat. Mater.*, 8(1):62–67, 2009. doi:10.1038/nmat2339.

[281] M.A. Khan, Unnat S. Bhansali, and H. N. Alshareef. High-Performance Non-Volatile Organic Ferroelectric Memory on Banknotes. *Adv. Mater.*, 24(16):2165–2170, 2012. doi:10.1002/adma.201200626.

[282] R. C. G. Naber, C. Tanase, P. W. M. Blom, G. H. Gelinck, A. W. Marsman, F. J. Touwslager, S. Setayesh, and D. M. de Leeuw. High-performance solution-processed polymer ferroelectric field-effect transistors. *Nat. Mater.*, 4(3):243–248, 2005. doi:10.1038/nmat1329.

[283] A. V. Bune, V. M. Fridkin, S. Ducharme, L. M. Blinov, S. P. Palto, A. V. Sorokin, S. G. Yudin, and A. Zlatkin. Two-dimensional ferroelectric films. *Nature*, 391(6670):874–877, 1998. doi:10.1038/36069.

[284] T. Nakajima, R. Abe, Y. Takahashi, and T. Furukawa. Intrinsic Switching Characteristics of Ferroelectric Ultrathin Vinylidene Fluoride/Trifluoroethylene Copolymer Films Revealed Using Au Electrode. *Jpn. J. Appl. Phys.*, 44(10L):L1385, 2005. doi:10.1143/JJAP.44.L1385.

[285] R. V. Gaynutdinov, O. A. Lysova, S. G. Yudin, A. L. Tolstikhina, A. L. Kholkin, V. M. Fridkin, and S. Ducharme. Polarization switching kinetics of ferroelectric nanomesas of vinylidene fluoride-trifluoroethylene copolymer. *Appl. Phys. Lett.*, 95(2):023303, 2009. doi:10.1063/1.3176213.

[286] P. Sharma, T. J. Reece, S. Ducharme, and A. Gruverman. High-resolution studies of domain switching behavior in nanostructured ferroelectric polymers. *Nano Lett.*, 11(5):1970–1975, 2011. doi:10.1021/nl200221z.

[287] B. Chu. A Dielectric Polymer with High Electric Energy Density and Fast Discharge Speed. *Science*, 313(5785):334–336, 2006. doi:10.1126/science.1127798.

[288] X. Chen, L. Liu, S-Z. Liu, Y-S. Cui, X-Z. Chen, H-X. Ge, and Q-D. Shen. P(VDF-TrFE-CFE) terpolymer thin-film for high performance nonvolatile memory. *Appl. Phys. Lett.*, 102(6):063103, 2013. doi:10.1063/1.4791598.

List of Figures

List of Tables

LIST OF TABLES

Publications List

List of publications included in this thesis

1. T. Raman Venkatesan, M. Wübbenhorst and R. Gerhard. Structure-Property Relationships in Three-phase Relaxor-Ferroelectric P(VDF-TrFE-CFE) Terpolymers. *Ferroelectrics*, 586(1):60-81, 2022. doi:10.1080/00150193.2021.2014260.

2. T. Raman Venkatesan, D. Smykalla, B. Ploss, M. Wübbenhorst and R. Gerhard. Tuning Tuning the Relaxor-Ferroelectric properties of Poly(vinylidenefluoride-trifluoroethylene-chlorofluoroethylene) Terpolymer Films by Means of Thermally Induced Micro- and Nanostructures. Under review in Macromolecules, 2022.

3. T. Raman Venkatesan, D. Smykalla, B. Ploss, M. Wübbenhorst and R. Gerhard. Non-Linear Dielectric Spectroscopy for Detecting and Evaluating Structure-Property Relations in a P(VDF-TrFE-CFE) Relaxor-Rerroelectric Terpolymer. *Appl. Phys. A*, 127(10): 756 (10 pages), 2021. doi: 10.1007/s00339-021-04876-0.

4. T. Raman Venkatesan and R. Gerhard. Origin of the Mid-Temperature Transition in Vinylidene fluoride-based Ferro-, Pyro- and Piezoelectric Homo-, Co- and Ter-polymers. *Mater. Res. Express*, 7(6): 065301 (7 pages), 2020. doi:10.1088/2053-1591/ab842c.

5. T. Raman Venkatesan, A. A. Gulyakova, and R. Gerhard. Influence of Film Stretching on Crystalline Phases and Dielectric Properties of a 70/30 mol% Poly(vinylidenefluoride-tetrafluoroethylene) Copolymer. *J. Adv. Dielect*, 10(5): 2050023 (10 pages), 2020. doi:10.1142/S2010135X2050023X.

6. T. Raman Venkatesan, M. Wübbenhorst, B. Ploss, X. Qiu, T. Nakajima, and T. Furukawa. The Mystery Behind the Mid-Temperature Transition(s) in Vinylidene fluoride-based Homo-, Co- and Terpolymers – Has the Puzzle Been Solved? *IEEE Trans. Dielectr. Electr. Insul.* , 27(5): 1446-1464, 2020. doi:0.1109/TDEI.2020.008865.

List of publications not included in this thesis

7. X. Qiu, A. J. Benjamin, T. Raman Venkatesan, G. C. Schmidt, R. A. Q. Soler, P. M. Panicker, R. Gerhard and A. C. Hübler. Dielectric and electroacoustic assessment of screen-printed piezoelectric polymer layers as flexible transducers: Influence of the electrode material. *IEEE Trans. Dielectr. Electr. Insul.* , 27(5): 1683-1690, 2020. doi:10.1109/TDEI.2020.008864.

8. Q. D. Nguyen, T. Raman Venkatesan, W. Wirges and R. Gerhard. Non-Uniform Polarization Profiles in P(VDF-TrFE) Copolymer Films after Cyclical Poling. *Proceedings IEEE International Symposium on Applications of Ferroelectrics (ISAF), Lausanne, Switzerland*, 1-4, 2019. doi:10.1109/ISAF43169.2019.9034937.

9. T. Raman Venkatesan, A. A. Gulyakova, P. Frübing, R. Gerhard. Electrical Polarization Phenomena, Dielectric Relaxations and Structural Transitions in a Relaxor-Ferroelectric Terpolymer Investigated with Electrical Probing Techniques. *Mater. Res. Express*, 6(12): 125301 (7 pages), 2019. doi: 10.1088/2053-1591/ab5352.

10. T. Raman Venkatesan, P. Frübing, R. Gerhard. Influence of Composition and Preparation on Crystalline Phases and Morphology in Poly(vinylidene fluoride-trifluoroethylene-chlorofluoroethylene) Relaxor-Ferroelectric Terpolymer. *Proceedings IEEE International Conference on Dielectrics (ICD)*, Budapest, Hungary, 1-4, 2018.

    doi10.1109/ICD.2018.8514758.

11. T. Raman Venkatesan, A. A. Gulyakova, P. Frübing, R. Gerhard. Relaxation processes and Structural Transitions in Poly(vinylidene fluoride-trifluoroethylene-chlorofluoroethylene) Relaxor-Ferro - electric Terpolymers as seen in Dielectric Spectroscopy. *IEEE Trans. Dielectr. Electr. Insul.* , 25(6): 2229-2235, 2018. doi10.1109/TDEI.2018.007440.

Acknowledgements

I would like to convey my first and foremost thanks, and gratitude to my advisors Prof. Dr. Reimund Gerhard and Prof. Dr. Michael Wübbenhorst for giving me this unique opportunity to do my doctoral research within the scope of a bi-national Ph.D. I am indebted to both of them for taking me under their tutelage, giving me the necessary freedom to work on my ideas and helping me with their knowledge, wisdom and experience during every step of my thesis. Prof. Gerhard has lead by example on the importance of conducting research with integrity, honesty and sound ethics. From him, I have understood the qualities that make a responsible researcher, leader, and above all a good and caring human being. The passion and un-satiable hunger of Prof. Wübbenhorst towards doing research and experiments has greatly inspired me. His enthusiasm and energy has motivated me even during difficult times.

My extended thanks to the members of my supervisory and examination committee Prof. Dr. Andreas Taubert, Prof. Dr. Pavrik Lettinga and Prof. Dr. Ruth Cardinaels for their time and interest in my thesis and providing me with constructive feedback. I take this opportunity to thank Prof. Dr. Yuri Feldman (The Hebrew University of Jerusalem) for serving as the external reviewer and his interest in my thesis, to thank Prof. Dr. Dieter Neher and Prof. Dr. Valeri Afanasiev for being the chair of my defence in University of Potsdam and KU Leuven, respectively.

Special thanks to Prof. Dr. Bernd Ploss (University of Applied Sciences Jena (UAS Jena)), Prof. Dr. Xunlin Qiu (East China University of Science and Technology, Shanghai), Dr. Anna Gulyakova (Herzen State Pedagogical University (HSPU), St. Petersburg) for their successful collaborations and discussions that as contributed immensely towards preparing this thesis. I am also desirous of acknowledging Dr. Peter Frübing, for his scientific advice and his help with setting up the rapid-quenching device.

I am indebted to Arkema-Piezotech and to Dr. Fabrice Domingues dos Santos for providing P(VDF-TrFE-CFE) terpolymer, to F2ME (Russia), Dr. Dmitry Temnov (HSPU) for the

extruded P(VDF-TFE) films. My sincere thanks to Dip.-Ing. Werner Wirges, Dip.-Ing. Andreas Pucher, Manuel Schulze (all University of Potsdam (UP)) and Werner Neefs (KU Leuven (KUL)) for stimulating discussions and helping me with the experimental setups. My heart-felt thanks to Stefan Mies (UP) for his kind help with the numerous DSC measurements and to Dr. Savitha Thayumanasundaram (KUL) for performing the mDSC measurements. Also, my sincere thanks to Dr. Christina Günter (UP) and Dr. Sylvie Tencé-Girault (PIMM-Arkema) for helping to perform X-ray Diffraction measurements and providing me with scientific inputs. Hearty thanks to Mr. David Smykalla (UAS Jena) for his invaluable help and time in performing non-linear dielectric spectroscopy and dielectric hysteresis measurements.

I am very fortunate to have been part of an open, dynamic and friendly research group both at the University of Potsdam and KU Leuven. I thank them for their love, support, encouragement and providing me with a healthy and happy work environment. Special thanks to my former group members at the University of Potsdam, Prof. Dr. Dmitry Rychkov, Dr. Gunnar Gidion, Dr. Quyet D. Nguyen, Dr. Jingwen Wang, Tobias Stubning (Robert Bosch GmbH) for their good company and assistance. My heartfelt thanks to the Professors and the group members at the Soft Matter and Biophysics group in KU Leuven, especially, Prof. Dr. Christ Glorieux, Prof. Dr. Enrico Carlon, Dr. Alessia Gennaro, Tommaso Seresini, Léopold Kritly, Hailong Pan, Dr. Pengfei Zhang, Dr. Liwang Liu, Cynthia Micallef, Dr. Gideon Wackers, Dr. Derick Yongabi, Enrico Skoruppa, Yannick Sluyts for their help, conversations and making my stay in Leuven memorable.

I am immensely indebted to Prof. Dr. Carsten Beta (UP) and Prof. Dr. Regina Hoffmann-Vogel (UP) for their support and to Ms. Beatrice Unger (formerly UP), Danielle Verachtert (KUL), Esther Balogh (KUL), Graziella Del Savio (Arensberg Doctoral School), Dr. Antonia Menski (UP) for their kind administrative help and support. I would like to also convey my special thanks to Dr. Claudia Rößling from the Welcome Center Potsdam and Christine Ludwig for their kind help with matters concerning my stay in Germany and personal well-being. Finally, I would like to extend my thanks to my family and friends for their constant motivation and encouragement.